RESEARCH ARTICLE

A Novel Subtype of Myeloproliferative Neoplasms Driven by a MYC-Alarmin Axis

Nicole D. Vincelette,[1,*] Xiaoqing Yu,[2] Andrew T. Kuykendall,[1] Jungwon Moon,[1] Siyuan Su,[3] Chia-Ho Cheng,[2] Rinzine Sammut,[1,4] Tiffany N. Razabdouski,[1] Hai Vu Nguyen,[5] Erika A. Eksioglu,[6] Onyee Chan,[1] Najla Al Ali,[1] Parth C. Patel,[1,7] Dae Hyun Lee,[8] Shima Nakanishi,[9] Renan B. Ferreira,[10] Qianxing Mo,[2] Suzanne Cory,[5] Harshani R. Lawrence,[10] Ling Zhang,[11] Daniel J. Murphy,[12,13] Rami S. Komrokji,[1] Daesung Lee,[3] Scott H. Kaufmann,[14] John L. Cleveland,[9] and Seongseok Yun[1,15,*]

[1]Department of Malignant Hematology, Moffitt Cancer Center & Research Institute, Tampa, FL 33612 USA
[2]Department of Bioinformatics and Biostatistics, Moffitt Cancer Center & Research Institute, Tampa, FL 33612, USA
[3]Department of Chemistry, University of Illinois Chicago, Chicago, IL 60607, USA
[4]Département d'hématologie clinique, Centre hospitalier universitaire de Nice, 06200 Nice, France
[5]The Walter and Eliza Hall Institute of Medical Research, Parkville, Victoria 3052, Australia
[6]Department of Immunology, Moffitt Cancer Center & Research Institute, Tampa, FL 33612, USA
[7]Department of Internal Medicine, University of South Florida, Tampa, FL 33602 USA
[8]Division of Cardiovascular Science, Department of Internal Medicine, University of South Florida, Tampa, FL 33602 USA
[9]Department of Tumor Biology, Moffitt Cancer Center & Research Institute, Tampa, FL 33612, USA
[10]Department of Drug Discovery, Moffitt Cancer Center & Research Institute, Tampa, FL 33612, USA
[11]Department of Pathology and Laboratory Medicine, Moffitt Cancer Center & Research Institute, Tampa, FL 33612, USA
[12]School of Cancer Sciences, University of Glasgow, Garscube Estate, Glasgow, United Kingdom
[13]Cancer Research UK Beatson Institute, Garscube Estate, Glasgow, United Kingdom
[14]Department of Molecular Pharmacology and Experimental Therapeutics, and Department of Oncology, Mayo Clinic, Rochester, MN 55905, USA.
[15]Lead contact

***Correspondence:**
Seongseok Yun, Moffitt Cancer Center & Research Institute, 12902 Magnolia Drive, Tampa, FL 33612, USA.
Phone: 813-745-4520; Fax: 813-745-5888;
E-mail: seongseok.yun@moffitt.org

Nicole D. Vincelette, Moffitt Cancer Center & Research Institute, 12902 Magnolia Drive, Tampa, FL 33612, USA Phone: 813-745-8110; Fax: 813-745-5888;
E-mail: nicole.vincelette@moffitt.org

Running title: Oncogenic Role of the MYC-S100A9 Circuit in MPN

Key words: MYC, myelofibrosis, trisomy 8, S100A9, alarmin

Main text word counts: 5,322

ABSTRACT

Despite advances in understanding the genetic abnormalities in myeloproliferative neoplasms (MPNs) and the development of JAK2 inhibitors, there is an urgent need to devise new treatment strategies, particularly for triple negative myelofibrosis (MF) patients whose MPNs lack mutations in the JAK2 kinase pathway and have very poor clinical outcomes. Here we report that *MYC* copy number gain and increased MYC expression frequently occur in triple negative MF, and that MYC-directed activation of S100A9, an alarmin protein that plays pivotal roles in inflammation and innate immunity, is necessary and sufficient to drive development and progression of MF. Notably, the MYC-S100A9 circuit provokes a complex network of inflammatory signaling that involves various hematopoietic cell types in the bone marrow microenvironment. Accordingly, genetic ablation of *S100A9* or treatment with small molecules targeting the MYC-S100A9 pathway effectively ameliorates MF phenotypes, highlighting the MYC-alarmin axis as a novel therapeutic vulnerability for this subgroup of MPNs.

SIGNIFICANCE

This study establishes that MYC expression is increased in triple negative MPNs via trisomy 8, that a MYC-S100A9 circuit manifest in these cases is sufficient to provoke myelofibrosis and inflammation in diverse hematopoietic cell types in the BM niche, and that the MYC-S100A9 circuit is targetable in triple negative MPN.

INTRODUCTION

Myelofibrosis (MF) is an aggressive myeloproliferative neoplasm (MPN) characterized by constitutional symptoms, cytopenias, splenomegaly, extramedullary hematopoiesis, bone marrow (BM) fibrosis, and a propensity for transformation to acute myeloid leukemia (AML)[1-3]. Approximately 85% of MF cases are driven by recurrent mutations in the *JAK2*, *CALR*, and *MPL* genes[4-9] that result in constitutive activation of JAK/STAT, PI3K/AKT, and MEK/ERK signaling pathways and a robust production of pro-inflammatory cytokines, leading to chronic inflammation and BM fibrosis[10,11]. Accordingly, the FDA has approved the JAK2 inhibitors ruxolitinib, fedratinib, and pacritinib, which provide significant improvement in constitutional symptoms, splenomegaly and overall survival (OS) for MF patients[12-15]. The clinical benefits of JAK2 inhibition largely reflect anti-inflammatory effects, as current JAK2 inhibitors are not disease modifying agents and subgroups of MF patients have inferior response to these drugs, particularly in triple negative MF (TN-MF) cases that lack *JAK2/CALR/MPL* mutations[12-14,16-18]. Thus, the field is focused on developing new therapeutic strategies to improve clinical outcomes in MF, especially TN-MF[19].

MYC is a basic-helix-loop-helix leucine zipper (bHLH-Zip) transcription factor that coordinates expression of genes controlling cell proliferation, survival, and metabolism[20-22]. Although MYC was originally identified as a transforming oncogene in lymphoid neoplasms[23-25], our studies and those of others have shown that MYC has important oncogenic roles in several myeloid malignancies[26-34]. For example, copy number gain of the *MYC* gene, located on chromosome (chr) 8q24, frequently occurs across all myeloid malignancies via trisomy 8[35-39], a genomic abnormality associated with increased MYC expression and adverse outcomes in AML and myelodysplastic

syndrome (MDS)[26,27,34]. Further, as a direct downstream target of JAK/STAT signaling, MYC has been shown to play key roles in MPN cell survival and JAK2 inhibitor resistance[40-42]. However, whether MYC serves as an independent oncogenic driver in MPN is not known.

Here we report that *MYC* copy number gain frequently occurs in TN-MF, a subgroup of MPN with the worst clinical outcomes, and is associated with increased MYC levels in hematopoietic stem cells (HSCs). Further, using transgenic mouse models that conditionally overexpress low levels of MYC in HSCs, we demonstrate that MYC can provoke MF-like disease independent of JAK2 pathway mutations, that this requires upregulation of S100A9, an alarmin protein that plays a key role in inflammation and innate immunity[43-48], and that the MYC-S100A9 axis represents a therapeutic vulnerability for MF

RESULTS

MYC copy number gain frequently occurs in TN-MF

To identify potential oncogenic drivers of TN-MF, we first performed cytogenetic analyses and targeted exome sequencing of 98 genes commonly mutated in myeloid malignancies in DNA from 584 MF patients who were identified in the Moffitt Cancer Center Total Cancer Care database as previously described[49]. Our MF cohort includes total 379 (65.0%) primary MF, 83 (14.2%) post-PV (polycythemia vera) MF, and 122 (20.9%) post-ET (essential thrombocythemia) MF (Figure 1A; Table S1), with the most common somatic mutation in *JAK2* followed by *ASXL1, TET2, CALR*, and *SRSF2* (Figures 1B-C and S1A). Consistent with previous reports[12-14,16-18], TN-MF patients in our cohort showed significantly shorter leukemia free survival (LFS) and OS compared to

JAK2/CALR/MPL mutant patients (Figures S1B-C). Notably, there was no significant difference in mutation profiles (other than JAK2 activating mutations) between TN *vs. JAK2/CALR/MPL* mutant MF (Figure S1A). However, we observed that trisomy 8 occurs more frequently in TN-MF *vs.* other subtypes (Figures 1D and S1D). Supporting a potential pathogenic role of trisomy 8 in TN-MF, patients with trisomy 8 had significantly shorter LFS (median LFS 21.4 *vs.* 32.9 years, p=0.0005) and OS (median OS 3.1 *vs.* 8.9 years, p=0.0011) (Figures 1E-F and S1E-F).

To screen oncogenic drivers in trisomy 8+ TN-MF, scRNA-seq analysis was performed comparing BM cells collected from healthy donors (HD) (n=3) and a treatment-naïve TN-MF patient with trisomy 8 (n=1) (Figures S1H-I; Table S2). Analysis of 18,651 cells (n=15,850 from HD; n=2,801 from the TN-MF patient) identified a total of 34 clusters that exhibit distinct gene expression profiles (Figures 1G and S1J-K). Distributions of these clusters were not significantly different between these two groups in the UMAP analyses (Figure 1H), indicating that hematopoietic cells in this TN-MF patient maintain gene expression profiles that are similar to normal cells. Cell component analyses, however, revealed expansion of HSCs, megakaryocytes, $CD8^+$ T-cells, and $CD56^+$ NK-cells in TN-MF, and reductions in multipotent lymphoid progenitors (MLPs), B-cells, and basophils (Figures 1I and S1L-M). In addition, the percentages of cells in S or G2/M phase were markedly increased in HSCs and common myeloid progenitors (CMPs) of trisomy 8+ TN-MF patient compared to HD (Figure S1N).

Copy number variation was also inferred using the scRNA-seq dataset. As expected, there was a distinct pattern of chr8 gain across major cell types (e.g., HSCs, CMPs, MLPs, erythroblasts, dendritic cells, and NK-cells) in trisomy 8+ TN-MF, but not in HD (Figures S1O-P). Of note, trisomy 8 was associated with bimodal distribution of AddModule score that was calculated based on

mRNA expression levels of 571 chr8 genes detected in our scRNA-seq analysis (Figure 1J). These results suggest that the additional copy of chr8 increases levels of chr8 gene expression. Subsequent comparison of 674 coding genes on chr8 *vs.* 1,260 genes that are differentially regulated in HSCs of trisomy 8+ TN-MF (compared to HD) identified a total of 131 chr8 genes (Figures 1K-L). Among these, *MYC* ranked second based on mRNA levels (Figure 1M) and was preferentially upregulated in HSCs (Figure 1N). Further, the MYC pathway was more active in the majority of major cell types (including HSCs/CMPs) in trisomy 8+ TN-MF based on PROGENy analysis (Figure S1Q; Table S3). Importantly, a comparison of trisomy 8+ *vs.* trisomy 8- cells in the same TN-MF patient, revealed that *MYC* levels were also significantly higher in trisomy 8+ HSCs/CMPs (Figure S1R); thus, increased *MYC* levels in trisomy 8+ TN-MF patient cells do not result from individual variation, but instead reflect gene copy number.

These findings were validated using immunohistochemistry (IHC) staining. In particular, BM MYC protein levels were significantly higher in trisomy 8+ *vs.* trisomy 8- TN-MF cells (Figures 1O-P and S1G). Of note, we did not observe any significant difference in somatic mutation profiles, cytogenetics, or clinical parameters between MYC negative *vs.* positive cases that potentially contribute to different levels of MYC expression other than trisomy 8 (Figure S1S; Table S4). Collectively, these results support the hypothesis that elevated MYC expression driven by *MYC* copy number gain may play an oncogenic role in MF independent of JAK2 pathway mutations.

MYC provokes an MPN that resembles MF *in vivo*

To assess the effects of MYC in HSCs and potential roles of MYC in MPN development, we established two independent transgenic mouse models: Mx1-Cre$^{+/-}$;Rosa26$^{LSL\text{-}MYC/LSL\text{-}MYC}$ and Scl-

CreERT$^{+/-}$;Rosa26$^{LSL\text{-}MYC/LSL\text{-}MYC}$ that inducibly overexpress human *MYC* in HSCs following Cre enzyme-mediated removal of a *LoxP-stop-LoxP* transcriptional stop cassette (Figures 2A-C and S2A)[50]. MYC protein levels in the Mx1-Cre$^{+/-}$;Rosa26$^{LSL\text{-}MYC/LSL\text{-}MYC}$ mice were initially compared with those expressed in lymphomas of Eμ-*Myc* transgenic mice[51,52] and in MYC10 VavP-*MYC* mice that express low levels of MYC and develop myeloid disease[53]. BM MYC levels in Mx1-Cre$^{+/-}$;Rosa26$^{LSL\text{-}MYC/LSL\text{-}MYC}$ mice were significantly lower than levels in Eμ-*Myc* B lymphoma cells (Figure 2D) but were similar to those in MYC10 BM cells (Figure 2E). These findings indicate that Mx1-Cre$^{+/-}$;Rosa26$^{LSL\text{-}MYC/LSL\text{-}MYC}$ mice express biologically relevant levels of MYC to study myeloid neoplasms[25,53].

The consequences of MYC overexpression in HSCs of Mx1-Cre$^{+/-}$;Rosa26$^{LSL\text{-}MYC/LSL\text{-}MYC}$ mice were evident following examination of peripheral blood (PB) of these mice, which displayed profound anemia and low grade monocytosis, as well as mild leukocytosis without significant changes in the neutrophil percentages and platelet counts (Figures 2F-H, S2B-D; Table S5). Mx1-Cre$^{+/-}$;Rosa26$^{LSL\text{-}MYC/LSL\text{-}MYC}$ mice also had significant increases in serum lactate dehydrogenase (LDH), slower weight gain, larger spleens, and shorter OS (median OS 258 *vs.* 385 days *vs.* not reached (NR) in MYC homozygous *vs.* heterozygous *vs.* wild type (WT), respectively, $p<0.0001$) (Figures 2I-M). Further, MYC homozygous mice had marked increases in atypical megakaryocytes[54,55], extramedullary hematopoiesis, and fibrosis of the spleen, liver, and, to a lesser extent, BM (Figures 2N and S2E-G). Notably, there was no evidence of acute leukemia (e.g., increased blasts), MDS (e.g., dysplastic cells) or lymphoma (e.g., bulky lymph nodes). An extensive comparison of MYC heterozygous *vs.* homozygous mice revealed that both develop the same

disease phenotypically, with heterozygous mice having delayed disease onset and lower disease burden (Figures 2F-N and S2B-G).

In independent experiments using Scl-CreERT$^{+/-}$;Rosa26$^{LSL\text{-}MYC/LSL\text{-}MYC}$ mice, we observed the same phenotypes as Mx1-Cre$^{+/-}$;Rosa26$^{LSL\text{-}MYC/LSL\text{-}MYC}$ mice, but with slower disease onset and progression (Figures S2H-T; Table S6). Collectively, these results indicate that modest levels of MYC overexpression in HSCs are sufficient to provoke a chronic myeloid neoplasm that is phenotypically and pathologically most similar to primary MF based on WHO diagnostic criteria[56-58].

MYC increases HSCs and myeloid progenitors with limited self-renewal capacity

Experiments characterizing hematopoietic sub-populations of Mx1-Cre$^{+/-}$;Rosa26$^{LSL\text{-}MYC/LSL\text{-}MYC}$ mice revealed that MYC promotes expansion of HSCs, multipotent progenitors (MPPs), myeloid progenitors such as CMPs, granulomonocytic progenitors (GMPs), and megakaryocyte erythrocyte progenitors (MEPs), as well as Gr-1^{+}/CD11b^{+} mature myeloid cells. In contrast, there were reductions in the percentages of B- and T-lymphocytes in the BM and spleen (Figures 3A-C and S3A-C). Although MYC increased the percentages of HSCs and progenitors in the Lin^{-} population, there was no significant change in the proportion of individual components (i.e., LT-HSC, ST-HSC, MPP2, and MPP3) and there was no significant lineage bias in myeloid progenitors (Figures S3B-C). A similar expansion of HSCs/MPPs without changes in the proportion of individual components was observed in Scl-CreERT$^{+/-}$;Rosa26$^{LSL\text{-}MYC/LSL\text{-}MYC}$ and Scl-CreERT$^{+/-}$;Rosa26$^{LSL\text{-}MYC/+}$ mice compared to control mice (Figure S3D). Notably, MYC homozygous progenitors had increased monocytic colony forming units (M-CFU) and granulomonocytic CFU

(GM-CFU) in BM cells and all CFU in spleen cells, but these displayed limited self-renewal capacity ex vivo (Figures 3D-E and S3E-J); thus, this MYC-driven myeloid neoplasm is not acute leukemia. Conversely, in myeloid progenitors isolated from the BM of Rosa26-CreERT2$^{+/-}$;*Myc*$^{fl/fl}$ mice, *Myc* loss provoked marked reductions in CFU, specifically in GM-CFU (Figure S3K-M).

In further studies, CD45.1^{+}/CD45.2^{+} mice were transplanted with CD45.2^{+} Mx1-Cre$^{+/-}$;Rosa26$^{LSL\text{-}MYC/LSL\text{-}MYC}$ and CD45.1^{+} WT *vs.* CD45.2^{+} Mx1-Cre$^{+/-}$;Rosa26$^{+/+}$ and CD45.1^{+} WT BM cells that are mixed at 1:1 ratio (Figure 3F). In these competitive transplant studies, the proliferative advantage associated with MYC overexpression was maintained in vivo (Figure 3G-I). Further, the transplanted MYC homozygous BM cells provoked a phenotypically indistinguishable disease in recipient mice and reduced their OS (median OS 315 days in Mx1-Cre$^{+/-}$;Rosa26$^{LSL\text{-}MYC/LSL\text{-}MYC}$ *vs.* NR in control transplanted group, p=0.0396) (Figures 3J-O; Table S7), indicating that the transplanted cells were sufficient to induce an MF-like chronic myeloid malignancy in the normal BM niche.

MYC-driven expansion and proliferation of HSCs and myeloid progenitors is independent of JAK/STAT signaling

To identify the mechanism by which MYC drives MF, scRNA-seq analysis was performed comparing BM cells harvested from Mx1-Cre$^{+/-}$;Rosa26$^{LSL\text{-}MYC/LSL\text{-}MYC}$ *vs.* Mx1-Cre$^{+/-}$;Rosa26$^{+/+}$ mice at 20 weeks following pIpC injection (Figure S4A). By analyzing 25,232 cells (n=13,552 from control and n=11,680 from Mx1-Cre$^{+/-}$;Rosa26$^{LSL\text{-}MYC/LSL\text{-}MYC}$ mouse), we identified a total of 33 clusters and 23 major cell types (Figures 4A and S4B-D). As in analyses of human TN-MF and healthy human donors (Figure 1H), distributions of these clusters were not significantly different

between MYC homozygous vs. control mice (Figure 4B). Cell component analyses revealed that the percentages of HSCs, myeloid progenitors, and mature myeloid cells, including monocytes and macrophages, were increased, whereas erythroblasts, B- and T-lymphocytes were reduced in MYC homozygous mice (Figures 4C-D). Notably, MYC homozygous mouse has an increased percentages of cells in S or G2/M phase, specifically in HSCs, myeloid progenitors, monoblasts, and monocytes (Figure S4E). These findings are consistent with the results from complete blood counts (CBC) with differential and flow-cytometry (Figures 2H, S2O, 3A-C, 3K, S3C, S3E, S3I, and S3M), further supporting the role of MYC in driving myeloid proliferation.

To assess MYC-driven transcriptomic changes in each cellular component, we performed differential gene expression analysis followed by semantic analysis in individual major cell types (Figures S4F-G; Table S8). Many of the well-known MYC target pathways (e.g., ribosome biogenesis, regulation of translation, p53 and intrinsic apoptosis[22]) were significantly activated in MYC homozygous HSCs (Figure 4E). In mature myeloid cells such as monocytes, MYC activated genes involved in metabolic processes, including oxidative phosphorylation and carbohydrate catabolism, and suppressed genes involved in myeloid differentiation (Figure 4F). Unexpectedly, MYC also suppressed cytokine signaling and inflammatory response pathways (Figure 4F). Indeed, PROGENy analysis revealed that the JAK/STAT, PI3K/AKT, and MAPK pathways as well as TNF-α and TGF-β signaling that play critical roles in chronic inflammation in the *JAK2/CALR/MPL* mutant MPN[10,11] are inactive in most of the major cell types that overexpress MYC, whereas p53 and alarmin pathways are substantially activated by MYC (Figure 4G; Table S9). These findings were validated by immunoblotting that showed a marked increase in p53 in MYC overexpressing

BM and spleen cells *vs*. control cells but no significant differences in the levels of phosphorylated Stat3, Akt, and Erk1/2 (Figures S4H-I).

Further underscoring a negligible role of the JAK pathway in MYC-driven MF, ruxolitinib treatment had minimal effects on the levels of phosphorylated Stat3, Akt, and Erk1/2 as well as apoptosis in homozygous MYC BM cells, although the same ruxolitinib concentrations induced robust cell death and/or downregulated levels of phospho-Stat3, -Akt, and -Erk1/2 in the *JAK2*^{V617F} mutant SET-2 and HEL MPN cells (Figures S4J-M). Collectively, these findings suggest that MYC provokes MF independent of the JAK pathway.

MYC induces S100A9-mediated chronic inflammation

Because the alarmin pathway upregulated by MYC (Figures 4G) can induce inflammation independent of the JAK/STAT pathway, we next focused on defining MYC targets that play critical roles in the alarmin pathway. Among genes that are differentially regulated by MYC in individual clusters (Figures S4F-G), increased MYC was accompanied by *S100a9* upregulation in most of the major cell types as well as increased expression of *S100a8* and *ASC* in several of the cell types (Figures 4H-O, S4N-Q; Table S8). These findings were validated by qRT-PCR, ELISA, and immunoblotting (Figures 4P-R, S4H-I, S4R). Supporting the clinical relevance of S100A9 in MF pathogenesis, *S100A9* levels in CD34^{+} BM cells were significantly elevated in MF patients *vs.* HD regardless of *JAK2*^{V617F} mutation status (Figures 5A-B)[59,60]. Importantly, in the TN-MF cohort, cells with *MYC* expression showed significantly higher S100A9 levels in their BM cells compared to cells not expressing *MYC* (Figures 1O-P and 5C-E). In addition, *S100A8/A9* levels in megakaryocytes, neutrophils (i.e., cluster 16), as well as *ASC* levels in CMPs, neutrophil, NK-, T-,

and B-cells were markedly increased in trisomy 8+ TN-MF compared to HD (Figures S5A-C). Finally, MYC induced a marked increase in cleaved caspase-1 and dimerized ASC (Figures S4H-I and S4S), which are hallmarks of activation of S100a8/a9-dependent inflammation[61]. Collectively, these observations suggest that increased MYC in HSCs induces S100a9-mediated inflammation.

A complex network of S100A9-mediated inflammatory signaling is manifest in MYC-driven MF

Interestingly, MYC-directed S100a8/a9 upregulation was completely lost when cells were cultured ex vivo (Figure 5F), indicating that an intact BM niche is critical for the MYC-driven inflammation. Notably, following the induction of MYC expression there were several marked changes in cell-cell interactions. First, a significant portion of S100a8/a9 signal was derived from cells in the granulocyte lineage (i.e., myeloblasts, myelocytes, neutrophils) (Figures 4N-O, S4N, S4P, 5G-N, S5D-F; Table S10). However, for HSCs, myeloid progenitors (i.e., CMPs, GMPs, MEPs), and lymphocytes (i.e., T-, B-, NK cells) that are normally less inflammatory, MYC expression also resulted in elevated levels of *S100a9*, thus affecting many other cell types expressing S100a9 receptors such as ALCAM[62] (Figures 5G-J). Second, even though MYC did not affect the frequency or pattern of interactions of some of the ligand-receptor pairs such as S100a8/a9-CD68 (Figures 5K-N, S5E-F), the intensity of S100a8/a9-mediated interactions was markedly increased in cells with elevated MYC levels (Figures 5O-P, S5G). Third, cells of myelomonocytic lineage (i.e., myeloblasts, myelocytes, monoblasts, monocytes, and macrophages) in MYC homozygous mice were most affected by S100a8/a9 signaling (Figures 5G-N, S5D-F). Accordingly, levels of the inflammatory marker ASC were significantly increased in these cell types in MYC homozygous

mice (Figures S4O, S4Q) and there was a marked expansion of monocytes and macrophages (Figures 2H, S2O, 3C-E, 3K, S3E, S3I, and S3M), especially M1 macrophages (Figures 5Q-R) that are known to be expanded by activation of S100A9 and CD68 and play pivotal roles in MF pathogenesis[63-65]. Finally, TNFα- and CSF-1-mediated cell-cell interactions were downregulated in MYC homozygous cells (Figures S5H-L; Table S10), further supporting negligible roles for the JAK2 pathway in this MYC-driven model of TN-MF. Collectively, these findings suggest that MYC provokes a unique inflammatory network that is mediated by S100A8/A9 within the BM niche.

S100a9 contributes to development of MYC-driven MF

To test whether S100a9 upregulation is required for MYC-driven MF development, we generated Mx1-Cre$^{+/-}$;Rosa26$^{LSL\text{-}MYC/LSL\text{-}MYC}$;*S100a9*$^{-/-}$ mice and compared them with Mx1-Cre$^{+/-}$;Rosa26$^{LSL\text{-}MYC/LSL\text{-}MYC}$ mice (Figure 6A). MYC levels in BM and spleen cells of these two cohorts were similar and were significantly higher than MYC levels in WT or *S100a9*$^{-/-}$ mice (Figures 6B-C). Conversely, S100a9 (in BM and spleen), as well as S100a8/a9 heterodimers (in serum) were undetectable in both *S100a9*$^{-/-}$ and Mx1-Cre$^{+/-}$;Rosa26$^{LSL\text{-}MYC/LSL\text{-}MYC}$;*S100a9*$^{-/-}$ mice (Figures 6C-D). *S100a9* deficiency impaired MYC-induced anemia and monocytosis, and increased platelet counts (Figures 6E-F, S6A-C; Table S11), indicating that S100a9 contributes to MYC-induced MF. Further, Mx1-Cre$^{+/-}$;Rosa26$^{LSL\text{-}MYC/LSL\text{-}MYC}$;*S100a9*$^{-/-}$ mice displayed significant improvements in weight gain, reduced spleen size, and prolonged OS compared to Mx1-Cre$^{+/-}$;Rosa26$^{LSL\text{-}MYC/LSL\text{-}MYC}$ mice (median OS NR *vs.* 225 days, p=0.0345) (Figures 6G-H, S6D; Table S11). Flow cytometric analyses revealed that *S100a9* loss in Mx1-Cre$^{+/-}$;Rosa26$^{LSL\text{-}MYC/LSL\text{-}MYC}$ mice (i) substantially reduced the percentages of HSCs, myeloid progenitors, and macrophages in BM and/or spleen; (ii) significantly reduced

the percentages of $Gr1^+/CD11b^+$ myeloid cells in spleen; and (iii) restored the percentages of $B220^+$ and $CD3^+$ cells close to normal levels in spleen (Figures 6I-N). Notably, *S100a9* deficiency alone did not affect normal hematopoiesis, as CFU in *S100a9*$^{-/-}$ progenitors were similar to those of WT mice (Figures S6E-G). Finally, loss of *S100a9* effectively suppressed MYC-driven megakaryocytic atypia, fibrosis, and extramedullary hematopoiesis (Figures 6O, S6H). However, the size of spleens and the percentages of HSCs/progenitors in Mx1-Cre$^{+/-}$;Rosa26$^{LSL\text{-}MYC/LSL\text{-}MYC}$;*S100a9*$^{-/-}$ mice were still higher than those of WT or Mx1-Cre$^{+/-}$;Rosa26$^{+/+}$ mice (Figures 6G and 6I-J), and there was residual megakaryocytic atypia and extramedullary hematopoiesis in Mx1-Cre$^{+/-}$;Rosa26$^{LSL\text{-}MYC/LSL\text{-}MYC}$;S100a9$^{-/-}$ mice (Figures 6O, S6H). Thus, S100a9 plays a major role in the pathogenesis of MYC-driven MF, but additional targets downstream of MYC might also contribute to myeloid proliferation and MF pathogenesis.

Enforced S100a9 expression is sufficient to provoke MF phenotypes

To test whether S100a9 overexpression would phenocopy the effects of MYC in driving MF, we assessed the phenotypes manifest in S100a9 transgenic (S100a9Tg) mice that overexpress *S100a9* under the control of the H2-K promoter (Figure S6I)[66]. Although there was no significant difference in *S100a9* mRNA levels in BM of S100a9Tg and WT mice (Figure S6J), most likely due to the abundance of neutrophils that express very high levels of *S100a9* in BM (Figures 4A and 4N), there were significantly higher levels of S100a9 mRNA and protein in the spleen of S100a9Tg mice (Figures S6K-L). At age >12 months, serum levels of S100a8/a9 dimers in S100a9Tg mice were also significantly elevated compared to age-matched control mice (Figure S6M). There was

no positive or negative correlation between S100a9 and MYC protein levels in S100a9Tg (Figure S6L), indicating S100A9 does not affect MYC expression.

Notably, S100a9 overexpression alone was sufficient to provoke anemia, lymphopenia, monocytosis, neutrophilia, and thrombocytopenia in ~60% of S100a9Tg mice, but these phenotypes only became prominent after 11 months of age (Figures S6N-R; Table S12). Forced expression of S100a9 also induced marked splenomegaly and significantly reduced OS (median OS 371 days *vs.* NR, p=0.0104) (Figure S6S-U). Further, S100a9 promoted expansion of HSCs, MPPs, and mature myeloid cells, and provoked decreases in B- and T-cells in BM and spleen (Figure S6V). Finally, S100a9 overexpression induced marked increase in megakaryocytic atypia, extramedullary hematopoiesis, and fibrosis of BM, spleen, and liver (Figure S6W). Collectively, these data confirm that S100A9 plays a pivotal role in MYC-driven MF.

Based on these findings, we assessed effects of pharmacologic inhibition of S100a9 in vivo using Tasquinimod, a small molecule that binds to S100a9 and prevents its interaction with its receptors[67,68] (Figure S7A). Phenocopying some of the effects of *S100a9* deletion, treatment of Mx1-Cre$^{+/-}$;Rosa26$^{LSL\text{-}MYC/LSL\text{-}MYC}$ mice with Tasquinimod (i) increased platelet counts, (ii) reduced spleen size, and (iii) partially reversed MYC-driven expansion of myeloid progenitors in spleen and of macrophages in BM (Figures S7B-H; Table S13). Further, Mx1-Cre$^{+/-}$;Rosa26$^{LSL\text{-}MYC/LSL\text{-}MYC}$ mice treated with Tasquinimod showed reduced megakaryocytic atypia, fibrosis, and extramedullary hematopoiesis (Figure S7I). Nonetheless, Tasquinimod failed to improve OS (median OS 251 *vs.* 208 days, p=0.7715) (Figure S7J). Instead, prolonged treatment with Tasquinimod (>3 months) provoked profound anemia and neutrophilia (Figures S7B, S7D), which were not seen in Mx1-Cre$^{+/-}$;Rosa26$^{LSL\text{-}MYC/LSL\text{-}MYC}$;*S100a9*$^{-/-}$ mice (Figures 6E, S6B). These changes,

which are likely off-target effects of Tasquinimod, may explain the failure of this agent to phenocopy *S100a9* knockout and significantly improve OS.

Targeting of the MYC-S100A9 circuit with a small molecule antagonizing MYC

In further studies, we examined the impact of directly targeting MYC using MYCi975, a small molecule that directly binds to the HLH domain of MYC, reducing MYC protein stability and transcriptional activity[69]. MYCi975, at concentrations that downregulate MYC protein in *JAK2*^{V617F} mutant MPN cells and MYC-dependent AML cells, induced robust PARP cleavage and apoptosis in primary BM cells from Mx1-Cre$^{+/-}$;Rosa26$^{LSL\text{-}MYC/LSL\text{-}MYC}$ mice ex vivo (Figures S7K-O), indicating that this model of TN-MF is addicted to MYC.

To test whether MYC inhibition can suppress disease progression in vivo, lethally irradiated CD45.1^{+}/CD45.2^{+} WT mice were transplanted with BM cells harvested from CD45.2^{+} Mx1-Cre$^{+/-}$;Rosa26$^{LSL\text{-}MYC/LSL\text{-}MYC}$ mice that were treated with pIpC 20 weeks prior to the transplant (Figure 7A). Engraftment of donor-derived CD45.2^{+} BM cells was confirmed by flow-cytometry at 4 weeks post-transplant, and mice were then randomized to either MYCi975 or vehicle treatment and monitored for disease progression (Figure 7A). MYCi975 effectively reduced MYC and S100a8/a9 levels in BM and spleen cells in vivo (Figure 7B). Consistent with these results, MYCi975 slowed disease progression and even caused disease regression in some mice (Figure 7C). Further, MYCi975 effectively suppressed MYC-driven MF phenotypes (Figures 7D-F, S7P; Table S14). Finally, these changes were associated with significantly improved OS (median OS NR *vs.* 252 days in MYCi975- *vs.* vehicle-treated group, respectively, p=0.0109) (Figure 7G).

Based on these results, the effects of MYC inhibition were assessed in a patient-derived

xenograft (PDX) from a trisomy 8+ TN-MF patient. First, BM samples were collected at the time of diagnosis from a trisomy 8+ TN-MF patient who had splenomegaly and profound constitutional symptoms (Figure 7H; Table S2). Staining of the BM biopsy revealed a hypercellular marrow with megakaryocytic atypia, grade 1 reticulin fibrosis, and elevated MYC protein levels (Figure 7H). scRNA-seq analysis of BM cells confirmed increased *MYC* and *S100A8/A9* in HSCs and neutrophils, respectively (Figure 7J). BM cells from this patient were then transplanted via intratibial injection into sublethally irradiated NSG-SGM3 mice. Following confirmation of engraftment of human $CD45^+$ cells at 9 weeks post-transplant, mice were randomized to treatment with MYCi975, ruxolitinib, or vehicle (Figure 7K). MYCi975 treatment effectively suppressed disease progression as evidenced by a significantly lower percentage of $hCD45^+$ cells in PB compared to mice treated with ruxolitinib or vehicle (Figure 7K). Importantly, treatment of the patient with fedratinib for 6 months showed only a modest improvement in spleen size without significant changes in BM cellularity, the percentage of trisomy 8+ and MYC+ cells, and reticulin fibrosis (Figures 7H-I, S7Q). These results indicate MYC as a clinically actionable target in MYC-driven TN-MF (Figure 7L). Further, our studies suggest that a small molecule targeting MYC can potentially irradicate malignant trisomy 8+ TN-MF clones, which is a major advance as malignant clones in MF are not eradicated by current JAK2 inhibitors[18,19].

DISCUSSION

While increased MYC expression in lymphoid malignancies is mainly driven by *MYC* gene rearrangements[23-25] and *MYC* somatic mutations have been identified in a variety of cancers[4-

[9,39,70-76], these changes are rare in myeloid neoplasms[39,71-76]. However, the *MYC* gene is located on chr 8q24 where copy number gain is frequently observed across all myeloid malignancies[35-39], and we and others have shown that *MYC* copy number gain is associated with increased MYC levels and inferior survival outcomes in AML and MDS[26,27,34]. Although *MYC* copy number gain is also frequent in MF patients[36-38,77], its oncogenic role in MF is largely unknown. Here we have shown that trisomy 8 commonly occurs in TN-MF, but not in other molecular subtypes, and is associated with adverse clinical outcomes. Further, our scRNA-seq and IHC analysis of BM cells revealed significantly higher levels of MYC mRNA and protein in HSCs from trisomy 8+ TN-MF patients compared to normal donors. These observations, along with subsequent findings discussed below, identify MYC as an oncogenic driver of TN-MF that is independent of JAK2 pathway mutations.

MYC transcriptional programs are activated as HSCs differentiate into myeloid progenitors[78], and these programs control the balance of HSCs self-renewal and differentiation into mature myeloid cells[79]. In accord with these findings, there was a dramatic reduction in GM-CFU following *Myc* silencing in Rosa26-CreERT2$^{+/-}$;*Myc*$^{fl/fl}$ mice, and the opposite effect upon MYC overexpression in Mx1-Cre$^{+/-}$;Rosa26$^{LSL\text{-}MYC/LSL\text{-}MYC}$ mice. Although these effects of MYC up- or down-regulation on myeloid progenitors ex vivo have been observed across many pre-clinical studies, the in vivo effects of increased MYC expression in HSCs have been variable[26,53,79-81]. For example, studies using retroviral-mediated MYC overexpression in HSCs have shown that MYC can provoke AML in vivo, and recent studies using human CD34^{+} cord blood stem cells have shown that lentiviral-mediated MYC overexpression in HSCs drives AML only in the presence of continuing IL-3/GM-CSF co-stimulus[32,33]. In contrast, culture of HSCs ex vivo following MYC

transduction yields highly homogeneous committed myeloid progenitors[82-86]. These varied findings might reflect the effects of different MYC expression levels. Previous in vivo studies using the VavP-*MYC* transgenic mouse model established that MYC levels govern hematopoietic tumor type, with high HSCs MYC levels favoring lymphoma development and lower MYC levels inducing the formation of marrows having megakaryocyte atypia and cytokine hypersensitivity, all of which are hallmarks of MPN, although the precise disease phenotypes and underlying mechanisms were not fully characterized[25,53].

Using two independent transgenic mouse models that inducibly increase MYC expression to levels found in myeloid disease-prone VavP-*MYC* transgenic mice, we have shown that low levels of MYC overexpression in HSCs induce a myeloid malignancy that is most consistent with MF[56,57]. Further, using in vivo transplant studies, pharmacologic inhibition of MYC was shown to effectively reverse MYC-driven MF phenotypes and significantly improve OS. Importantly, the MYC inhibitor also suppressed disease progression in a PDX model using primary BM cells from a TN-MF patient with trisomy 8. Accordingly, this study is the first to show that MYC levels are increased in a subgroup of TN-MF patients, specifically in patients with trisomy 8 and that MYC provokes MF independent of JAK2 pathway mutations, and suggest that this MYC circuit is targetable using a small molecule inhibitor.

Chronic inflammation is a hallmark of MF pathogenesis. While pro-inflammatory cytokines induced by constitutive activation of JAK/STAT pathway play pivotal roles in MF development in patients with *JAK2/CALR/MPL* mutations, the oncogenic drivers that promote inflammation in TN-MF have heretofore been unclear. Our studies establish that increased MYC expression in HSCs induces S100A8/A9-mediated chronic inflammation, and that *S100a9* deficiency

significantly impairs MYC-driven MF development, leading to improved OS. Importantly, MYC-driven MF cells are not sensitive to JAK2 inhibitors ex vivo, a finding supported by additional PDX experiments and clinical studies performed in parallel. Collectively, these findings suggest that MF patients whose disease depends on MYC activation need alternative therapeutic strategies using agents targeting the MYC-alarmin axis rather than JAK2 inhibitors.

One of the most striking findings is the complex nature of the inflammatory network driven by the MYC-alarmin axis. This inflammatory network requires an intact BM niche and likely involves various hematopoietic and non-hematopoietic cells. Even though S100a8/a9 levels are significantly increased by MYC in BM and/or spleen cells in vivo, MYC-directed upregulation of S100a8/a9 is completely abolished in BM cells cultured ex vivo. scRNA-seq analyses also suggest that this inflammatory network likely includes contributions of various hematopoietic and non-hematopoietic cells. Indeed, a wide range of hematopoietic cells that are minimally inflammatory under normal conditions (e.g., HSCs, myeloid progenitors, T-lymphocytes) can affect diverse cell types via S100a8/a9 when MYC is activated. This is especially manifest in myelomonocytic lineage cells (e.g., monoblasts, monocytes, macrophages) that are predominantly affected by S100a8/a9 signals through various receptors (e.g., ALCAM, CD68) to promote the selective expansion of highly inflammatory M1 macrophages[87,88]. Notably, MF patients have increased macrophages in their BMs compared to patients with other MPN subtypes or normal BM[89], and depletion of macrophages effectively prevents MF development in a model of *JAK2*^{V617F} driven MF[63]. Taken together, our data suggest that expansion of inflammatory monocytes and macrophages plays a key role in MF development regardless of JAK2 pathway mutations. If so, selective targeting of these sub-populations using small molecules or monoclonal antibodies could be an alternative

therapeutic approach.

Our studies raise several important questions. First, MYC, as a direct downstream target of the JAK/STAT pathway, also plays key roles in MPN cell survival and resistance to JAK2 inhibitors[40-42,90,91]. Although *S100A9* levels were elevated in the $CD34^+$ cells of *JAK2*^{V617F} mutant MF patients[59,60], it is unclear whether the MYC-S100A9 circuit also plays an active role in MPN driven by *JAK2* pathway mutations. The answer to this clinically important question will have consequences for eligibility criteria in future clinical trials using agents targeting the MYC-S100A9 pathway and for the design of optimal combination therapies. Second, S100A9 from mesenchymal stromal cells (MSCs) is known to play an essential role in the $JAK2^{V617F}$- and TPO-driven MF pathogenesis[45]. Indeed, $Gli1^+$ or $LepR^+$ MSCs have been identified as fibrosis-driving myofibroblasts in the context of *JAK2* pathway mutations[92-94], but it remains to be determined whether MYC in HSCs can also activate $Gli1^+$ or $LepR^+$ MSCs. Third, consistent with observations from other MPN mouse models[95-101], we observed significant fibrosis in the spleen and liver, but less in the BM in MYC-driven murine MF. While it is possible that inherently higher levels of *S100A8/A9* in the normal mouse BM niche *vs.* human BM reflect a tolerability of higher S100A8/A9 levels in murine BM before fibrosis occurs, other differences in the BM niche between mouse and human, as well as between mouse BM and spleen, also need to be explored as potential explanations for the differences in fibrosis phenotypes. Fourth, *S100a9* deficiency only partially abrogated MYC-driven MF phenotypes, suggesting that additional targets downstream of MYC also contribute to MF pathogenesis. As S100A9-directed agents become available, it will be important to see whether inhibition of S100A9-mediated inflammation will translate into improved survival outcomes in patients with pre-existing MF and to address this question

separately in patients with MYC-driven MF vs. *JAK2/CALR/MPL*-driven MF. Fifth, even though Tasquinimod acutely inhibits S100A9 signaling and has been well studied in both mice and humans[67,68], this agent showed modest effects in suppressing MYC-driven MF phenotypes and, upon long-term treatment, was associated with effects such as anemia and neutrophilia that were not seen with *S100a9* knockout, indicating the need for developing S100A9 inhibitors with improved efficacy and safety profiles. Sixth, because TN-MF is associated with higher risk of transformation into AML *vs*. other molecular subtypes, identifying secondary genetic alterations and defining how they cooperate with MYC to promote AML transformation will be critical to improve clinical outcomes in these patients. Finally, trisomy 8 also occurs in HSCs in the normal population, with a prevalence that increases with aging[102-105] in much the same fashion as somatic mutations (e.g., *JAK2, DNMT3A, TET2*) in HSCs that drive clonal hematopoiesis and provoke a pro-inflammatory state linked to other co-morbidities such as cardiovascular disease[106-109]. Thus, the systemic impact of inflammatory signals that can arise from MYC-dependent clonal hematopoiesis warrants future investigation.

In summary, the studies reported herein are the first to describe an oncogenic role of MYC in MF pathogenesis, reveal a previously undescribed circuit that connects MYC, alarmins, and inflammation, and validate the MYC-S100A9 axis as a novel therapeutic vulnerability in a subgroup of MF patients with very poor outcomes. Accordingly, our results provide a strong rationale for testing agents targeting MYC or S100A9 in early phase clinical trials in MF patients having increased MYC activity.

METHODS

Human subjects and clinical data

Using the Moffitt Cancer Center (MCC) Total Cancer Care (TCC) dataset, we retrospectively identified cases diagnosed with primary and secondary myelofibrosis (MF) from 2000 to 2021. The patients had provided written informed consent to be included in the dataset, and our study was approved by the MCC IRB (protocols MCC#14690 and MCC#18864). MYC and S100A9 protein expression were assessed by immunohistochemistry (IHC) staining as described below. Somatic mutations were assessed using targeted exome sequencing (developed at MCC) examining 54 or 98 myeloid genes as previously described[110,111]. Clinical variables and disease-related prognostic factors, including age, gender, cytogenetics, and treatment regimens, were characterized at the time of MF diagnosis, and were annotated using descriptive statistics. The LFS and OS were estimated with the Kaplan-Meier method and compared using log-rank test. All statistical analyses were performed using SPSS v24.0 and GraphPad Prism 7.

Animal studies

All animal studies were performed in compliance with the National Institutes of Health Guidelines under a protocol approved by the H. Lee Moffitt Cancer Center & Research Institute and the University of South Florida Institutional Animal Care and Use Committee (IACUC). Mouse genotypes from tail biopsies were determined using real time PCR with specific probes designed for each gene (Transnetyx). All mice used in our in vivo studies were C57BL/6J background except PDX studies that used NSG-SGM3 mice (see Table S15).

Mx1-Cre$^{+/-}$;Rosa26$^{LSL\text{-}MYC/LSL\text{-}MYC}$ and Scl-CreERT$^{+/-}$;Rosa26$^{LSL\text{-}MYC/LSL\text{-}MYC}$ mice were generated by crossing Mx1-Cre$^{+/-}$ or Scl-CreERT$^{+/-}$ mice with Rosa26$^{LSL\text{-}MYC/LSL\text{-}MYC}$ mice, respectively. Mx1-Cre$^{+/-}$;Rosa26$^{LSL\text{-}MYC/LSL\text{-}MYC}$;S100a9$^{-/-}$ mice were generated by crossing Mx1-Cre$^{+/-}$;Rosa26$^{LSL\text{-}MYC/LSL\text{-}MYC}$ mice with S100a9$^{-/-}$ mice. Mice at age 6~11 weeks in both experimental and control groups were treated with pIpC (250μg/kg, d1 and d3, prepared in normal saline, i.p.) or tamoxifen (250mg/kg, d1-5, prepared in corn oil, po) to induce MYC gene expression. Using peripheral blood (PB) samples, complete blood counts (CBC) with differential were assessed 1 week prior to pIpC or tamoxifen treatment (baseline), and then every 4 weeks following drug treatment. Mice at pre-defined endpoints were sacrificed and primary BM, spleen, and liver tissues/cells were analyzed via the assays described below. Pre-defined endpoints used in our in vivo studies include (i) substantial weight loss (≥20% loss), (ii) abnormalities with movement or breathing, (iii) excessive lethargy, tremors, restlessness, failure to groom causing unkempt appearance, teeth grinding, or guarding (protecting the painful area), (iv) failure to show normal patterns of inquisitiveness, and (v) inability to urinate or defecate.

For competitive congenic transplant experiments, mice were placed on Baytril water (0.25 mg/ml) 72 hr prior to irradiation to prevent opportunistic bacterial infections. Lethally irradiated (1100cGy) CD45.1^{+}/CD45.2^{+} WT recipient mice were transplanted with a total of 1 million CD45.2^{+} Mx1-Cre$^{+/-}$;Rosa26$^{LSL\text{-}MYC/LSL\text{-}MYC}$ or Mx1-Cre$^{+/-}$;Rosa26$^{+/+}$ (that were treated with pIpC 20 weeks prior to transplant) and CD45.1^{+} WT helper cells (mixed at 1:1 ratio) via tail vein injection 24 hr after irradiation. To confirm successful engraftment, PB samples were collected at 4 weeks following transplant, then incubated in ACK buffer twice for 5 min to lyse RBC. Disease burden was measured every 4 weeks by performing serial CBC with differential and flow cytometry as

described below. Mice were harvested at pre-defined endpoints and primary BM and spleen cells were harvested for RNA extraction and qRT-PCR, immunoblotting, and ELISA assays. Femur, tibia, spleen, and liver tissues were also harvested. Tissues were incubated in Neutral Buffered Formalin for 24 hr, then stored in 70% EtOH until used. H&E, trichrome, and reticulin staining were performed as described[112] or as noted below. Spleen and body weight were measured per protocol.

Tissue culture

Cell lines were propagated at densities of <1 x 10^6 cells/ml in RPMI 1640 medium containing 10% heat-inactivated fetal bovine serum (FBS), 100 units/ml penicillin G, and 2 mM glutamine (medium A) except for SET-2 cells, which were cultured in medium with 15% FBS. Primary BM cells were harvested from Mx1-Cre$^{+/-}$;Rosa26$^{+/+}$, Mx1-Cre$^{+/-}$;Rosa26$^{LSL\text{-}MYC/+}$, Mx1-Cre$^{+/-}$;Rosa26$^{LSL\text{-}MYC/LSL\text{-}MYC}$, Rosa26-CreERT2$^{+/-}$;*Myc*$^{+/+}$, and Rosa26-CreERT2$^{+/-}$;*Myc*$^{fl/fl}$ mice. BM cells were homogenized in PBS with 2% FBS, filtered through a 100-µm strainer and cultured in RPMI 1640 medium containing FBS (15%), glutamine (2 mM), mouse IL-3 (10 ng/ml), mouse IL-6 (10 ng/ml), mouse SCF (10 ng/ml), and penicillin G (100 units/ml).

Colony forming assays

Primary mouse BM and spleen cells were harvested under sterile conditions. Cells were centrifuged for 5 min at 1,000 rpm and pellets were resuspended in RBC lysis buffer. Samples were then centrifuged for 5 min at 1,000 rpm and resuspended in 2% FBS IMDM media to 2 x 10^4 cells/100 µl stock for BM cells and 2 x 10^5 cells/100 µl for spleen cells. After mixing 400 µl of each

stock with 4 ml of Methocult^{TM} GF M3434, 1.1ml of the mixture (2 x 10^4 BM cells and 2 x 10^5 spleen cells) was plated in triplicate into 6-well dishes (SmartDish^{TM}, STEMCELL Technology). After incubation for 10 days, colonies were manually counted.

Immunoblotting

Following treatment with the indicated concentrations of drugs or isolation of the primary cells from BM and spleen, cells (5x10^6/aliquot) were washed with cold Dulbecco's phosphate buffered saline (PBS), lysed with RIPA buffer (10 mM Tris [pH 7.4], 100 mM NaCl, 1 mM EDTA, 1 mM EGTA, 1% Triton X-100, 10% glycerol 0.1%SDS, 0.5% deoxycholate) or ARF buffer (50 mM HEPES [pH 7.5], 150 mM NaCl, 1 mM EDTA, 2.5 mM EGTA, 0.1% Tween-20) that contained a complete protease inhibitor mini-tablet (1 tablet/10 ml), PMSF (1 mM), beta-glycerophosphate (10 mM), sodium fluoride (1 mM), and sodium orthovanadate (1 mM). After lysates were sonicated, and centrifuged at 15,000 rpm for 30 sec or 2 min, supernatants were carefully collected. Protein concentration was determined using a BCA Assay. Protein was separated on SDS-PAGE, transferred to nitrocellulose membranes, and blotted with specific primary antibodies as listed in the Table S15. Images were captured using Odyssey Fc Imaging System (LI-COR).

ASC crosslinking assays

Primary BM and spleen cells (1 x 10^7 cells per mouse) were lysed with RIPA buffer following RBC lysis as described above. Cell lysates were sheared 30 times through a 21-guage needle in microcentrifuge tubes, then centrifugated for 8 min at 1,800 rpm. Supernatants were incubated on ice for 10 min, then split into two tubes; one for immunoblotting as described above and the

other for ASC speck cross-linking. For cross-linking, lysates were centrifugated for 10 min at 5,000 rpm and supernatants were removed. After pellets were washed twice with PBS, freshly made disuccimidyl suberate solution (dissolved in anhydrous DMSO, final concentration 2 mM) was added into each pellet followed by incubation at room temperature for 30 min on a rotator. Samples were centrifugated for 10 min at 5,000 rpm, supernatants were discarded, pellets were resuspended with 30 µl of 1x Laemmli buffer (2% SDS, 5% 2-mercaptoethanol, 10% glycerol, 0.002% bromophenol blue, 0.0625M Tris-HCl, pH 6.8) and subjected to SDS-PAGE as described above. Loading volumes were adjusted based on protein concentration of whole cell lysates.

Enzyme-linked immunosorbent assay

Serum was collected from mice at the specified times in each protocol. Following incubation of whole blood at room temperature for 30-40 min, clots were removed by centrifugating blood samples at 2,000 x *g* for 10 min in a refrigerated centrifuge. This step was repeated one more time to remove residual blood clots, then serum samples were stored at -80°C until used. ELISA was performed following the manufacturer's protocol (R&D System). Briefly, a 96-well microplate was coated with capture antibody (100 µL per well) overnight at room temperature. After plates were blocked with blocking buffer (300 µl per well) for 1 hr at room temperature, 100 µl of serum samples (diluted at 1:10 ratio with reagent diluent) or standard were added to the plate, which was then incubated for 2 hr at room temperature. After washing and addition of 100 µl of detection antibody to each well, plates were incubated for 2 hr at room temperature. Streptavidin-HRP, substrate solution and stop solution were added per protocol. Optical density was immediately measured using a microplate reader. Values measured at 450 nm were

subtracted from values measured at 540 nm.

RNA preparation and qRT-PCR assays

RNA from primary BM or spleen cells, tumor tissues of Eμ-*Myc* mice, or human MPN cells was isolated using NucleoSpin RNA II kit. cDNA was prepared using iScript^{TM} cDNA synthesis kit and qRT-PCR was performed using a CFX96 Touch Real-Time PCR Detection System (BioRad). Data were analyzed using the following equations: ΔCt = Ct(sample) - Ct(endogenous control); ΔΔCt = ΔCt(sample) - ΔCt(untreated or control); Fold Change = $2^{-\Delta\Delta Ct}$. *Ubiquitin* and *Actin* served as the endogenous controls. Primers are listed in the Table S16.

Lactate dehydrogenase activity

Serum lactate dehydrogenase (LDH) levels were quantified according to a protocol provided with the CyQUANT LDH Cytotoxicity Assay Kit. A 50 μl serum sample was aliquoted into 96-well microplate, then mixed with 50 μl of reaction mixture provided in the kit. Following incubation for 30 min at room temperature in the dark, 50 μl of stop solution was added into each well and mixed by gentle tapping. Absorbance was measured at 490 nm and 680 nm. LDH activity was calculated by subtracting the 680 nm absorbance value (background) from the 490 nm absorbance.

Flow cytometry analyses

Primary BM and spleen cells were harvested as above. Following RBC lysis using ACK buffer, cells were resuspended in PBS with 2% FBS. To characterize changes in individual hematopoietic

lineages, cells were stained with Zombie near IR (ZNIR, viability dye), mouse anti-CD16/32 (Fc block), -Ter119-V450, -B220-PE, -Ly-6G/Ly-6C-APC, -CD11b-BUV737, -CD3-BV786, and -F4/80-BUV395 fluorochrome-conjugated antibodies. To characterize the hematopoietic stem cells and progenitor populations, cells were stained with mouse Lin cocktail (BV421), anti-CD34-PE, -CD117-APC, -Ly-6A/Ly-6E-BB515, -CD150-PE-Dazzle 594, -CD48-Brilliant Violet 711, and -CD16/CD32-BUV395 conjugated antibodies. Cells were fixed with 4% paraformaldehyde for 10 min, washed with FACS buffer three times, and then subjected to flow cytometry.

In competitive transplant and xenograft experiments, cells were incubated with ZNIR and washed with PBS. After incubation with mouse FC blocking antibody for 10 min, cells were stained with anti-mouse CD45.1 and CD45.2 antibodies, fixed with 4% paraformaldehyde for 10 min, washed with FACS buffer three times, and subjected to flow cytometry as described[113]. To assess apoptosis, cells were treated with drugs as indicated, stained with Annexin-V and propidium iodide (PI), and then the percentage of AnnexinV/PI positive populations were quantified by flow cytometry as described[114].

Immunohistochemistry

Paraffin-embedded BM trephine biopsies were used for immunohistochemistry (IHC) analyses as described[34]. Blocks were sectioned to 4-μm in thickness. Unstained slides were deparaffinized using automated system with EZ Prep solution (Ventana Medical System) and stained with MYC or S100A9 antibody using a Ventana Discovery XT automated system (Ventana) per the manufacturer's protocols. Slides were reviewed by an independent hematopathologist. Protein expression levels were calculated as % (0~100%) of MYC or S100A9 positive cells multiplied by

staining intensity (1^{+}~3^{+}) as described[28].

Reticulin and trichrome staining

The reticulin and trichrome stains were based on the method of Gomori and Snook (Artisan Reticulin-Nuclear Fast Red Stain Kit) and the original Masson's procedure (Artisan Masson's Trichrome Stain Kit). Staining was performed by using Artisan Staining System following protocols provided by manufacturer.

Single cell library production and sequencing

Primary mouse BM cells, healthy donor BM MNCs, and MF patient BM MNCs were prepared following the protocol provided by 10x Genomics (CG000392, Rev A). For single cell encapsulation and library production, we used the Chromium Single Cell 3' Reagent Kits (v2) per user guideline (CG00052, Rev D). Sequencing was performed on a Nextseq 2000 platform (Illumina) aiming for a minimum of 50,000 reads/cell.

Single-cell RNA-seq data processing, filtering, batch effect correction, and clustering

A customized reference genome was built by adding MYC sequences to the GRCm38 mouse transcriptome using the *mkref* module of Cell Ranger (v6.0, 10X Genomics). Raw sequencing reads from single cells were aligned against the customized mouse reference and processed using *count* module of Cell Ranger. Gene-barcode matrices containing only barcodes with UMI counts passing threshold were imported to Seurat[115] for further analysis. Genes detected in less than 3 cells were excluded; cells with less than 200 genes detected or greater than 10% mitochondrial

UMIs were also filtered out. Doublets were detected using Scrublet[116], DoubletFinder[117], scDblFinder[118], and doubletCells implemented in scran[119], assuming 0.08% doublet rate for every 1,000 sequenced cells. Cells identified as doublets by at least two algorithms were removed from further analysis. Raw UMI counts were log normalized and the top 5,000 variable genes were identified using "vst" method implemented in the *FindVaribleFeatures* function in Seurat. T cell receptor and immunoglobulin genes were removed from the variable genes to prevent clustering based on V(D)J transcripts. S and G2/M cell cycle phase scores were assigned to cells using *CellCycleScoring* function.

To further remove batch effects, individual samples were then integrated using *FindIntegrationAnchors* and *IntegrateData* functions[120] with 8,000 anchor genes and 40 dimensions of canonical correlation analysis (CCA). Briefly, dimension reduction was performed on each sample using diagonalized CCA, and L2-normalization was applied to the canonical correlation vectors to project all samples into a shared space. The mutual nearest neighbors (MNS) across cells from different datasets were used as "anchors" to encode the cellular relationship between samples. Samples were integrated based on correction vectors for sample calculated form anchors.

Integrated data were further scaled using *ScaleData* function by regressing against total read count, percentages of mitochondrial UMIs, and cell cycle phase scores (S and G2/M). A shared nearest neighbor (SNN) based graph was constructed using the top 40 principal components, and clusters were identified using the Louvain algorithm using *FindCluster* function at resolution = 1 (33 clusters). Uniform Manifold Approximation and Projection (UMAP) were generated by *RunUMAP* function and used for visualization.

Mouse bone marrow cluster annotation

Differential expression analysis comparing each cluster *vs.* all others was performed using *FindAllMarkers* function in Seurat with default settings. Genes with log2(fold-change) >0.25 and Bonferroni-corrected p-value <0.05 were considered differentially expressed. Clusters were annotated by comparing the cluster-specific genes to canonical markers for Hematopoietic Stem cells (HSCs) (*Myct1, Angpt1, Rgs1, Pde4b, Ncl*), Erythroblasts (*Car2, Gypa, Prdx2, Alas2, Slc4a*1), Monoblasts (*F13a1, Tmsb10, Ly86, Lgals1, Ccr2*), Monocytes (*Pld4, S100a4, Itgb7, Ahnak, Pid*1), Myeloblasts (*Elane, Mpo, Ms4a3, Ctsg, Prtn3*), Myelocytes (*Anxa1, Ltf, Lcn2, Fcnb, Camp*), Megakaryocytes (*Timp3, Rab27b, Pls1, P2rx1*), Basophils (*Ccl3, Fcer1a, Ms4a2, Hdc, Cyp4f18*), Macrophages (*Cd300e, Batf3, C1qb, Cd68*), M1 macrophages (*Cxcl9, Cxcl10, Cxcl11, Il1a, Tnf, Il6, Ccl5, Ccl2, Ccl4, Cxcl1, Ccl7, Il27, Il10, Cxcl3, Tnfsf15, Ccl3, Il11*), M2 macrophages (*Ccl24, Ccl8, Ccl12, Ccl9, Cxcl12, Ccl6*), Neutrophils (*S100a9, S1000a8, Mmp9, Il1rn, Cxcr2*), Granulocyte-monocyte progenitors (GMPs) (*Mpo, Cstg, Prtn3, H2afy*), Megakaryocyte-erythroid progenitors (MEPs) (*Pf4, Gata2, Cdk6, Gas5*), Common Myeloid progenitors (CMPs) (*Cd34, Npm1, Eef1g, H2afy*), T cells (*Cd3e, Cd3d, Cd4, Cd8a*), NK cells (*Klrd1, Ncr1, Klra4*), Pro-B cells (*Vpreb3, Akap12, Cd79b, Chchd10, Cecr2*), Pre-B cells (*H2-Ab1, Shisa5, March1, Cd74, H2-DMb2*), Plasma cells (*Igkc, Ighm, Jchain*), Endothelial cells (*Kdr, Lrg1, Cldn5, Fam167b, Osmr*), pDC (*Siglech, Ccr9, Bst2, Pacsin1, Tcf4*), and Adipose cells (*Cxcl12, Igfpb5, Bgn, Igfbp4*). To confirm cell annotation, enrichment scores were calculated using *AUCell* algorithm implemented in SCENIC[121] for signature genes reported in previous single-cell RNA-seq studies on BM, AML, and hematopoietic cells[122-125]. Human signatures were converted to their mouse homologs using R package biomaRt

before sending for enrichment analysis. Expression of marker genes was visualized on UMAP or by violin plot using log normalized UMI counts. Heatmaps were used to visualize the z-score normalized average expression across clusters. The 33 clusters were further grouped into 23 major cell types based on their annotation. Differential gene expression analysis was performed to generate cell type specific marker genes.

Human bone marrow cluster annotation

Human bone marrow (BM) scRNA-seq data were analyzed as described above. A shared nearest neighbor (SNN) based graph was constructed using the top 40 principal components, and clusters were identified using the Louvain algorithm using *FindCluster* function at resolution = 1 (34 clusters). Clusters were annotated by comparing the cluster-specific genes to canonical markers for Hematopoietic Stem cells (HSCs) (*SPINK2, CRHBP, MEIS1, MLLT3*), Erythroblasts (*BROX2, AHSP, HBB, ALAS2*), Basophils (*GATA2, LTC4S, CLC, IL3RA*), Macrophages (*CD68, CD163, CD300E*), Neutrophils (*CXCL8, S1000A8, S1000A9, CSF3R, CXCR2*), Megakaryocytes (*PPBP, PF4, GP9, SDPR*), Common myeloid progenitors (CMPs) (*MPO, FLT3, CEBPA, ELANE*), multi-lymphoid progenitors (*DNTT*, *CXCR4*, *BLNK*, *IGLL1*, *EBF1*), T cells (*CD3E, CD3D, CD4, CD8A*), Naïve T cells (*TCF7*, *IL7R*, *TCF7*, *CCR7*), Naïve-memory T cells (*CCL5*, *IFITM1*, *LTB*, KLF2), Effector-memory T cells (*GZMK*, *EOMES*, *KLRG1*, *CD27*), Effector T cells (*CCL3*, CCL4, *GZMB*, *GZMA*, PRF1), $CD16^+$ NK cells (*FCGR3A, KLRB1, KLRD1*), $CD56^+$ NK cells (*NCAM1*, *KLRB1*, *KLRD1)*, Pro-B cells (*CD79A*, *SOX4, IL7R, RAG2, LEF1*), Mature-B cells (*CD79A*, *MS4A1, TNFRSF13C, ITGAM*), Plasma cells (*IGHA1, IGHG1, IGHG2, IGHG4*), pDC (*LILRA4, IRF7, IL3RA, TCF4, PACSIN1*), and cDC2 (*CD1C, FCER1A, CLEC10A,*

HLA-DQA1). Cell annotation was further confirmed by AUCell scores of signature genes reported in previous scRNA-seq studies on human BM cells[122-126].

InferCNV analysis

Copy number variation patterns in human BM single cells were extracted using InferCNV v3.1.5. (https://github.com/broadinstitute/inferCNV, Trinity CTAT Project). 3000 cells from the three HD samples were randomly selected and served as reference normal cells for de-noise control. Cells from the TN-MF patient were selected as observations. InferCNV analysis was performed using "denoise" mode to correct for batch effects from different patients. Clusters of cells with copy number gain observed on chr8 were determined as trisomy 8+ cells in the TN-MF patient. The trisomy status was further confirmed by expression of chr8 genes. Briefly, 571 genes located on chromosome 8 were identified from Gencode annotation. Overall expression of these genes was calculated by *AddModuleScore* function in Seurat and visualized by histogram.

Differential gene expression comparing MYC *vs.* WT mouse bone marrow cells

Composition (%) of the 23 cell types was calculated and compared between MYC *vs.* WT samples and was visualized using ggplot2 stacked bar plot. The composition difference of each cell type between MYC *vs.* WT was calculated as log2(% in MYC/% in WT) and visualized as a bar plot. Differential expression analysis was performed to compare MYC *vs.* WT cells in each cell type using *FindMarkers* function of Seurat with default settings. Genes with log2(fold-change) >0.25 and Bonferroni-corrected p-value <0.05 were considered differentially expressed. The MYC differential genes were compared among clusters within HSCs and Progenitors, Myeloblasts and

Myelocytes, Monoblasts and Monocytes, Neutrophils, T and NK cells, and B and Plasma cells, and visualized by Venn Diagram.

Semantic analyses

First, differential gene expression analysis was performed with Seurat (v 4.0.2)[120] between MYC and NULL phenotypes for all 23 major types. Genes with adjusted p value < 0.05 were considered for GO.bp enrichment analysis using clusterProfiler (v4.4.4)[127]. The obtained GO.bp terms from up-reg (fold change > 1) and down-reg genes (fold change < 1) were summarized via the REVIGO web application (http://revigo.irb.hr/)[128] using p value of GO term as input metric allowing a similarity of 0.7.

Cell-cell interaction (ligand-receptor) analyses

To identify and visualize cell-cell (ligand-receptor) interactions in MYC and WT cells, we loaded the scRNA-seq normalized gene expression data with cell type information into the R package CellChat [129]. We also built mouse reference for cell-cell interactions with the data from OmniPath database (https://omnipathdb.org/)[130] using R packages liana[131] and OmniPathR[132]. A total of 5,964 mouse ligand-receptor interactions were used as a priori network information. The standard CellChat pre-processing steps were applied to identify overexpressed ligand-receptor interactions (identifyOverExpressedInteractions), compute the communication probability/strength between any interacting cell groups (computeCommunProb) and the communication probability/strength on the signaling pathway level, by summarizing all of the related ligands/receptors (computeCommunProbPathway); this resulted in 800 and 814

significant interactions for the MYC and WT groups, respectively. The selected interactions are visualized in a circular plot and the thicker edge line indicates a stronger signal based on the number of interactions. To visualize the difference in intensity of cell-cell interactions between the MYC and WT groups, we calculated both ligand and receptor expression means for the selected interaction in each pair of cell type, subtracted WT from MYC, and then visualized the difference of interaction intensity using the significant interactions ($p<0.05$).

Pathway activity inference

A panel of 16 pathways was constructed with the 14 signaling pathways derived by PROGENy[133] (Androgen, Estrogen, EGFR, Hypoxia, JAK-STAT, MAPK, NF-κB, PI3K, p53, TGF-β, TNF-α, Trail, VEGF, and WNT), known MYC target genes[134], and the Alarmin pathway[135,136]. From the differential expression analysis comparing MYC *vs*. WT in each cell type, genes were ranked based on -log10(p-value)*(sign of log2(fold-change)), with the most up-regulated genes ranked at the top and the most down-regulated genes ranked at the bottom of the list. Pre-ranked Gene Set Enrichment Analysis (GSEA) was performed on these ranked gene lists against the 16 pathways using R package fgsea[137] with 10,000 permutations. The normalized enrichment scores (NES) were used to denote the activity of each pathway and visualized by hierarchically clustered heatmap using R package ComplexHeatmap[138], where positive NES presented up-regulated activity while negative NES presented down-regulated activity in MYC compared to WT.

Synthesis of Tasquinimod

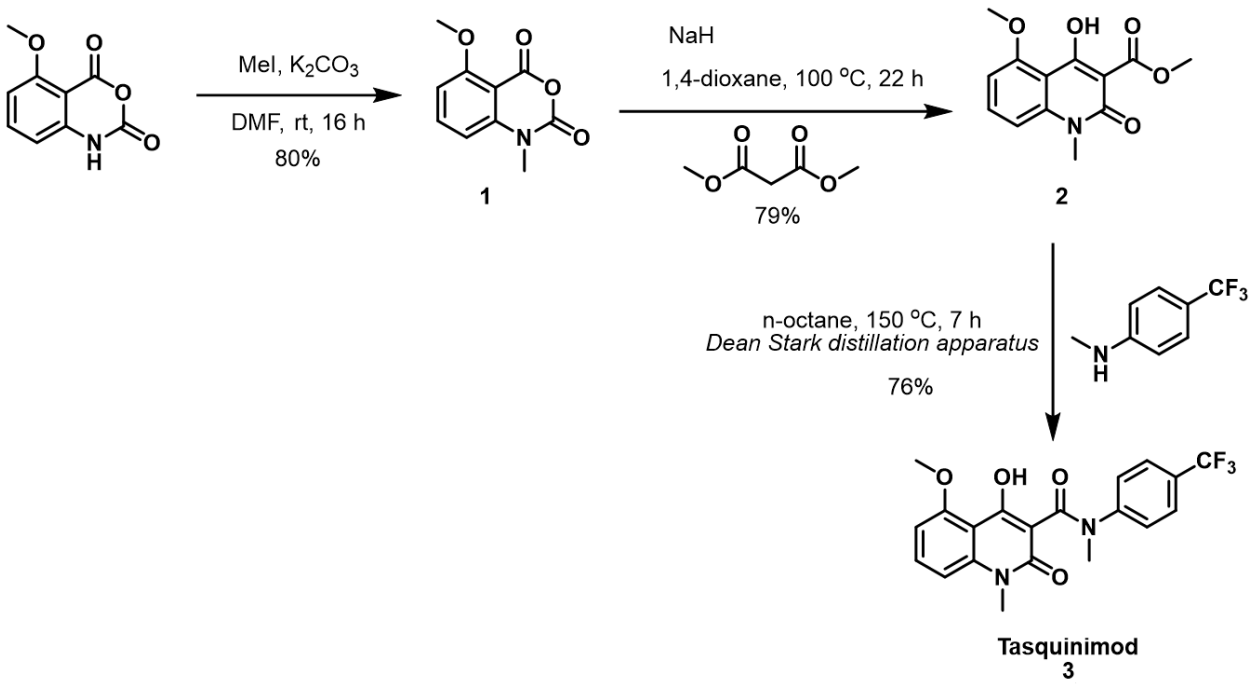

Synthesis of 5-Methoxy-1-methyl-2H-benzo[d][1,3]oxazine-2,4(1H)-dione (compound **1**): A dry 100 mL round-bottom flask with a stirring bar under inert (argon) atmosphere, was charged with 5-methoxy-2H-benzo[d][1,3]oxazine-2,4(1H)-dione (3.00 g, 15.53 mmol, 1 equiv) and DMF (32 mL). K_2CO_3 (2.73 g, 19.7 mmol, 1.27 equiv) and MeI (1.04 mL, 16.8 mmol, 1.08 equiv) were added to the resulting solution and the mixture was stirred at room temperature for 16 hr. After this period, HCl (1 M, 66 mL) was added slowly and carefully. After complete addition of HCL, the mixture was stirred for 30 min and the solid obtained was filtered. The solid was washed with water (3 x 20 mL) and dried under vacuum to afford intermediate dione 1 (2.57 g, 12.4 mmol, 80% yield) as a white solid. ^{1}H NMR (500 MHz, DMSO) δ 7.76 (t, *J* = 8.5 Hz, 1H), 6.95 (t, *J* = 8.6 Hz, 2H), 3.91 (s, 3H), 3.42 (s, 3H).^{13}C NMR (126 MHz, DMSO) δ 161.4, 154.7, 148.1, 144.0, 137.8, 106.6, 106.4, 100.5, 56.4, 32.2. HPLC–MS (ESI+): *m/z* 208.1 $(M+H)^+$. *m/z* calculated for $C_{10}H_{10}NO_4^+$ $(M+H)^+$ 208.06.

Methyl-4-hydroxy-5-methoxy-1-methyl-2-oxo-1,2-dihydroquinoline-3-carboxylate (compound **2**): A dry 100 mL round-bottomed flask, equipped with a stirring bar and a condenser, under inert (argon) atmosphere, was charged with 1 (2.00 g, 9.65 mmol, 1 equiv) and 1,4-dioxane (13 mL), followed by NaH (60% dispension in mineral oil, 425 mg, 10.6 mmol, 1.1 equiv). Dimethyl malonate (1.21 mL, 10.6 mmol, 1.1 equiv) was added dropwise and the resulting mixture was stirred at 100 ^{o}C for 22 hr. After this period, the reaction mixture was cooled to room temperature and quenched with water (61 mL). The aqueous solution was acidified with 1 M aq HCl to pH 3 and left in the refrigerator for 4-16 hr to precipitate the product. The solid obtained was collected by filtration, washed with water (3x 20 mL) and dried under vacuum to afford intermediate 2 (2.02 g, 7.67 mmol, 79% yield) as a pale yellow solid. ^{1}H NMR (500 MHz, $CDCl_3$) δ 7.57 (t, *J* = 8.5 Hz, 1H), 6.95 (d, *J* = 8.7 Hz, 1H), 6.74 (d, *J* = 7.6 Hz, 1H), 4.01 (s, 4H), 4.00 (s, 3H), 3.64 (s, 3H). ^{13}C NMR (126 MHz, $CDCl_3$) δ 171.8, 170.9, 159.9, 159.8, 143.2, 134.4, 107.4, 105.2, 104.3, 99.1, 56.6, 52.9, 30.1. HPLC–MS (ESI+): *m/z* 264.1 $(M+H)^+$. *m/z* calculated for $C_{13}H_{14}NO_5^+$ $(M+H)^+$ 264.09.

4-Hydroxy-5-methoxy-N,1-dimethyl-2-oxo-N-(4-(trifluoromethyl)phenyl)-1,2-dihydroquinoline-3-carboxamide (Tasquinimod, Compound **3**): A dry 100 mL round bottom flask equipped with a stirring bar, a Dean Stark distillation apparatus, and a condenser, under inert (argon) atmosphere, was charged with intermediate 2 (1.50 g, 5.70 mmol, 1 equiv), *N*-methyl-4-(trifluoromethyl) aniline (1.58 mL, 11.4 mmol, 2 equiv), and *n*-octane (40 mL). The reaction mixture was heated to 150^{o}C (oil bath temperature) to reflux, and the mixture was stirred at this temperature for 7 hr, approximately 20 mL of volatiles were collected in the Dean Stark apparatus. The reaction mixture was cooled down to room temperature and the solvent was

removed under vacuum. The crude product was purified by column chromatography (SiO_2, 50-100% EtOAc in hexanes) to afford the final compound **3** (Tasquinimod) (1.77 g, 4.36 mmol, 76% yield) as an off-white solid.

Characterization of Tasquinimod

^{1}H NMR of Tasquinimod

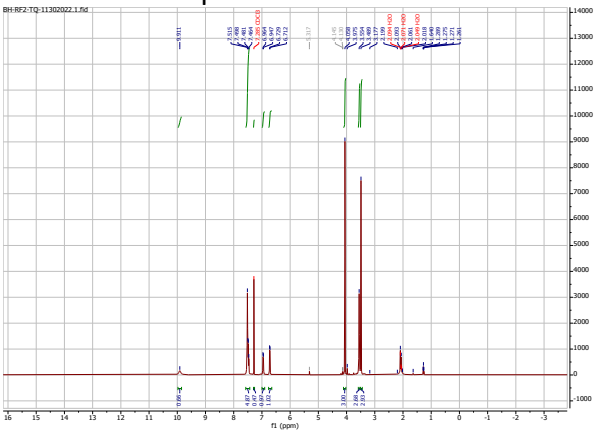

^{13}C NMR of Tasquinimod

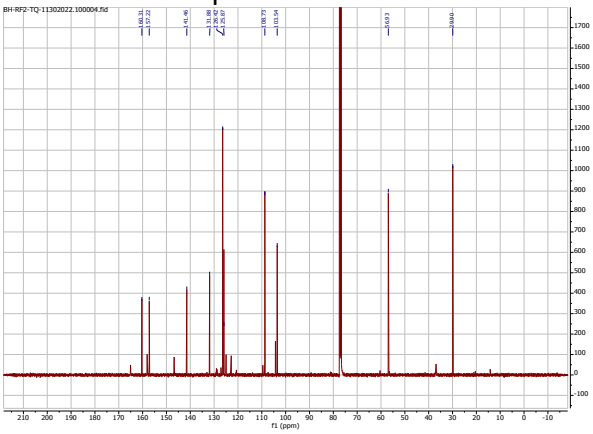

^{19}F NMR of Tasquinimod

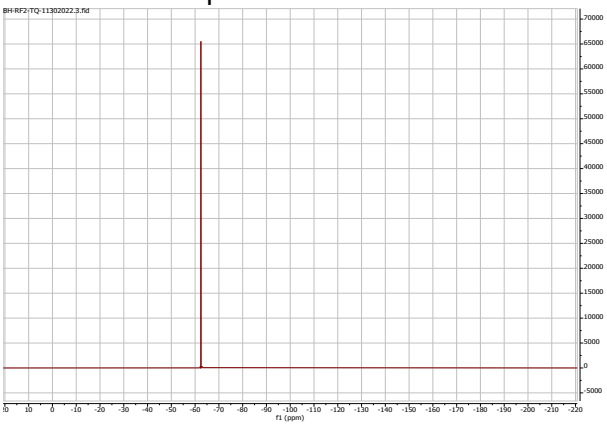

HPLC of Tasquinimod

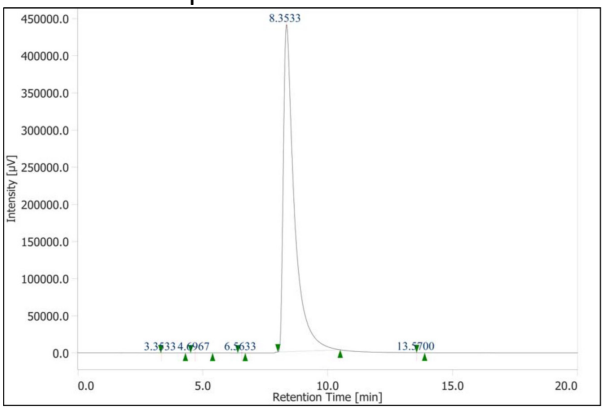

HPLC 99% (t_R = 8.35 min, 5-95% CH_3OH in water (0.1% TFA), 1mL/min, 20 min); 99% (t_R = 4.92 min, 40% CH_3OH in water (0.1% TFA), 1mL/min, 20 min). ^{1}H NMR (500 MHz, $CDCl_3$) δ 9.91 (s, 1H), 7.53 – 7.46 (m, 5H), 6.94 (d, *J* = 8.5 Hz, 1H), 6.70 (d, *J* = 8.2 Hz, 1H), 4.04 (s, 3H), 3.55 (s, 3H), 3.49 (s, 3H). ^{19}F NMR (471 MHz, $CDCl_3$) δ -62.42. ^{13}C NMR (126 MHz, $CDCl_3$) δ 165.1, 160.3, 158.1,

157.2, 146.8, 141.5, 131.9, 128.9 (q, $^{2}J_{CF}$ = 31.5Hz), 126.4, 125.9 (q, $^{3}J_{CF}$ = 3.8 Hz), 123.9 (q, $^{1}J_{CF}$ = 272.1 Hz), 109.6, 108.7, 104.3, 103.5, 56.9, 36.9, 29.9. HPLC–MS (ESI+): *m/z* 407.1 $(M+H)^{+}$. TOF-LCMS *m/z* calculated for $C_{20}H_{18}F_3N_2O_4^{+}$ $(M+H)^{+}$ 407.1214, found 407.1222.

Treatment of mice with Tasquinimod

Mx1-Cre$^{+/-}$;Rosa26$^{LSL\text{-}MYC/LSL\text{-}MYC}$ mice were treated with pIpC, and mice were then randomized to Tasquinimod *vs.* vehicle treatment. Tasquinimod treatment was initiated 5 days after the first dose of pIpC and Tasquinimod (30mg/kg/day) was administered via drinking water. Tasquinimod was dissolved in DMSO (final concentration 5%), then mixed with sucrose (final concentration 3%) and PEG300 (final concentration 2%) containing water. Vehicle group mice were treated with water containing DMSO (5%), sucrose (3%), and PEG300 (2%). Drinking water bottles were replaced every 3 days. Treatment was continued until endpoints.

Synthesis of MYCi975

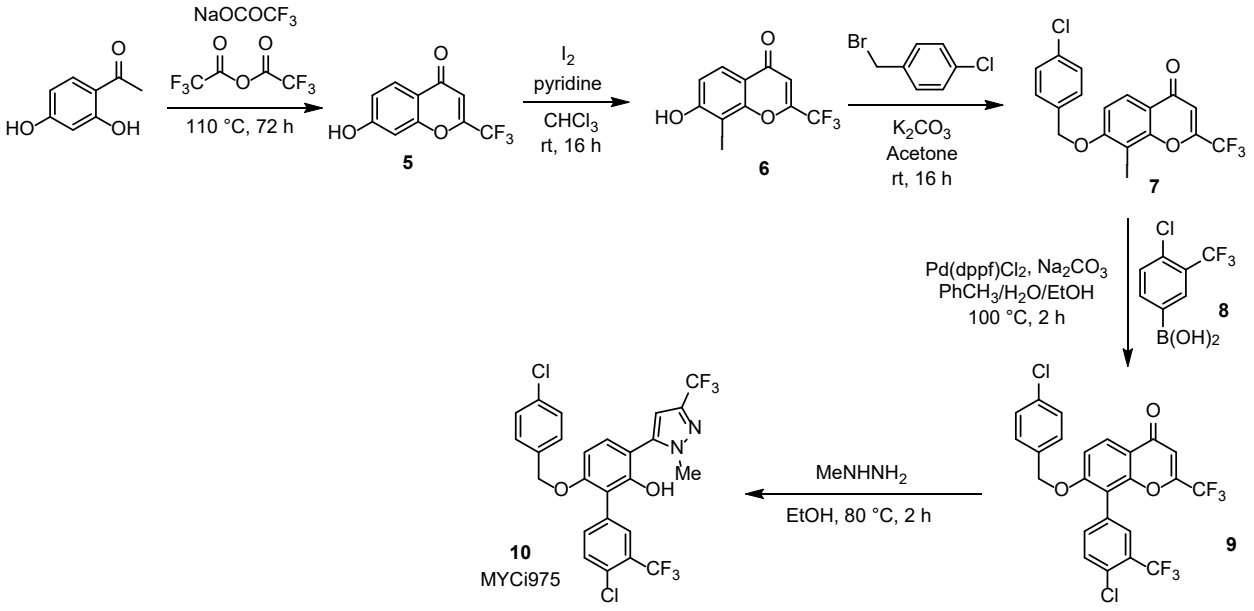

MYCi975 was prepared according to the reported procedure with minor modifications[69].

Synthesis of compound **5**: To an oven-dry Schlenk flask (250 mL) was charged with (2,4-dihydroxyphenyl)ethan-1-one (5.00 g, 32.9 mmol, 1 equiv), sodium trifluoroacetate (9.84 g, 72,4 mmol, 2.2 equiv), and trifluoroacetic anhydride (18.5 mL, 131.6 mmol, 4 equiv). The flask was then tightly sealed with a polytetrafluoroethylene (Teflon) screw, and the reaction mixture was stirred at 110°C for 72 hr. The resulting mixture was allowed to cool down to approximately 70°C, and 200 mL of EtOAc was added in three batches to dilute the crude material. The solution was then transferred into a 1000 mL Erlenmeyer flask and neutralized with saturated aqueous K_2CO_3 solution until pH reached approximately 7. The organic layer was separated, and the water layer was washed with EtOAc (150 mL × 3). The combined organic layers were dried over anhydrous Na_2SO_4, filtered, and concentrated *in vacuo* to approximately 200 mL. The flask was kept open at room temperature for 2–3 days until no more solid was precipitated. Compound **5** (3.55g, 47%) was obtained by vacuum filtration.

Synthesis of compound **6**: To a suspension of 5 (4.00 g, 17.4 mmol, 1 equiv) in $CHCl_3$ (110 mL) was added molecular iodine (17.6 g, 69.5 mmol, 4 equiv) and pyridine (5.62 mL, 69.5 mmol, 4 equiv). The mixture was allowed to stir at room temperature for 16 hr, and the reaction was quenched by saturated $Na_2S_2O_3$ solution (120 mL). The organic layer was separated, and the aqueous layer was extracted with CH_2Cl_2 (80 mL × 3). The combined organic layers were washed with brine, dried over anhydrous Na_2SO_4, and concentrated *in vacuo* to give compound **6** (5.33 g, 86%).

Synthesis of compound **7**: To a suspension of 6 (2.00 g, 5.60 mmol) in acetone (20 mL) was added 4-chlorobenzyl bromide (1.50 g, 7.28 mmol, 1.3 equiv) and K_2CO_3 (1.55 g, 11.2 mmol, 2

equiv). The mixture was allowed to stir at room temperature for 16 hr. Upon completion, the mixture was filtered, and the filtrate was collected and concentrated *in vacuo* to give the dark-brown solids. The solids were then suspended in 75 mL of water, and crude material of 7 was obtained after vacuum filtration. No further purification was required.

Synthesis of compound **9**: To a round-bottom flask (50 mL) was added 7 (1.50 g, 3.12 mmol, 1 equiv), boronic acid 8 (770 mg, 3.43 mmol, 1.1 equiv), sodium carbonate (661 mg, 6.24 mmol, 2 equiv), and Pd(dppf)Cl_2 (228 mg, 0.312 mmol, 10 mol %). Toluene (10 mL), water (4 mL), and ethanol (2 mL) were then introduced into the flask, and the mixture was bubbled with nitrogen gas for 10 minutes. The reaction was allowed to stir at 100 ^oC for 2 hr. Upon completion, the solution was diluted by 75 mL of EtOAc and washed with 50 mL of saturated NH_4Cl solution. Crude material was obtained after drying over anhydrous Na_2SO_4, filtration, and concentration *in vacuo*. After SiO_2 chromatography (Hexanes : EtOAc = 4 : 1) pure product 9 was obtained (1.12 g, 67%).

Synthesis of compound **10** (MYCi975): To a suspension of 9 (1.50 g, 2.81 mmol, 1 equiv) in ethanol (11 mL) was introduced methylhydrazine (444 µL, 8.43 mmol, 3 equiv). The mixture was allowed to reflux (80^oC) for 2 hr. Crude material was obtained by concentration *in vacuo*, and after SiO_2 chromatography (Hexanes : EtOAc = 20 : 1 to 2 : 1) pure compound **10** was obtained (631 mg, 40%).

Characterization of MYCi975

HPLC 93.3% (t_R = 8.10 min), 85% CH_3OH in water (0.1% TFA), 1mL/min, 20 min); ^{1}H NMR (500 MHz, $CDCl_3$) 7.79 (d, *J* = 2.0 Hz, 1H), 7.63 (d, *J* = 8.0 Hz, 1H), 7.53 (dd, *J* = 8.0, 2.0 Hz, 1H), 7.31 – 7.30 (m, 2H), 7.21 (d, *J* = 8.5 Hz, 1H), 7.16 – 7.14 (m, 2H), 6.72 (d, *J* = 8.5 Hz, 1H), 6.57 (s, 1H), 5.09

(s, 1H), 5.05 (s, 2H), 3.81 (s, 3H); ^{19}F NMR (471 MHz, $CDCl_3$) -62.02 (s, 3F), -62.60 (s, 3F); HPLC–MS (ESI+) *m/z* 559.8 and 558.7 $(M-H)^+$.

^{1}H NMR of MYCi975

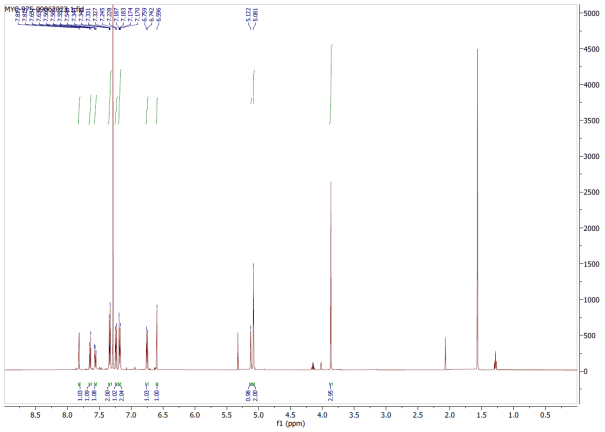

^{19}F NMR of MYCi975

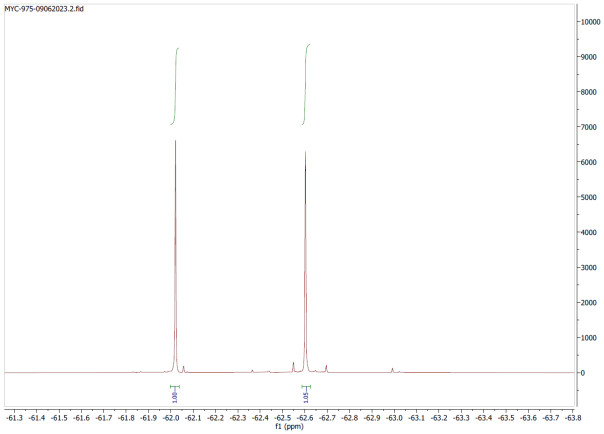

HPLC of MYCi975

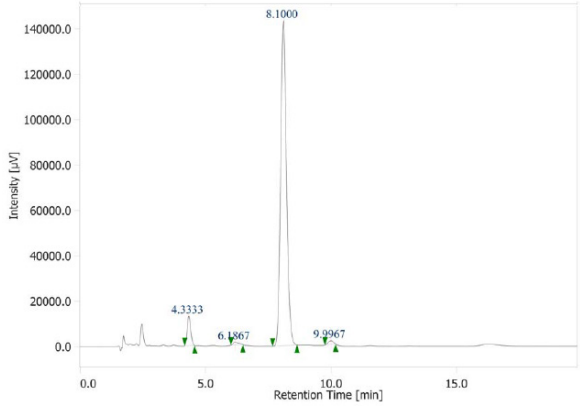

HPLC-MS of MYCi975

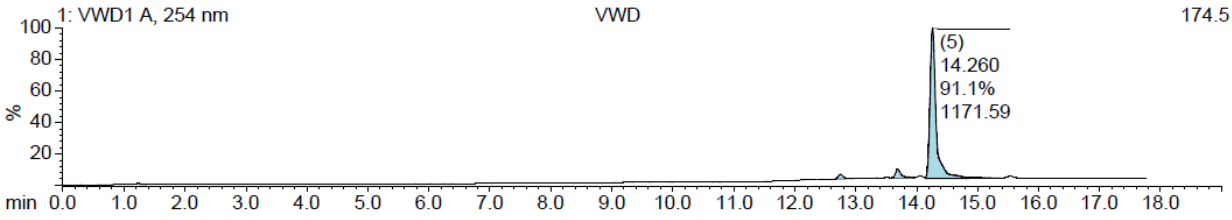

Treatment of mice with MYCi975

CD45.2^{+} BM cells were harvested from Mx1-Cre$^{+/-}$;Rosa26$^{LSL\text{-}MYC/LSL\text{-}MYC}$ mice that was treated with pIpC 20 weeks prior. After RBC lysis, a total of 1 x 10^6 cells were transplanted via tail vein into lethally irradiated CD45.1^{+} WT C57BL/6 recipient mice. Peripheral blood was collected at 4 weeks post-transplant, mononuclear cells were isolated following RBC lysis, and successful engraftment was confirmed by flow cytometry after staining cells with ZNIR viability dye, and anti-Ter-119, -CD45.1, and -CD45.2 antibodies. Mice were randomized to MYCi975 (100mg/kg/day, d1-5, 3 weeks on, 3 weeks off) *vs.* vehicle treatment. MYCi975 was initiated at 5 weeks post-transplant and drug was delivered via oral gavage. MYCi975 was dissolved in DMSO (final concentration 5%), mixed with corn oil, then vortexed multiple times until completely dissolved. Vehicle group was treated with corn oil. Treatment was continued until endpoints.

Patient-derived xenograft studies

Primary BM cells from a TN-MF patient were collected under the TCC protocol. Somatic mutation in *JAK2, MPL,* or *CALR* gene was assessed by NGS. Trisomy 8 was assessed by both conventional karyotyping and FISH analyses. After isolating BM MNCs following SepMate^{TM} PBMC isolation protocol, cells were frozen in DMEM media supplemented with 20% FBS and 20% DMSO until used. After thawing BM MNCs were cultured in serum free SFEM II media (STEMCELL Technologies) supplemented with Pen-Strep (50 U/ml), human SCF (100 ng/ml), human TPO (100 ng/ml), and human FLT3L (100 ng/ml) for 16 hours. A total 1.6 x 10^5 cells (in 30-µl of PBS) were transplanted via intra-tibial injection into sublethally irradiated (200 cGy) NSG-SGM3 mice. Engraftment of MF cells were confirmed by measuring human CD45^{+} cells in peripheral blood by

flow cytometry at 9 weeks post-transplant. Mice were then randomized to vehicle, MYCi975 (100mg/kg, po, once a day, d1-5, 3 weeks on, 2 weeks off), or ruxolitinib (180mg/kg, po, once a day, d1-5, 3 weeks on, 2 weeks off) treatment.

Statistical analysis

Under the assumption of independent variables, normal distribution, and equal variance of samples, statistical significance was assessed using unpaired two-tailed Student's *t*-test for in vitro and ex vivo experiments. Error bars presented in the figures indicate the mean ± SEM. The statistical parameters are described in the individual figure legends. For survival analyses, LFS and OS were estimated using the Kaplan-Meier method and compared using a log-rank test. Statistical analyses were performed using SPSS v24.0 and GraphPad Prism 7. A *p*-value less than 0.05 was considered statistically significant.

Data Sharing Statement

scRNA-Seq data from mouse and human BM cells have been deposited in the GEO under accession files GSE240963 and GSE242730, respectively.

AUTHORS' DISCLOSURE

D.J.M. has received funding from Merck Pharmaceuticals and PUMA Biotech for work unrelated to this project. A.T.K. received research funding from Bristol Myers Squibb, Novartis, Morphosys, GlaxoSmithKline, Janssesn. A.T.K. received honoraria from Abbvie, GlaxoSmithKline, MorphoSys, Incyte, Bristol Myers Squibb, CTI Biopharma, Kartos, and Karyopharm.

AUTHOR CONTRIBUTIONS

Study conception and design: N.D.V., J.L.C., and S.Y.; performed experiments, collected, and assembled the data: N.D.V., X.Y., A.T.K., J.M., C-H.C., R.S., H.V.N., A.A.N., P.C.P., D.H.L., T.N.R., Q.M., R.S.K., and S.Y.; analyzed and interpreted the data: N.D.V., X.Y., C-H.C., O.C., Q.M., L.Z., D.J.M., S.H.K., J.L.C., and S.Y.; writing and/or revision of the manuscript: N.D.V., X.Y., H.L., D.L., S.H.K., J.L.C., and S.Y.; review of manuscript: all authors reviewed the manuscript; administrative, technical or material support: N.D.V., X.Y., S.S., H.V.N., E.E., S.N., R.B.F., H.L., S.C., D.J.M., D.L., S.H.K., J.L.C., and S.Y.; study supervision: N.D.V. and S.Y.

ACKNOWLEDGEMENTS

The authors thank Jodi Kroeger, Dr. Neel Chaudhary, and the Moffitt Flow Cytometry Core; Sean Yoder, Dr. Chaomei Zhang, Dr. Lan Zhang, Tania Mesa, and the Moffitt Genomics Core for their help with scRNA-seq analyses; Dr. Eric Padron for providing Scl-CreERT mice; Dr. Peter Papenhausen and Dr. Liu Kenian for their assistance with conventional karyotyping and FISH studies; Jodi Balasi, Noel Clark, and the Moffitt Histology Core for their assistance with immunohistochemistry staining; Yamila Caraballo Perez, Janis De La Iglesia, and the Moffitt Clinical Pathology Lab for their help with reticulin, trichrome, and immunohistochemistry staining.

This work was supported in part by Deutsche Krebsilfe grant 109220 (D.J.M.), the program grant 1016701 from the Australian National Health and Medical Research Council (NHMRC) (S.C.), the Cortner-Couch Endowed Chair for Cancer Research from the University of South Florida

School of Medicine (J.L.C.), NIH grant K08 CA237627 (S.Y.), an American Society of Hematology (ASH) Research Training Award for Fellows (RTAF) (S.Y.), an ASH Scholar Award for Fellow (S.Y.), an ASH Scholar Award for Fellow to Faculty (N.V.D.), a Career Development Award from the American Society of Clinical Oncology (ASCO) (S.Y.), a Miles for Moffitt grant from the H. Moffitt Cancer Center & Research Institute (S.Y. and Q.M.), a research grant from the Graduate Medical Education (GME) at the University of South Florida (S.Y. and P.C.P.), a research grant from the Clinical Science Division at the H. Lee Moffitt Cancer Center & Research Institute (S.Y.), and NCI Comprehensive Cancer Grant P30-CA076292 to the H. Lee Moffitt Cancer Center & Research Institute.

NOTE

Supplemental data for this article are available at Blood Cancer Discovery Online.

FIGURE LEGENDS

Figure 1. Trisomy 8 is associated with elevated MYC expression in BM HSCs of TN-MF patients. A, The proportion of primary, post-PV, and post-ET MF in Moffitt MF dataset (n=584). **B,** The frequency of *JAK2/MPL/CALR* somatic mutations in the Moffitt MF cohort. Demographic and laboratory profiles are described in Table S1. **C,** Bar plot shows percentages of recurrently mutated genes; solid blue, driver mutations; and stripes, mutations included in the major diagnostic criteria for MF based on the WHO classification. **D,** The percentages of trisomy 8 in each molecular subtype of MF. **E-F,** Kaplan-Meier (KM) curves showing the LFS and OS based on presence of trisomy 8 in MF. G-H, UMAP plots of hematopoietic single cells in BM of normal HD (n=3) *vs.* trisomy 8+ TN-MF (n=1). Demographic and laboratory profiles are described in Table S2. **I-J,** Comparison of BM major cell types (I) and AddModule Score (J) of HD *vs.* trisomy 8+ TN-MF. AddModule Score was calculated based on a total of 571 coding genes located on chr8 and that were detected in scRNA-seq analysis. **K,** Volcano plot showing a total of 1,260 genes that are differentially regulated (q<0.05) in HSCs of trisomy 8+ TN-MF *vs.* HD. **L,** Venn diagram of coding genes on chr8 (n=674) and genes with differential changes in HSCs. **M,** Ranked list of log2-fold change of 131 chr8 genes differentially regulated in HSCs of trisomy 8+ TN-MF. **N,** Ridgeline plots comparing *MYC* mRNA levels in BM cells for each major cell types of trisomy 8+ TN-MF (red) *vs.* HD (blue). **O,** MYC IHC staining of BM core biopsy samples from TN-MF patients. **P,** Percentages of MYC positive cells in trisomy 8 negative (n=17) *vs.* positive (n=6) TN-MF. Demographic and laboratory profiles of TN-MF patients included in MYC IHC analysis are shown in Table S4.

Figure 2. MYC overexpression in HSCs provokes MF. **A,** Schematic of mouse *in vivo* studies. **B-C,** MYC mRNA (B) and protein (C) levels in BM and spleen cells of Mx1-Cre$^{+/-}$;Rosa26$^{+/+}$, Mx1-Cre$^{+/-}$;Rosa26$^{LSL\text{-}MYC/+}$, and Mx1-Cre$^{+/-}$;Rosa26$^{LSL\text{-}MYC/LSL\text{-}MYC}$ mice, respectively, at 20 weeks post-pIpC treatment. **D-E,** Comparison of MYC protein levels in Mx1-Cre$^{+/-}$;Rosa26$^{LSL\text{-}MYC/LSL\text{-}MYC}$ BM cells *vs.* Eμ-*Myc* lymphoma cells (D) or VavP-MYC10 mice BM cells (E) at age 8 weeks. **F-H,** Peripheral blood (PB) CBC analyses. Baseline CBC was performed 1 week prior to pIpC injection. **I,** LDH activity in serum samples from each experimental group. **J,** Comparison of body weight changes of experimental groups. Baseline body weights were determined 1 week prior to pIpC treatment. **K-L,** Spleen weight at endpoints. Mx1-Cre$^{+/-}$;Rosa26$^{+/+}$ mice were sacrificed as control when Mx1-Cre$^{+/-}$;Rosa26$^{LSL\text{-}MYC/+}$ and Mx1-Cre$^{+/-}$;Rosa26$^{LSL\text{-}MYC/LSL\text{-}MYC}$ mice were at their endpoints. Endpoints criteria is described in "Animal studies" section. **M,** KM curves of OS, calculated from the date of pIpC treatment. **N,** H&E, reticulin, and trichrome stained images of BM (left 3 columns) and spleen (right 3 columns) at week 20 post-pIpC. Demographic and laboratory profiles are shown in Table S5. Box plots in (F-I, L) represent data from 38-54 mice in each group. Error bars in (B) indicate mean ±SEM of at least 6 independent mice. *, P<0.05 compared with control group.

Figure 3. Forced MYC expression provokes expansion of HSCs and myeloid progenitors with limited self-renewal capacity. **A-C,** The percentages of HSCs/MPPs (A), myeloid progenitors (B), and $Gr1^+/CD11b^+$ mature myeloid cells (C) in each experimental group. **D-E,** Serial colony forming assays using primary BM cells collected from Mx1-$Cre^{+/-}$;$Rosa26^{+/+}$, Mx1-$Cre^{+/-}$;$Rosa26^{LSL\text{-}MYC/+}$ and Mx1-$Cre^{+/-}$;$Rosa26^{LSL\text{-}MYC/LSL\text{-}MYC}$ mice at 20 weeks post-pIpC. **F,** Competitive transplant using BM cells from $CD45.2^+$ Mx1-$Cre^{+/-}$;$Rosa26^{+/+}$ *vs.* Mx1-$Cre^{+/-}$;$Rosa26^{LSL\text{-}MYC/LSL\text{-}MYC}$ mice. BM cells were harvested from these mice 20 weeks post-pIpC injection, mixed 1:1 with $CD45.1^+$ WT BM cells, and a total of 1 million cells were injected via tail vein into lethally irradiated $CD45.1^+/CD45.2^+$ recipient mice. **G-H,** MYC mRNA (G) and protein (H) levels in BM and spleen cells from recipient mice at endpoints. **I,** Percentages of $CD45.2^+$ cells were assessed by serial PB flow cytometry analyses. **J-L,** CBC analyses at indicated times following transplantation. **M,** Spleen weight at endpoints. **N,** KM curves of OS, calculated from the date of transplant. **O,** H&E, reticulin, and trichrome stained images of BM, spleen, and liver. Mice transplanted with Mx1-$Cre^{+/-}$;$Rosa26^{+/+}$ BM cells were sacrificed as controls when mice transplanted with Mx1-$Cre^{+/-}$;$Rosa26^{LSL\text{-}MYC/LSL\text{-}MYC}$ BM cells approached their endpoints. Error bars in (A-C, E, G, I) indicate mean ±SEM of at least 4 independent mice. *, $P<0.05$ compared with control group.

Figure 4. Characterization of MYC-driven MF at the single cell level. **A-B,** UMAP plots of single hematopoietic cells in BM of Mx1-Cre$^{+/-}$;Rosa26$^{+/+}$ (control) *vs.* Mx1-Cre$^{+/-}$;Rosa26$^{LSL\text{-}MYC/LSL\text{-}MYC}$ (MYC) mice at 20 weeks post-pIpC injection. **C-D,** Bar plots of percentages of major cell types in control *vs.* MYC mouse. **E-F,** Semantic plots of HSCs (E) and monocytes (F). Upregulated and downregulated pathways in MYC *vs.* control cells are highlighted in red and blue, respectively. **G,** PROGENy analysis comparing MYC *vs.* control cells. Individual column and row are major cell types and pathways known to contribute to MPN pathogenesis, respectively. **H-M,** Venn diagram of MYC-controlled, differentially expressed genes by scRNA-seq (log2fold change>0.25, q<0.05) in major cell types. **N,** Expression levels of *S100a9* in individual cells are projected onto the UMAP space. **O,** Ridgeline plots comparing *S100a9* mRNA levels in MYC (red) vs. control (blue) BM cells in each major cell type. **P-Q,** qRT-PCR assays were used to assess the levels of *S100a8/a9* mRNA in BM and spleen cells. **R,** ELISA was used to assess the levels of S100a8/a9 heterodimer in the serum at their end points. Error bars in (P-Q) indicate mean ±SEM of at least 6 independent mice. Box plot in (R) represents data from 6-16 mice in each group. *, *P*<0.05 compared with control group.

Figure 5. MYC-directed changes in cell-cell interactions in the BM niche. **A,** Comparison of $CD34^+$ BM cells of *JAK2*^{V617F} mutant MF patients (n=9) *vs.* HD (n=6) identified 200 differentially regulated genes. Among these, 9 are also regulated by MYC, including *S100A9*. **B,** A total of 144 genes were identified as upregulated in $CD34^+$ BM cells from *JAK2* WT MF patients (n=5) vs. control (total human universal RNA), and *S100A9* is one of 4 genes that is also increased by MYC. **C-E,** IHC staining analysis of BM demonstrates increased levels of S100A9 protein in TN-MF patients with positive MYC expression vs. patients lacking MYC expression in their BM. **F,** Levels of *MYC, S100a8*, and *S100a9* in *ex vivo* cultured (for 9~10 days) primary BM cells harvested from the indicated mice. **G-P,** Network plots of ligands (S100a8, S100a9) and receptors (ALCAM, CD68) interactions. S100a8/a9 signals originating from HSCs, GMPs, MEPs, myelocytes, neutrophils, and T-cells in WT (G, K) and MYC (H, L) mice, and S100a8/9 signals coming to monoblasts, monocytes, or macrophages in WT (I, M) and MYC (J, N) mice are presented in different colors. Thicker line in **G-N,** indicates a more frequent interaction between cell types and differences in intensity of interactions are shown in (O-P); higher and lower signal activity in MYC cells (*vs.* WT) are in red and blue, respectively. **Q,** Percentages of M1 *vs.* M2 macrophages in MYC *vs.* WT mice based on scRNA-seq analysis. R, Percentages of macrophages ($CD11b^+$ and $F4/80^+$ cells) in BM and spleen were assessed by flow cytometry at 20 weeks post-pIpC injection as indicated. Error bars in (D-F, R) indicate mean ±SEM of at least 3 independent samples or assays. *, $P<0.05$ compared with control group.

Figure 6. *S100a9* loss impairs MYC-driven MF. A, Schematic of in vivo mouse studies. **B-D,** Levels of MYC, S100a9, and S100a8/a9 heterodimers in BM, spleen, and serum, respectively, in *S100a9*$^{+/+}$, *S100a9*$^{-/-}$, Mx1-Cre$^{+/-}$;Rosa26$^{LSL\text{-}MYC/LSL\text{-}MYC}$, and Mx1-Cre$^{+/-}$;Rosa26$^{LSL\text{-}MYC/LSL\text{-}MYC}$;*S100a9*$^{-/-}$ mice. *S100a9*$^{+/+}$ and *S100a9*$^{-/-}$ mice were sacrificed as age matched controls when Mx1-Cre$^{+/-}$;Rosa26$^{LSL\text{-}MYC/LSL\text{-}MYC}$ mice were at their endpoints. Mx1-Cre$^{+/-}$;Rosa26$^{LSL\text{-}MYC/LSL\text{-}MYC}$;*S100a9*$^{-/-}$ mice were sacrificed at ~32 weeks post-pIpC treatment, which is equivalent to the median OS of Mx1-Cre$^{+/-}$;Rosa26$^{LSL\text{-}MYC/LSL\text{-}MYC}$ mice (see panel H). **E-F,** PB CBC analyses. Baseline CBC was performed 1 week prior to pIpC injection. **G,** Comparison of spleen weight. Mice were sacrificed as described in panels (B-D). **H,** KM curves of OS. **I-N,** Percentages of HSCs/MPPs (I), myeloid progenitors (J), Gr1^{+}/CD11b^{+} myeloid cells (K), macrophages (L), B-cells (M), and T-cells (N) in each group. **O,** H&E stained images of BM, SP, and liver at week 32 post-pIpC injection. Demographic and laboratory profiles are described in Table S11. Actin blots in (C) were from the same samples run on different gels. Box plots in (D-G) represent data from at least 6 mice in each group. Experiments in (I-N) were performed simultaneously with experiments in Figure 3A-C and Figure S3B, thus, control and some of experimental groups are shared among these experiments. Error bars in (B, I-N) indicate mean ±SEM of at least 2 independent assays. *, P<0.05 compared with control group.

Figure 7. Inhibition of MYC effectively suppresses TN-MF disease progression. A, Schematic of in vivo mouse studies. **B,** MYC, S100a8, and S100a9 protein levels in the BM and spleen cells of vehicle- *vs.* MYCi975- treated mice (that were transplanted with BM cells from a Mx1-Cre$^{+/-}$;Rosa26$^{LSL\text{-}MYC/LSL\text{-}MYC}$ mouse) were compared to protein levels in Mx1-Cre$^{+/-}$;Rosa26$^{+/+}$ control mice. **C,** Disease burden (CD45.2^{+} cells as % of total CD45.1^{+}+CD45.2^{+} cells) was serially assessed by flow cytometry at the indicated time points using PB samples. **D-E,** PB CBC analyses. Baseline CBC was performed 1 week prior to transplant. **F,** Spleen weight at endpoints. MYCi975-treated mice were sacrificed at the same time when vehicle-treated mice approach their endpoints for paired analyses. **G,** KM curves of OS. Demographic and laboratory profiles are described in Table S14. **H-I,** H&E, reticulin, and MYC IHC staining, as well as cytogenetics and spleen size in a trisomy 8+ TN-MF patient before and after 6 months treatment of fedratinib (400mg po daily). **J,** *MYC* and *S100A8/A9* levels in HSCs/CMPs and neutrophils, respectively, in trisomy 8+ TN-MF *vs.* HD. **K,** PB disease burden (expressed as % of hCD45^{+} cells in hCD45^{+}+mCD45.1^{+} cells) in recipient mice treated with vehicle, ruxolitinib, or MYCi975. Mice were randomized at 9 weeks post-transplant, and disease burden was compared at 13 weeks post-transplant. **L,** Graphical summary of the MYC-S100A8/A9 circuit in TN-MF. Actin blots in (B) were from the same samples run on different gels. Box plots in (D-F, K) represent data from 6 and 4-5 mice in each group, respectively. *, P<0.05 compared with control group.

REFERENCES

1. Verstovsek, S., Yu, J., Scherber, R.M., Verma, S., Dieyi, C., Chen, C.-C., and Parasuraman, S. (2022). Changes in the incidence and overall survival of patients with myeloproliferative neoplasms between 2002 and 2016 in the United States. Leukemia & Lymphoma *63*, 694-702. 10.1080/10428194.2021.1992756.

2. Spivak, J.L. (2017). Myeloproliferative Neoplasms. N Engl J Med *376*, 2168-2181. 10.1056/NEJMra1406186.

3. Tefferi, A. (2021). Primary myelofibrosis: 2021 update on diagnosis, risk-stratification and management. Am J Hematol *96*, 145-162. https://doi.org/10.1002/ajh.26050.

4. Klampfl, T., Gisslinger, H., Harutyunyan, A.S., Nivarthi, H., Rumi, E., Milosevic, J.D., Them, N.C.C., Berg, T., Gisslinger, B., Pietra, D., et al. (2013). Somatic Mutations of Calreticulin in Myeloproliferative Neoplasms. N Engl J Med *369*, 2379-2390. 10.1056/NEJMoa1311347.

5. Nangalia, J., Massie, C.E., Baxter, E.J., Nice, F.L., Gundem, G., Wedge, D.C., Avezov, E., Li, J., Kollmann, K., Kent, D.G., et al. (2013). Somatic CALR Mutations in Myeloproliferative Neoplasms with Nonmutated JAK2. N Engl J Med *369*, 2391-2405. 10.1056/NEJMoa1312542.

6. Cabagnols, X., Favale, F., Pasquier, F., Messaoudi, K., Defour, J.P., Ianotto, J.C., Marzac, C., Le Couédic, J.P., Droin, N., Chachoua, I., et al. (2016). Presence of atypical thrombopoietin receptor (MPL) mutations in triple-negative essential thrombocythemia patients. Blood *127*, 333-342. 10.1182/blood-2015-07-661983 %J Blood.

7. Milosevic Feenstra, J.D., Nivarthi, H., Gisslinger, H., Leroy, E., Rumi, E., Chachoua, I., Bagienski, K., Kubesova, B., Pietra, D., Gisslinger, B., et al. (2016). Whole-exome sequencing identifies novel MPL and JAK2 mutations in triple-negative myeloproliferative neoplasms. Blood *127*, 325-332. 10.1182/blood-2015-07-661835 %J Blood.

8. Pikman, Y., Lee, B.H., Mercher, T., McDowell, E., Ebert, B.L., Gozo, M., Cuker, A., Wernig, G., Moore, S., Galinsky, I., et al. (2006). MPLW515L Is a Novel Somatic Activating Mutation in Myelofibrosis with Myeloid Metaplasia. PLOS Medicine *3*, e270. 10.1371/journal.pmed.0030270.

9. Grinfeld, J., Nangalia, J., Baxter, E.J., Wedge, D.C., Angelopoulos, N., Cantrill, R., Godfrey, A.L., Papaemmanuil, E., Gundem, G., MacLean, C., et al. (2018). Classification and Personalized Prognosis in Myeloproliferative Neoplasms. N Engl J Med *379*, 1416-1430. 10.1056/NEJMoa1716614.

10. Kleppe, M., Kwak, M., Koppikar, P., Riester, M., Keller, M., Bastian, L., Hricik, T., Bhagwat, N., McKenney, A.S., Papalexi, E., et al. (2015). JAK–STAT Pathway Activation in Malignant and Nonmalignant Cells Contributes to MPN Pathogenesis and Therapeutic Response. Cancer Discov *5*, 316-331. 10.1158/2159-8290.CD-14-0736 %J Cancer Discovery.

11. Tefferi, A., Vaidya, R., Caramazza, D., Finke, C., Lasho, T., and Pardanani, A. (2011). Circulating Interleukin (IL)-8, IL-2R, IL-12, and IL-15 Levels Are Independently Prognostic in Primary Myelofibrosis: A Comprehensive Cytokine Profiling Study. J Clin Oncol *29*, 1356-1363. 10.1200/jco.2010.32.9490.

12. Verstovsek, S., Mesa, R.A., Gotlib, J., Levy, R.S., Gupta, V., DiPersio, J.F., Catalano, J.V., Deininger, M., Miller, C., Silver, R.T., et al. (2012). A Double-Blind, Placebo-Controlled Trial of Ruxolitinib for Myelofibrosis. N Engl J Med *366*, 799-807. 10.1056/NEJMoa1110557.

13. Harrison, C., Kiladjian, J.-J., Al-Ali, H.K., Gisslinger, H., Waltzman, R., Stalbovskaya, V., McQuitty, M., Hunter, D.S., Levy, R., Knoops, L., et al. (2012). JAK Inhibition with Ruxolitinib versus Best Available Therapy for Myelofibrosis. N Engl J Med *366*, 787-798. 10.1056/NEJMoa1110556.

14. Pardanani, A., Harrison, C., Cortes, J.E., Cervantes, F., Mesa, R.A., Milligan, D., Masszi, T., Mishchenko, E., Jourdan, E., Vannucchi, A.M., et al. (2015). Safety and Efficacy of Fedratinib in Patients With Primary or Secondary Myelofibrosis: A Randomized Clinical Trial. JAMA Oncology *1*, 643-651. 10.1001/jamaoncol.2015.1590 %J JAMA Oncology.

15. Mascarenhas, J., Hoffman, R., Talpaz, M., Gerds, A.T., Stein, B., Gupta, V., Szoke, A., Drummond, M., Pristupa, A., Granston, T., et al. (2018). Pacritinib vs Best Available Therapy, Including Ruxolitinib, in Patients With Myelofibrosis: A Randomized Clinical Trial. JAMA Oncology *4*, 652-659. 10.1001/jamaoncol.2017.5818 %J JAMA Oncology.

16. Aguirre, L.E.E., Jain, A.G., Ball, S., Al Ali, N., Tinsley-Vance, S.M., Sallman, D.A., Sweet, K., Lancet, J.E., Padron, E., Kuykendall, A.T., and Komrokji, R.S. (2021). Triple-Negative Myelofibrosis: Disease Features, Response to Treatment and Outcomes. Blood *138*, 1494-1494. 10.1182/blood-2021-151978 %J Blood.

17. Tefferi, A., Lasho, T.L., Finke, C.M., Knudson, R.A., Ketterling, R., Hanson, C.H., Maffioli, M., Caramazza, D., Passamonti, F., and Pardanani, A. (2014). CALR vs JAK2 vs MPL-mutated or triple-negative myelofibrosis: clinical, cytogenetic and molecular comparisons. Leukemia *28*, 1472-1477. 10.1038/leu.2014.3.

18. Ross, D.M., Babon, J.J., Tvorogov, D., and Thomas, D. (2021). Persistence of myelofibrosis treated with ruxolitinib: biology and clinical implications. Haematologica *106*, 1244-1253. 10.3324/haematol.2020.262691.

19. Vachhani, P., Verstovsek, S., and Bose, P. (2022). Disease Modification in Myelofibrosis: An Elusive Goal? J Clin Oncol 10;40(11):1147-1154 JCO.21.02246. 10.1200/jco.21.02246.

20. Dang, C.V. (1999). c-Myc target genes involved in cell growth, apoptosis, and metabolism. Mol Cell Biol *19*, 1-11.

21. Dang, C.V. (2012). MYC on the path to cancer. Cell *149*, 22-35. 10.1016/j.cell.2012.03.003.

22. Dang, C.V., O'Donnell, K.A., Zeller, K.I., Nguyen, T., Osthus, R.C., and Li, F. (2006). The c-Myc target gene network. Semin Cancer Biol *16*, 253-264. 10.1016/j.semcancer.2006.07.014.

23. Adams, J.M., Harris, A.W., Pinkert, C.A., Corcoran, L.M., Alexander, W.S., Cory, S., Palmiter, R.D., and Brinster, R.L. (1985). The c-myc oncogene driven by immunoglobulin enhancers induces lymphoid malignancy in transgenic mice. Nature *318*, 533-538. 10.1038/318533a0.

24. Taub, R., Kirsch, I., Morton, C., Lenoir, G., Swan, D., Tronick, S., Aaronson, S., and Leder, P. (1982). Translocation of the c-myc gene into the immunoglobulin heavy chain locus in human Burkitt lymphoma and murine plasmacytoma cells. Proc Natl Acad Sci *79*, 7837-7841. doi:10.1073/pnas.79.24.7837.

25. Smith, D.P., Bath, M.L., Harris, A.W., and Cory, S. (2005). T-cell lymphomas mask slower developing B-lymphoid and myeloid tumours in transgenic mice with broad haemopoietic expression of MYC. Oncogene *24*, 3544-3553. 10.1038/sj.onc.1208399.

26. Yun, S., Vincelette, N.D., Yu, X., Watson, G.W., Fernandez, M.R., Yang, C., Hitosugi, T., Cheng, C.-H., Freischel, A.R., Zhang, L., et al. (2021). TFEB Links MYC Signaling to Epigenetic Control of Myeloid Differentiation and Acute Myeloid Leukemia. Blood Cancer Discov *2*, 162-185. 10.1158/2643-3230.BCD-20-0029 %J Blood Cancer Discovery.

27. Gajzer, D., Logothetis, C.N., Sallman, D.A., Calon, G., Babu, A., Chan, O., Vincelette, N.D., Volpe, V.O., Al Ali, N.H., Basra, P., et al. (2021). MYC overexpression is associated with an early disease progression from MDS to AML. Leuk Res *111*, 106733. https://doi.org/10.1016/j.leukres.2021.106733.

28. Ohanian, M., Rozovski, U., Kanagal-Shamanna, R., Abruzzo, L.V., Loghavi, S., Kadia, T., Futreal, A., Bhalla, K., Zuo, Z., Huh, Y.O., et al. (2018). MYC protein expression is an important prognostic factor in acute myeloid leukemia. Leukemia & Lymphoma *60*, 37-48. 10.1080/10428194.2018.1464158.

29. Sakamoto, K., Katayama, R., Asaka, R., Sakata, S., Baba, S., Nakasone, H., Koike, S., Tsuyama, N., Dobashi, A., Sasaki, M., et al. (2018). Recurrent 8q24 rearrangement in blastic plasmacytoid dendritic cell neoplasm: association with immunoblastoid

cytomorphology, MYC expression, and drug response. Leukemia *32*, 2590-2603. 10.1038/s41375-018-0154-5.

30. Sloand, E.M., Pfannes, L., Chen, G., Shah, S., Solomou, E.E., Barrett, J., and Young, N.S. (2006). CD34 cells from patients with trisomy 8 myelodysplastic syndrome (MDS) express early apoptotic markers but avoid programmed cell death by up-regulation of antiapoptotic proteins. Blood *109*, 2399-2405. 10.1182/blood-2006-01-030643 %J Blood.

31. Reavie, L., Buckley, Shannon M., Loizou, E., Takeishi, S., Aranda-Orgilles, B., Ndiaye-Lobry, D., Abdel-Wahab, O., Ibrahim, S., Nakayama, Keiichi I., and Aifantis, I. (2013). Regulation of c-Myc Ubiquitination Controls Chronic Myelogenous Leukemia Initiation and Progression. Cancer Cell *23*, 362-375. https://doi.org/10.1016/j.ccr.2013.01.025.

32. Luo, H., Li, Q., O'Neal, J., Kreisel, F., Le Beau, M.M., and Tomasson, M.H. (2005). c-Myc rapidly induces acute myeloid leukemia in mice without evidence of lymphoma-associated antiapoptotic mutations. Blood *106*, 2452-2461. 10.1182/blood-2005-02-0734.

33. Bulaeva, E., Pellacani, D., Nakamichi, N., Hammond, C.A., Beer, P.A., Lorzadeh, A., Moksa, M., Carles, A., Bilenky, M., Lefort, S., et al. (2020). MYC-induced human acute myeloid leukemia requires a continuing IL-3/GM-CSF costimulus. Blood *136*, 2764-2773. 10.1182/blood.2020006374 %J Blood.

34. Yun, S., Sharma, R., Chan, O., Vincelette, N.D., Sallman, D.A., Sweet, K., Padron, E., Komrokji, R., Lancet, J.E., Abraham, I., et al. (2019). Prognostic significance of MYC oncoprotein expression on survival outcome in patients with acute myeloid leukemia with myelodysplasia related changes (AML-MRC). Leuk Res *84*, 106194. https://doi.org/10.1016/j.leukres.2019.106194.

35. Haase, D. (2008). Cytogenetic features in myelodysplastic syndromes. Annals of Hematology *87*, 515-526. 10.1007/s00277-008-0483-y.

36. Wassie, E., Finke, C., Gangat, N., Lasho, T.L., Pardanani, A., Hanson, C.A., Ketterling, R.P., and Tefferi, A. (2015). A compendium of cytogenetic abnormalities in myelofibrosis: molecular and phenotypic correlates in 826 patients. Br J Haematol *169*, 71-76. https://doi.org/10.1111/bjh.13260.

37. Vaidya, R., Caramazza, D., Begna, K.H., Gangat, N., Van Dyke, D.L., Hanson, C.A., Pardanani, A., and Tefferi, A. (2011). Monosomal karyotype in primary myelofibrosis is detrimental to both overall and leukemia-free survival. Blood *117*, 5612-5615. 10.1182/blood-2010-11-320002 %J Blood.

38. Tefferi, A., Nicolosi, M., Mudireddy, M., Lasho, T.L., Gangat, N., Begna, K.H., Hanson, C.A., Ketterling, R.P., and Pardanani, A. (2018). Revised cytogenetic risk stratification in

primary myelofibrosis: analysis based on 1002 informative patients. Leukemia *32*, 1189-1199. 10.1038/s41375-018-0018-z.

39. Papaemmanuil, E., Gerstung, M., Bullinger, L., Gaidzik, V.I., Paschka, P., Roberts, N.D., Potter, N.E., Heuser, M., Thol, F., Bolli, N., et al. (2016). Genomic Classification and Prognosis in Acute Myeloid Leukemia. N Engl J Med *374*, 2209-2221. doi:10.1056/NEJMoa1516192.

40. Kleppe, M., Koche, R., Zou, L., van Galen, P., Hill, C.E., Dong, L., De Groote, S., Papalexi, E., Hanasoge Somasundara, A.V., Cordner, K., et al. (2018). Dual Targeting of Oncogenic Activation and Inflammatory Signaling Increases Therapeutic Efficacy in Myeloproliferative Neoplasms. Cancer Cell *33*, 29-43.e27. 10.1016/j.ccell.2017.11.009.

41. Huang, S.-M.A., Wang, A., Greco, R., Li, Z., Barberis, C., Tabart, M., Patel, V., Schio, L., Hurley, R., Cheng, H., et al. (2014). Combination of PIM and JAK2 inhibitors synergistically suppresses cell proliferation and overcomes drug resistance of myeloproliferative neoplasms. Oncotarget 30;5(10):3362-74.

42. Kim, S.-K., Knight, D.A., Jones, L.R., Vervoort, S., Ng, A.P., Seymour, J.F., Bradner, J.E., Waibel, M., Kats, L., and Johnstone, R.W. (2018). JAK2 is dispensable for maintenance of JAK2 mutant B-cell acute lymphoblastic leukemias. Genes Dev *32*, 849-864. 10.1101/gad.307504.117.

43. Wang, S., Song, R., Wang, Z., Jing, Z., Wang, S., and Ma, J. (2018). S100A8/A9 in Inflammation. Front Immunol *9,* 1298. 10.3389/fimmu.2018.01298.

44. Gleitz, H.F.E., Benabid, A., and Schneider, R.K. (2021). Still a burning question: the interplay between inflammation and fibrosis in myeloproliferative neoplasms. Curr Opin Hematol *28*, 364-371. 10.1097/moh.0000000000000669.

45. Leimkühler, N.B., Gleitz, H.F.E., Ronghui, L., Snoeren, I.A.M., Fuchs, S.N.R., Nagai, J.S., Banjanin, B., Lam, K.H., Vogl, T., Kuppe, C., et al. (2021). Heterogeneous bone-marrow stromal progenitors drive myelofibrosis via a druggable alarmin axis. Cell Stem Cell *28*, 637-652.e638. 10.1016/j.stem.2020.11.004.

46. Zambetti, Noemi A., Ping, Z., Chen, S., Kenswil, Keane J.G., Mylona, Maria A., Sanders, Mathijs A., Hoogenboezem, Remco M., Bindels, Eric M.J., Adisty, Maria N., Van Strien, Paulina M.H., et al. (2016). Mesenchymal Inflammation Drives Genotoxic Stress in Hematopoietic Stem Cells and Predicts Disease Evolution in Human Pre-leukemia. Cell Stem Cell *19*, 613-627. 10.1016/j.stem.2016.08.021.

47. Bresnick, A.R., Weber, D.J., and Zimmer, D.B. (2015). S100 proteins in cancer. Nature Reviews Cancer *15*, 96-109. 10.1038/nrc3893.

48. Vogl, T., Tenbrock, K., Ludwig, S., Leukert, N., Ehrhardt, C., van Zoelen, M.A.D., Nacken, W., Foell, D., van der Poll, T., Sorg, C., and Roth, J. (2007). Mrp8 and Mrp14 are

endogenous activators of Toll-like receptor 4, promoting lethal, endotoxin-induced shock. Nature Medicine *13*, 1042-1049. 10.1038/nm1638.

49. Yun, S., Geyer, S.M., Komrokji, R.S., Al Ali, N.H., Song, J., Hussaini, M., Sweet, K.L., Lancet, J.E., List, A.F., Padron, E., and Sallman, D.A. (2020). Prognostic significance of serial molecular annotation in myelodysplastic syndromes (MDS) and secondary acute myeloid leukemia (sAML). Leukemia. 35, 1145-1155 10.1038/s41375-020-0997-4.

50. Kruspig, B., Monteverde, T., Neidler, S., Hock, A., Kerr, E., Nixon, C., Clark, W., Hedley, A., Laing, S., Coffelt, S.B., et al. (2018). The ERBB network facilitates KRAS-driven lung tumorigenesis. Sci Transl Med *10*, eaao2565. 10.1126/scitranslmed.aao2565 %J Science Translational Medicine.

51. Harris, A.W., Pinkert, C.A., Crawford, M., Langdon, W.Y., Brinster, R.L., and Adams, J.M. (1988). The E mu-myc transgenic mouse. A model for high-incidence spontaneous lymphoma and leukemia of early B cells. Journal of Experimental Medicine *167*, 353-371. 10.1084/jem.167.2.353 %J Journal of Experimental Medicine.

52. Fernandez, M.R., Schaub, F.X., Yang, C., Li, W., Yun, S., Schaub, S.K., Dorsey, F.C., Liu, M., Steeves, M.A., Ballabio, A., et al. (2022). Disrupting the MYC-TFEB Circuit Impairs Amino Acid Homeostasis and Provokes Metabolic Anergy. Cancer Research *82*, 1234-1250. 10.1158/0008-5472.CAN-21-1168 %J Cancer Research.

53. Smith, D.P., Bath, M.L., Metcalf, D., Harris, A.W., and Cory, S. (2006). MYC levels govern hematopoietic tumor type and latency in transgenic mice. Blood *108*, 653-661. 10.1182/blood-2006-01-0172 %J Blood.

54. Ohshima, K., Kikuchi, M., and Takeshita, M. (1995). A megakaryocyte analysis of the bone marrow in patients with myelodysplastic syndrome, myeloproliferative disorder and allied disorders. J Pathol *177*, 181-189. https://doi.org/10.1002/path.1711770212.

55. Rabellino, E.M., Levene, R.B., Nachman, R.L., and Leung, L.L.K. (1984). Human Megakaryocytes III. Characterization in Myeloproliferative Disorders. Blood *63*, 615-622. https://doi.org/10.1182/blood.V63.3.615.615.

56. Arber, D.A., Orazi, A., Hasserjian, R., Thiele, J., Borowitz, M.J., Le Beau, M.M., Bloomfield, C.D., Cazzola, M., and Vardiman, J.W. (2016). The 2016 revision to the World Health Organization classification of myeloid neoplasms and acute leukemia. Blood *127*, 2391-2405. 10.1182/blood-2016-03-643544.

57. Guglielmelli, P., Pacilli, A., Rotunno, G., Rumi, E., Rosti, V., Delaini, F., Maffioli, M., Fanelli, T., Pancrazzi, A., Pietra, D., et al. (2017). Presentation and outcome of patients with 2016 WHO diagnosis of prefibrotic and overt primary myelofibrosis. Blood *129*, 3227-3236. 10.1182/blood-2017-01-761999 %J Blood.

58. Khoury, J.D., Solary, E., Abla, O., Akkari, Y., Alaggio, R., Apperley, J.F., Bejar, R., Berti, E., Busque, L., Chan, J.K.C., et al. (2022). The 5th edition of the World Health Organization Classification of Haematolymphoid Tumours: Myeloid and Histiocytic/Dendritic Neoplasms. Leukemia *36*, 1703-1719. 10.1038/s41375-022-01613-1.

59. Baumeister, J., Maié, T., Chatain, N., Gan, L., Weinbergerova, B., de Toledo, M.A.S., Eschweiler, J., Maurer, A., Mayer, J., Kubesova, B., et al. (2021). Early and late stage MPN patients show distinct gene expression profiles in CD34+ cells. Annals of Hematology *100*, 2943-2956. 10.1007/s00277-021-04615-8.

60. Čokić, V.P., Mossuz, P., Han, J., Socoro, N., Beleslin-Čokić, B.B., Mitrović, O., Subotički, T., Diklić, M., Leković, D., Gotić, M., et al. (2015). Microarray and Proteomic Analyses of Myeloproliferative Neoplasms with a Highlight on the mTOR Signaling Pathway. PLOS ONE *10*, e0135463. 10.1371/journal.pone.0135463.

61. Bergsbaken, T., Fink, S.L., and Cookson, B.T. (2009). Pyroptosis: host cell death and inflammation. Nature Reviews Microbiology *7*, 99-109. 10.1038/nrmicro2070.

62. von Bauer, R., Oikonomou, D., Sulaj, A., Mohammed, S., Hotz-Wagenblatt, A., Gröne, H.J., Arnold, B., Falk, C., Luethje, D., Erhardt, A., et al. (2013). CD166/ALCAM mediates proinflammatory effects of S100B in delayed type hypersensitivity. J Immunol *191*, 369-377. 10.4049/jimmunol.1201864.

63. Wakahashi, K., Minagawa, K., Kawano, Y., Kawano, H., Suzuki, T., Ishii, S., Sada, A., Asada, N., Sato, M., Kato, S., et al. (2019). Vitamin D receptor–mediated skewed differentiation of macrophages initiates myelofibrosis and subsequent osteosclerosis. Blood *133*, 1619-1629. 10.1182/blood-2018-09-876615 %J Blood.

64. Sunahori, K., Yamamura, M., Yamana, J., Takasugi, K., Kawashima, M., Yamamoto, H., Chazin, W.J., Nakatani, Y., Yui, S., and Makino, H. (2006). The S100A8/A9 heterodimer amplifies proinflammatory cytokine production by macrophages via activation of nuclear factor kappa B and p38 mitogen-activated protein kinase in rheumatoid arthritis. Arthritis Research & Therapy *8*, R69. 10.1186/ar1939.

65. Okada, K., Arai, S., Itoh, H., Adachi, S., Hayashida, M., Nakase, H., and Ikemoto, M. (2016). CD68 on rat macrophages binds tightly to S100A8 and S100A9 and helps to regulate the cells' immune functions. Journal of leukocyte biology *100*, 1093-1104. 10.1189/jlb.2A0415-170RRR.

66. Cheng , P., Corzo , C.A., Luetteke , N., Yu , B., Nagaraj , S., Bui , M.M., Ortiz , M., Nacken , W., Sorg , C., Vogl , T., et al. (2008). Inhibition of dendritic cell differentiation and accumulation of myeloid-derived suppressor cells in cancer is regulated by S100A9 protein. Journal of Experimental Medicine *205*, 2235-2249. 10.1084/jem.20080132 %J Journal of Experimental Medicine.

67. Björk, P., Björk, A., Vogl, T., Stenström, M., Liberg, D., Olsson, A., Roth, J., Ivars, F., and Leanderson, T. (2009). Identification of Human S100A9 as a Novel Target for Treatment of Autoimmune Disease via Binding to Quinoline-3-Carboxamides. PLOS Biology *7*, e1000097. 10.1371/journal.pbio.1000097.

68. Sternberg, C., Armstrong, A., Pili, R., Ng, S., Huddart, R., Agarwal, N., Khvorostenko, D., Lyulko, O., Brize, A., Vogelzang, N., et al. (2016). Randomized, Double-Blind, Placebo-Controlled Phase III Study of Tasquinimod in Men With Metastatic Castration-Resistant Prostate Cancer. J Clin Oncol *34*, 2636-2643. 10.1200/jco.2016.66.9697.

69. Han, H., Jain, A.D., Truica, M.I., Izquierdo-Ferrer, J., Anker, J.F., Lysy, B., Sagar, V., Luan, Y., Chalmers, Z.R., Unno, K., et al. (2019). Small-Molecule MYC Inhibitors Suppress Tumor Growth and Enhance Immunotherapy. Cancer Cell *36*, 483-497.e415. 10.1016/j.ccell.2019.10.001.

70. Bolouri, H., Farrar, J.E., Triche Jr, T., Ries, R.E., Lim, E.L., Alonzo, T.A., Ma, Y., Moore, R., Mungall, A.J., Marra, M.A., et al. (2017). The molecular landscape of pediatric acute myeloid leukemia reveals recurrent structural alterations and age-specific mutational interactions. Nature Medicine *24*, 103. 10.1038/nm.4439 https://www.nature.com/articles/nm.4439#supplementary-information.

71. Tyner, J.W., Tognon, C.E., Bottomly, D., Wilmot, B., Kurtz, S.E., Savage, S.L., Long, N., Schultz, A.R., Traer, E., Abel, M., et al. (2018). Functional genomic landscape of acute myeloid leukaemia. Nature *562*, 526-531. 10.1038/s41586-018-0623-z.

72. Bejar , R., Stevenson , K., Abdel-Wahab , O., Galili , N., Nilsson , B., Garcia-Manero , G., Kantarjian , H., Raza , A., Levine , R.L., Neuberg , D., and Ebert , B.L. (2011). Clinical Effect of Point Mutations in Myelodysplastic Syndromes. New England Journal of Medicine *364*, 2496-2506. 10.1056/NEJMoa1013343.

73. Haferlach, T., Nagata, Y., Grossmann, V., Okuno, Y., Bacher, U., Nagae, G., Schnittger, S., Sanada, M., Kon, A., Alpermann, T., et al. (2014). Landscape of genetic lesions in 944 patients with myelodysplastic syndromes. Leukemia *28*, 241-247. 10.1038/leu.2013.336.

74. Yoshizato, T., Nannya, Y., Atsuta, Y., Shiozawa, Y., Iijima-Yamashita, Y., Yoshida, K., Shiraishi, Y., Suzuki, H., Nagata, Y., Sato, Y., et al. (2017). Genetic abnormalities in myelodysplasia and secondary acute myeloid leukemia: impact on outcome of stem cell transplantation. Blood *129*, 2347-2358. 10.1182/blood-2016-12-754796.

75. Nagata, Y., Makishima, H., Kerr, C.M., Przychodzen, B.P., Aly, M., Goyal, A., Awada, H., Asad, M.F., Kuzmanovic, T., Suzuki, H., et al. (2019). Invariant patterns of clonal succession determine specific clinical features of myelodysplastic syndromes. Nature Communications *10*, 5386. 10.1038/s41467-019-13001-y.

76. Papaemmanuil, E., Gerstung, M., Malcovati, L., Tauro, S., Gundem, G., Van Loo, P., Yoon, C.J., Ellis, P., Wedge, D.C., Pellagatti, A., et al. (2013). Clinical and biological implications of driver mutations in myelodysplastic syndromes. Blood *122*, 3616-3627. 10.1182/blood-2013-08-518886.

77. Al-Ghamdi, Y.A., Lake, J., Bagg, A., Thakral, B., Wang, S.A., Bueso-Ramos, C., Masarova, L., Verstovsek, S., Rogers, H.J., Hsi, E.D., et al. (2023). Triple-Negative Primary Myelofibrosis: A Bone Marrow Pathology Group Study. Mod Pathol *36*. 10.1016/j.modpat.2022.100016.

78. Hérault, L., Poplineau, M., Mazuel, A., Platet, N., Remy, É., and Duprez, E. (2021). Single-cell RNA-seq reveals a concomitant delay in differentiation and cell cycle of aged hematopoietic stem cells. BMC Biology *19*, 19. 10.1186/s12915-021-00955-z.

79. Wilson, A., Murphy, M.J., Oskarsson, T., Kaloulis, K., Bettess, M.D., Oser, G.M., Pasche, A.-C., Knabenhans, C., MacDonald, H.R., and Trumpp, A. (2004). c-Myc controls the balance between hematopoietic stem cell self-renewal and differentiation. Genes Dev *18*, 2747-2763. 10.1101/gad.313104.

80. Guo, Y., Niu, C., Breslin, P., Tang, M., Zhang, S., Wei, W., Kini, A.R., Paner, G.P., Alkan, S., Morris, S.W., et al. (2009). c-Myc–mediated control of cell fate in megakaryocyte-erythrocyte progenitors. Blood *114*, 2097-2106. 10.1182/blood-2009-01-197947 %J Blood.

81. Felsher, D.W., and Bishop, J.M. (1999). Reversible Tumorigenesis by MYC in Hematopoietic Lineages. Molecular Cell *4*, 199-207. 10.1016/S1097-2765(00)80367-6.

82. Bhatia, M., Bonnet, D., Kapp, U., Wang, J.C.Y., Murdoch, B., and Dick, J.E. (1997). Quantitative Analysis Reveals Expansion of Human Hematopoietic Repopulating Cells After Short-term Ex Vivo Culture. Journal of Experimental Medicine *186*, 619-624. 10.1084/jem.186.4.619 %J Journal of Experimental Medicine.

83. Conneally, E., Cashman, J., Petzer, A., and Eaves, C. (1997). Expansion in vitro of transplantable human cord blood stem cells demonstrated using a quantitative assay of their lympho-myeloid repopulating activity in nonobese diabetic scid/scid mice. Proc Natl Acad Sci *94*, 9836-9841. doi:10.1073/pnas.94.18.9836.

84. Gammaitoni, L., Bruno, S., Sanavio, F., Gunetti, M., Kollet, O., Cavalloni, G., Falda, M., Fagioli, F., Lapidot, T., Aglietta, M., and Piacibello, W. (2003). Ex vivo expansion of human adult stem cells capable of primary and secondary hemopoietic reconstitution. Experimental Hematology *31*, 261-270. 10.1016/S0301-472X(02)01077-9.

85. Ueda, T., Tsuji, K., Yoshino, H., Ebihara, Y., Yagasaki, H., Hisakawa, H., Mitsui, T., Manabe, A., Tanaka, R., Kobayashi, K., et al. (2000). Expansion of human NOD/SCID-

repopulating cells by stem cell factor, Flk2/Flt3 ligand, thrombopoietin, IL-6, and soluble IL-6 receptor. The Journal of Clinical Investigation *105*, 1013-1021. 10.1172/JCI8583.

86. Marx-Blümel, L., Marx, C., Sonnemann, J., Weise, F., Hampl, J., Frey, J., Rothenburger, L., Cirri, E., Rahnis, N., Koch, P., et al. (2021). Molecular characterization of hematopoietic stem cells after in vitro amplification on biomimetic 3D PDMS cell culture scaffolds. Scientific Reports *11*, 21163. 10.1038/s41598-021-00619-6.

87. Italiani, P., and Boraschi, D. (2014). From Monocytes to M1/M2 Macrophages: Phenotypical vs. Functional Differentiation. Front Immunol *5*. 514 10.3389/fimmu.2014.00514.

88. Orecchioni, M., Ghosheh, Y., Pramod, A.B., and Ley, K. (2019). Macrophage Polarization: Different Gene Signatures in M1(LPS+) vs. Classically and M2(LPS–) vs. Alternatively Activated Macrophages. Front Immunol *10*. 1084 10.3389/fimmu.2019.01084.

89. Molitor, D.C.A., Boor, P., Buness, A., Schneider, R.K., Teichmann, L.L., Körber, R.-M., Horvath, G.L., Koschmieder, S., and Gütgemann, I. (2021). Macrophage frequency in the bone marrow correlates with morphologic subtype of myeloproliferative neoplasm. Annals of Hematology *100*, 97-104. 10.1007/s00277-020-04304-y.

90. Funakoshi-Tago, M., Sumi, K., Kasahara, T., and Tago, K. (2013). Critical Roles of Myc-ODC Axis in the Cellular Transformation Induced by Myeloproliferative Neoplasm-Associated JAK2 V617F Mutant. PLOS ONE *8*, e52844. 10.1371/journal.pone.0052844.

91. Wernig, G., Gonneville, J.R., Crowley, B.J., Rodrigues, M.S., Reddy, M.M., Hudon, H.E., Walz, C., Reiter, A., Podar, K., Royer, Y., et al. (2008). The Jak2V617F oncogene associated with myeloproliferative diseases requires a functional FERM domain for transformation and for expression of the Myc and Pim proto-oncogenes. Blood *111*, 3751-3759. 10.1182/blood-2007-07-102186 %J Blood.

92. Decker, M., Martinez-Morentin, L., Wang, G., Lee, Y., Liu, Q., Leslie, J., and Ding, L. (2017). Leptin-receptor-expressing bone marrow stromal cells are myofibroblasts in primary myelofibrosis. Nature Cell Biology *19*, 677-688. 10.1038/ncb3530.

93. Schneider, R.K., Mullally, A., Dugourd, A., Peisker, F., Hoogenboezem, R., Van Strien, P.M.H., Bindels, E.M., Heckl, D., Büsche, G., Fleck, D., et al. (2017). Gli1+ Mesenchymal Stromal Cells Are a Key Driver of Bone Marrow Fibrosis and an Important Cellular Therapeutic Target. Cell Stem Cell *20*, 785-800.e788. 10.1016/j.stem.2017.03.008.

94. Kramann, R., and Schneider, R.K. (2018). The identification of fibrosis-driving myofibroblast precursors reveals new therapeutic avenues in myelofibrosis. Blood *131*, 2111-2119. 10.1182/blood-2018-02-834820 %J Blood.

95. Mullally, A., Lane, S.W., Ball, B., Megerdichian, C., Okabe, R., Al-Shahrour, F., Paktinat, M., Haydu, J.E., Housman, E., Lord, A.M., et al. (2010). Physiological Jak2V617F

Expression Causes a Lethal Myeloproliferative Neoplasm with Differential Effects on Hematopoietic Stem and Progenitor Cells. Cancer Cell *17*, 584-596. 10.1016/j.ccr.2010.05.015.

96. Akada, H., Yan, D., Zou, H., Fiering, S., Hutchison, R.E., and Mohi, M.G. (2010). Conditional expression of heterozygous or homozygous Jak2V617F from its endogenous promoter induces a polycythemia vera–like disease. Blood *115*, 3589-3597. 10.1182/blood-2009-04-215848 %J Blood.

97. Li, J., Spensberger, D., Ahn, J.S., Anand, S., Beer, P.A., Ghevaert, C., Chen, E., Forrai, A., Scott, L.M., Ferreira, R., et al. (2010). JAK2 V617F impairs hematopoietic stem cell function in a conditional knock-in mouse model of JAK2 V617F–positive essential thrombocythemia. Blood *116*, 1528-1538. 10.1182/blood-2009-12-259747 %J Blood.

98. Marty, C., Lacout, C., Martin, A., Hasan, S., Jacquot, S., Birling, M.-C., Vainchenker, W., and Villeval, J.-L. (2010). Myeloproliferative neoplasm induced by constitutive expression of JAK2V617F in knock-in mice. Blood *116*, 783-787. 10.1182/blood-2009-12-257063 %J Blood.

99. Chapeau, E.A., Mandon, E., Gill, J., Romanet, V., Ebel, N., Powajbo, V., Andraos-Rey, R., Qian, Z., Kininis, M., Zumstein-Mecker, S., et al. (2019). A conditional inducible JAK2V617F transgenic mouse model reveals myeloproliferative disease that is reversible upon switching off transgene expression. PLOS ONE *14*, e0221635. 10.1371/journal.pone.0221635.

100. Li, J., Kent, D.G., Chen, E., and Green, A.R. (2011). Mouse models of myeloproliferative neoplasms: JAK of all grades. Disease Models & Mechanisms *4*, 311-317. 10.1242/dmm.006817 %J Disease Models & Mechanisms.

101. Jacquelin, S., Kramer, F., Mullally, A., and Lane, S.W. (2020). Murine Models of Myelofibrosis. Cancer (Basel)*12*, 2381.

102. Niroula, A., Sekar, A., Murakami, M.A., Trinder, M., Agrawal, M., Wong, W.J., Bick, A.G., Uddin, M.M., Gibson, C.J., Griffin, G.K., et al. (2021). Distinction of lymphoid and myeloid clonal hematopoiesis. Nature Medicine *27*, 1921-1927. 10.1038/s41591-021-01521-4.

103. Saiki, R., Momozawa, Y., Nannya, Y., Nakagawa, M.M., Ochi, Y., Yoshizato, T., Terao, C., Kuroda, Y., Shiraishi, Y., Chiba, K., et al. (2021). Combined landscape of single-nucleotide variants and copy number alterations in clonal hematopoiesis. Nature Medicine *27*, 1239-1249. 10.1038/s41591-021-01411-9.

104. Loh, P.-R., Genovese, G., and McCarroll, S.A. (2020). Monogenic and polygenic inheritance become instruments for clonal selection. Nature *584*, 136-141. 10.1038/s41586-020-2430-6.

105. Loh, P.-R., Genovese, G., Handsaker, R.E., Finucane, H.K., Reshef, Y.A., Palamara, P.F., Birmann, B.M., Talkowski, M.E., Bakhoum, S.F., McCarroll, S.A., and Price, A.L. (2018). Insights into clonal haematopoiesis from 8,342 mosaic chromosomal alterations. Nature *559*, 350-355. 10.1038/s41586-018-0321-x.

106. Hormaechea-Agulla, D., Matatall, K.A., Le, D.T., Kain, B., Long, X., Kus, P., Jaksik, R., Challen, G.A., Kimmel, M., and King, K.Y. (2021). Chronic infection drives Dnmt3a-loss-of-function clonal hematopoiesis via IFNγ signaling. Cell Stem Cell *28*, 1428-1442.e1426. 10.1016/j.stem.2021.03.002.

107. Liao, M., Chen, R., Yang, Y., He, H., Xu, L., Jiang, Y., Guo, Z., He, W., Jiang, H., and Wang, J. (2022). Aging-elevated inflammation promotes DNMT3A R878H-driven clonal hematopoiesis. Acta Pharmaceutica Sinica B *12*, 678-691. https://doi.org/10.1016/j.apsb.2021.09.015.

108. Fuster, J.J., MacLauchlan, S., Zuriaga, M.A., Polackal, M.N., Ostriker, A.C., Chakraborty, R., Wu, C.-L., Sano, S., Muralidharan, S., Rius, C., et al. (2017). Clonal hematopoiesis associated with TET2 deficiency accelerates atherosclerosis development in mice. Science *355*, 842-847. doi:10.1126/science.aag1381.

109. Fidler, T.P., Xue, C., Yalcinkaya, M., Hardaway, B., Abramowicz, S., Xiao, T., Liu, W., Thomas, D.G., Hajebrahimi, M.A., Pircher, J., et al. (2021). The AIM2 inflammasome exacerbates atherosclerosis in clonal haematopoiesis. Nature *592*, 296-301. 10.1038/s41586-021-03341-5.

110. Sallman, D.A., Komrokji, R., Vaupel, C., Cluzeau, T., Geyer, S.M., McGraw, K.L., Al Ali, N.H., Lancet, J., McGinniss, M.J., Nahas, S., et al. (2016). Impact of TP53 mutation variant allele frequency on phenotype and outcomes in myelodysplastic syndromes. Leukemia *30*, 666-673. 10.1038/leu.2015.304.

111. Yun, S., Komrokji, R., Al Ali, N., Song, J., Vaupel, C., Hussaini, M., Sweet, K., Lancet, J., Hall, J., List, A., et al. (2017). Prognostic Significance of Serial Molecular Annotation in Myelodysplastic Syndromes (MDS) and Secondary Acute Myeloid Leukemia (sAML). Clinical Lymphoma, Myeloma and Leukemia *17*, S344-S345. 10.1016/j.clml.2017.07.166.

112. Feldman, A.T., and Wolfe, D. (2014). Tissue Processing and Hematoxylin and Eosin Staining. In Histopathology: Methods and Protocols, C.E. Day, ed. (Springer New York), pp. 31-43. 10.1007/978-1-4939-1050-2_3.

113. Yoshimi, A., Balasis, M.E., Vedder, A., Feldman, K., Ma, Y., Zhang, H., Lee, S.C.-W., Letson, C., Niyongere, S., Lu, S.X., et al. (2017). Robust patient-derived xenografts of MDS/MPN overlap syndromes capture the unique characteristics of CMML and JMML. Blood *130*, 397-407. 10.1182/blood-2017-01-763219.

114. Yun, S., Vincelette, N.D., Knorr, K.L., Almada, L.L., Schneider, P.A., Peterson, K.L., Flatten, K.S., Dai, H., Pratz, K.W., Hess, A.D., et al. (2016). 4EBP1/c-MYC/PUMA and NFκB/EGR1/BIM pathways underlie cytotoxicity of mTOR dual inhibitors in malignant lymphoid cells. Blood. 10.1182/blood-2015-02-629485.

115. Satija, R., Farrell, J.A., Gennert, D., Schier, A.F., and Regev, A. (2015). Spatial reconstruction of single-cell gene expression data. Nat Biotechnol *33*, 495-502. 10.1038/nbt.3192.

116. Wolock, S.L., Lopez, R., and Klein, A.M. (2019). Scrublet: Computational Identification of Cell Doublets in Single-Cell Transcriptomic Data. Cell Syst *8*, 281-291 e289. 10.1016/j.cels.2018.11.005.

117. McGinnis, C.S., Murrow, L.M., and Gartner, Z.J. (2019). DoubletFinder: Doublet Detection in Single-Cell RNA Sequencing Data Using Artificial Nearest Neighbors. Cell Syst *8*, 329-337 e324. 10.1016/j.cels.2019.03.003.

118. Germain, P., Lun, A., Macnair, W., and Robinson, M. (2021). Doublet identification in single-cell sequencing data using scDblFinder [version 1; peer review: 1 approved, 1 approved with reservations]. F1000Research *10*. 10.12688/f1000research.73600.1.

119. Lun, A.T., McCarthy, D.J., and Marioni, J.C. (2016). A step-by-step workflow for low-level analysis of single-cell RNA-seq data with Bioconductor. F1000Res *5*, 2122. 10.12688/f1000research.9501.2.

120. Hao, Y., Hao, S., Andersen-Nissen, E., Mauck, W.M., 3rd, Zheng, S., Butler, A., Lee, M.J., Wilk, A.J., Darby, C., Zager, M., et al. (2021). Integrated analysis of multimodal single-cell data. Cell *184*, 3573-3587 e3529. 10.1016/j.cell.2021.04.048.

121. Aibar, S., González-Blas, C.B., Moerman, T., Huynh-Thu, V.A., Imrichova, H., Hulselmans, G., Rambow, F., Marine, J.-C., Geurts, P., Aerts, J., et al. (2017). SCENIC: single-cell regulatory network inference and clustering. Nature Methods *14*, 1083-1086. 10.1038/nmeth.4463.

122. Stumpf, P.S., Du, X., Imanishi, H., Kunisaki, Y., Semba, Y., Noble, T., Smith, R.C.G., Rose-Zerili, M., West, J.J., Oreffo, R.O.C., et al. (2020). Transfer learning efficiently maps bone marrow cell types from mouse to human using single-cell RNA sequencing. Communications Biology *3*, 736. 10.1038/s42003-020-01463-6.

123. van Galen, P., Hovestadt, V., Wadsworth Ii, M.H., Hughes, T.K., Griffin, G.K., Battaglia, S., Verga, J.A., Stephansky, J., Pastika, T.J., Lombardi Story, J., et al. (2019). Single-Cell RNA-Seq Reveals AML Hierarchies Relevant to Disease Progression and Immunity. Cell *176*, 1265-1281.e1224. 10.1016/j.cell.2019.01.031.

124. Buenrostro, J.D., Corces, M.R., Lareau, C.A., Wu, B., Schep, A.N., Aryee, M.J., Majeti, R., Chang, H.Y., and Greenleaf, W.J. (2018). Integrated Single-Cell Analysis Maps the

Continuous Regulatory Landscape of Human Hematopoietic Differentiation. Cell *173*, 1535-1548.e1516. https://doi.org/10.1016/j.cell.2018.03.074.

125. Pishesha, N., Thiru, P., Shi, J., Eng, J.C., Sankaran, V.G., and Lodish, H.F. (2014). Transcriptional divergence and conservation of human and mouse erythropoiesis. Proceedings of the National Academy of Sciences *111*, 4103-4108. doi:10.1073/pnas.1401598111.

126. Hay, S.B., Ferchen, K., Chetal, K., Grimes, H.L., and Salomonis, N. (2018). The Human Cell Atlas bone marrow single-cell interactive web portal. Experimental Hematology *68*, 51-61. 10.1016/j.exphem.2018.09.004.

127. Wu, T., Hu, E., Xu, S., Chen, M., Guo, P., Dai, Z., Feng, T., Zhou, L., Tang, W., Zhan, L., et al. (2021). clusterProfiler 4.0: A universal enrichment tool for interpreting omics data. The Innovation *2*. 10.1016/j.xinn.2021.100141.

128. Supek, F., Bošnjak, M., Škunca, N., and Šmuc, T. (2011). REVIGO Summarizes and Visualizes Long Lists of Gene Ontology Terms. PLOS ONE *6*, e21800. 10.1371/journal.pone.0021800.

129. Jin, S., Guerrero-Juarez, C.F., Zhang, L., Chang, I., Ramos, R., Kuan, C.-H., Myung, P., Plikus, M.V., and Nie, Q. (2021). Inference and analysis of cell-cell communication using CellChat. Nature Communications *12*, 1088. 10.1038/s41467-021-21246-9.

130. Türei, D., Korcsmáros, T., and Saez-Rodriguez, J. (2016). OmniPath: guidelines and gateway for literature-curated signaling pathway resources. Nature Methods *13*, 966-967. 10.1038/nmeth.4077.

131. Dimitrov, D., Türei, D., Garrido-Rodriguez, M., Burmedi, P.L., Nagai, J.S., Boys, C., Ramirez Flores, R.O., Kim, H., Szalai, B., Costa, I.G., et al. (2022). Comparison of methods and resources for cell-cell communication inference from single-cell RNA-Seq data. Nature Communications *13*, 3224. 10.1038/s41467-022-30755-0.

132. Türei, D., Valdeolivas, A., Gul, L., Palacio-Escat, N., Klein, M., Ivanova, O., Ölbei, M., Gábor, A., Theis, F., Módos, D., et al. (2021). Integrated intra- and intercellular signaling knowledge for multicellular omics analysis. Mol Syst Biol *17*, e9923. https://doi.org/10.15252/msb.20209923.

133. Holland, C.H., Tanevski, J., Perales-Patón, J., Gleixner, J., Kumar, M.P., Mereu, E., Joughin, B.A., Stegle, O., Lauffenburger, D.A., Heyn, H., et al. (2020). Robustness and applicability of transcription factor and pathway analysis tools on single-cell RNA-seq data. Genome Biology *21*, 36. 10.1186/s13059-020-1949-z.

134. Sabò, A., Kress, T.R., Pelizzola, M., de Pretis, S., Gorski, M.M., Tesi, A., Morelli, M.J., Bora, P., Doni, M., Verrecchia, A., et al. (2014). Selective transcriptional regulation by Myc in cellular growth control and lymphomagenesis. Nature *511*, 488.

10.1038/nature13537https://www.nature.com/articles/nature13537#supplementary-information.

135. Rouillard, A.D., Gundersen, G.W., Fernandez, N.F., Wang, Z., Monteiro, C.D., McDermott, M.G., and Ma'ayan, A. (2016). The harmonizome: a collection of processed datasets gathered to serve and mine knowledge about genes and proteins. Database *2016*. 10.1093/database/baw100.

136. Chan, J.K., Roth, J., Oppenheim, J.J., Tracey, K.J., Vogl, T., Feldmann, M., Horwood, N., and Nanchahal, J. (2012). Alarmins: awaiting a clinical response. The Journal of Clinical Investigation *122*, 2711-2719. 10.1172/JCI62423.

137. Sergushichev, A.A. (2016). An algorithm for fast preranked gene set enrichment analysis using cumulative statistic calculation. bioRxiv, 060012. 10.1101/060012.

138. Gu, Z., Eils, R., and Schlesner, M. (2016). Complex heatmaps reveal patterns and correlations in multidimensional genomic data. Bioinformatics *32*, 2847-2849. 10.1093/bioinformatics/btw313.

Figure 1

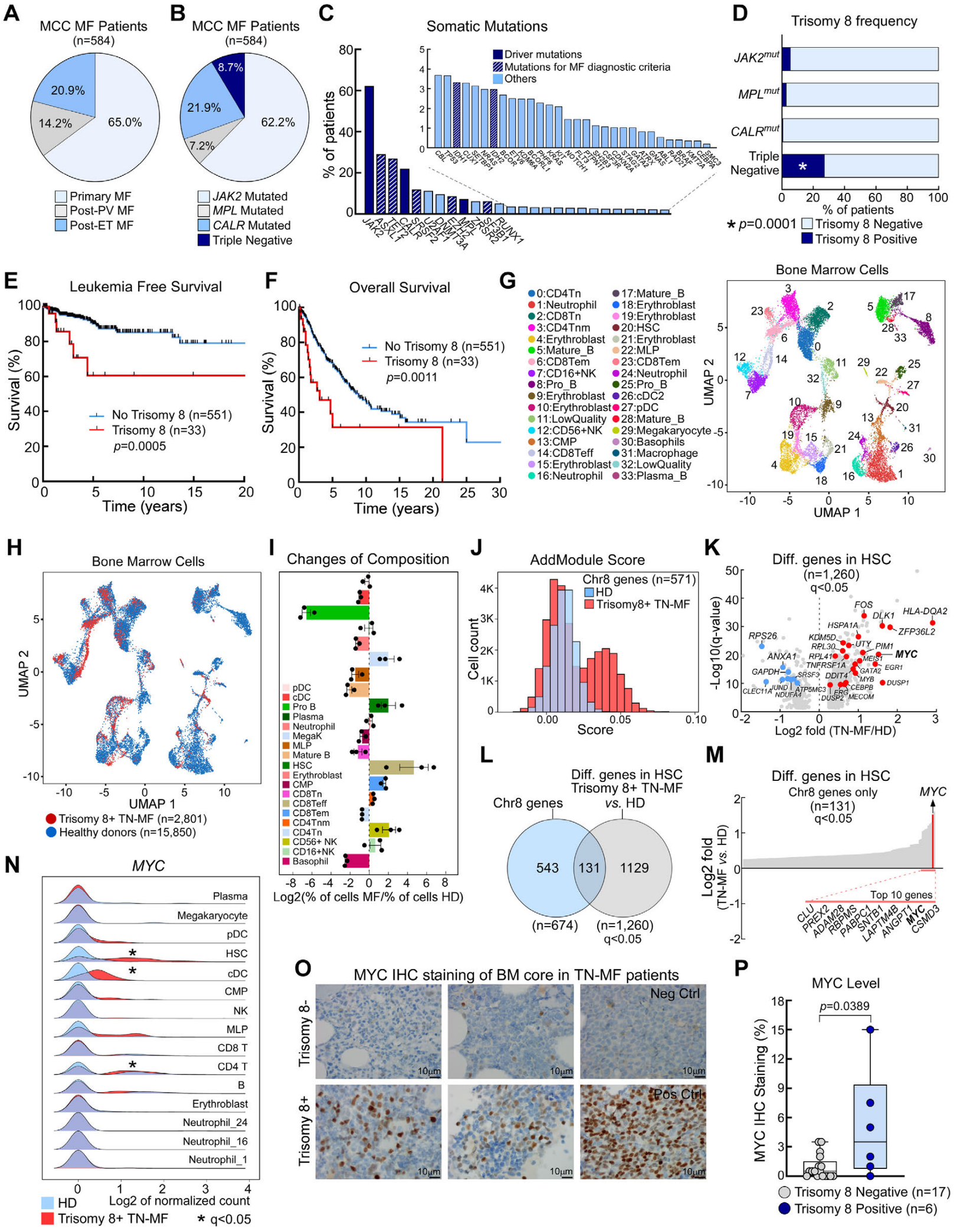
A
MCC MF Patients
(n=584)
20.9%
14.2%
65.0%
Primary MF
Post-PV MF
Post-ET MF
B
MCC MF Patients
(n=584)
8.7%
21.9%
7.2%
62.2%
JAK2 Mutated
MPL Mutated
CALR Mutated
Triple Negative
C
Somatic Mutations
% of patients
Driver mutations
Mutations for MF diagnostic criteria
Others
JAK2
ASXL1
TET2
CALR
SRSF2
U2AF1
DNMT3A
EZH2
MPL
IDH2
IDH1
TP53
RUNX1
SRSF2
D
Trisomy 8 frequency
JAK2mut
MPLmut
CALRmut
Triple Negative
% of patients
* p=0.0001
Trisomy 8 Negative
Trisomy 8 Positive
E
Leukemia Free Survival
Survival (%)
No Trisomy 8 (n=551)
Trisomy 8 (n=33)
p=0.0005
Time (years)
F
Overall Survival
Survival (%)
No Trisomy 8 (n=551)
Trisomy 8 (n=33)
p=0.0011
Time (years)
G
0:CD4Tn
1:Neutrophil
2:CD8Tn
3:CD4Tnm
4:Erythroblast
5:Mature_B
6:CD8Tem
7:CD16+NK
8:Pro_B
9:Erythroblast
10:Erythroblast
11:LowQuality
12:CD56+NK
13:CMP
14:CD8Teff
15:Erythroblast
16:Neutrophil
17:Mature_B
18:Erythroblast
19:Erythroblast
20:HSC
21:Erythroblast
22:MLP
23:CD8Tem
24:Neutrophil
25:Pro_B
26:cDC2
27:pDC
28:Mature_B
29:Megakaryocyte
30:Basophils
31:Macrophage
32:LowQuality
33:Plasma_B
Bone Marrow Cells
UMAP 1
UMAP 2
H
Bone Marrow Cells
UMAP 1
UMAP 2
Trisomy 8+ TN-MF (n=2,801)
Healthy donors (n=15,850)
I
Changes of Composition
pDC
cDC
Pro B
Plasma
Neutrophil
MegaK
MLP
Mature B
HSC
Erythroblast
CMP
CD8Tn
CD8Teff
CD8Tem
CD4Tnm
CD4Tn
CD56+ NK
CD16+NK
Basophil
Log2(% of cells MF/% of cells HD)
J
AddModule Score
Chr8 genes (n=571)
HD
Trisomy8+ TN-MF
Cell count
Score
K
Diff. genes in HSC
(n=1,260)
q<0.05
-Log10(q-value)
Log2 fold (TN-MF/HD)
FOS
DLK1
HLA-DQA2
HSPA1A
ZFP36L2
RPS26
KDM5D
UTY
PIM1
RPL30
ANXA1
RPL41
MEIS1
MYC
TNFRSF1A
EGR1
GAPDH
SRSF3
DDIT4
GATA2
MYB
DUSP1
CLEC11A
UND
NDUFA1
ATP5MC3
ERG
DUSP2
CEBPB
MECOM
L
Diff. genes in HSC
Trisomy 8+ TN-MF
Chr8 genes
vs. HD
543
131
1129
(n=674)
(n=1,260)
q<0.05
M
Diff. genes in HSC
Chr8 genes only
(n=131)
q<0.05
MYC
Log2 fold
(TN-MF vs. HD)
Top 10 genes
CLU
PREX2
ADAM28
RBPMS
PABPC1
SNTB1
LAPTM4B
ANGPT1
MYC
CSMD3
N
MYC
Plasma
Megakaryocyte
pDC
HSC
cDC
CMP
NK
MLP
CD8 T
CD4 T
B
Erythroblast
Neutrophil_24
Neutrophil_16
Neutrophil_1
HD
Trisomy 8+ TN-MF
Log2 of normalized count
* q<0.05
O
MYC IHC staining of BM core in TN-MF patients
Trisomy 8-
Trisomy 8+
Neg Ctrl
Pos Ctrl
10μm
P
MYC Level
p=0.0389
MYC IHC Staining (%)
Trisomy 8 Negative (n=17)
Trisomy 8 Positive (n=6)

Figure S1

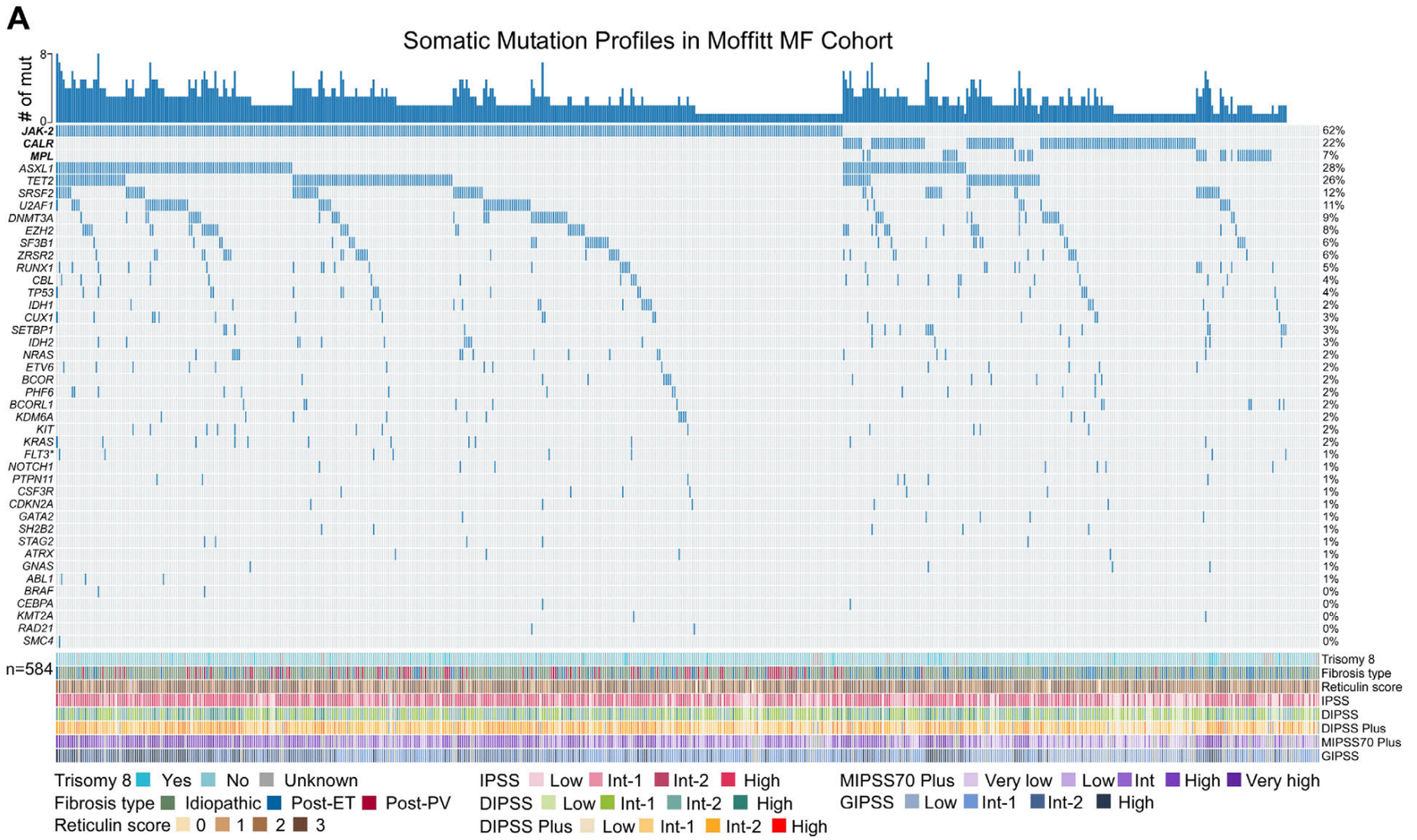

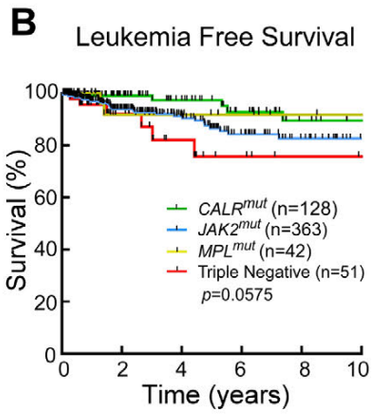

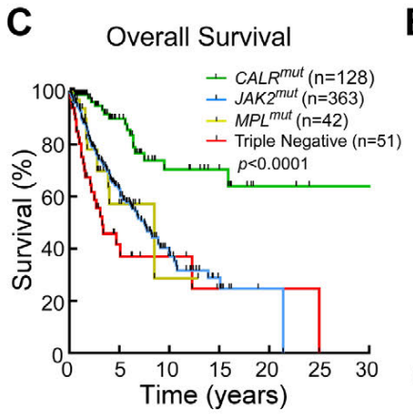

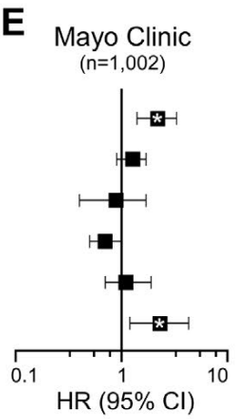

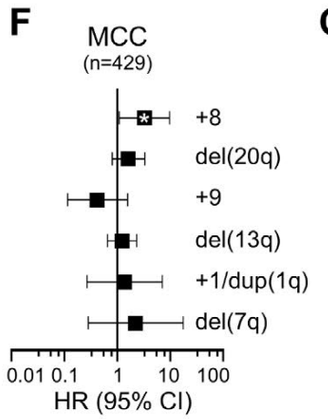

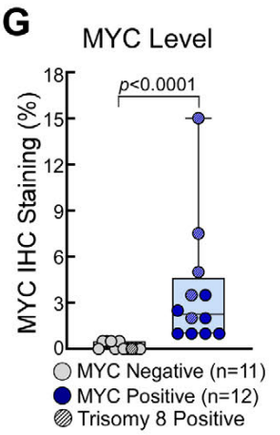

∗ p<0.05
compared to normal karyotype

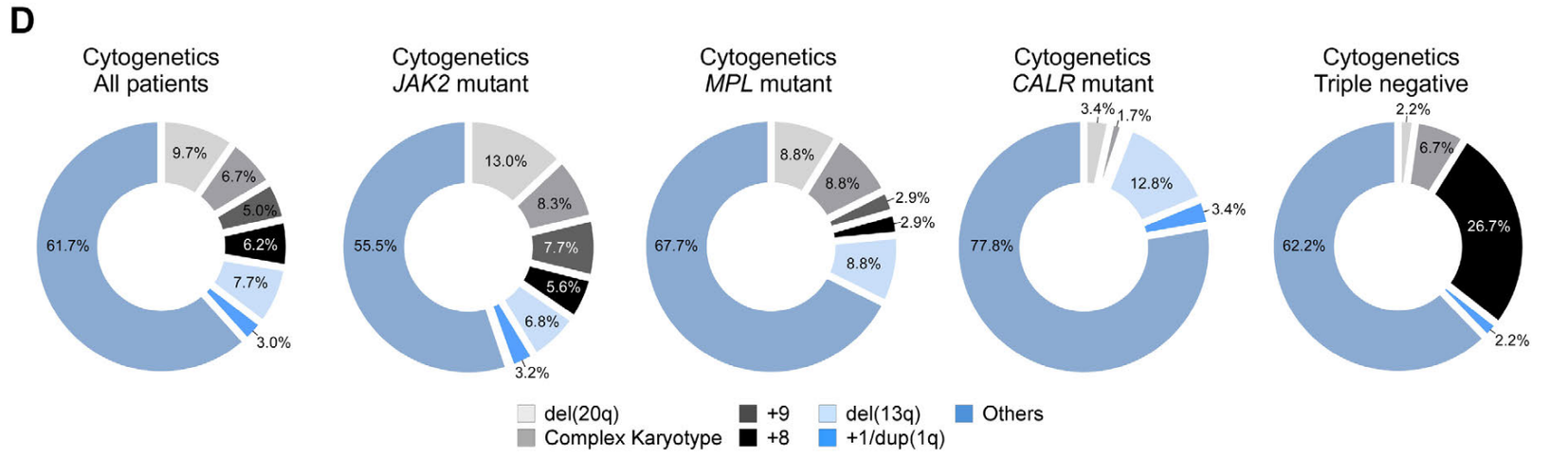

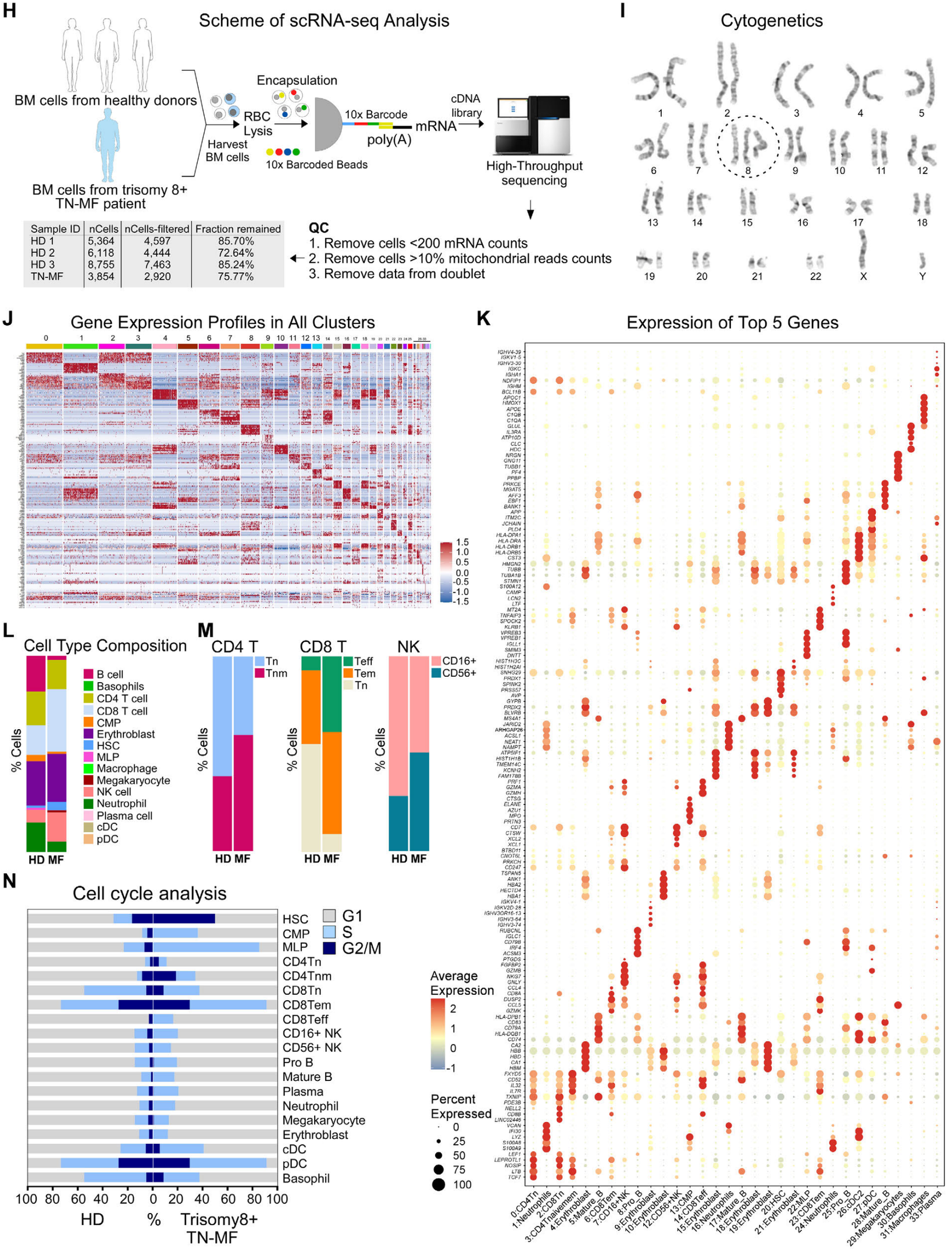
H
Scheme of scRNA-seq Analysis
BM cells from healthy donors
BM cells from trisomy 8+ TN-MF patient
Harvest BM cells
RBC Lysis
Encapsulation
10x Barcoded Beads
10x Barcode
poly(A)
mRNA
cDNA library
High-Throughput sequencing
Sample ID | nCells | nCells-filtered | Fraction remained
HD 1 | 5,364 | 4,597 | 85.70%
HD 2 | 6,118 | 4,444 | 72.64%
HD 3 | 8,755 | 7,463 | 85.24%
TN-MF | 3,854 | 2,920 | 75.77%
QC
1. Remove cells <200 mRNA counts
2. Remove cells >10% mitochondrial reads counts
3. Remove data from doublet
I
Cytogenetics
J
Gene Expression Profiles in All Clusters
K
Expression of Top 5 Genes
L
Cell Type Composition
B cell
Basophils
CD4 T cell
CD8 T cell
CMP
Erythroblast
HSC
MLP
Macrophage
Megakaryocyte
NK cell
Neutrophil
Plasma cell
cDC
pDC
% Cells
HD MF
M
CD4 T
Tn
Tnm
CD8 T
Teff
Tem
Tn
NK
CD16+
CD56+
N
Cell cycle analysis
G1
S
G2/M
HSC
CMP
MLP
CD4Tn
CD4Tnm
CD8Tn
CD8Tem
CD8Teff
CD16+ NK
CD56+ NK
Pro B
Mature B
Plasma
Neutrophil
Megakaryocyte
Erythroblast
cDC
pDC
Basophil
HD % Trisomy8+ TN-MF
Average Expression
Percent Expressed
0:CD4Tn
1:Neutrophils
2:CD8Tn
3:CD4Tnaivemem
4:Erythroblast
5:Mature_B
6:CD8Tem
7:CD16+NK
8:Pro_B
9:Erythroblast
10:Erythroblast
11:CD56+NK
12:CMP
13:CD8Teff
14:CD8Teff
15:Erythroblast
16:Neutrophils
17:Mature_B
18:Erythroblast
19:Erythroblast
20:HSC
21:Erythroblast
22:MLP
23:CD8Tem
24:Neutrophils
25:Pro_B
26:cDC2
27:pDC
28:Mature_B
29:Megakaryocytes
30:Basophils
31:Macrophages
33:Plasma

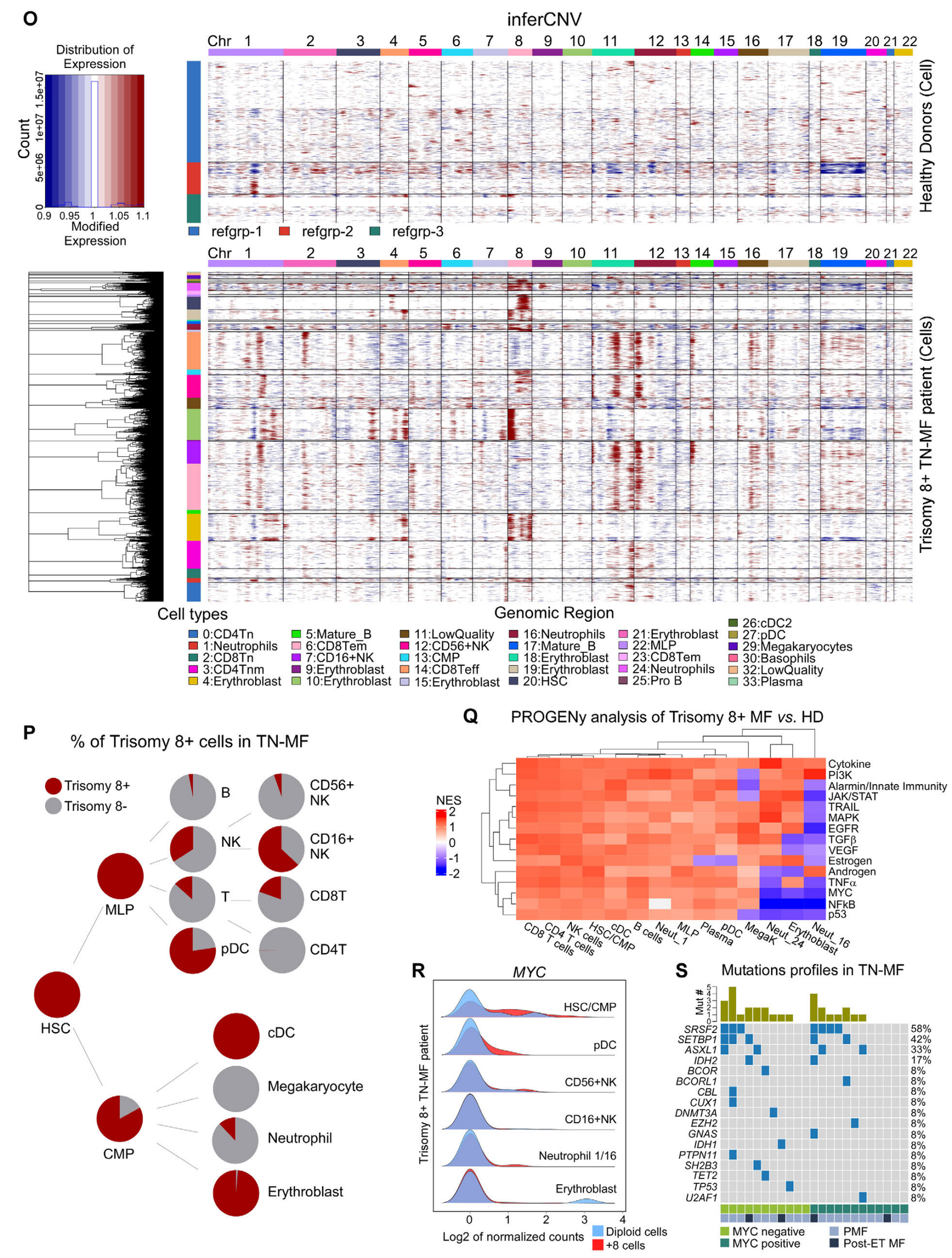
O
inferCNV
Distribution of Expression
Count
Modified Expression
Chr 1 2 3 4 5 6 7 8 9 10 11 12 13 14 15 16 17 18 19 20 21 22
Healthy Donors (Cell)
refgrp-1 refgrp-2 refgrp-3
Trisomy 8+ TN-MF patient (Cells)
Cell types
0:CD4Tn
1:Neutrophils
2:CD8Tn
3:CD4Tnm
4:Erythroblast
5:Mature_B
6:CD8Tem
7:CD16+NK
9:Erythroblast
10:Erythroblast
11:LowQuality
12:CD56+NK
13:CMP
14:CD8Teff
15:Erythroblast
16:Neutrophils
17:Mature_B
18:Erythroblast
19:Erythroblast
20:HSC
21:Erythroblast
22:MLP
23:CD8Tem
24:Neutrophils
25:Pro B
26:cDC2
27:pDC
29:Megakaryocytes
30:Basophils
32:LowQuality
33:Plasma
Genomic Region
P
% of Trisomy 8+ cells in TN-MF
Trisomy 8+
Trisomy 8-
HSC
MLP
CMP
B
NK
T
pDC
CD56+ NK
CD16+ NK
CD8T
CD4T
cDC
Megakaryocyte
Neutrophil
Erythroblast
Q
PROGENy analysis of Trisomy 8+ MF vs. HD
NES
Cytokine
PI3K
Alarmin/Innate Immunity
JAK/STAT
TRAIL
MAPK
EGFR
TGFβ
VEGF
Estrogen
Androgen
TNFα
MYC
NFkB
p53
CD8 T cells
CD4 T cells
NK cells
HSC/CMP
cDC
B cells
Neut_1
MLP
Plasma
pDC
MegaK
Neut_24
Erythoblast
Neut_16
R
MYC
Trisomy 8+ TN-MF patient
HSC/CMP
pDC
CD56+NK
CD16+NK
Neutrophil 1/16
Erythroblast
Log2 of normalized counts
Diploid cells
+8 cells
S
Mutations profiles in TN-MF
Mut #
SRSF2 58%
SETBP1 42%
ASXL1 33%
IDH2 17%
BCOR 8%
BCORL1 8%
CBL 8%
CUX1 8%
DNMT3A 8%
EZH2 8%
GNAS 8%
IDH1 8%
PTPN11 8%
SH2B3 8%
TET2 8%
TP53 8%
U2AF1 8%
MYC negative
MYC positive
PMF
Post-ET MF

Figure 2

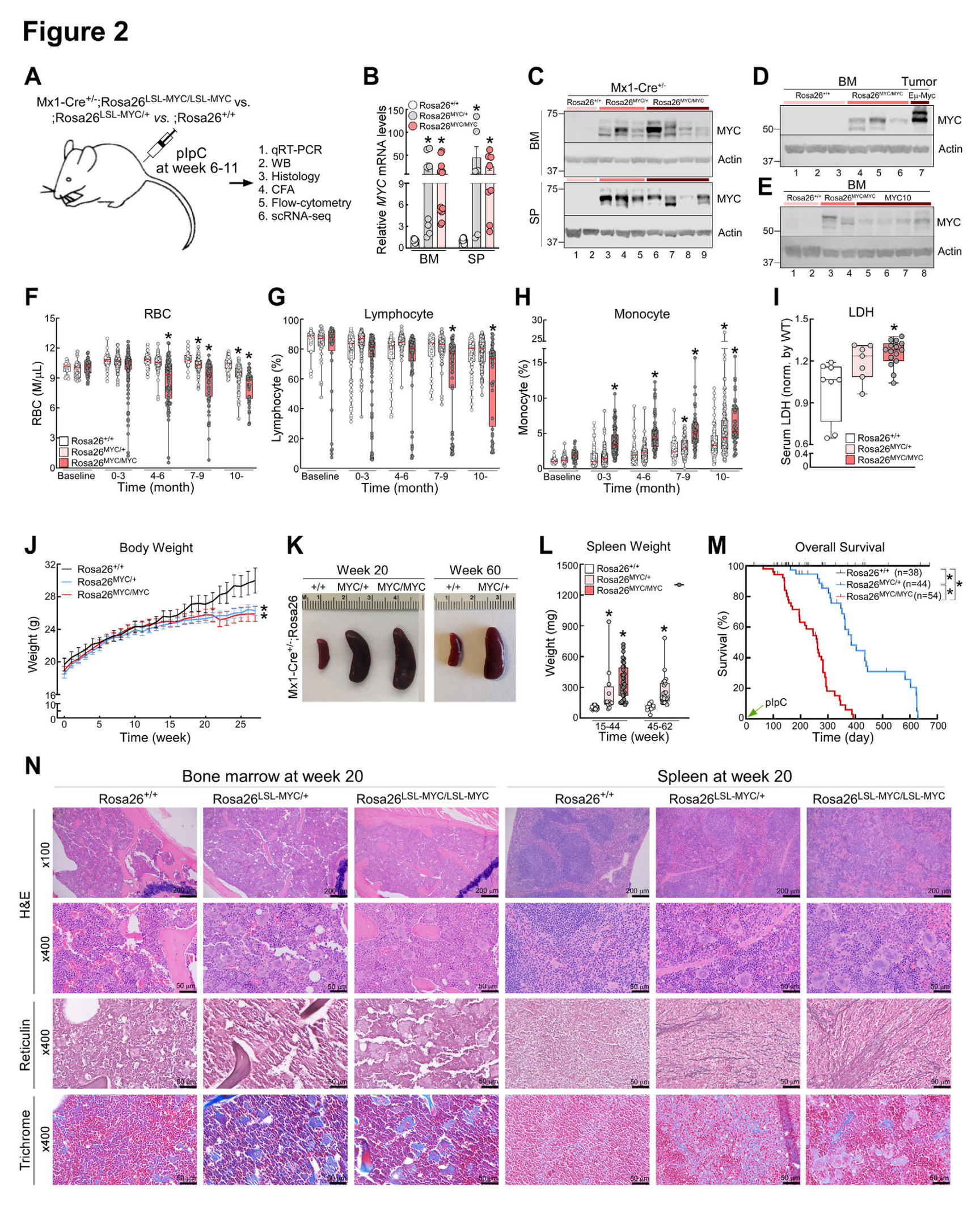
A
Mx1-Cre+/-;Rosa26LSL-MYC/LSL-MYC vs.
;Rosa26LSL-MYC/+ vs. ;Rosa26+/+
pIpC
at week 6-11
1. qRT-PCR
2. WB
3. Histology
4. CFA
5. Flow-cytometry
6. scRNA-seq
B
Relative MYC mRNA levels
Rosa26+/+
Rosa26MYC/+
Rosa26MYC/MYC
BM
SP
C
Mx1-Cre+/-
BM
SP
MYC
Actin
D
BM
Tumor
Eμ-Myc
E
MYC10
F
RBC
RBC (M/μL)
Time (month)
G
Lymphocyte
Lymphocyte (%)
H
Monocyte
Monocyte (%)
I
LDH
Serum LDH (norm. by WT)
J
Body Weight
Weight (g)
Time (week)
K
Week 20
Week 60
Mx1-Cre+/-;Rosa26
L
Spleen Weight
Weight (mg)
15-44
45-62
M
Overall Survival
Survival (%)
Rosa26+/+ (n=38)
Rosa26MYC/+ (n=44)
Rosa26MYC/MYC (n=54)
pIpC
Time (day)
N
Bone marrow at week 20
Spleen at week 20
Rosa26+/+
Rosa26LSL-MYC/+
Rosa26LSL-MYC/LSL-MYC
H&E
Reticulin
Trichrome
x100
x400

Figure S2

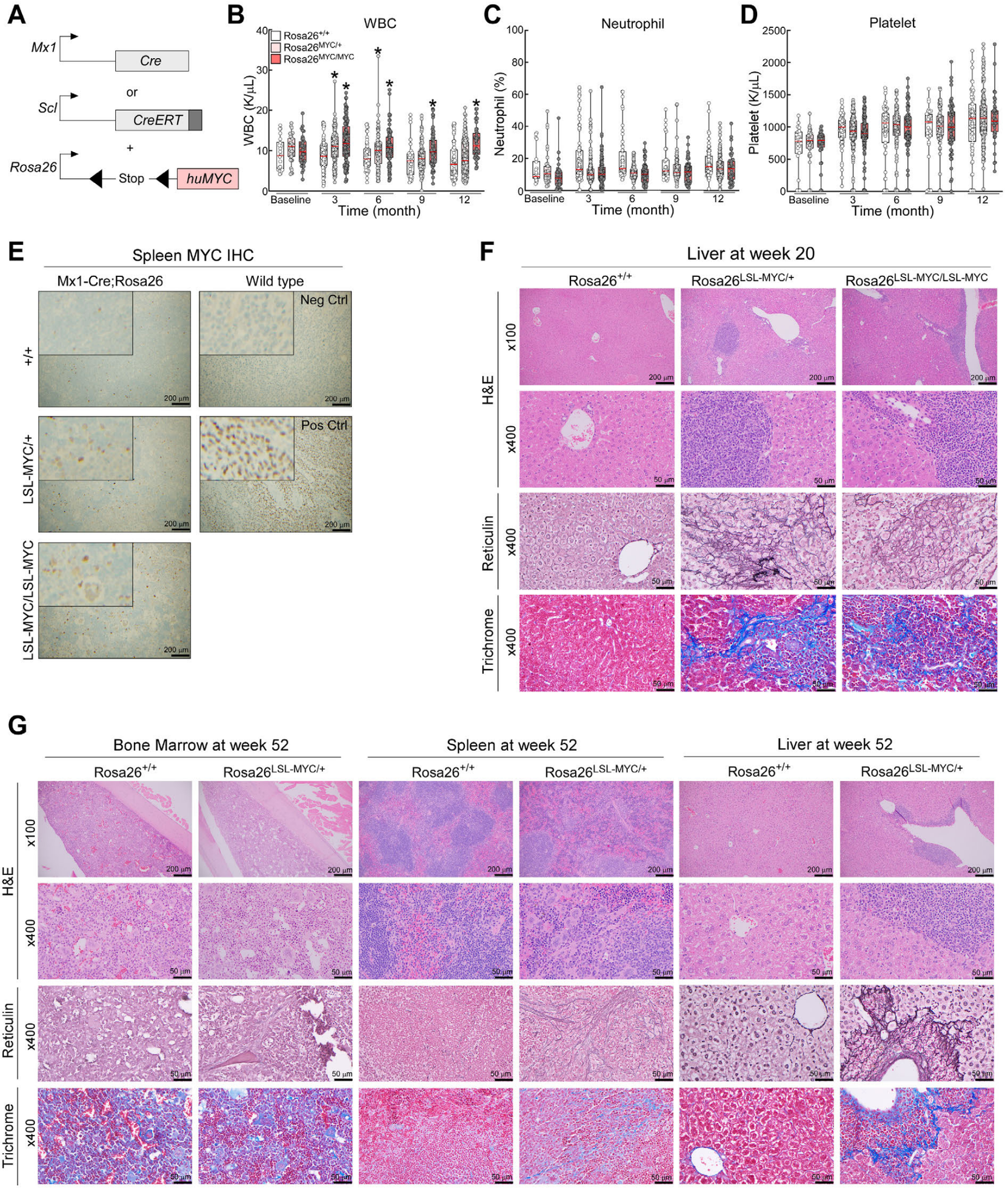
A
Mx1
Cre
or
Scl
CreERT
+
Rosa26
Stop
huMYC
B
WBC
Rosa26+/+
Rosa26MYC/+
Rosa26MYC/MYC
WBC (K/μL)
Baseline
3
6
9
12
Time (month)
C
Neutrophil
Neutrophil (%)
Time (month)
D
Platelet
Platelet (K/μL)
Time (month)
E
Spleen MYC IHC
Mx1-Cre;Rosa26
Wild type
Neg Ctrl
Pos Ctrl
+/+
LSL-MYC/+
LSL-MYC/LSL-MYC
200 μm
F
Liver at week 20
Rosa26+/+
Rosa26LSL-MYC/+
Rosa26LSL-MYC/LSL-MYC
H&E
x100
x400
Reticulin
Trichrome
200 μm
50 μm
G
Bone Marrow at week 52
Spleen at week 52
Liver at week 52
Rosa26+/+
Rosa26LSL-MYC/+
H&E
x100
x400
Reticulin
Trichrome
200 μm
50 μm

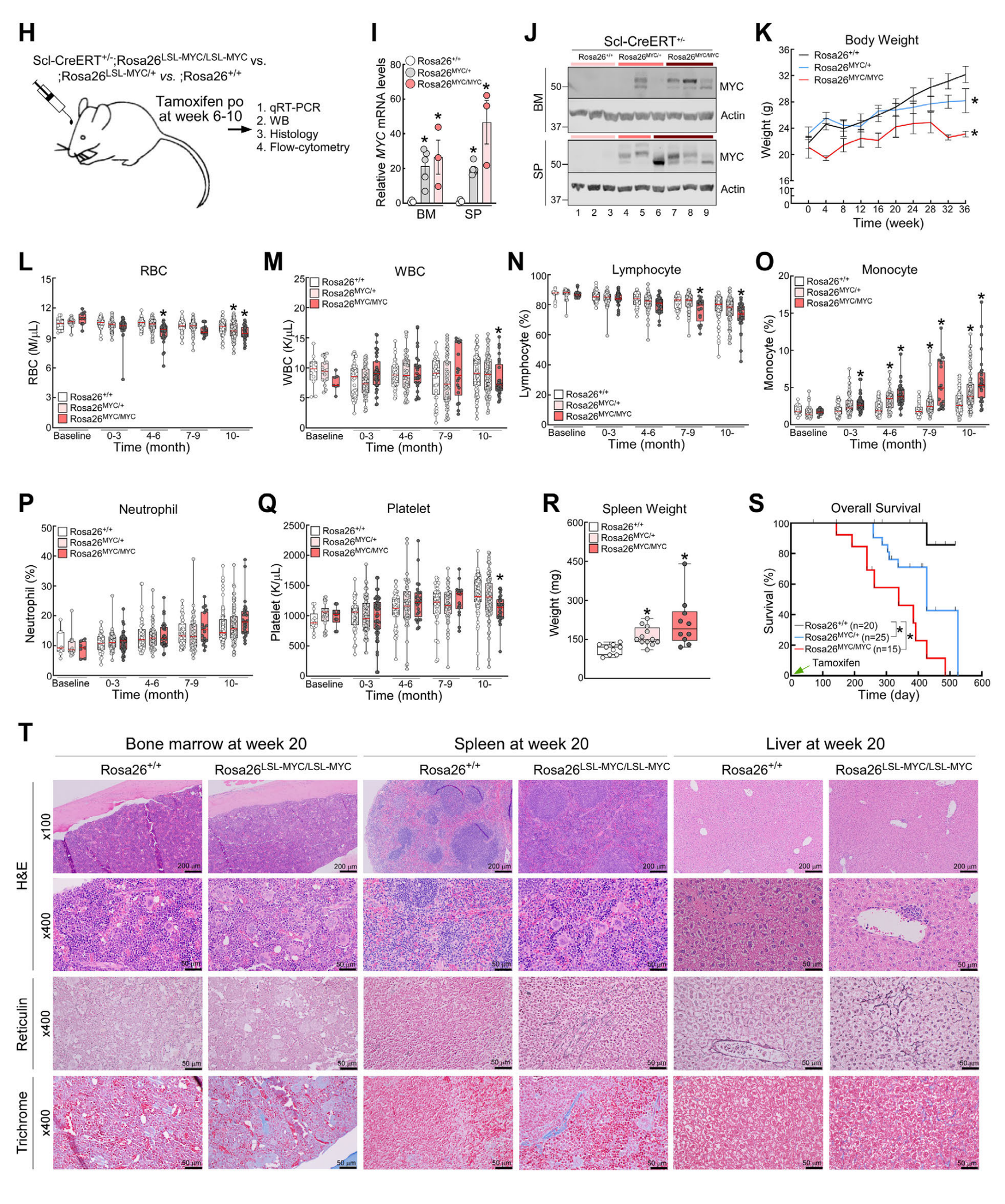
H
Scl-CreERT+/-;Rosa26LSL-MYC/LSL-MYC vs.
;Rosa26LSL-MYC/+ vs. ;Rosa26+/+
Tamoxifen po
at week 6-10
1. qRT-PCR
2. WB
3. Histology
4. Flow-cytometry
I
Relative MYC mRNA levels
Rosa26+/+
Rosa26MYC/+
Rosa26MYC/MYC
BM
SP
J
Scl-CreERT+/-
Rosa26+/+
Rosa26MYC/+
Rosa26MYC/MYC
BM
SP
MYC
Actin
K
Body Weight
Weight (g)
Time (week)
L
RBC
RBC (M/μL)
Time (month)
M
WBC
WBC (K/μL)
N
Lymphocyte
Lymphocyte (%)
O
Monocyte
Monocyte (%)
P
Neutrophil
Neutrophil (%)
Q
Platelet
Platelet (K/μL)
R
Spleen Weight
Weight (mg)
S
Overall Survival
Survival (%)
Rosa26+/+ (n=20)
Rosa26MYC/+ (n=25)
Rosa26MYC/MYC (n=15)
Tamoxifen
Time (day)
T
Bone marrow at week 20
Spleen at week 20
Liver at week 20
Rosa26+/+
Rosa26LSL-MYC/LSL-MYC
H&E
Reticulin
Trichrome
x100
x400
200 μm
50 μm

Figure 3

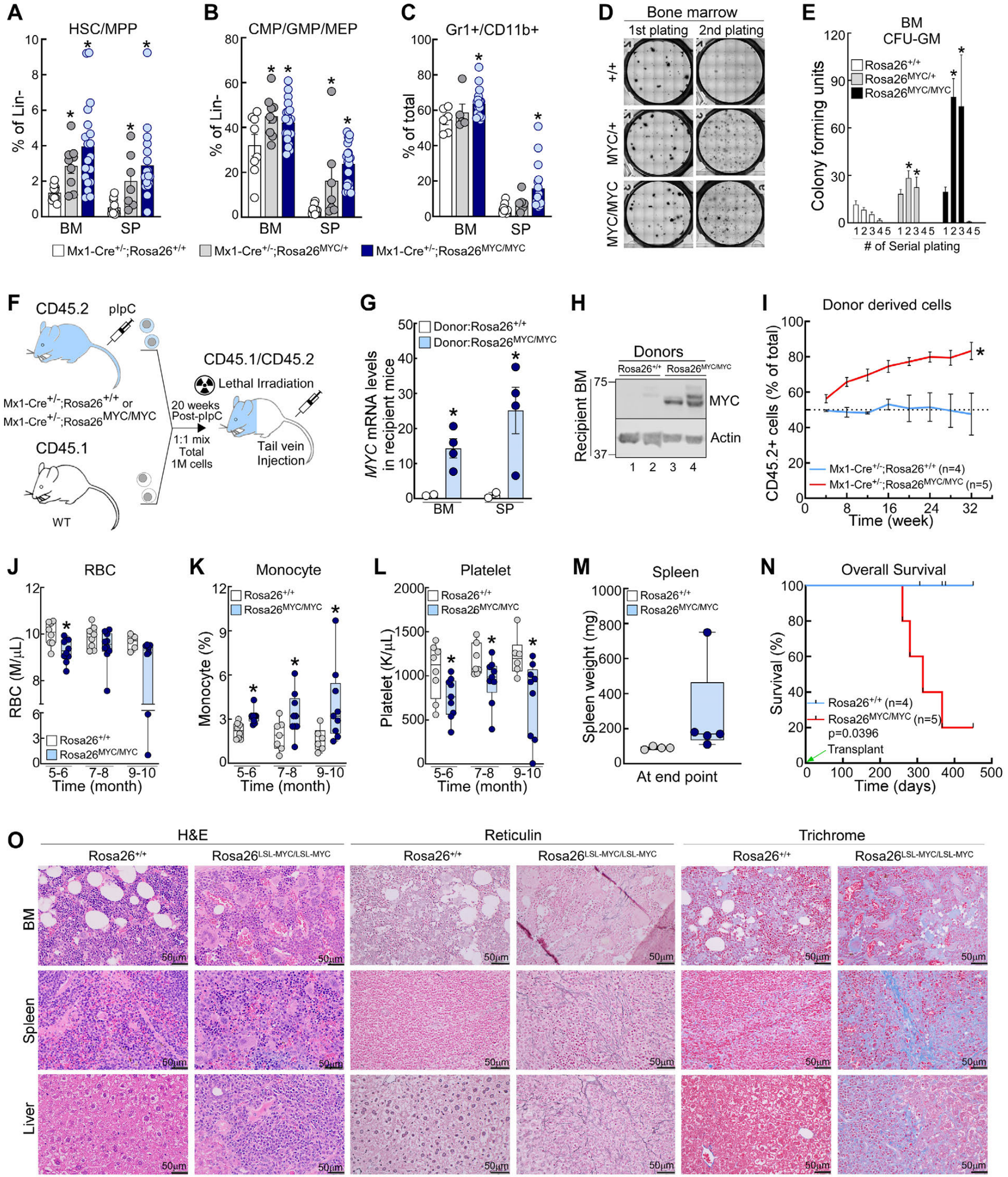
A
HSC/MPP
% of Lin-
BM
SP
B
CMP/GMP/MEP
% of Lin-
C
Gr1+/CD11b+
% of total
Mx1-Cre+/-;Rosa26+/+
Mx1-Cre+/-;Rosa26MYC/+
Mx1-Cre+/-;Rosa26MYC/MYC
D
Bone marrow
1st plating
2nd plating
+/+
MYC/+
MYC/MYC
E
BM
CFU-GM
Rosa26+/+
Rosa26MYC/+
Rosa26MYC/MYC
Colony forming units
# of Serial plating
F
CD45.2
pIpC
Mx1-Cre+/-;Rosa26+/+ or
Mx1-Cre+/-;Rosa26MYC/MYC
CD45.1/CD45.2
Lethal Irradiation
20 weeks
Post-pIpC
1:1 mix
Total
1M cells
Tail vein
Injection
CD45.1
WT
G
Donor:Rosa26+/+
Donor:Rosa26MYC/MYC
MYC mRNA levels
in recipient mice
BM
SP
H
Donors
Rosa26+/+
Rosa26MYC/MYC
Recipient BM
MYC
Actin
I
Donor derived cells
CD45.2+ cells (% of total)
Mx1-Cre+/-;Rosa26+/+ (n=4)
Mx1-Cre+/-;Rosa26MYC/MYC (n=5)
Time (week)
J
RBC
RBC (M/μL)
Rosa26+/+
Rosa26MYC/MYC
5-6
7-8
9-10
Time (month)
K
Monocyte
Monocyte (%)
L
Platelet
Platelet (K/μL)
M
Spleen
Spleen weight (mg)
At end point
N
Overall Survival
Survival (%)
Rosa26+/+ (n=4)
Rosa26MYC/MYC (n=5)
p=0.0396
Transplant
Time (days)
O
H&E
Reticulin
Trichrome
Rosa26+/+
Rosa26LSL-MYC/LSL-MYC
BM
Spleen
Liver
50μm

Figure S3

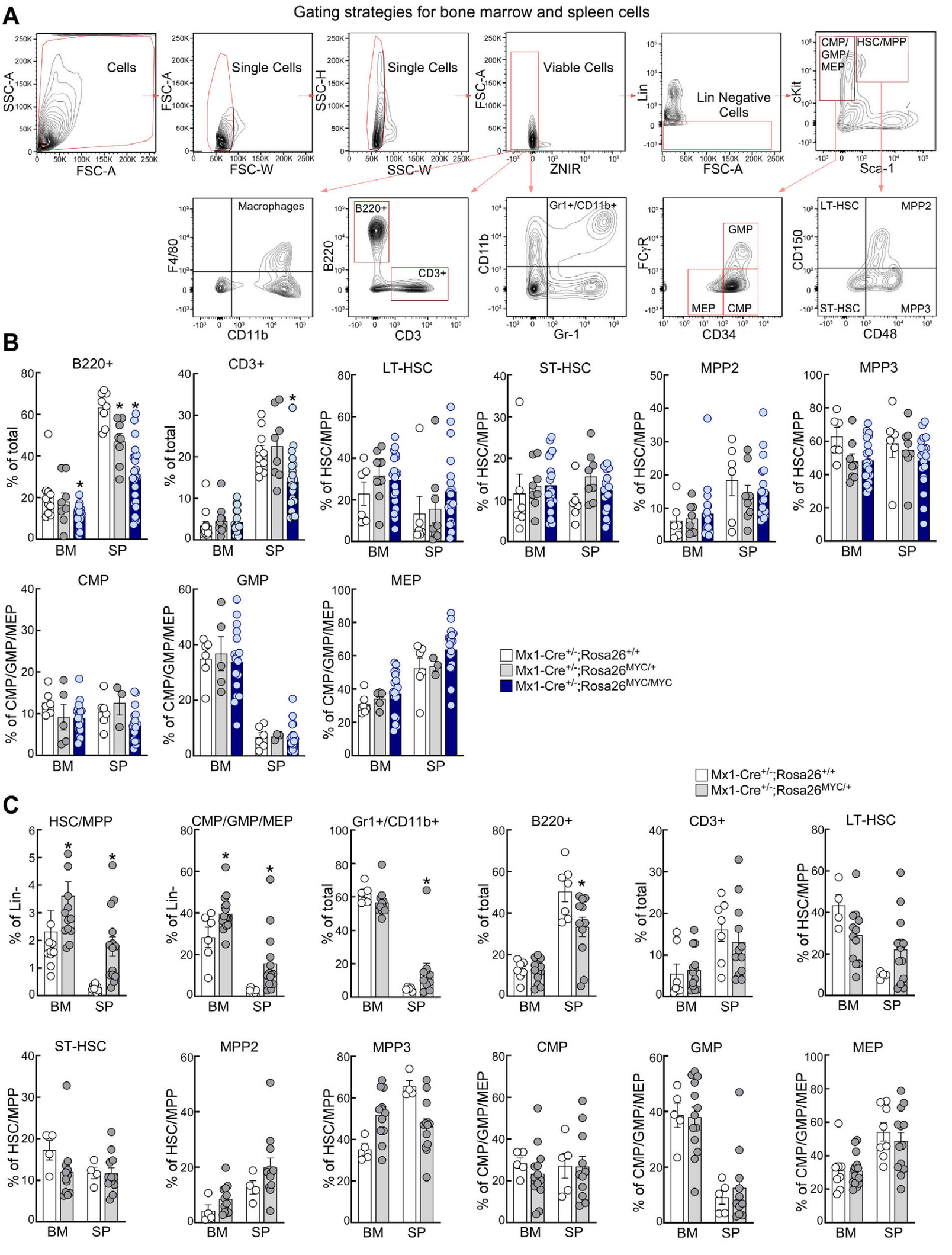
A
Gating strategies for bone marrow and spleen cells
Cells
Single Cells
Single Cells
Viable Cells
Lin Negative Cells
CMP/ GMP/ MEP
HSC/MPP
Macrophages
B220+
CD3+
Gr1+/CD11b+
GMP
MEP
CMP
LT-HSC
MPP2
ST-HSC
MPP3
B
B220+
CD3+
LT-HSC
ST-HSC
MPP2
MPP3
CMP
GMP
MEP
% of total
% of HSC/MPP
% of CMP/GMP/MEP
BM
SP
Mx1-Cre+/-;Rosa26+/+
Mx1-Cre+/-;Rosa26MYC/+
Mx1-Cre+/-;Rosa26MYC/MYC
C
HSC/MPP
CMP/GMP/MEP
Gr1+/CD11b+
B220+
CD3+
LT-HSC
ST-HSC
MPP2
MPP3
CMP
GMP
MEP
% of Lin-
% of total
% of HSC/MPP
% of CMP/GMP/MEP
BM
SP
Mx1-Cre+/-;Rosa26+/+
Mx1-Cre+/-;Rosa26MYC/+

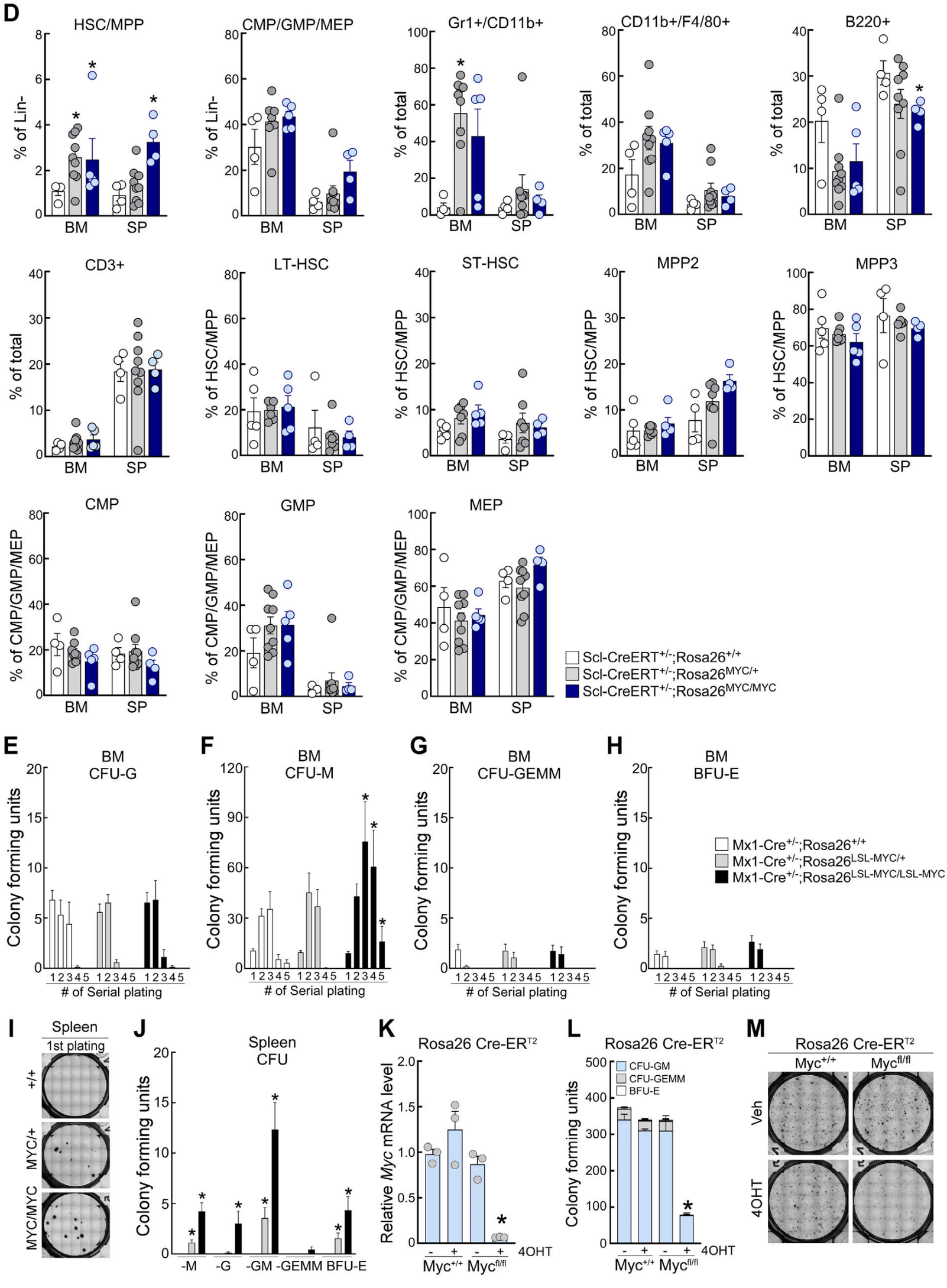
D
HSC/MPP
CMP/GMP/MEP
Gr1+/CD11b+
CD11b+/F4/80+
B220+
CD3+
LT-HSC
ST-HSC
MPP2
MPP3
CMP
GMP
MEP
% of Lin-
% of total
% of HSC/MPP
% of CMP/GMP/MEP
BM
SP
Scl-CreERT+/-;Rosa26+/+
Scl-CreERT+/-;Rosa26MYC/+
Scl-CreERT+/-;Rosa26MYC/MYC
E
BM
CFU-G
F
BM
CFU-M
G
BM
CFU-GEMM
H
BM
BFU-E
Colony forming units
# of Serial plating
Mx1-Cre+/-;Rosa26+/+
Mx1-Cre+/-;Rosa26LSL-MYC/+
Mx1-Cre+/-;Rosa26LSL-MYC/LSL-MYC
I
Spleen
1st plating
+/+
MYC/+
MYC/MYC
J
Spleen
CFU
Colony forming units
-M
-G
-GM
-GEMM
BFU-E
K
Rosa26 Cre-ERT2
Relative Myc mRNA level
4OHT
Myc+/+
Mycfl/fl
L
Rosa26 Cre-ERT2
Colony forming units
CFU-GM
CFU-GEMM
BFU-E
4OHT
Myc+/+
Mycfl/fl
M
Rosa26 Cre-ERT2
Myc+/+
Mycfl/fl
Veh
4OHT

Figure 4

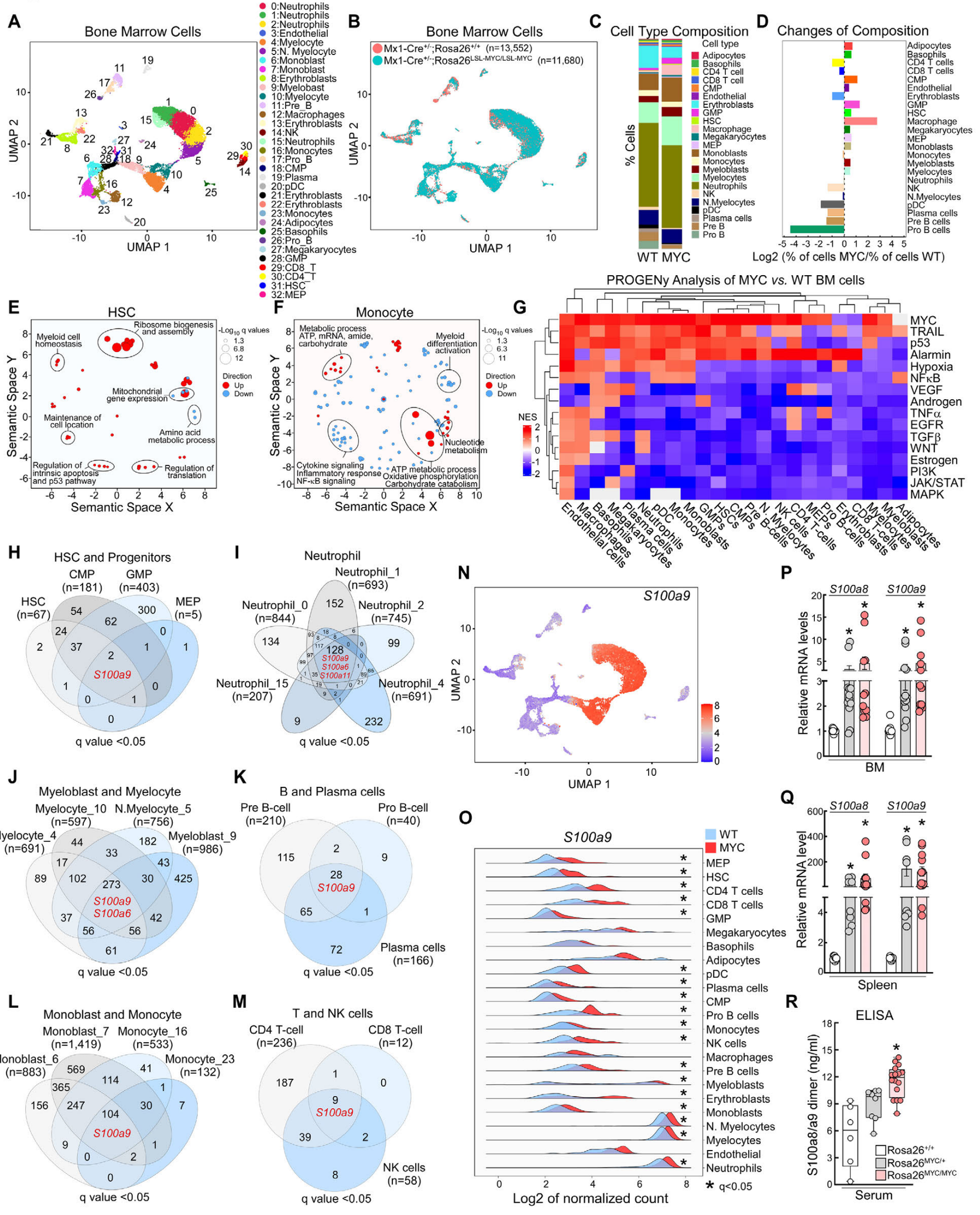
A
Bone Marrow Cells
UMAP 1
UMAP 2
0:Neutrophils
1:Neutrophils
2:Neutrophils
3:Endothelial
4:Myelocyte
5:N. Myelocyte
6:Monoblast
7:Monoblast
8:Erythroblasts
9:Myelobast
10:Myelocyte
11:Pre_B
12:Macrophages
13:Erythroblasts
14:NK
15:Neutrophils
16:Monocytes
17:Pro_B
18:CMP
19:Plasma
20:pDC
21:Erythroblasts
22:Erythroblasts
23:Monocytes
24:Adipocytes
25:Basophils
26:Pro_B
27:Megakaryocytes
28:GMP
29:CD8_T
30:CD4_T
31:HSC
32:MEP
B
Bone Marrow Cells
Mx1-Cre+/-;Rosa26+/+ (n=13,552)
Mx1-Cre+/-;Rosa26LSL-MYC/LSL-MYC (n=11,680)
C
Cell Type Composition
% Cells
WT MYC
Cell type
Adipocytes
Basophils
CD4 T cell
CD8 T cell
CMP
Endothelial
Erythroblasts
GMP
HSC
Macrophage
Megakaryocytes
MEP
Monoblasts
Monocytes
Myeloblasts
Myelocytes
Neutrophils
NK
N.Myelocytes
pDC
Plasma cells
Pre B
Pro B
D
Changes of Composition
Log2 (% of cells MYC/% of cells WT)
E
HSC
Semantic Space X
Semantic Space Y
Myeloid cell homeostasis
Ribosome biogenesis and assembly
Mitochondrial gene expression
Maintenance of cell location
Amino acid metabolic process
Regulation of intrinsic apoptosis and p53 pathway
Regulation of translation
-Log10 q values
Direction
Up
Down
F
Monocyte
Metabolic process ATP, mRNA, amide, carbohydrate
Myeloid differentiation activation
Nucleotide metabolism
Cytokine signaling
Inflammatory response
NF-κB signaling
ATP metabolic process
Oxidative phosphorylation
Carbohydrate catabolism
G
PROGENy Analysis of MYC vs. WT BM cells
NES
MYC
TRAIL
p53
Alarmin
Hypoxia
NFκB
VEGF
Androgen
TNFα
EGFR
TGFβ
WNT
Estrogen
PI3K
JAK/STAT
MAPK
Endothelial cells
Macrophages
Basophils
Megakaryocytes
Plasma cells
Neutrophils
pDC
Monocytes
Monoblasts
GMPs
HSCs
CMPs
Pre B-cells
N. Myelocytes
NK cells
CD4 T-cells
MEPs
Pro B-cells
Erythroblasts
CD8 T-cells
Myelocytes
Myeloblasts
Adipocytes
H
HSC and Progenitors
HSC (n=67)
CMP (n=181)
GMP (n=403)
MEP (n=5)
S100a9
q value <0.05
I
Neutrophil
Neutrophil_0 (n=844)
Neutrophil_1 (n=693)
Neutrophil_2 (n=745)
Neutrophil_15 (n=207)
Neutrophil_4 (n=691)
S100a9
S100a6
S100a11
q value <0.05
N
S100a9
UMAP 1
UMAP 2
P
S100a8
S100a9
Relative mRNA levels
BM
J
Myeloblast and Myelocyte
Myelocyte_10 (n=597)
N.Myelocyte_5 (n=756)
Myelocyte_4 (n=691)
Myeloblast_9 (n=986)
S100a9
S100a6
q value <0.05
K
B and Plasma cells
Pre B-cell (n=210)
Pro B-cell (n=40)
Plasma cells (n=166)
S100a9
q value <0.05
O
S100a9
WT
MYC
Log2 of normalized count
* q<0.05
Q
S100a8
S100a9
Relative mRNA level
Spleen
L
Monoblast and Monocyte
Monoblast_7 (n=1,419)
Monocyte_16 (n=533)
Monoblast_6 (n=883)
Monocyte_23 (n=132)
S100a9
q value <0.05
M
T and NK cells
CD4 T-cell (n=236)
CD8 T-cell (n=12)
NK cells (n=58)
S100a9
q value <0.05
R
ELISA
S100a8/a9 dimer (ng/ml)
Rosa26+/+
Rosa26MYC/+
Rosa26MYC/MYC
Serum

Figure S4

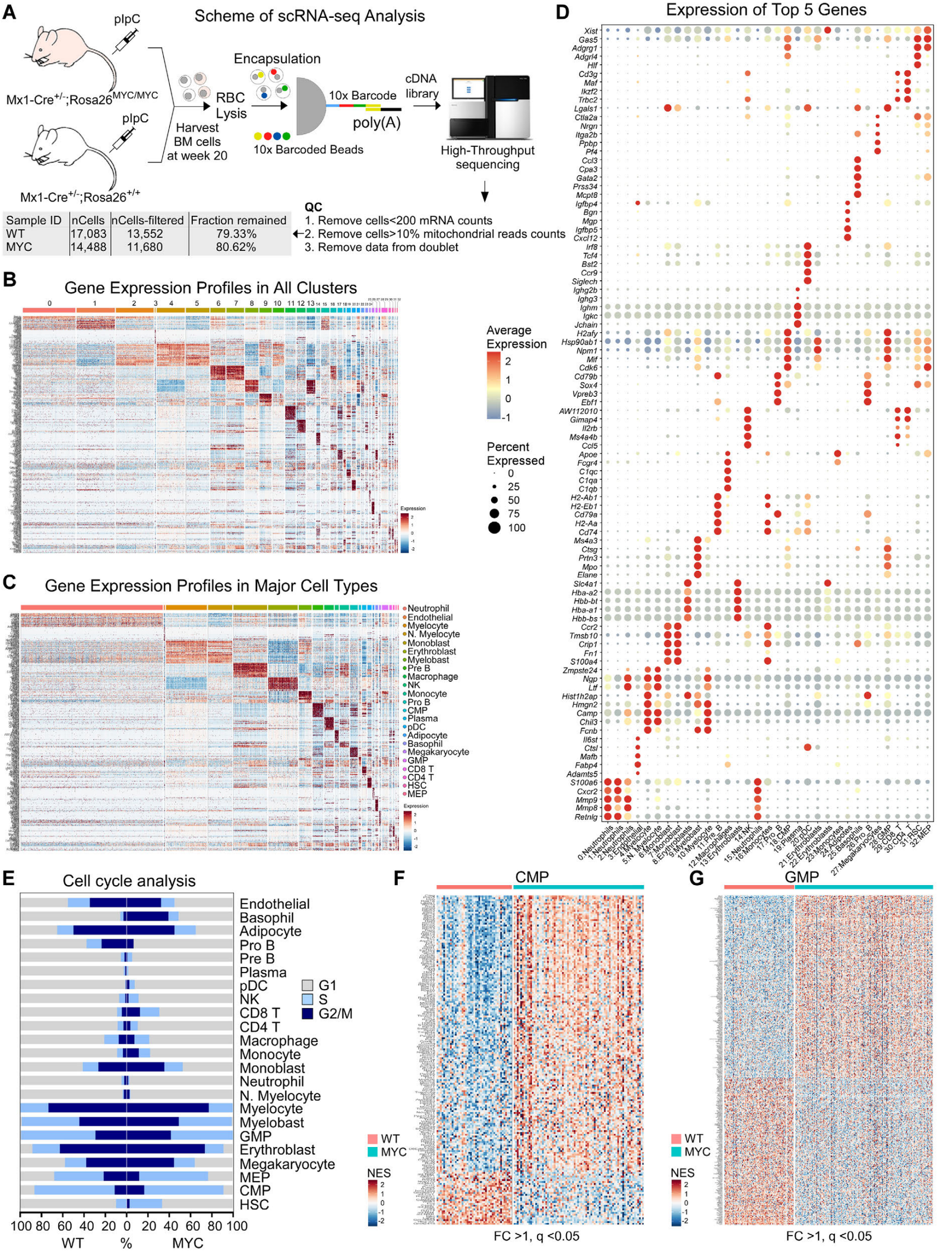
A
Scheme of scRNA-seq Analysis
pIpC
Mx1-Cre+/-;Rosa26MYC/MYC
pIpC
Mx1-Cre+/-;Rosa26+/+
Harvest BM cells at week 20
RBC Lysis
Encapsulation
10x Barcoded Beads
10x Barcode
poly(A)
cDNA library
High-Throughput sequencing
QC
1. Remove cells<200 mRNA counts
2. Remove cells>10% mitochondrial reads counts
3. Remove data from doublet
Sample ID | nCells | nCells-filtered | Fraction remained
WT | 17,083 | 13,552 | 79.33%
MYC | 14,488 | 11,680 | 80.62%
B
Gene Expression Profiles in All Clusters
Average Expression
Percent Expressed
C
Gene Expression Profiles in Major Cell Types
Neutrophil
Endothelial
Myelocyte
N. Myelocyte
Monoblast
Erythroblast
Myelobast
Pre B
Macrophage
NK
Monocyte
Pro B
CMP
Plasma
pDC
Adipocyte
Basophil
Megakaryocyte
GMP
CD8 T
CD4 T
HSC
MEP
D
Expression of Top 5 Genes
Xist
Gas5
Adgrg1
Adgrl4
Hlf
Cd3g
Maf
Ikzf2
Trbc2
Lgals1
Ctla2a
Nrgn
Itga2b
Ppbp
Pf4
Ccl3
Cpa3
Gata2
Prss34
Mcpt8
Igfbp4
Bgn
Mgp
Igfbp5
Cxcl12
Irf8
Tcf4
Bst2
Ccr9
Siglech
Ighg2b
Ighg3
Ighm
Igkc
Jchain
H2afy
Hsp90ab1
Npm1
Mif
Cdk6
Cd79b
Sox4
Vpreb3
Ebf1
AW112010
Gimap4
Il2rb
Ms4a4b
Ccl5
Apoe
Fcgr4
C1qc
C1qa
C1qb
H2-Ab1
H2-Eb1
Cd79a
H2-Aa
Cd74
Ms4a3
Ctsg
Prtn3
Mpo
Elane
Slc4a1
Hba-a2
Hbb-bt
Hba-a1
Hbb-bs
Ccr2
Tmsb10
Crip1
Fn1
S100a4
Zmpste24
Ngp
Ltf
Hist1h2ap
Hmgn2
Camp
Chil3
Fcnb
Il6st
Ctsl
Mafb
Fabp4
Adamts5
S100a6
Cxcr2
Mmp9
Mmp8
Retnlg
0.Neutrophils
1.Neutrophils
2.Neutrophils
3.Endothelial
4.Myelocyte
5.N. Myelocyte
6.Monoblast
7.Monoblast
8.Erythroblasts
9.Myelobast
10.Myelocyte
11.Pre B
12.Macrophages
13.Erythroblasts
14.NK
15.Neutrophils
16.Monocytes
17.Pro B
18.CMP
19.Plasma
20.pDC
21.Erythroblasts
22.Erythroblasts
23.Monocytes
24.Adipocytes
25.Basophils
26.Pro B
27.Megakaryocytes
28.GMP
29.CD8 T
30.CD4 T
31.HSC
32.MEP
E
Cell cycle analysis
Endothelial
Basophil
Adipocyte
Pro B
Pre B
Plasma
pDC
NK
CD8 T
CD4 T
Macrophage
Monocyte
Monoblast
Neutrophil
N. Myelocyte
Myelocyte
Myelobast
GMP
Erythroblast
Megakaryocyte
MEP
CMP
HSC
G1
S
G2/M
100 80 60 40 20 0 20 40 60 80 100
WT % MYC
F
CMP
WT
MYC
NES
FC >1, q <0.05
G
GMP
WT
MYC
NES
FC >1, q <0.05

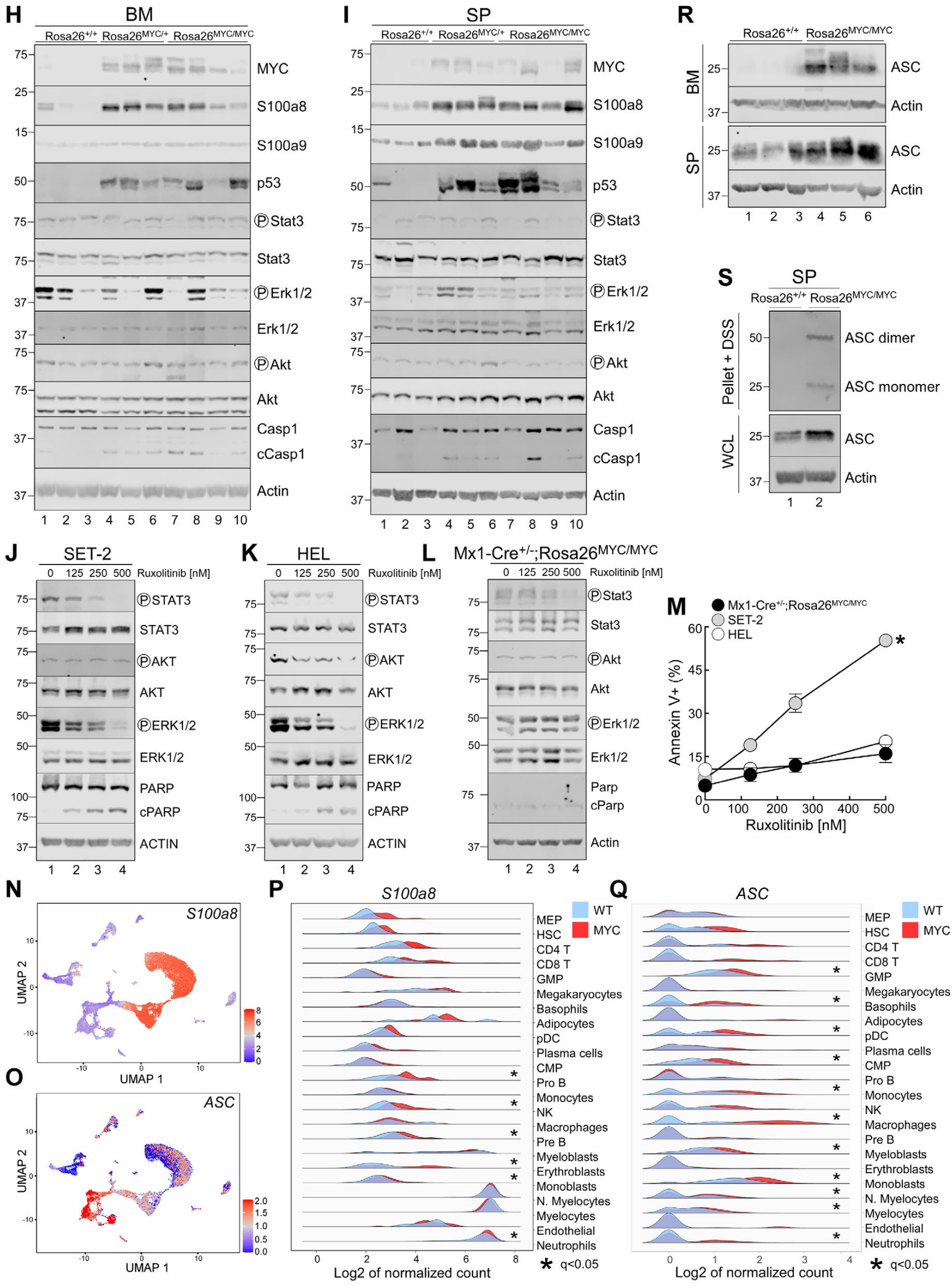
H
BM
Rosa26+/+ Rosa26MYC/+ Rosa26MYC/MYC
MYC
S100a8
S100a9
p53
ⓅStat3
Stat3
ⓅErk1/2
Erk1/2
ⓅAkt
Akt
Casp1
cCasp1
Actin
1 2 3 4 5 6 7 8 9 10
I
SP
Rosa26+/+ Rosa26MYC/+ Rosa26MYC/MYC
MYC
S100a8
S100a9
p53
ⓅStat3
Stat3
ⓅErk1/2
Erk1/2
ⓅAkt
Akt
Casp1
cCasp1
Actin
1 2 3 4 5 6 7 8 9 10
R
Rosa26+/+ Rosa26MYC/MYC
BM
SP
ASC
Actin
1 2 3 4 5 6
S
SP
Rosa26+/+ Rosa26MYC/MYC
Pellet + DSS
WCL
ASC dimer
ASC monomer
ASC
Actin
1 2
J
SET-2
0 125 250 500 Ruxolitinib [nM]
ⓅSTAT3
STAT3
ⓅAKT
AKT
ⓅERK1/2
ERK1/2
PARP
cPARP
ACTIN
1 2 3 4
K
HEL
0 125 250 500 Ruxolitinib [nM]
ⓅSTAT3
STAT3
ⓅAKT
AKT
ⓅERK1/2
ERK1/2
PARP
cPARP
ACTIN
1 2 3 4
L
Mx1-Cre+/-;Rosa26MYC/MYC
0 125 250 500 Ruxolitinib [nM]
ⓅStat3
Stat3
ⓅAkt
Akt
ⓅErk1/2
Erk1/2
Parp
cParp
Actin
1 2 3 4
M
Mx1-Cre+/-;Rosa26MYC/MYC
SET-2
HEL
Annexin V+ (%)
Ruxolitinib [nM]
N
S100a8
UMAP 2
UMAP 1
O
ASC
UMAP 2
UMAP 1
P
S100a8
WT
MYC
MEP
HSC
CD4 T
CD8 T
GMP
Megakaryocytes
Basophils
Adipocytes
pDC
Plasma cells
CMP
Pro B
Monocytes
NK
Macrophages
Pre B
Myeloblasts
Erythroblasts
Monoblasts
N. Myelocytes
Myelocytes
Endothelial
Neutrophils
Log2 of normalized count
* q<0.05
Q
ASC
WT
MYC
Log2 of normalized count
* q<0.05

Figure 5

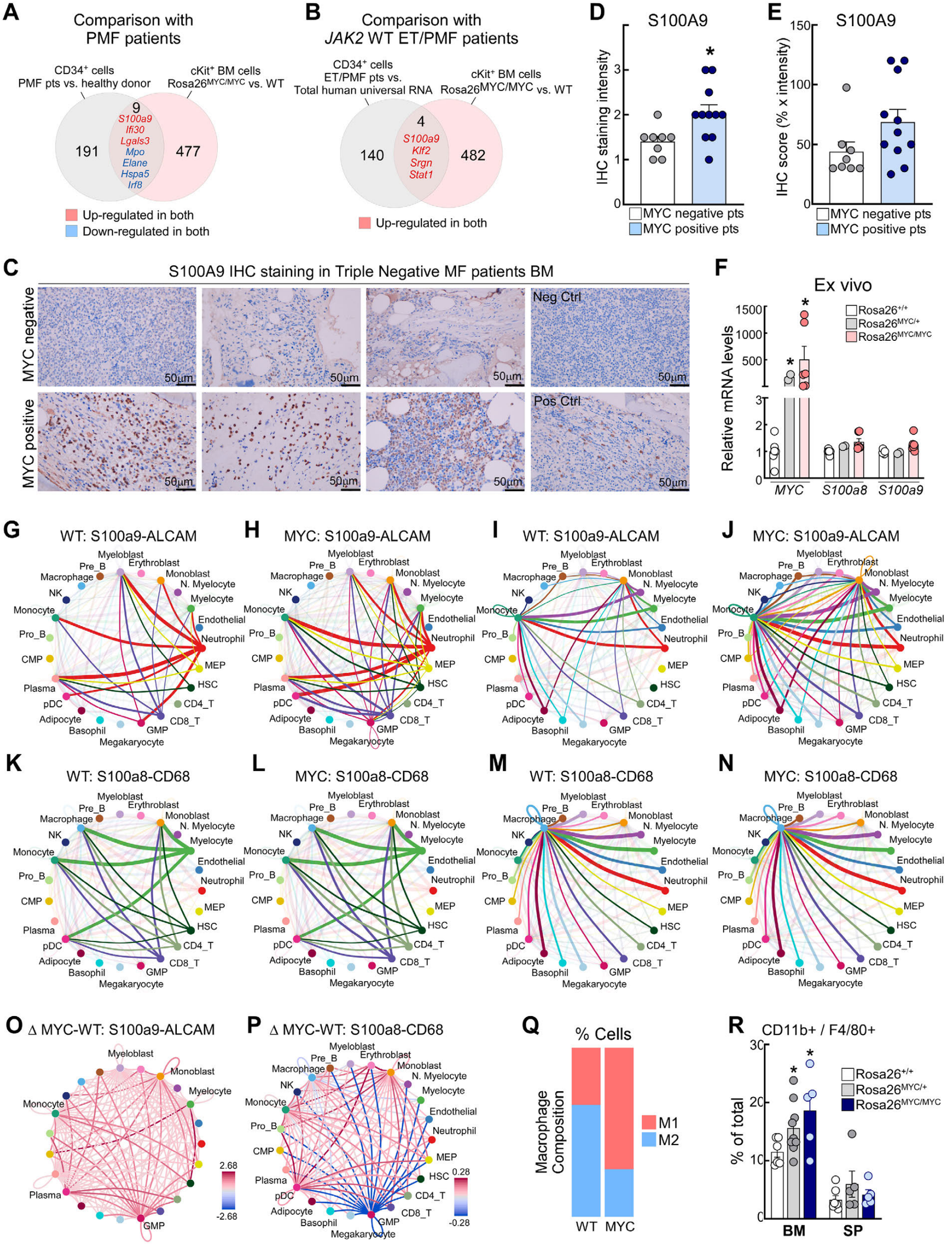
A
Comparison with PMF patients
CD34+ cells PMF pts vs. healthy donor
cKit+ BM cells Rosa26MYC/MYC vs. WT
191
9
S100a9
Ifi30
Lgals3
Mpo
Elane
Hspa5
Irf8
477
Up-regulated in both
Down-regulated in both
B
Comparison with JAK2 WT ET/PMF patients
CD34+ cells ET/PMF pts vs. Total human universal RNA
cKit+ BM cells Rosa26MYC/MYC vs. WT
140
4
S100a9
Klf2
Srgn
Stat1
482
Up-regulated in both
D
S100A9
IHC staining intensity
MYC negative pts
MYC positive pts
E
S100A9
IHC score (% x intensity)
MYC negative pts
MYC positive pts
C
S100A9 IHC staining in Triple Negative MF patients BM
MYC negative
MYC positive
Neg Ctrl
Pos Ctrl
50µm
F
Ex vivo
Relative mRNA levels
Rosa26+/+
Rosa26MYC/+
Rosa26MYC/MYC
MYC
S100a8
S100a9
G
WT: S100a9-ALCAM
H
MYC: S100a9-ALCAM
I
WT: S100a9-ALCAM
J
MYC: S100a9-ALCAM
K
WT: S100a8-CD68
L
MYC: S100a8-CD68
M
WT: S100a8-CD68
N
MYC: S100a8-CD68
Myeloblast
Pre_B
Erythroblast
Macrophage
Monoblast
NK
N. Myelocyte
Monocyte
Myelocyte
Endothelial
Pro_B
Neutrophil
CMP
MEP
Plasma
HSC
pDC
CD4_T
Adipocyte
CD8_T
Basophil
GMP
Megakaryocyte
O
Δ MYC-WT: S100a9-ALCAM
2.68
-2.68
P
Δ MYC-WT: S100a8-CD68
0.28
-0.28
Q
% Cells
Macrophage Composition
M1
M2
WT
MYC
R
CD11b+ / F4/80+
% of total
Rosa26+/+
Rosa26MYC/+
Rosa26MYC/MYC
BM
SP

Figure S5

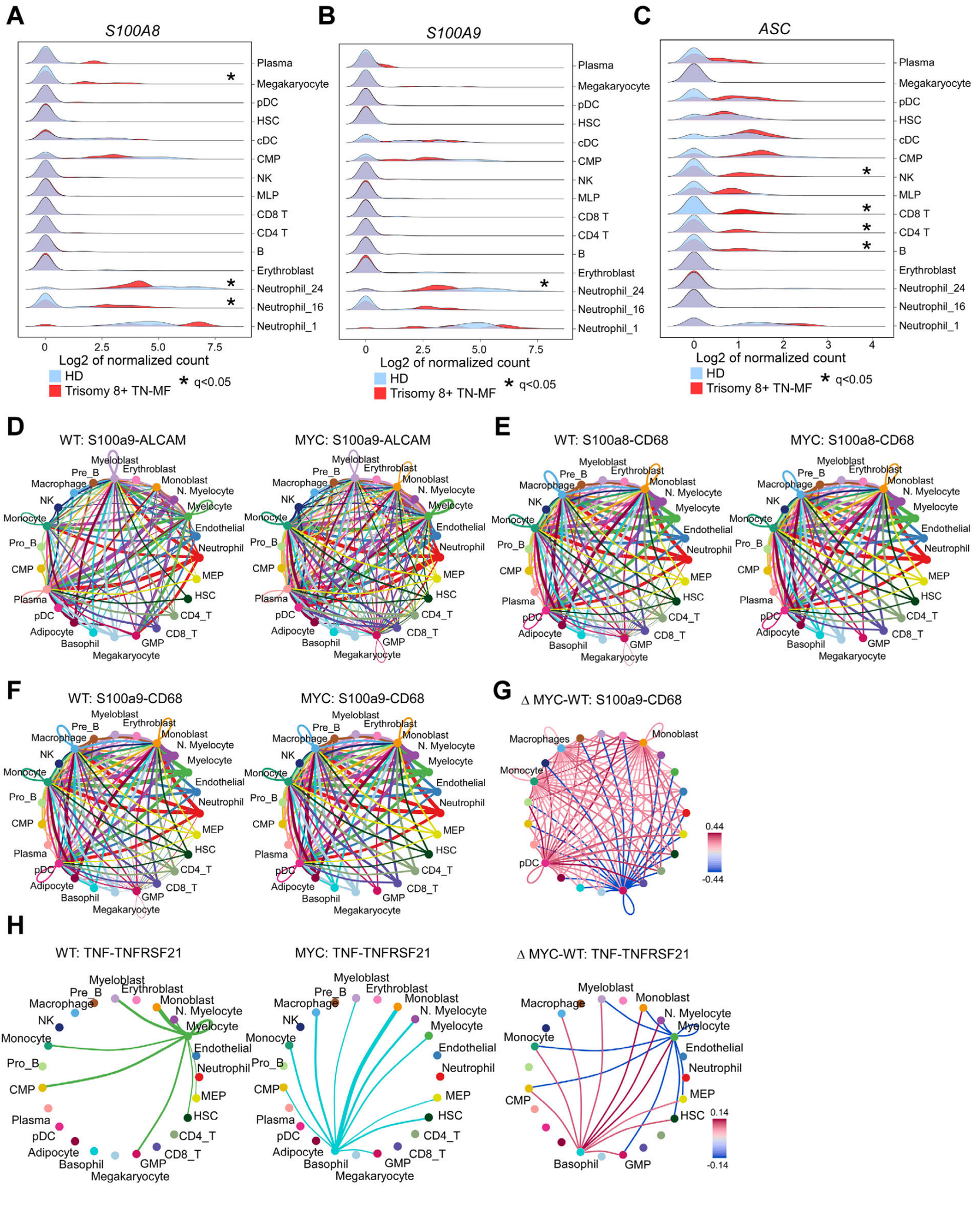
A
S100A8
B
S100A9
C
ASC
Plasma
Megakaryocyte
pDC
HSC
cDC
CMP
NK
MLP
CD8 T
CD4 T
B
Erythroblast
Neutrophil_24
Neutrophil_16
Neutrophil_1
0
2.5
5.0
7.5
1
2
3
4
Log2 of normalized count
HD
Trisomy 8+ TN-MF
* q<0.05
D
WT: S100a9-ALCAM
MYC: S100a9-ALCAM
E
WT: S100a8-CD68
MYC: S100a8-CD68
Myeloblast
Pre_B
Erythroblast
Macrophage
Monoblast
N. Myelocyte
NK
Myelocyte
Monocyte
Endothelial
Pro_B
Neutrophil
CMP
MEP
Plasma
HSC
pDC
CD4_T
Adipocyte
CD8_T
Basophil
GMP
Megakaryocyte
F
WT: S100a9-CD68
MYC: S100a9-CD68
G
Δ MYC-WT: S100a9-CD68
Macrophages
Monocyte
Monoblast
pDC
0.44
-0.44
H
WT: TNF-TNFRSF21
MYC: TNF-TNFRSF21
Δ MYC-WT: TNF-TNFRSF21
0.14
-0.14

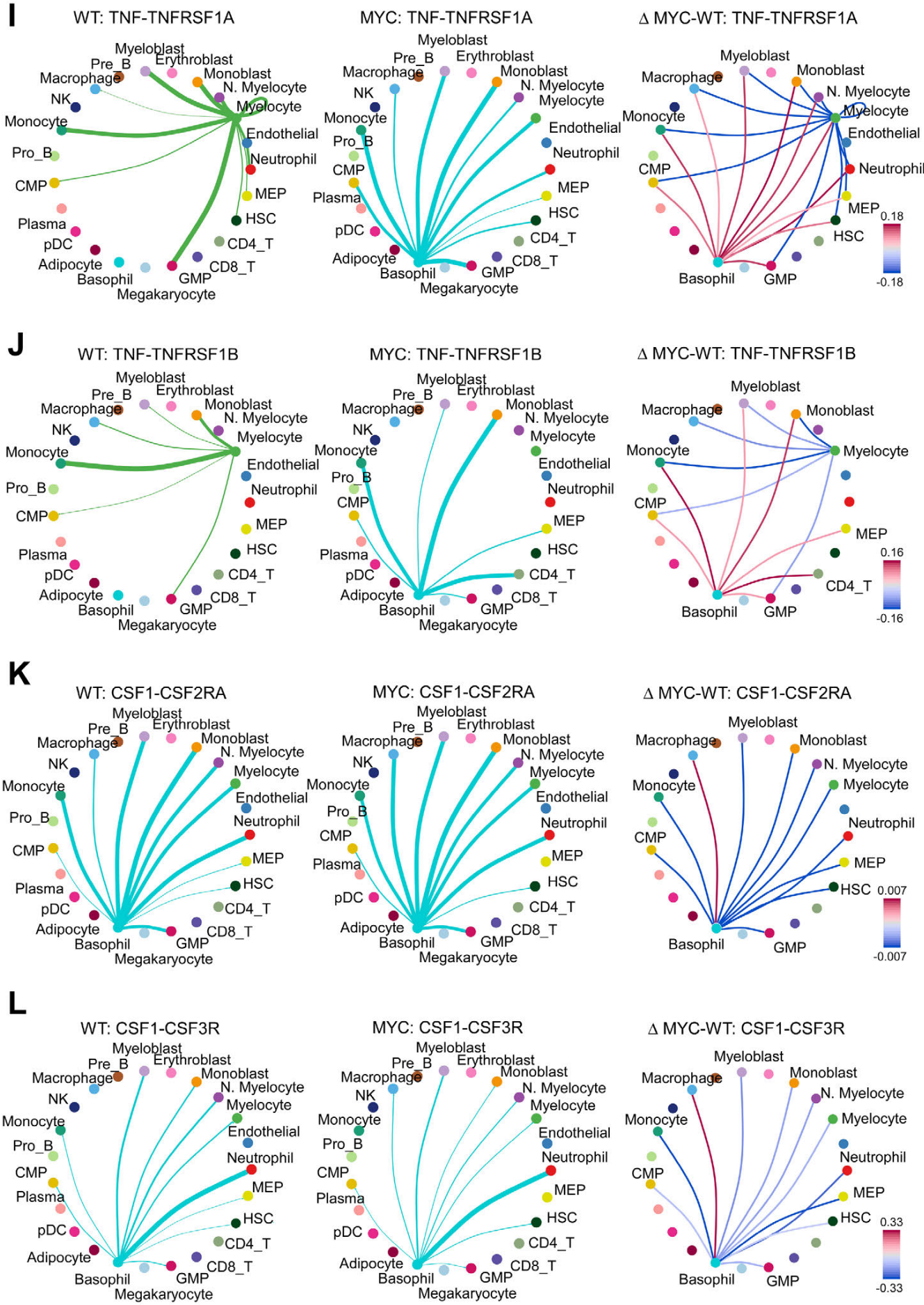
I
WT: TNF-TNFRSF1A
MYC: TNF-TNFRSF1A
Δ MYC-WT: TNF-TNFRSF1A
J
WT: TNF-TNFRSF1B
MYC: TNF-TNFRSF1B
Δ MYC-WT: TNF-TNFRSF1B
K
WT: CSF1-CSF2RA
MYC: CSF1-CSF2RA
Δ MYC-WT: CSF1-CSF2RA
L
WT: CSF1-CSF3R
MYC: CSF1-CSF3R
Δ MYC-WT: CSF1-CSF3R
Myeloblast
Pre_B
Erythroblast
Macrophage
Monoblast
N. Myelocyte
NK
Myelocyte
Monocyte
Endothelial
Pro_B
Neutrophil
CMP
MEP
Plasma
HSC
pDC
CD4_T
Adipocyte
CD8_T
Basophil
GMP
Megakaryocyte
0.18
-0.18
0.16
-0.16
0.007
-0.007
0.33
-0.33

Figure 6

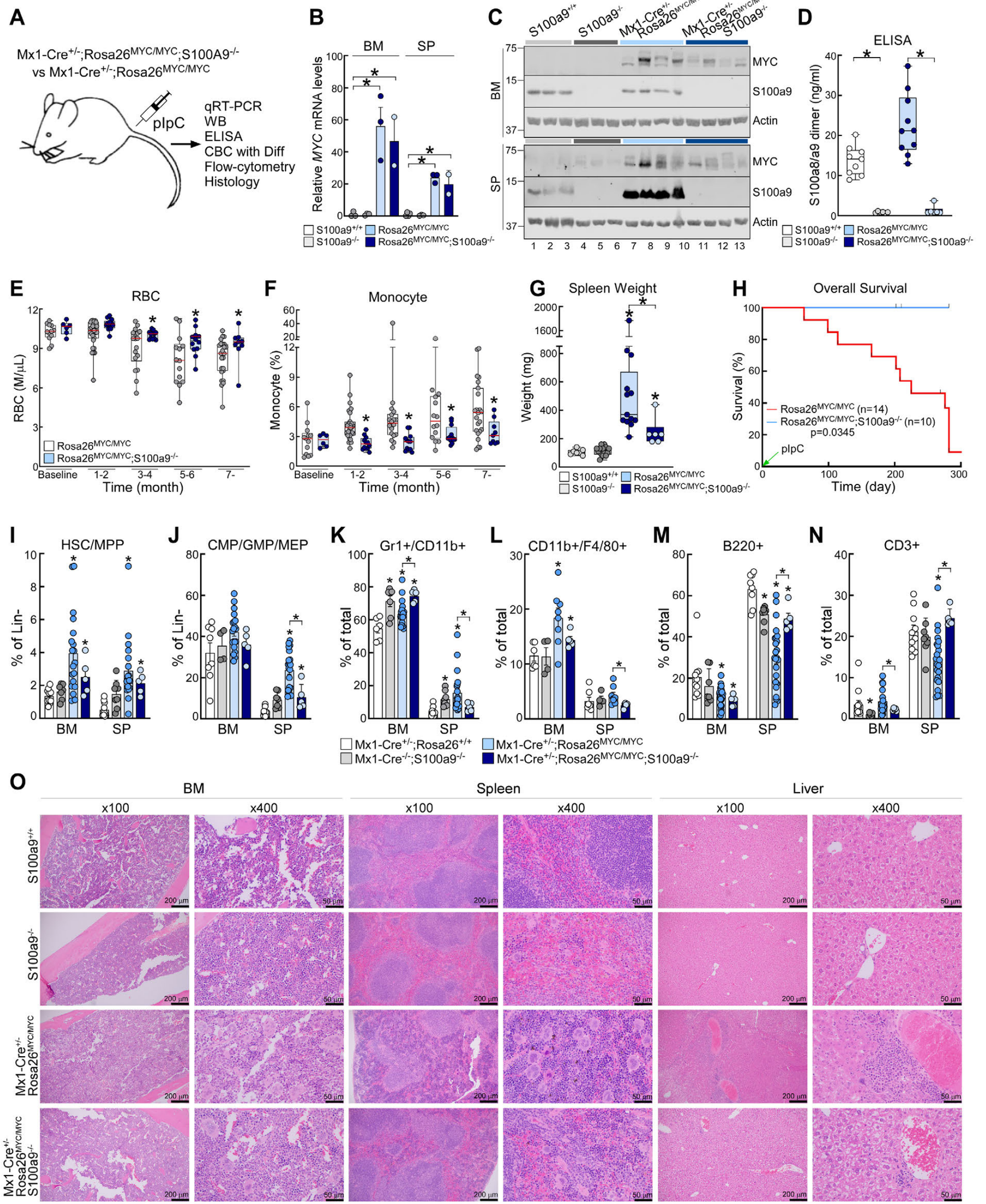
A
Mx1-Cre+/-;Rosa26MYC/MYC;S100A9-/-
vs Mx1-Cre+/-;Rosa26MYC/MYC
pIpC
qRT-PCR
WB
ELISA
CBC with Diff
Flow-cytometry
Histology
B
BM
SP
Relative MYC mRNA levels
S100a9+/+
S100a9-/-
Rosa26MYC/MYC
Rosa26MYC/MYC;S100a9-/-
C
S100a9+/+
S100a9-/-
Mx1-Cre+/- Rosa26MYC/MYC
Mx1-Cre+/- Rosa26MYC/MYC S100a9-/-
BM
SP
MYC
S100a9
Actin
1 2 3 4 5 6 7 8 9 10 11 12 13
D
ELISA
S100a8/a9 dimer (ng/ml)
E
RBC
RBC (M/μL)
Rosa26MYC/MYC
Rosa26MYC/MYC;S100a9-/-
Baseline
1-2
3-4
5-6
7-
Time (month)
F
Monocyte
Monocyte (%)
G
Spleen Weight
Weight (mg)
H
Overall Survival
Survival (%)
Rosa26MYC/MYC (n=14)
Rosa26MYC/MYC;S100a9-/- (n=10)
p=0.0345
pIpC
Time (day)
I
HSC/MPP
% of Lin-
J
CMP/GMP/MEP
% of Lin-
K
Gr1+/CD11b+
% of total
L
CD11b+/F4/80+
% of total
M
B220+
% of total
N
CD3+
% of total
BM
SP
Mx1-Cre+/-;Rosa26+/+
Mx1-Cre-/-;S100a9-/-
Mx1-Cre+/-;Rosa26MYC/MYC
Mx1-Cre+/-;Rosa26MYC/MYC;S100a9-/-
O
BM
Spleen
Liver
x100
x400
S100a9+/+
S100a9-/-
Mx1-Cre+/- Rosa26MYC/MYC
Mx1-Cre+/- Rosa26MYC/MYC S100a9-/-
200 μm
50 μm

Figure S6

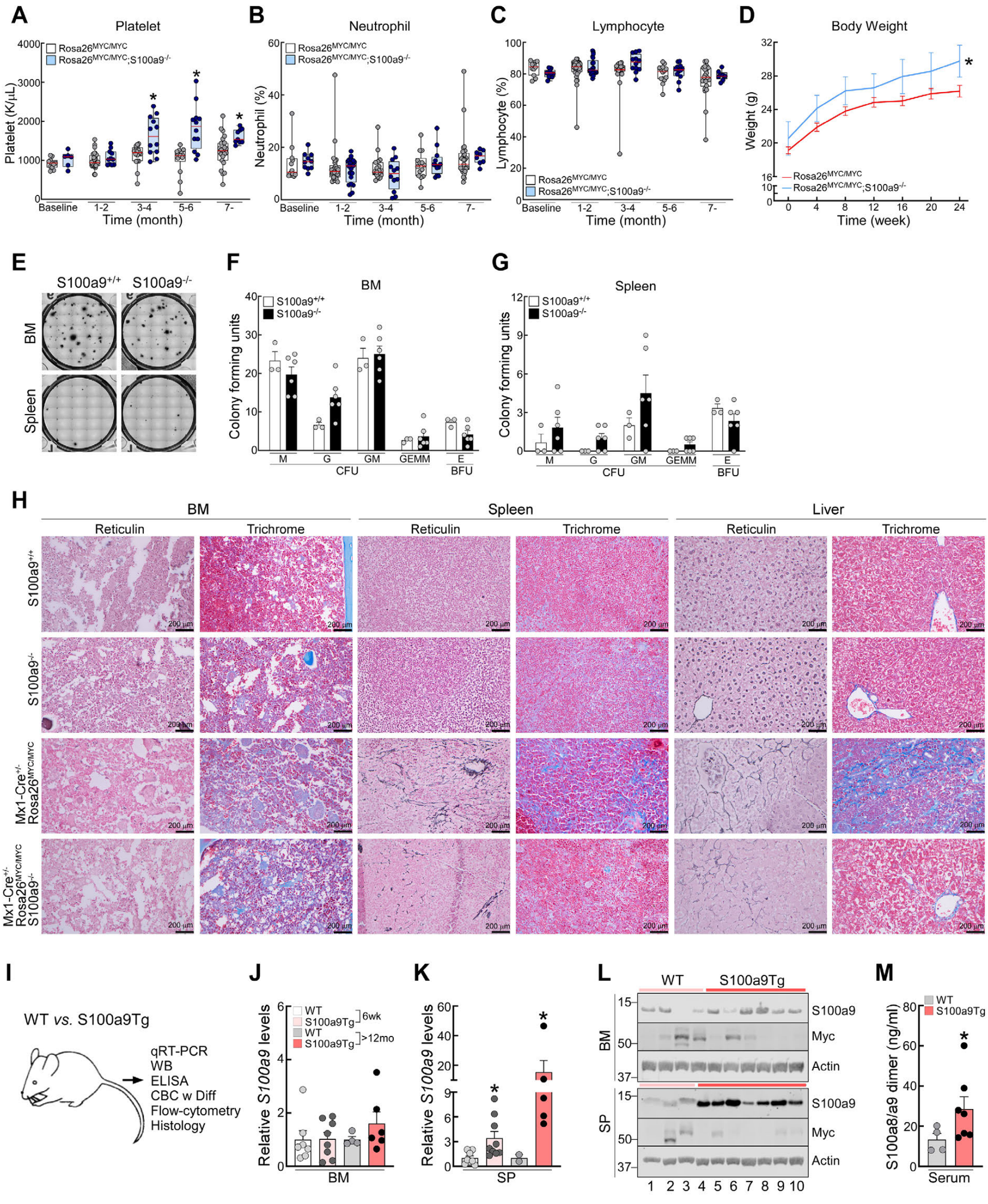
A
Platelet
Rosa26MYC/MYC
Rosa26MYC/MYC;S100a9-/-
Platelet (K/μL)
Baseline
1-2
3-4
5-6
7-
Time (month)
B
Neutrophil
Neutrophil (%)
C
Lymphocyte
Lymphocyte (%)
D
Body Weight
Weight (g)
Time (week)
E
S100a9+/+
S100a9-/-
BM
Spleen
F
BM
Colony forming units
M
G
GM
GEMM
E
CFU
BFU
G
Spleen
H
BM
Spleen
Liver
Reticulin
Trichrome
S100a9+/+
S100a9-/-
Mx1-Cre+/- Rosa26MYC/MYC
Mx1-Cre+/- Rosa26MYC/MYC S100a9-/-
200 μm
I
WT vs. S100a9Tg
qRT-PCR
WB
ELISA
CBC w Diff
Flow-cytometry
Histology
J
Relative S100a9 levels
WT
S100a9Tg
6wk
>12mo
BM
K
SP
L
WT
S100a9Tg
S100a9
Myc
Actin
M
S100a8/a9 dimer (ng/ml)
Serum

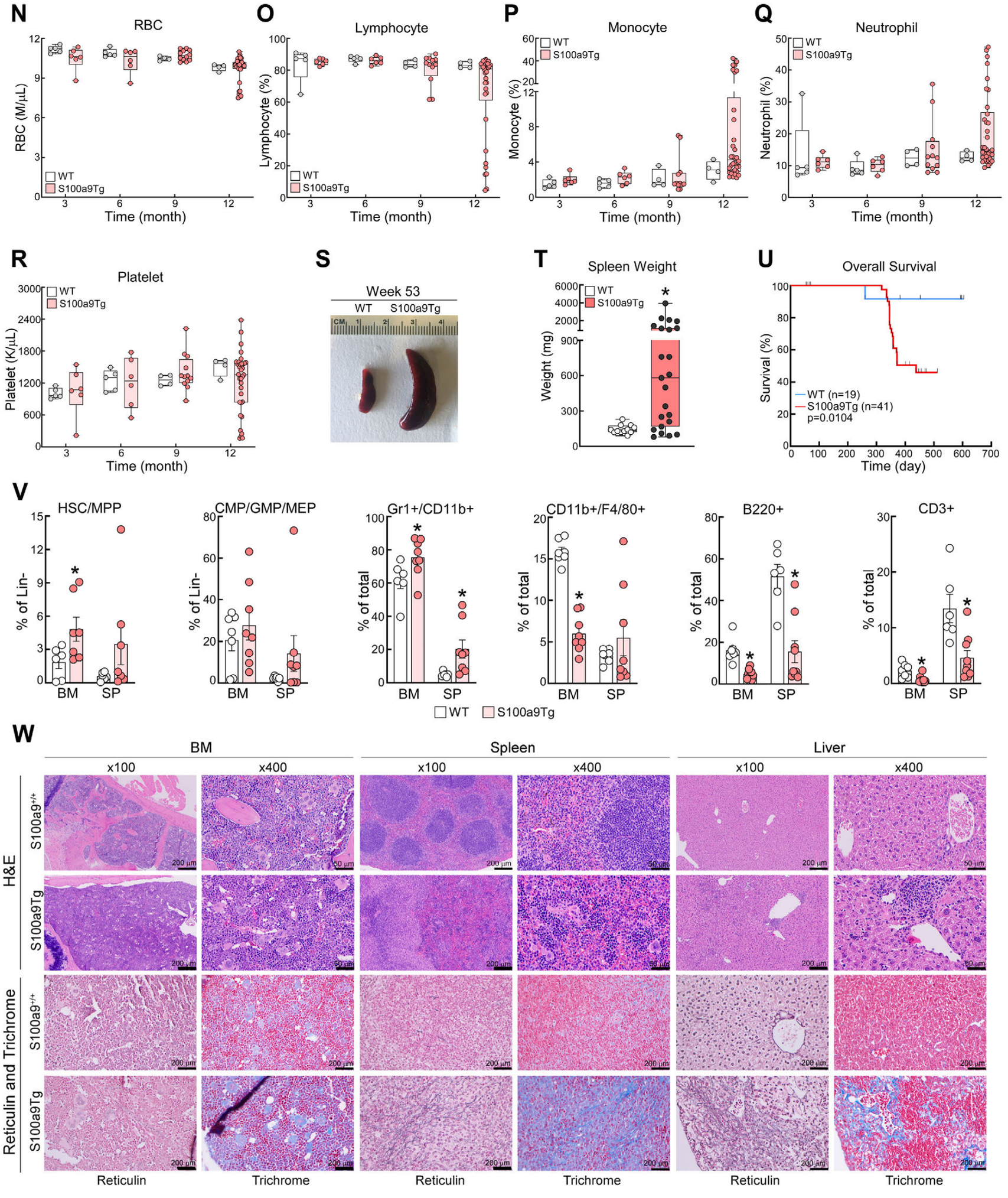
N
RBC
RBC (M/μL)
WT
S100a9Tg
Time (month)
O
Lymphocyte
Lymphocyte (%)
P
Monocyte
Monocyte (%)
Q
Neutrophil
Neutrophil (%)
R
Platelet
Platelet (K/μL)
S
Week 53
WT
S100a9Tg
T
Spleen Weight
Weight (mg)
U
Overall Survival
Survival (%)
WT (n=19)
S100a9Tg (n=41)
p=0.0104
Time (day)
V
HSC/MPP
CMP/GMP/MEP
Gr1+/CD11b+
CD11b+/F4/80+
B220+
CD3+
% of Lin-
% of total
BM
SP
W
BM
Spleen
Liver
x100
x400
H&E
Reticulin and Trichrome
S100a9+/+
S100a9Tg
Reticulin
Trichrome

Figure 7

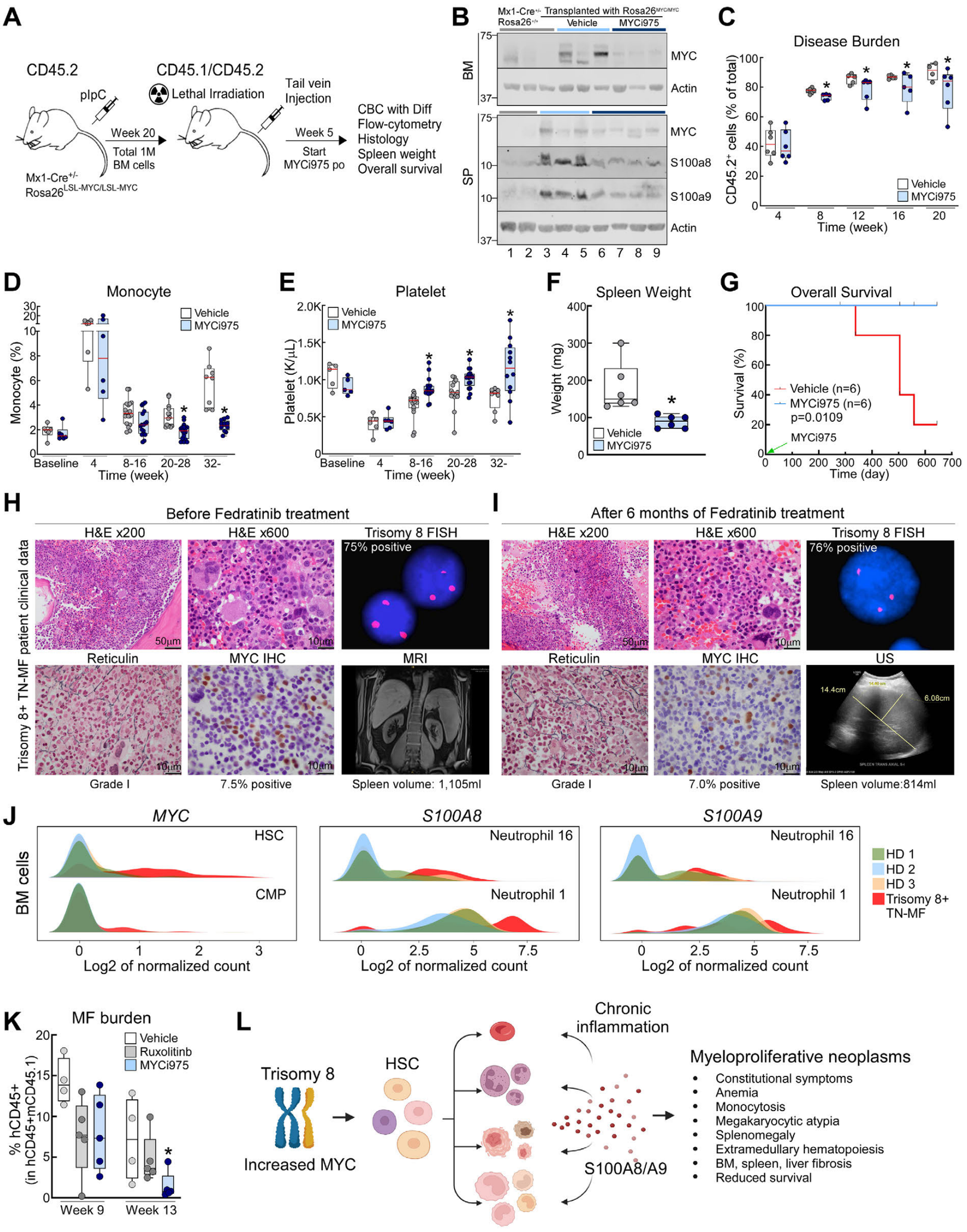
A
CD45.2
pIpC
Mx1-Cre+/-
Rosa26LSL-MYC/LSL-MYC
Week 20
Total 1M
BM cells
CD45.1/CD45.2
Lethal Irradiation
Tail vein
Injection
Week 5
Start
MYCi975 po
CBC with Diff
Flow-cytometry
Histology
Spleen weight
Overall survival
B
Mx1-Cre+/- Transplanted with Rosa26MYC/MYC
Rosa26+/+
Vehicle
MYCi975
BM
SP
MYC
Actin
S100a8
S100a9
C
Disease Burden
CD45.2+ cells (% of total)
Vehicle
MYCi975
Time (week)
D
Monocyte
Monocyte (%)
Baseline
8-16
20-28
32-
Time (week)
E
Platelet
Platelet (K/μL)
F
Spleen Weight
Weight (mg)
G
Overall Survival
Survival (%)
Vehicle (n=6)
MYCi975 (n=6)
p=0.0109
Time (day)
H
Before Fedratinib treatment
patient clinical data
H&E x200
H&E x600
Trisomy 8 FISH
75% positive
Trisomy 8+ TN-MF
Reticulin
MYC IHC
MRI
Grade I
7.5% positive
Spleen volume: 1,105ml
I
After 6 months of Fedratinib treatment
76% positive
US
14.4cm
6.08cm
Grade I
7.0% positive
Spleen volume:814ml
J
MYC
S100A8
S100A9
BM cells
HSC
CMP
Neutrophil 16
Neutrophil 1
HD 1
HD 2
HD 3
Trisomy 8+ TN-MF
Log2 of normalized count
K
MF burden
Vehicle
Ruxolitinb
MYCi975
% hCD45+ (in hCD45+mCD45.1)
Week 9
Week 13
L
Trisomy 8
Increased MYC
HSC
Chronic inflammation
S100A8/A9
Myeloproliferative neoplasms
Constitutional symptoms
Anemia
Monocytosis
Megakaryocytic atypia
Splenomegaly
Extramedullary hematopoiesis
BM, spleen, liver fibrosis
Reduced survival

Figure S7

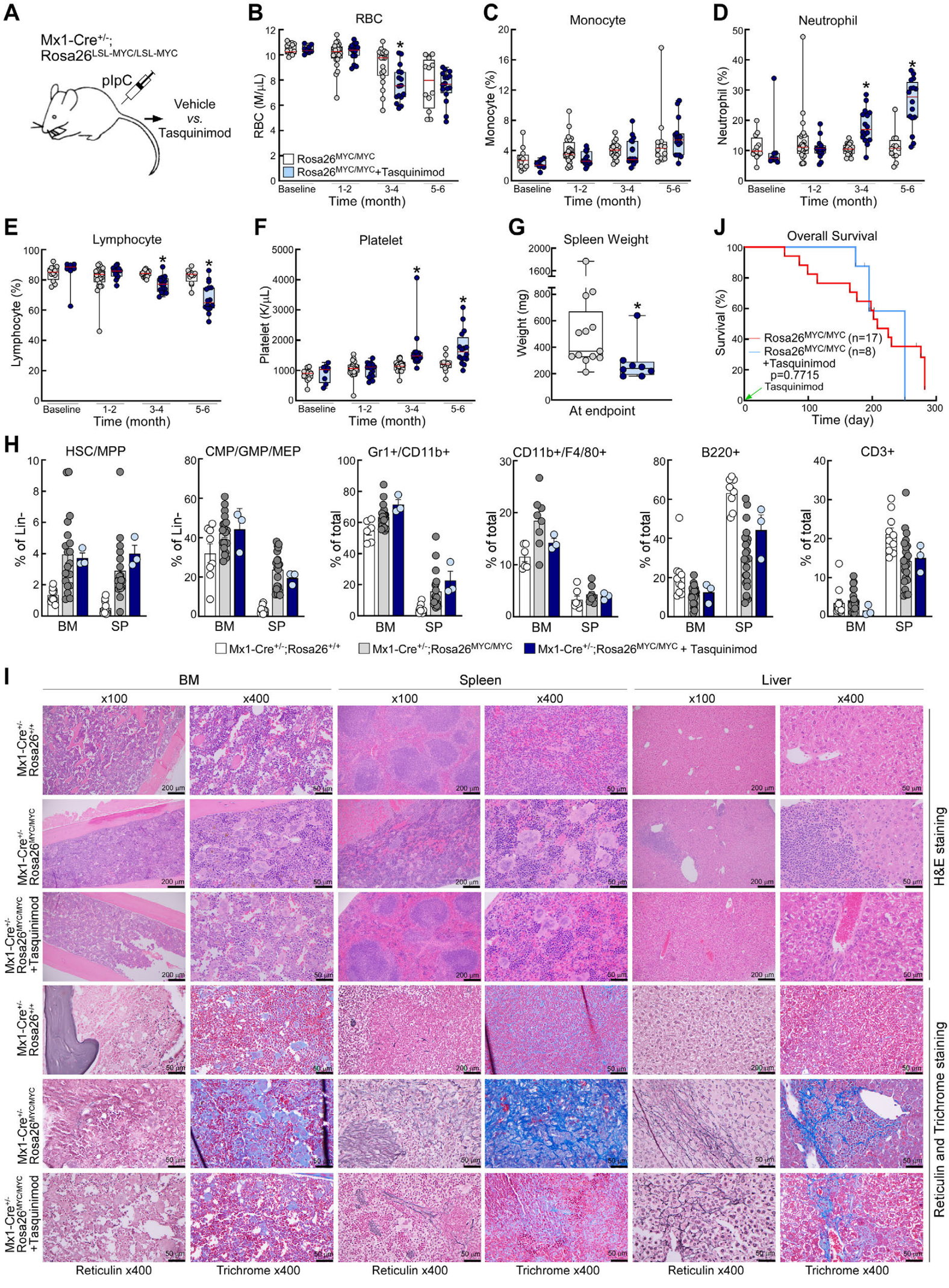
A
Mx1-Cre+/-;
Rosa26LSL-MYC/LSL-MYC
pIpC
Vehicle
vs.
Tasquinimod
B
RBC
RBC (M/μL)
Rosa26MYC/MYC
Rosa26MYC/MYC+Tasquinimod
Baseline
1-2
3-4
5-6
Time (month)
C
Monocyte
Monocyte (%)
Time (month)
D
Neutrophil
Neutrophil (%)
Time (month)
E
Lymphocyte
Lymphocyte (%)
Time (month)
F
Platelet
Platelet (K/μL)
Time (month)
G
Spleen Weight
Weight (mg)
At endpoint
J
Overall Survival
Survival (%)
Rosa26MYC/MYC (n=17)
Rosa26MYC/MYC (n=8)
+Tasquinimod
p=0.7715
Tasquinimod
Time (day)
H
HSC/MPP
CMP/GMP/MEP
Gr1+/CD11b+
CD11b+/F4/80+
B220+
CD3+
% of Lin-
% of total
BM
SP
Mx1-Cre+/-;Rosa26+/+
Mx1-Cre+/-;Rosa26MYC/MYC
Mx1-Cre+/-;Rosa26MYC/MYC + Tasquinimod
I
BM
Spleen
Liver
x100
x400
Mx1-Cre+/- Rosa26+/+
Mx1-Cre+/- Rosa26MYC/MYC
Mx1-Cre+/- Rosa26MYC/MYC +Tasquinimod
H&E staining
Reticulin and Trichrome staining
Reticulin x400
Trichrome x400

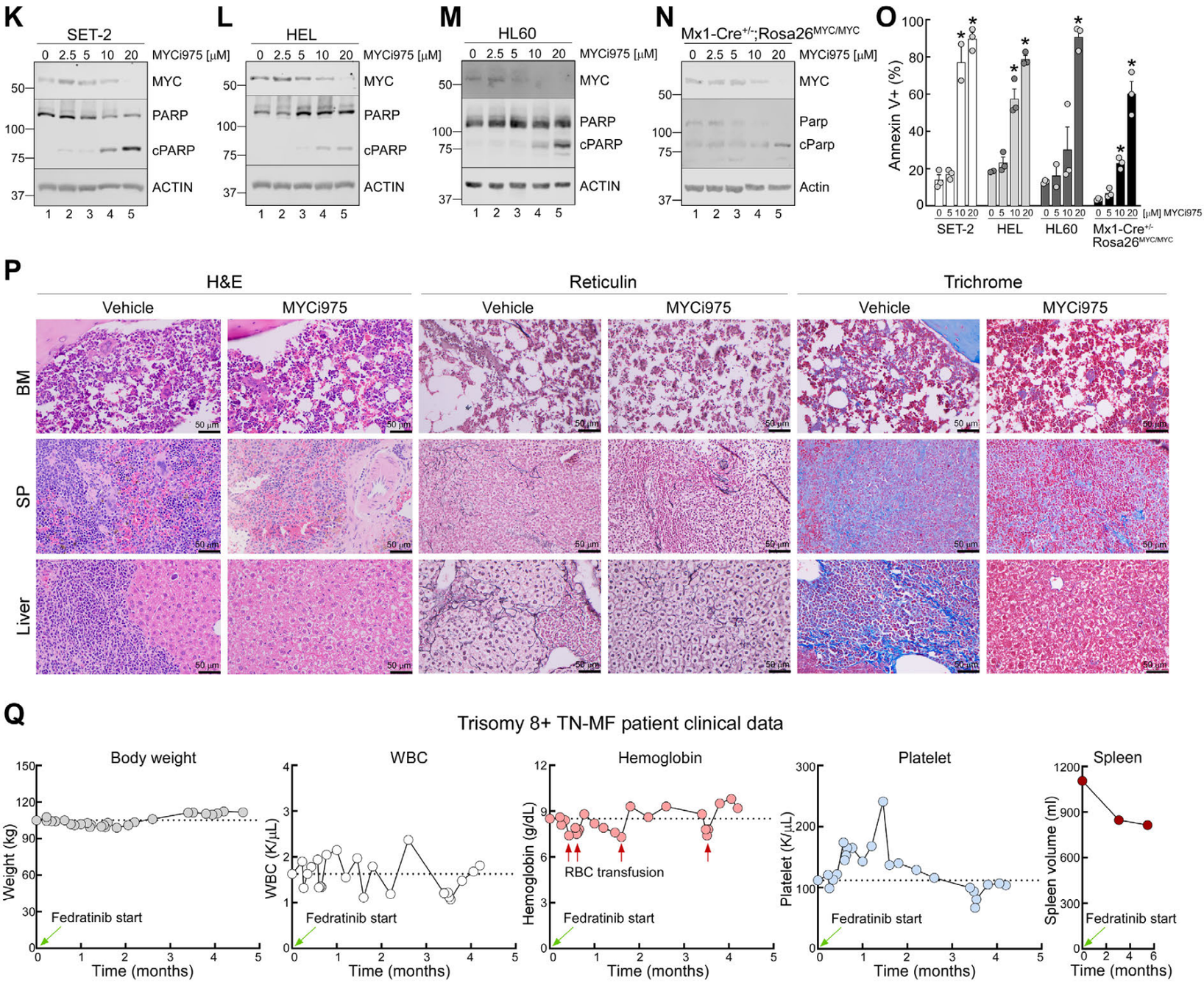
K
SET-2
0 2.5 5 10 20 MYCi975 [μM]
MYC
PARP
cPARP
ACTIN
50
100
75
37
1 2 3 4 5
L
HEL
0 2.5 5 10 20 MYCi975 [μM]
MYC
PARP
cPARP
ACTIN
50
100
75
37
1 2 3 4 5
M
HL60
0 2.5 5 10 20 MYCi975 [μM]
MYC
PARP
cPARP
ACTIN
50
100
75
37
1 2 3 4 5
N
Mx1-Cre+/-;Rosa26MYC/MYC
0 2.5 5 10 20 MYCi975 [μM]
MYC
Parp
cParp
Actin
50
100
75
37
1 2 3 4 5
O
Annexin V+ (%)
100
80
60
40
20
0
0 5 10 20 [μM] MYCi975
SET-2
HEL
HL60
Mx1-Cre+/-
Rosa26MYC/MYC
P
H&E
Reticulin
Trichrome
Vehicle
MYCi975
BM
SP
Liver
50 μm
Q
Trisomy 8+ TN-MF patient clinical data
Body weight
Weight (kg)
150
120
90
60
30
0
Fedratinib start
0 1 2 3 4 5
Time (months)
WBC
WBC (K/μL)
4
3
2
1
0
Fedratinib start
0 1 2 3 4 5
Time (months)
Hemoglobin
Hemoglobin (g/dL)
12
9
6
3
0
RBC transfusion
Fedratinib start
0 1 2 3 4 5
Time (months)
Platelet
Platelet (K/μL)
300
200
100
0
Fedratinib start
0 1 2 3 4 5
Time (months)
Spleen
Spleen volume (ml)
1200
900
600
300
0
Fedratinib start
0 2 4 6
Time (months)

Supplemental Information

A Novel Subtype of Myeloproliferative Neoplasms Driven by a MYC-Alarmin Axis

Nicole D. Vincelette,[1,*] Xiaoqing Yu,[2] Andrew T. Kuykendall,[1] Jungwon Moon,[1] Siyuan Su,[3] Chia-Ho Cheng,[2] Rinzine Sammut,[1,4] Tiffany N. Razabdouski,[1] Hai Vu Nguyen,[5] Erika A. Eksioglu,[6] Onyee Chan,[1] Najla Al Ali,[1] Parth C. Patel,[1,7] Dae Hyun Lee,[8] Shima Nakanishi,[9] Renan B. Ferreira,[10] Qianxing Mo,[2] Suzanne Cory,[5] Harshani R. Lawrence,[10] Ling Zhang,[11] Daniel J. Murphy,[12,13] Rami S. Komrokji,[1] Daesung Lee,[3] Scott H. Kaufmann,[14] John L. Cleveland,[9] and Seongseok Yun[1,15, *]

[1]Department of Malignant Hematology, Moffitt Cancer Center & Research Institute, Tampa, FL 33612 USA
[2]Department of Bioinformatics and Biostatistics, Moffitt Cancer Center & Research Institute, Tampa, FL 33612, USA
[3]Department of Chemistry, University of Illinois Chicago, Chicago, IL 60607, USA
[4]Département d'hématologie clinique, Centre hospitalier universitaire de Nice, 06200 Nice, France
[5]The Walter and Eliza Hall Institute of Medical Research, Parkville, Victoria 3052, Australia
[6]Department of Immunology, Moffitt Cancer Center & Research Institute, Tampa, FL 33612, USA
[7]Department of Internal Medicine, University of South Florida, Tampa, FL 33602 USA
[8]Division of Cardiovascular Science, Department of Internal Medicine, University of South Florida, Tampa, FL 33602 USA
[9]Department of Tumor Biology, Moffitt Cancer Center & Research Institute, Tampa, FL 33612, USA
[10]Department of Drug Discovery, Moffitt Cancer Center & Research Institute, Tampa, FL 33612, USA
[11]Department of Pathology and Laboratory Medicine, Moffitt Cancer Center & Research Institute, Tampa, FL 33612, USA
[12]School of Cancer Sciences, University of Glasgow, Garscube Estate, Glasgow, United Kingdom
[13]Cancer Research UK Beatson Institute, Garscube Estate, Glasgow, United Kingdom
[14]Department of Molecular Pharmacology and Experimental Therapeutics, and Department of Oncology, Mayo Clinic, Rochester, MN 55905, USA.
[15]Lead contact

*Correspondence:
Seongseok Yun, H. Lee Moffitt Cancer Center & Research Institute, 12902 Magnolia Drive, Tampa, FL 33612, USA. Phone: 813-745-4520; Fax: 813-745-5888;
E-mail: seongseok.yun@moffitt.org

Nicole D. Vincelette, H. Lee Moffitt Cancer Center & Research Institute, 12902 Magnolia Drive, Tampa, FL 33612, USA Phone: 813-745-8110; Fax: 813-745-5888;
E-mail: nicole.vincelette@moffitt.org

Supplementary Information includes:

Supplementary Figures S1-S7

Supplementary Tables S1-S16

SUPPLEMENTAL FIGURE LEGENDS

Figure S1. Landscape of somatic mutations and cytogenetics in Moffitt MF cohort. A, Somatic mutation profiles in Moffitt MF patients. Individual columns and rows represent each patient and somatic mutation, respectively. Positive mutations are highlighted in dark blue. Numbers of total mutations in individual patients and percentages of somatic mutations in the total number of patients are described in the top and right side of the plot, respectively. Trisomy 8 status, subtypes of MF, reticulin fibrosis score, and prognostic scores are described at the bottom of the plot. Demographic profiles and laboratory parameters are described in Table S1. **B-C,** Kaplan-Meier curves showing the LFS (B) and OS (C). **D,** Percentages of cytogenetic abnormalities (top 5 most frequent aberrations) and complex karyotype (defined as at least 3 concurrent chromosomal abnormalities) in individual molecular subtypes and all MF patients. **E-F,** Forest plots showing hazard ratio (HR) and 95% confidence intervals associated with individual cytogenetic abnormalities in the Mayo Clinic (E) and Moffitt MF (F) cohorts, respectively. Patients with more than one chromosomal abnormality were excluded from the analyses. Data in (E) were re-analyzed using the original published data[38]. **G,** Levels of MYC protein expression in BM cells of TN-MF patients. MYC positivity was defined as at least 1% of cells that express MYC protein. **H,** Schematic diagram describing scRNA-seq analyses of human BM cells. **I,** Conventional karyotyping of TN-MF patient BM cells used in scRNA-seq analysis. **J,** Heatmaps depicting differentially expressed genes between healthy donors (n = 3) vs. trisomy 8+ TN-MF patient in the indicated individual clusters. **K,** Cell type markers (top 5 genes) in the indicated individual clusters. **L-M,** Cell type composition of BM cells in healthy donors *vs.* trisomy

8+ TN-MF patient. **N,** Percentages of cells in G1, S, and G2/M phase of cell cycle in individual major cell types of healthy donors *vs.* trisomy 8+ TN-MF patient. **O,** inferCNV analysis based on scRNA-seq data. Top and bottom panels represent data from normal donors (used as reference) and trisomy 8+ TN-MF, respectively. Columns represent individual chromosomes and rows represent major cell types. **P,** Pie charts showing percentages of trisomy 8+ *vs.* diploid cells in individual major cell types in trisomy 8+ TN-MF patient BM.**Q,** PROGENy analysis comparing trisomy 8+ TN-MF *vs.* healthy donors BM cells. Individual columns and rows represent major cell types and pathways that are known to contribute to MPN pathogenesis. **R,** Ridgeline plots of *MYC* mRNA levels in diploid (blue) *vs.* trisomy 8+ (red) BM cells for each major cell type of the trisomy 8+ TN-MF patient. **S,** Somatic mutation profiles in MYC negative (n = 11) *vs.* positive (n = 12) TN-MF patients. Individual columns and rows represent each patient and somatic mutation, respectively. Positive and negative mutations are highlighted in dark blue and grey, respectively. Number of total mutations in individual patients and the percentages of somatic mutations in total patients are described in the top and right side, respectively. Subtypes of MF and MYC status are described at the bottom of the plot. Abbreviations: MF, myelofibrosis; Triple negative MF, TN-MF; LFS, leukemia free survival; OS, overall survival; MCC, Moffitt Cancer Center; IPSS, International Prognostic Scoring System; DIPSS, Dynamic IPSS; MIPSS70, Mutation-Enhanced IPSS; GIPSS, Genetically Inspired Prognostic Scoring System.

Figure S2. Effects of enforced MYC expression in HSCs in vivo. A, Schematic of the *Mx1-Cre, Scl-CreERT*, and *Rosa26-LSL-MYC* alleles. **B-D,** PB CBC analyses of white blood cells (WBC) (B), neutrophils (C), and platelets (D). Baseline CBC was performed 1 week prior to pIpC treatment. **E,** MYC IHC staining of spleen tissue. **F,** H&E, reticulin, and trichrome stained images of liver tissues at week 20 following pIpC injection. **G,** H&E, reticulin, and trichrome stained images of BM, spleen, and liver at week 52 post-pIpC treatment. Demographic profiles and laboratory parameters are described in Table S4. **H,** Schematic of in vivo studies using Scl-CreERT2$^{+/-}$;Rosa26$^{LSL\text{-}MYC/LSL\text{-}MYC}$ mice. **I-J,** MYC mRNA (I) and protein (J) levels in BM and spleen of Scl-CreERT$^{+/-}$;Rosa26$^{+/+}$, Scl-CreERT$^{+/-}$;Rosa26$^{LSL\text{-}MYC/+}$, and Scl-CreERT$^{+/-}$;Rosa26$^{LSL\text{-}MYC/LSL\text{-}MYC}$ mice, respectively. **K,** Comparison of body weight between the indicated experimental groups. **L-Q,** PB CBC analyses of RBC (L), WBC (M), lymphocytes (N), monocytes (O), neutrophils (P), and platelets (Q). Baseline CBC was performed 1 week prior to tamoxifen treatment. **R,** Spleen weight at endpoints. Scl-CreERT$^{+/-}$;Rosa26$^{+/+}$ mice were sacrificed as control when Scl-CreERT$^{+/-}$;Rosa26$^{LSL\text{-}MYC/+}$ and Scl-CreERT$^{+/-}$;Rosa26$^{LSL\text{-}MYC/LSL\text{-}MYC}$ mice were at their endpoints. Endpoints criteria is described in "Animal studies" section. **S,** Kaplan-Meier curves of OS, calculated from the date of tamoxifen treatment. **T,** H&E, reticulin, and trichrome stained images of BM, spleen, and liver at week 20 following tamoxifen treatment. Demographic profiles and laboratory parameters are described in Table S6. Error bars in (I) and (K) indicate mean ±SEM of at least 3 independent mice. Box plots in panels (B-D) and (L-Q) represent data from 38-54 and 15-25 mice, respectively, in each experimental group. * In panels (B, I, K-O, and Q-S), P<0.05 compared with control group.

Figure S3. MYC-induced changes in hematopoietic sub-populations and colony forming potential. A, Gating strategies used to quantify hematopoietic subpopulations. **B,** Percentages of $B220^+$ B-cells, $CD3^+$ T-cells, LT-HSC, ST-HSC, MPP2, MPP3, CMPs, GMPs, and MEPs in BM or spleen of the indicated groups before 45 weeks from pIpC treatment. **C,** Percentages of individual hematopoietic subpopulations in Mx1-$Cre^{+/-}$;$Rosa26^{+/+}$ and Mx1-$Cre^{+/-}$;$Rosa26^{LSL\text{-}MYC/+}$ mice, respectively, after 45 weeks from pIpC treatment. **D,** Comparison of individual hematopoietic cell types in BM and spleen of Scl-$CreERT^{+/-}$;$Rosa26^{+/+}$, Scl-$CreERT^{+/-}$;$Rosa26^{LSL\text{-}MYC/+}$ and Scl-$CreERT^{+/-}$;$Rosa26^{LSL\text{-}MYC/LSL\text{-}MYC}$ mice. **E-H,** Serial colony forming assays using primary BM cells from Mx1-$Cre^{+/-}$;$Rosa26^{+/+}$, Mx1-$Cre^{+/-}$;$Rosa26^{LSL\text{-}MYC/+}$ and Mx1-$Cre^{+/-}$;$Rosa26^{LSL\text{-}MYC/LSL\text{-}MYC}$ mice at 20 weeks post-pIpC. A total $1x10^4$ cells were plated from each experimental group, cultured for 10 days, and CFU-G (E), CFU-M (F), CFU-GEMM (G), and BFU-E (H) were then counted manually. **I-J,** Serial colony forming assays using the indicated primary spleen cells. **K-M,** Colony forming assays using primary BM cells harvested from 7-week old Rosa26-Cre-$ERT2^{+/-}$;$Myc^{+/+}$ and Rosa26-Cre-$ERT2^{+/-}$;$Myc^{fl/fl}$ mice. Cells were cultured ex vivo with vehicle or 4-OHT (1μM) for 10 days, and then assessed for colony forming units. Knockout of *Myc* was confirmed by qRT-PCR assays (K). Error bars in (B-H and J-L) indicate mean ±SEM of at least 3 independent mice. * in (B-D, F, and J-L), $P<0.05$ compared with control group.

Figure S4. JAK/STAT, PI3K/AKT, MEK/ERK, and alarmin pathways in MYC-driven MF. A, Schematic of scRNA-seq analyses of mouse BM cells. **B-C,** Heatmaps depicting differentially expressed genes between Mx1-Cre$^{+/-}$;Rosa26$^{+/+}$ control *vs.* Mx1-Cre$^{+/-}$;Rosa26$^{LSL\text{-}MYC/LSL\text{-}MYC}$ mouse in individual clusters (B) and major cell types (C). **D,** Cell type markers (top 5 genes) in individual clusters. **E,** Percentages of cells in G1, S, and G2/M phase of cell cycle in each major cell type of Mx1-Cre$^{+/-}$;Rosa26$^{LSL\text{-}MYC/LSL\text{-}MYC}$ (MYC) *vs.* control (WT) mice. **F-G,** Heatmaps showing differentially expressed genes (log2 fold change>0.25, q<0.05) between Mx1-Cre$^{+/-}$;Rosa26$^{+/+}$ *vs.* Mx1-Cre$^{+/-}$;Rosa26$^{LSL\text{-}MYC/LSL\text{-}MYC}$ mouse in the CMPs (F) and GMPs (G) clusters. **H-I,** Immunoblotting of BM (H) and spleen cells (I) harvested from Mx1-Cre$^{+/-}$;Rosa26$^{+/+}$, Mx1-Cre$^{+/-}$;Rosa26$^{LSL\text{-}MYC/+}$ and Mx1-Cre$^{+/-}$;Rosa26$^{LSL\text{-}MYC/LSL\text{-}MYC}$ mice. **J-M,** SET-2, HEL, and primary BM cells harvested from Mx1-Cre$^{+/-}$;Rosa26$^{LSL\text{-}MYC/LSL\text{-}MYC}$ mice were incubated with vehicle *vs.* ruxolitinib as indicated for 48 hr, and then assessed for changes in phospho-STAT3, -ERK1/2, -AKT, and cleaved PARP protein levels (J-L) and apoptosis (M, % Annexin V$^+$ cells). **N-Q,** *S100a8* and *ASC* mRNAs levels in single cell are projected onto the UMAP plots (N, O, respectively) and changes in these genes in the individual major cell types in MYC (red) *vs.* control (blue) BM cells are presented in the ridgeline plots (P, Q). **R,** Immunoblotting of BM (top panel) and spleen cells (bottom panel) harvested from Mx1-Cre$^{+/-}$;Rosa26$^{+/+}$ and Mx1-Cre$^{+/-}$;Rosa26$^{LSL\text{-}MYC/LSL\text{-}MYC}$ mice. **S,** ASC speck cross-linking using spleen cells harvested from Mx1-Cre$^{+/-}$;Rosa26$^{+/+}$ and Mx1-Cre$^{+/-}$;Rosa26$^{LSL\text{-}MYC/LSL\text{-}MYC}$ mice. See method for the details. Actin blots in panels (H-L) were from the same samples run on different gels. Error bars in (M) indicate mean ±SEM of 3 independent assays. * In (M, P, and Q), P<0.05 compared with control group.

Figure S5. Changes in signaling in BM of trisomy 8+ TN-MF patient and MYC MF mice. A-C, Ridgeline plots comparing *S100A8/A9* and *ASC* mRNA levels in each major BM cell type of trisomy 8+ TN-MF patient *vs.* normal healthy donors. **D-G,** Network plots of interactions of ligands (S100a8 or S100a9) and receptors (ALCAM or CD68). Ligand signals originating from individual major cell types are presented in different colors. Thicker lines in (D-F) indicate a more frequent interaction between cell types. Differences in intensity of interactions are presented in (G). Higher and lower signal activity in MYC homozygous cells (compared to WT) are presented in red and blue, respectively. **H-L,** Network plots of interactions of ligands (TNF-α or CSF-1) and receptors (TNFRSF21, TNFRSF1A, TNFRSF1B, CSF2RA, or CSF3R) in mouse BM cells. Differences in intensity of interactions are presented in the third plots of the individual panels. Higher and lower signal activity in MYC cells (compared to WT) are presented in red and blue, respectively. * in panels (A-C), $P<0.05$ compared with control group.

Figure S6. Effects of silencing in MYC-driven MF or overexpression of S100a9. A-C, PB CBC analyses in Mx-Cre$^{+/-}$;Rosa26$^{LSL\text{-}MYC/LSL\text{-}MYC}$ and Mx-Cre$^{+/-}$;Rosa26$^{LSL\text{-}MYC/LSL\text{-}MYC}$;*S100A9*$^{-/-}$ mice following pIpC treatment. Baseline CBC was performed 1 week prior to pIpC. **D,** Comparison of body weight of Mx-Cre$^{+/-}$;Rosa26$^{LSL\text{-}MYC/LSL\text{-}MYC}$ and Mx-Cre$^{+/-}$;Rosa26$^{LSL\text{-}MYC/LSL\text{-}MYC}$;*S100A9*$^{-/-}$ mice following treatment with pIpC. **E-G,** Comparison of colony forming units between WT *vs. S100a9*$^{-/-}$ mice. **H,** Reticulin and trichrome stained images of BM, spleen, and liver in the indicated mice. Demographic profiles and laboratory parameters are described in Table S11. **I,** Schematic of in vivo S100a9Tg mouse studies. **J-K,** Levels of S100a9 mRNA in BM (J) and spleen (K) cells of S100a9Tg *vs*. control mice at indicated time points. **L,** Levels of S100a9 protein in BM (top panels) and spleen (bottom panels) of S100a9Tg mice at age >12 months. Age-matched control mice were sacrificed at the same time for paired analysis. **M,** Serum levels of S100a8/a9 heterodimers in S100a9Tg *vs*. control mice at age >12 months. **N-R,** PB CBC analyses of RBC (N), lymphocytes (O), monocytes (P), neutrophils (Q), and platelets (R) in S100a9Tg *vs*. control mice at indicated time points. **S-T,** Spleen weight of S100a9Tg mice at age >12 months. Age-matched control mice were sacrificed as control. **U,** Kaplan-Meier curves of OS, calculated from date of birth. **V,** Percentages of HSCs and MPPs, myeloid progenitors, Gr1^{+}/CD11b^{+} mature myeloid cells, macrophages, B-cells, and T-cells in each cohort. **W,** H&E, reticulin, and trichrome stained images of BM, spleen, and liver of S100a9Tg *vs.* control mice at age >12 months. Clinical parameters are described in Table S12. Actin blots in (L) were from the same samples run on different gels. Box plots in (A-C, N-R, and T) represent data from at least 5 mice in each group. Error bars in (D, F, G, J, K, M, and V) indicate mean ±SEM of at least 5 independent assays. * in (A, D, K, M and V), $P<0.05$ compared with control group.

Figure S7. Effects of inhibition of S100a9 or MYC in MYC-driven MF. A, Schematic of in vivo Tasquinimod efficacy studies. Mice were randomized to vehicle *vs.* Tasquinimod treatment following pIpC treatment. **B-F,** PB CBC analyses of RBC (B), monocytes (C), neutrophils (D), lymphocytes (E), and platelets (F) in Tasquinimod *vs.* vehicle treated cohorts. Baseline CBC was performed 1 week prior to drug treatment. **G,** Spleen weight at endpoints. Tasquinimod treated mice were sacrificed at ~32 weeks post-pIpC treatment, which is equivalent to the median OS of vehicle treated Mx1-Cre$^{+/-}$;Rosa26$^{LSL\text{-}MYC/LSL\text{-}MYC}$ mice. **H,** Percentages of HSCs and MPPs, myeloid progenitors, Gr1^{+}/CD11b^{+} mature myeloid cells, macrophages, B-cells, and T-cells in each cohort. **I,** H&E, reticulin, and trichrome stained images of BM, spleen, and liver at week 32 following pIpC injection in each group. **J,** Kaplan-Meier curves of OS. OS was calculated from the first date of Tasquinimod treatment. Demographic profiles and laboratory parameters are described in Table S13. **K-O,** Changes in MYC and cleaved PARP levels (K-N) by immunoblotting and apoptosis (O, % Annexin V^{+} cells) were assessed following 48 hr incubation with MYCi975 at the indicated concentrations. **P,** H&E, reticulin, and trichome stained images of BM, spleen, and liver at MYCi975 study endpoints. **Q,** Serial clinical data in trisomy 8+ TN-MF patient before and during fedratinib treatment. Body weight, WBC, hemoglobin, platelets counts and spleen volume were serially assessed as indicated. Experiments in (H) were performed simultaneously with experiments in Figure 3A-C and Figure S3B. Actin blots in (K-N) were from the same samples run on different gels. Box plots in panels (B-G) represent data from at least 8 mice in each group. Error bars in (H and O) indicate mean ±SEM of at least 3 independent assays. * in (B, D-G and O), $P<0.05$ compared with control group.

SUPPLEMENTAL TABLES

Table S1. Demographics of Moffitt Total Cancer Care MF patients

Parameters	*JAK2* mutant patients (n = 363)	*MPL* mutant patients (n = 42)	*CALR* mutant patients (n = 128)	TN patients (n = 51)	All patients (n = 584)
Median age at diagnosis, years (range)	67 (19-94)	69 (47-86)	61 (31-87)	70 (19-86)	67 (19-94)
Sex, n (%)					
Male	209 (58)	23 (55)	71 (55)	29 (57)	332 (57)
Female	154 (42)	19 (45)	57 (45)	22 (43)	252 (43)
Type of MF, n (%)					
PMF	227 (63)	30 (71)	79 (62)	43 (84)	378 (65)
Post-ET	55 (15)	12 (29)	48 (38)	8 (16)	122 (21)
Post-PV	81 (22)	0 (0)	2 (2)	0 (0)	83 (14)
Labs at Diagnosis (range)					
WBC, K/µL	10.3 (1.4-184.4)	8.1 (1.9-49.8)	7.5 (1.5-87.5)	8.5 (2.0-85.9)	9.1 (1.4-184.4)
Hemoglobin, g/dL	11.2 (4.9-17.4)	10.1 (6.4-13.7)	10.7 (5.6-16.3)	10.1 (3.4-15.6)	10.9 (3.4-17.4)
Platelet, K/µL	263.5 (8-2195)	315 (37-1307)	381 (18-1459)	156.5 (8-1238)	287 (8-2195)
Monocyte, K/µL	0.6 (0.0-31.2)	0.6 (0.1-9.5)	0.5 (0.0-3.9)	0.6 (0.1-5.9)	0.6 (0.1-5.9)
ANC, K/µL	7.4 (0.4-165.8)	4.7 (1.1-30.1)	5.2 (0.6-56.9)	6.3 (0.2-53.5)	6.2 (0.2-14.1)
ALC, K/µL	1.5 (0-14.1)	1.5 (0.5-4.9)	1.5 (0.4-10.2)	1.5 (0.4-5.0)	1.5 (0.0-14.1)
BM assessment					
Blast, % (range)	0 (0-15)	0 0-8)	0 (0-5)	0 (0-4)	0 (0-15)
Reticulin fibrosis, grade (range)	2 (1-3)	2 (1-3)	2 (1-3)	2 (1-3)	2 (1-3)
Cytogenetics, n (%) *	n = 339	n = 34	n = 117	n = 45	n = 535
+1/dup(1q)	11 (3)	0 (0)	4 (3)	1 (2)	16 (3)
Del(17p)	1 (0.4)	0 (0)	0 (0)	1 (2)	2 (0.4)
Del(13q)	23 (7)	3 (9)	15 (13)	0 (0)	41 (8)
+9	26 (8)	1 (3)	0 (0)	0 (0)	27 (5)
Del(20q)	44 (13)	3 (9)	4 (3)	1 (2)	52 (10)
+8	19 (6)	1 (3)	1 (1)	12 (27)	33 (6)
Complex karyotype **	28 (8)	3 (9)	2 (2)	3 (7)	36 (7)
Spleen size, cm (range)	16.5 (10-36)	15 (8-29)	15.5 (7.6-30)	14.8 (9.9-23.1)	16 (7.6-36)
DIPSS, n (%)	n = 360	n = 42	n = 128	n = 51	n = 581
Low	26 (7)	3 (7)	24 (19)	8 (16)	61 (10)
Intermediate-1	158 (44)	15 (36)	56 (44)	18 (35)	247 (43)
Intermediate-2	130 (36)	17 (40)	40 (31)	16 (31)	203 (35)
High	46 (13)	7 (17)	8 (6)	9 (18)	70 (12)

Abbreviations: Myelofibrosis (MF), triple negative (TN), primary MF (PMF), essential thrombocythemia (ET), polycythemia vera (PV), white blood cells (WBC), absolute neutrophil counts (ANC), absolute lymphocyte counts (ALC), bone marrow (BM), Dynamic International Prognostic Scoring System (DIPSS).

*Cytogenetics were assessed by conventional karyotyping and/or Fluorescence In Situ Hybridization (FISH). Six most common cytogenetic abnormalities are presented.

**Complex karyotype was defined as 3 or more cytogenetic abnormalities.

Table S2. Demographic Profile of trisomy 8+ TN-MF patient and healthy donors used in scRNA-seq analysis and PDX studies

ID	Age (yr)	Gender	Diagnosis	Conventional Karyotyping	FISH	Somatic mutations	Previous treatments
PDX	40	Male	MF	47,XY,+8[20]	Trisomy 8+ in 75%	*ASXL1* p.G646Wfs*12, VAF 36.6% *U2AF1* p.S34F, VAF 48.4%	None
HD1	22	Female	HD	NA	NA	NA	None
HD2	20	Male	HD	NA	NA	NA	None
HD3	19	Female	HD	NA	NA	NA	None

Abbreviations: Fluorescence in situ hybridization (FISH), variant allele frequency (VAF), healthy donor (HD), single cell RNA sequencing (scRNA-seq), patient-derived xenograft (PDX), not assessed (NA). See Figure S1I and Figure 7H for the conventional karyotyping and FISH results, respectively, of trisomy 8+ TN-MF patient.

Table S3. List of genes used for PROGENy analysis of human BM cells

JAK/STAT	*CCL2 CCR2 CLCF1 F2 F2R FGFR3 HCLS1 HGS IFNAR1 IFNAR2 IFNL1 IL12A IL20 IL22RA2 IL31RA LYN NF2 NMI PIAS1 PIGU SOCS1 SOCS2 SOCS3 SOCS6 STAMBP STAT1 STAT2 STAT3 STAT4 STAT5A STAT5B*
MAPK	*ABCA7 ABL1 ACE2 ACKR3 ACTA2 ADAM8 ADAM9 ADCYAP1 ADIPOQ ADORA1 ADRA1A ADRA1B ADRA2A ADRA2B ADRA2C ADRB2 ADRB3 AGER AGT AIDA AJUBA AKAP12 AKAP13 ALKAL1 ALKAL2 ALOX12B ALOX15 AMBP ANGPT1 ANKRD6 APELA APIP APOA1 APOE APP AR ARHGAP8 ARHGEF5 ARHGEF6 ARL6IP5 ARRB1 ARRB2 ASH1L ATF2 ATF3 ATP6AP2 AVP AVPI1 AVPR1B AXIN1 BANK1 BCAR3 BIRC7 BMP2 BMP4 BMP7 BMPER BRAF BRAP BTN2A2 C1QL4 C1QTNF1 C3orf33 C5AR1 CALCR CAMKK2 CARD9 CARTPT CASC2 CASR CAV1 CAV2 CAV3 CAVIN3 CBLC CCL1 CCL11 CCL13 CCL14 CCL15 CCL16 CCL17 CCL18 CCL19 CCL2 CCL20 CCL21 CCL22 CCL23 CCL24 CCL25 CCL26 CCL3 CCL3L1 CCL3L3 CCL4 CCL5 CCL7 CCL8 CCM2 CCN1 CCN2 CCR1 CCR5 CCR7 CD24 CD27 CD300A CD36 CD4 CD40 CD44 CD74 CD81 CDC42 CDC42EP5 CDH2 CDK1 CDK10 CDK5RAP3 CDON CEACAM1 CFLAR CHI3L1 CHRNA10 CHRNA7 CHRNA9 CIB1 CNKSR3 COPS5 CRK CRKL CRYAB CRYBA1 CSF1R CSK CSPG4 CTNNB1 CTSH CX3CL1 CXCL17 CYLD DAB2 DAB2IP DACT1 DAG1 DAXX DDR1 DDR2 DDT DEFB114 DENND2B DHX33 DIRAS1 DIRAS2 DIXDC1 DKK1 DLG1 DNAJA1 DNAJC27 DOK1 DOK2 DOK3 DOK4 DOK5 DOK6 DRD2 DRD4 DSTYK DUSP1 DUSP10 DUSP13 DUSP16 DUSP19 DUSP2 DUSP22 DUSP26 DUSP29 DUSP3 DUSP4 DUSP5 DUSP6 DUSP7 DUSP8 DUSP9 DVL2 DVL3 EDA2R EDAR EDN1 EDN3 EFNA1 EGF EGFR EIF2AK2 EIF3A ELANE EMILIN1 EPGN EPHA2 EPHA4 EPHA7 EPHA8 EPHB1 EPHB2 EPO ERBB2 ERBB4 ERCC6 ERN1 ERN2 ERP29 ERRFI1 EZH2 EZR F2R F2RL1 FAM83D FAS FBLN1 FBXW7 FCGR2B FCRL3 FERMT2 FFAR4 FGA FGB FGD2 FGF1 FGF10 FGF13 FGF18 FGF19 FGF2 FGF20 FGF21 FGF23 FGF4 FGF8 FGFR1 FGFR2 FGFR3 FGFR4 FGG FKTN FLCN FLT1 FLT3 FLT4 FN1 FOXM1 FOXO1 FPR2 FRS2 FSHR FZD10 FZD4 FZD5 FZD7 FZD8 GADD45A GADD45B GADD45G GAREM1 GAS6 GATA4 GBA1 GBP1 GCG GCNT2 GDF15 GDF6 GFRAL GH1 GHR GHRL GLIPR2 GNAI2 GPBAR1 GPER1 GPNMB GPR183 GPR37 GPR37L1 GPR55 GPS1 GPS2 GRAP GRAP2 GRB10 GRB2 GREM1 GRM1 GRM4 GRM5 GSDME GSTP1 HACD3 HAND2 HAVCR2 HCRTR1 HDAC3 HESX1 HGF HIPK2 HIPK3 HLA-DRB1 HMGB1 HMGCR HRAS HRH4 HSF1 HTR2A HTR2B HTR2C HYAL2 IAPP ICAM1 IGBP1 IGF1 IGF1R IGF2 IGFBP3 IGFBP4 IGFBP6 IKBKB IL11 IL18 IL1A IL1B IL26 IL31RA IL34 IL6 INAVA INHBA INPP5K INS INSR IQGAP1 IQGAP3 IRAK1 IRAK3 IRAK4 ITCH ITGA1 ITGAV ITGB1BP1 ITGB3 ITPKB JAK2 JCAD JUN KARS1 KDR KISS1 KIT KITLG KL KLB KLHDC10 KLHL31 KRAS KSR1 LAMTOR1 LAMTOR2 LAMTOR3 LAPTM5 LAX1 LBH LEMD2 LEP LGALS9 LIF LILRA5 LILRB4 LMO3 LPAR1 LPAR2 LPAR3 LRRK2 LTBR LYN MADD MAGED1 MAP2K1 MAP2K2 MAP2K3 MAP2K4 MAP2K5 MAP2K6 MAP2K7 MAP3K1 MAP3K10 MAP3K11 MAP3K12 MAP3K13 MAP3K15 MAP3K2 MAP3K20 MAP3K21 MAP3K3 MAP3K4 MAP3K5 MAP3K6 MAP3K7 MAP3K9 MAP4K1 MAP4K2 MAP4K3 MAP4K4 MAP4K5 MAPK1 MAPK10 MAPK11 MAPK12 MAPK13 MAPK14 MAPK15 MAPK3 MAPK4 MAPK6 MAPK7 MAPK8 MAPK8IP1 MAPK8IP2 MAPK8IP3 MAPK9 MAPKAPK2 MAPKAPK3 MAPKAPK5 MAPKBP1 MARCO MARVELD3 MBIP MBP MDFIC MECOM MEF2A MEF2C MEN1 MFAP3 MFHAS1 MID1 MIF MINK1 MIR126 MIR133A1 MIR133B MIR138-1 MIR145 MIR181A2 MIR181B1 MIR181D MIR185 MIR200C MIR205 MIR20A MIR21 MIR218-1 MIR221 MIR222 MIR23A MIR24-1 MIR26A1 MIR27A MIR27B MIR29B1 MIR424 MIR503 MIR519D MIR92A1 MIRLET7B MMP8 MOS MST1R MT3 MTURN MUSK MYC MYD88 MYDGF MYOC NAIP NBR1 NCF1 NCOR1 NDRG2 NDRG4 NDST1 NECAB2 NEK10 NELFE NENF NF1 NF2 NFKB1 NLK NLRP12 NLRP6 NOD1 NOD2 NODAL NOTCH1 NOTCH2 NOX1 NOX4 NPFFR2 NPHS1 NPNT NPPA NPR2 NPSR1 NPTN NPY NPY5R NRAS NRG1 NRP1 NRTN NTF3 NTRK1 NTRK2 NTRK3 NUP62 OPRK1 OPRM1 OR2AT4 OSM OXTR P2RX7 P2RY1 P2RY6 PABPN1 PAFAH1B1 PAGE4 PAK1 PAK2 PAK3 PAK4 PAK5 PAK6 PAQR3 PBK PDCD10 PDCD4 PDE5A PDE6G PDE6H PDE8A PDGFA PDGFB PDGFC PDGFD PDGFRA PDGFRB PEA15 PEBP1 PELI2 PER1 PHB1 PHB2 PHLPP1 PIK3CB PIK3CG PIK3R2 PIK3R5 PIK3R6 PIN1 PINK1 PJA2 PKHD1 PLA2G1B PLA2G2A PLA2G5 PLCB1 PLCE1 PLCG2 PLVAP POU4F2 PPARG PPEF2 PPIA PPM1L PPP1CB PPP1CC PPP2R1A PPP5C PRDM11 PRDM15 PRDX1 PRDX2 PRKCA PRKCD PRKCE PRKCZ PRKD2 PRKN PRMT1 PRMT5 PROK1 PRXL2C PSCA PSEN1 PSMD10 PTEN PTGER4 PTK2B PTPN1 PTPN11 PTPN2 PTPN22 PTPN3 PTPN6 PTPN7 PTPRC PTPRJ PTPRR PYCARD QARS1 RAF1 RAMP3 RANBP9 RAP1A RAP1B RAP1GDS1 RAP2A RAPGEF2 RASGRP1 RASGRP3 RASSF2 RB1CC1 RBX1 RCE1 RELL1 RELL2 REN RET RGS14 RGS2 RHBDD3 RIPK1 RIPK2 RIT2 RNF149 RNF41 ROBO1 ROCK1 ROCK2 ROR1 ROR2 ROS1 RPS3 RPS6KA6 RRAS RYK S100A12 S100A7 SASH1 SBK2 SCG2 SCIMP SDCBP SEMA3A SEMA4C SEMA6A SEMA7A SERPINB3 SERPINF2 SETX SFRP1 SFRP2 SH2B3 SH2D3A SH2D3C SH3RF1 SH3RF2 SH3RF3 SHANK3 SHC1 SIRPA SLA SLAMF1 SLC30A10 SLC9A3R1 SMAD1 SMAD3 SMAD4 SMPD1 SOD1 SORBS3 SORL1 SOX2 SOX9 SPAG9 SPHK1 SPI1 SPRED1 SPRED2 SPRED3 SPRY1 SPRY2 SPRY3 SPRY4 SRC SSTR4 STK25 STK3 STK38 STK39 STK4 STK40 STRADB STYX STYXL2 SULT1A3 SULT1A4 SYK SYNGAP1 SYNJ2BP SYT14P1 TAB1 TAOK1 TAOK2 TAOK3 TBC1D10C TBX1 TDGF1 TEK TENM1 TF TGFA TGFB1 TGFB2 TGFB3 TGFBR1 TGFBR3 THBS1 THPO TIMP3 TIRAP TLR3 TLR4 TLR6 TLR7 TLR9 TMEM106A TNF TNFAIP8L3 TNFRSF11A TNFRSF19 TNFSF11 TNIK TNIP1 TP73 TPBG TPD52L1 TRAF1 TRAF2 TRAF3 TRAF4 TRAF5 TRAF6 TRAF7 TREM2 TRIB1 TRIM5 TRPV4 UCHL1 ULK4 UNC5CL USP17L2 VEGFA VRK2 VRK3 WDR54 WNK2 WNK4 WNT16 WNT5A WNT7A WNT7B WWC1 XCL1 XCL2 XDH XIAP YWHAE YWHAZ ZC3H12A ZDHHC17 ZDHHC9 ZFP36 ZFP36L1 ZFP36L2 ZMYND11 ZNF622 ZNF675*
EGFR	*ABL1 ACP4 ADAM17 ADORA1 ADRA2A AFAP1L2 AGR2 AGT AKT1 AREG BCAR1 BCAR3 BRAF BTC CADM1 CAMLG CBL CBLB CBLC CCDC88A CDH13 CEACAM1 CHMP6 CNOT9 CPNE3 CUL5 DAB2IP DGKD DUSP3 EFEMP1 EGF EGFR EPGN ERBB2 ERBB3 ERBB4 ERBIN EREG ERRFI1 FAM83A FAM83B FAM83C FASLG FBXW7 FER GAB1 GAREM1 GPER1 GPRC5A GRB2 GRB7 HAP1 HBEGF HIP1 HIP1R IFI6 IQGAP1 ITGA1 KIF16B LGMN MAPK1 MIR133A1 MIR21 MIR29A MMP9 MVB12A MVB12B MVP MYOC NCF1 NCK2 NEU3 NEURL1 NPR2 NRG1 NRG3 NRG4 NUP62 PDE6G PDE6H PDPK1 PIGR PIK3C2A PIK3CA PLAUR PLCE1 PLCG1 PRICKLE1 PSEN1 PTK2 PTK2B PTK6 PTPN11 PTPN12 PTPN18 PTPN2 PTPN3 PTPRJ PTPRR RAB7A RALA RALB RASSF2 RBPJ REPS2 RHBDF1 RHBDF2 RNF115 RNF126 RTN4 SH3TC2 SHC1 SHC3 SHKBP1 SLC30A10 SNX5 SNX6 SOCS4 SOCS5 SOS1 SOX9 SRC STUB1 TDGF1 TGFA TGFB1 TSG101 VIL1 VPS25 WDR54 ZFYVE28 ZGPAT*
PI3K	*AGT AKT1 ANGPT1 BECN1 BTN2A2 C1QBP CAT CBL CCL5 CD160 CD28 CEACAM1 CEP55 CRNN CRYBA1 CSF3 DAB2IP DCN DDR1 DDR2 DIPK2A EDN1 EGF EGFR ERBB2 ERBB3 ERBB4 F2 F2R F2RL1 FBXL2 FCGR3A FGF2 FGFR1 FGR FLT1 FLT3 FN1 FSHR GATA3 GH1 GPER1 HAX1 HCLS1 HCST HGF HTR2A HTR2B IGF1 IGF1R IL18 INPP5E INS INSR IRS1 JAK2 KBTBD2 KDR KIT LEP LIME1 LTK MAZ MIR126 MIR206 MIR20A MIR21 MIR449A MUSK MYDGF MYO16 MYOC NCF1 NEDD4 NF1 NKX3-1 NLRC3 NOP53 NTRK1 NTRK2 NTRK3 NYAP1 NYAP2 OSM PDGFA PDGFB PDGFC PDGFD PDGFRA PDGFRB PEAR1 PIK3AP1 PIK3C2A PIK3C2B PIK3C2G PIK3CA PIK3CB PIK3CD PIK3CG PIK3IP1 PIK3R1 PIK3R2 PIK3R5 PIP5K1A PIP5K1B PIP5K1C PLEKHA1 PLXNB1 PPARD PPP1R16B*

	PREX2 PRR5 PRR5L PTEN PTK2 PTPN13 PTPN6 RASGRP1 RELN RGL2 ROR1 ROR2 SELP SEMA3E SEMA4D SERPINA12 SERPINE2 SIRT1 SIRT2 SLC9A3R1 SOX9 SRC STAMBP TEK TGFB2 TNF TREM2 TSC2 TWIST1 TYRO3 UBE3A UNC5B WNT16 ZFP36L1
TGF-β	*ACVR1 ACVRL1 ADAM17 ADAM9 ADAMTSL2 AMHR2 APOA1 APPL1 APPL2 ARID4A ARID4B ARRB2 ASPN AXIN1 BAMBI BCL9 BCL9L BMP2 BMPR1A BRMS1 BRMS1L C20orf27 CAV1 CAV2 CAV3 CD109 CDH5 CDKN1C CDKN2B CHST11 CIDEA CILP CITED1 CITED2 CLDN5 COL1A2 COL3A1 CREBBP DAB2 DAND5 DKK3 DNM2 DUSP22 EID2 EMILIN1 ENG EP300 FAM89B FBN1 FBN2 FERMT1 FERMT2 FKBP1A FLCN FMOD FNTA FOLR1 FOS FOXH1 FSHB FURIN FUT8 GCNT2 GDF10 GDF15 GDF5 GDF9 GIPC1 GLG1 HDAC1 HDAC2 HIPK2 HPGD HSP90AB1 HSPA1A HSPA5 HTRA1 HTRA3 HTRA4 ID1 IL17F IL17RD ING1 ING2 ITGA3 ITGA8 ITGB1 ITGB5 ITGB6 ITGB8 JUN LATS1 LATS2 LDLRAD4 LEFTY1 LEMD3 LOX LPXN LRG1 LRRC32 LTBP1 LTBP2 LTBP3 LTBP4 MAP3K7 MEN1 MIR15B MIR17 MIR183 MIR18A MIR20A MIR21 MIR212 MIR26A1 MIR29B1 MIR30A MIR30B MIR342 MIR498 MIRLET7F1 MIRLET7G MSTN MTMR4 MYOCD NKX2-1 NLK NODAL NPNT NREP NRROS OGT ONECUT1 ONECUT2 PALS1 PARP1 PBLD PDPK1 PEG10 PIN1 PMEPA1 PML PPARA PPARG PPM1A PRDM16 PSG9 PTK2 PTPRK PXN RASL11B RBBP4 RBBP7 RNF111 SAP130 SAP30 SAP30L SDCBP SIN3A SINHCAF SIRT1 SKI SKIL SKOR2 SLC2A10 SMAD1 SMAD2 SMAD3 SMAD4 SMAD5 SMAD6 SMAD7 SMAD9 SMURF1 SMURF2 SNW1 SNX25 SNX6 SOX11 SPI1 SPRED1 SPRED2 SPRED3 SPRY1 SPRY2 SRC STAT3 STK11 STRAP STUB1 SUDS3 TAB1 TET1 TGFB1 TGFB1I1 TGFB2 TGFB3 TGFBR1 TGFBR2 TGFBR3 TGFBRAP1 THBS1 TNXB TP53 TRIM33 TWSG1 USP15 USP9X USP9Y VASN VEPH1 WFIKKN1 WFIKKN2 WNT1 ZBTB7A ZEB1 ZEB2 ZFYVE9 ZMIZ1 ZMIZ2 ZNF451 ZNF703 ZYX*
TNF-α	*ACTN4 ADAM17 ADIPOQ AIM2 APOA1 BIRC2 BIRC3 BIRC7 CARD14 CARD16 CARD8 CASP1 CASP4 CASP8 CCDC3 CD70 CDIP1 CHUK CLDN18 COMMD7 CPNE1 CYLD EDA2R EIF5A EXT1 F2RL1 FAS FOXO3 GAS6 GPS2 GSTP1 H2BC11 HIPK1 HSPA1A HSPA1B IKBKB ILK JAK2 KRT18 KRT8 LAPTM5 LIMS1 MIR1246 MIR152 MIR24-1 MIR27B MIR34A NAIP NFKBIA NKIRAS1 NKIRAS2 NLRP2B NR1H4 OTULIN PELI3 PIAS3 PIAS4 PLVAP PPP2CB PRKN PTK2B PTPN2 PYCARD PYDC1 PYDC2 RELA RFFL RIPK1 RRAGA SHARPIN SPATA2 SPHK1 SPPL2A SPPL2B ST18 STAT1 SYK TMSB4X TNF TNFAIP3 TNFRSF11A TNFRSF13C TNFRSF14 TNFRSF17 TNFRSF18 TNFRSF19 TNFRSF1A TNFRSF1B TNFRSF25 TNFRSF4 TNFSF11 TNFSF13B TNFSF18 TP53 TRADD TRAF1 TRAF2 TRAF3 TRAF3IP2 TRAF4 TRAF5 TRAF6 TRAIP TRIM32 TXNDC17 UBE2K UMOD XIAP ZNF675*
VEGF	*ADAMTS3 ADGRA2 CADM4 CCBE1 CD63 DAB2IP DCN DLL1 FBXW7-AS1 FLT1 FLT3 FLT4 FOXC1 GAB1 HRG HSPB1 IL12A IL12B JCAD KDR MIR16-1 MIR199A1 MIR21 MIR26A1 MIR329-1 MIR342 MIR424 MYO1C NRP1 NRP2 NUS1 PDGFRA PDGFRB PGF PIK3CA PIK3CB PIK3CD PRKD1 PRKD2 PTP4A3 ROBO1 SEMA6A SMOC2 SPRY2 TNXB VEGFA VEGFB VEGFC VEGFD XDH*
p53	*ACER2 ANKRD1 ATM ATR ATRX BATF BCL3 BRCA2 CASP2 CD44 CD74 CDKN1A CDKN1B CHEK2 COPS3 CRADD DDX5 DYRK1A DYRK3 E2F7 EEF1E1 FOXM1 GML GTSE1 HIC1 HIPK2 ING4 KAT5 KDM1A KMT5A MARCHF7 MDM2 MDM4 MIF MSX1 MUC1 MYO6 NBN NDRG1 PAXIP1 PIDD1 PLA2R1 PLK2 PLK3 PMAIP1 PML PPM1D PRAP1 PSMD10 PTTG1IP PYHIN1 RPL26 RPS27L RPS6KA6 SESN2 SIRT1 SMYD2 SNAI1 SNAI2 SOX4 SP100 SPRED1 SPRED2 TFAP4 TP53 TRIAP1 TWIST1 USP10 YJU2 ZMPSTE24 ZNF385A ZNHIT1*
Estrogen	*AR ARID1A BRCA1 CARM1 CNOT1 CNOT2 CNOT9 CYP7B1 DDRGK1 DDX17 DDX5 DDX54 DEFA1 DEFA1B DEFA3 DNAAF4 EGLN2 ESR1 ESR2 FOXA1 FOXH1 ISL1 KANK2 KMT2D LATS1 LBH MED1 NCOA4 PADI2 PAGR1 PAK1 PARP1 PHB2 POU4F2 PPARGC1B RBFOX2 SAFB SKP2 SRARP SRC STRN3 TADA3 TAF7 TP63 TRIP4 UBA5 UFL1 UFM1 UFSP2 VPS11 VPS18 WBP2 YAP1 ZNF366*
Androgen	*AR ARID1A CST11 DAB2 DAXX DDX17 DDX5 DNAJA1 EP300 FKBP4 FOXH1 FOXP1 HDAC1 HDAC6 HEYL KDM1A KDM3A KDM4C KDM5D NCOR1 NCOR2 NKX3-1 NODAL PARK7 PHB1 PIAS2 PKN1 PLPP1 PMEPA1 PRMT2 RHOA RHOXF1 RNF14 RNF6 RWDD1 SAFB2 SCGB2A1 SCGB2A2 SFRP1 SIRT1 SMARCA4 TCF21 TMF1 TRIM68 UBE3A ZBTB7A ZMIZ1*
TRAIL	*ATF3 CASP8 FADD MIR221 MIR222 PARK7 PTEN SPI1 TIMP3 TNFRSF10A TNFRSF10B TNFRSF10C ZDHHC3*
NF-κB	*ACTN4 ADGRG3 ADIPOR1 AGER AGO3 AKIP1 AKT1 ALK APP BCL3 BIRC2 BIRC3 BMP7 C1QTNF3 C1QTNF4 C20orf27 CALR CARD10 CARD14 CCL19 CCN3 CD14 CD27 CD86 CHI3L1 CHUK COPS8 CPNE1 CYLD DDX3X DICER1 DLG1 EDA EDAR EDN1 EGFR EIF2AK2 EP300 EZR GREM1 HAVCR2 HDAC7 IFI35 IKBKE IL12B IL18 IL18R1 IL1B IL23A ILK IRAK1 LAPTM5 LGALS9 LIME1 LIMS1 LITAF LRRC19 MALT1 MAP3K14 MAP3K7 MAS1 MIR125B1 MIR130A MIR132 MIR146A MIR149 MIR15B MIR182 MIR204 MIR21 MIR223 MIR27A MIR27B MIR29B1 MIR30C2 MIR329-1 MIR508 MIR766 MIR9-1 MKRN2 MMP8 NDUFC2 NFAT5 NFKB1 NFKB2 NFKBIA NLRC3 NLRP12 NLRP3 NMI NOD1 NOD2 NR3C2 PDCD4 PHB1 PHB2 PPM1A PPM1B PPP4C PRDX1 PTP4A3 PTPN22 PYDC2 RASSF2 RBCK1 RC3H1 RC3H2 REL RELA RELB RHOA RIPK3 RPS3 RTKN2 SASH1 SPHK1 SPI1 TCIM TERF2IP TIRAP TLR2 TLR3 TLR4 TLR6 TLR7 TLR9 TMSB4X TNF TNFRSF10A TNFRSF10B TNFSF14 TNFSF15 TRADD TRAF2 TRAF4 TRAF6 TREM2 TRIM40 TRIM44 TRIM6 TRIP6 TSPAN6 UACA ZC3H12A ZFP91*
MYC	*AMD1 ARL1 ARRB2 ASAH1 ATF4 ATM ATP5B ATP5C1 ATP5E ATP5G2 BARD1 BCKDHA BCKDHB BLK CACNB1 CAD CALM2 CALR CAPZA1 CD79B CD97 CDC6 CDC25B CDK6 CDKN1B CTSC CISH CKS2 CLCN2 CLCN3 CLCN6 CLN3 SLC31A1 COX7C COX15 CR2 CREB1 CREBL2 CSF2RB CSTF3 CYBA DAXX DBI DBP DDB1 DDX1 DDX3X DDX5 DDX10 DPAGT1 DPYSL3 EIF2S1 EIF2S3 ENO2 STOM ERCC6 ETF1 ETFA FABP5 FANCF FKBP2 FLOT2 FRAP1 FTH1 XRCC6 GABPA GAK GALC NR6A1 GCLC GMDS GNA12 GNL1 GNS GRK4 H2AFX H2AFZ HADHB HARS HIP2 HLA-A HLA-F HMMR HNRNPA1 HNRNPL HSPA2 HSPA9 HSPE1 IDH3B IFNAR1 IFNGR1 IGBP1 ILK ING1 IRF3 JARID2 KHK KIF11 KPNA3 RANBP5 LAMP1 LDHA FADS3 LNPEP LSP1 LTA4H M6PR NBR1 MAD2L1 SMAD3 MAGOH MAN2A1 MARS MAT2A MBNL1 MCM3 MCM5 MDH1 MAP3K5 RAB8A METTL1 MFAP1 MFNG MGAT2 MKLN1 MMP8 MMP15 MOCS2 MSH2 MST1R MT2A MT3 MTF1 MTHFD1 PPP1R12A NACA NAGA NUBP1 NCBP1 NCL NDUFA1 NDUFA2 NDUFA6 NDUFB1 NDUFB2 NDUFB3 NDUFB4 NDUFB5 NDUFB6 NDUFS1 NDUFV1 NDUFS6 DRG1 NFKBIB NME1 CNOT2 CNOT4 NUP88 OAZ1 PA2G4 PCM1 PCMT1 PCNA PCTK1 PCYT1A PDE4C PDE6D PDK1 PDK2 PDK3 SLC26A4 PER1 PET112L PEX6 PFKFB4 PFN1 PIGF PKM2 PMM2 PMS1 PMS2L3 UBL3 POLH POU2F1 PPA1 PPIA PPP1CB PPP1R7 PPP2CA PPP2R1B PPP2R4 PPP3CA PREP PRKAB1 PRKAB2 PRKAG1 PKN2 PRKCSH PRKDC MAPK7 MAP2K5 MAP2K7 PRKRIR PRPS2 PRPSAP1 PSMA1 PSMA5 PSMB1 PSMB5 PSMB7 PSMC4 PSMC5 PSMD3 PSMD5 PSMD7 PSMD8 PSMD10 PTPN1 PTPN6 PTPRF PYCR1 ALDH18A1 RAB1A RGL2 RAB3A RAC2 RAD9A RAP2B RASA1 ARID4A JARID1A RBBP8 RBL1 RBM4 RECQL RFX5 RGS16 RHEB RLN1 RNF4 ABCE1 RPL5 RPL8 RPL9 RPL13 RPL15 RPL18 RPL19 RPL27 RPL27A RPL31 RPL32 RPL37 RPLP1 RPS5 RPS6 RPS6KA2 RPS6KB1 RPS13 RPS17 RPS19 RPS20 RPS21 RPS25 RPS26 RPS27A RPS29 RRAS RXRB VPS52 SARS SCD SCO1 SDF2 SFRS2 SFRS5 SFRS7 SLC1A4 SLC2A4 SLC7A1 SLC12A2 SLC22A3 SLC22A4 SNAPC1 SNAPC3 SNRPA SNRPD3 SOD1 SOX12 SP4 SPIB SRD5A1 SRI SREBF2 SRP54 SRP68 SRPR SSB SUPT5H VAMP1 SYK SYPL1 CNTN2 TCEB3 C2orf3 TCF12 MLX TLE3 TLL2 TLOC1 TMF1 TMPO TMSB4X TNFAIP1 TP53 TPP2 TPR TPT1 HSP90B1 TSC2 TSPY1 TTC4 TUBG1 TULP3 TYK2 U2AF1 UBE2D3 UBE2G2 UCHL1 USP4 UQCRC2 USP1 VASP VCP VDAC2 VGF EIF4H XK YY1 YWHAH ZFPL1*

	ZNF7 ZNF12 ZNF35 ZNF85 ZNF134 ZNF136 ZNF142 TRIM25 ZNF174 ZNF192 ZNF225 PTP4A1 CSDE1 DAP3 FZD5 ARMET SLC39A7 EPM2A JTV1 UBXD6 GLRA3 CCDC6 CUL5 COIL ELL DPF1 DGCR6 LZTR1 HDHD1A USP11 JARID1C SMC1A TMEM187 LAGE3 HIST1H4I ACOX3 HIST1H2AI HIST1H2AK HIST1H2AJ HIST1H2AC HIST1H2AM HIST2H2AA3 HIST1H2BG HIST1H2BN HIST1H2BM HIST1H2BF HIST1H2BE HIST1H2BH HIST1H2BI HIST1H2BC HIST2H2BE HIST1H4B HIST1H4L PLA2G6 SLC25A11 TAGLN2 UXT EEA1 STX7 CMAH RAD54L GNPAT SIP1 RANBP3 SLC43A1 PEX3 PARG CSDA COPS3 AGPS BLZF1 PIAS1 DEGS1 MADD MKNK1 KHSRP AKR7A2 PRKRA USO1 DSCR2 RNASET2 EIF3I STX16 STX10 PLA2G4B JRKL SNX3 CRADD CD164 RAB11A RIPK2 PEX11B SUCLG1 TRIM24 DPM1 DPM2 SAP30 GGH ALKBH1 DLEU2 ARHGEF7 SQSTM1 SGPL1 CDC16 ZNF259 SLC5A6 HERC1 MBD4 HIST1H2AG HIST1H2BJ PLOD3 CH25H BAZ1B NFS1 ASH2L LATS1 RQCD1 AIFM1 RRP9 ATG12 EXO1 COX7A2L AP4M1 VAPA RPS6KA5 PSCD2 WDR46 SFRS11 COPS2 TRIP13 GTF3C5 GTF3C4 EFTUD2 PPT2 CIAO1 RECQL5 PEX16 MED17 GSTO1 LY86 EIF4E2 MED20 PMPCB FXR2 SPTLC2 EEF1E1 POLR1C CIR APBA3 H2AFY CHD1L H6PD NR1D1 SPAG6 RBM39 MPHOSPH1 IER2 PSCDBP RNF7 PTDSS1 MAML1 KEAP1 GINS1 AMMECR1 GOLGA5 HS3ST2 THRAP3 NUP153 DMTF1 HDAC6 SH2D3C SAE1 ABCB6 SCAMP3 ARPC4 ACTR3 NUBP2 RAD50 KIF20A FRY TRAP1 ARFRP1 AKAP9 CEBPZ RCL1 PSME3 MPHOSPH6 USPL1 PSMD14 TRIB1 NBR2 HRSP12 ABCC4 ZMPSTE24 STUB1 OPRS1 SDCCAG10 SAP18 DNAJA2 MAEA DLEU1 LANCL1 TMEM5 TMEM4 HMG20A CACNG3 TUBA1B SCML2 CEPT1 ANAPC10 PIAS3 PRMT5 TESK2 TIMM23 IFI30 TIMM17A HAX1 COG5 TIMM44 MYBBP1A CIB1 DDX17 HBXIP ARL6IP5 CCT7 ERLIN1 SPAG5 POLR3G IVNS1ABP RAD51AP1 TUSC4 PMVK RRAGA CCT8 AP4B1 MGEA5 NFAT5 PTGES3 AHCYL1 ARPP-19 ZNF274 WDR4 YIF1A SUGT1 RNPS1 SEC61B TMED10 MAPRE2 CYB561D2 TOPBP1 HSF2BP HNRPUL1 BTN2A1 POLR3A PWP1 AP4S1 NUDT6 MAP4K5 RASSF1 SUPT16H AKAP10 RPL35 PDCD10 DCTN3 PHB2 GABARAP MTF2 NCBP2 MAPRE1 ATF6 KCNH4 ITGB3BP AP4E1 ABCB10 CBX5 TTC33 DDX58 CORO1C CD2AP MKRN1 NUP62 ARFIP2 LYPLA3 ZKSCAN5 CARKL SDF2L1 MAFF FTSJ1 RAB3GAP2 SLC39A6 ATXN10 PRDX5 APPL1 FBXO5 MYCBP TIMM9 TIMM8B NUFIP1 DNAI1 ACAD8 ST6GALNAC4 TRAPPC3 CACYBP ATP5S SNX5 IL17C SERP1 ARHGEF16 TNFRSF21 LSM1 MOCS3 EIF3K RABGEF1 HTRA2 MAT2B NXT1 TMOD2 ABT1 UCRC RBM15B CPSF1 SNX15 HOOK2 HCFC2 PYCR2 TIMM22 GPR132 SERTAD1 POMT2 UBQLN1 ERO1L CXXC1 ZNRD1 DEF6 WDR42A RNF141 HEBP1 LOC51035 ZNF593 RPS27L POLR1D CCDC41 LOC51136 DYNC1LI1 MRTO4 DCTN4 NAGPA HSPA14 ATPBD1C C15orf15 ABI3 PIGP CDKL3 IER5 SCAND1 GMIP FKBP11 ZDHHC3 ATP6V1D PPME1 NOL7 DDX41 HSD17B7 SCLY MIR16 AZIN1 PCF11 TRIM33 CUTA LSR LIPT1 KIAA0859 TRMT6 STYXL1 GINS2 BRP44L ASB1 MPP6 LSM8 VPS29 PPP6C POLR3K RAPGEF6 RP6-213H19.1 ZAK BTBD1 NUP54 ADAM22 PTOV1 DSCR6 POLE3 H2BFS GDAP1 CCDC76 GNB1L LZTFL1 TRIM44 OCIAD1 CNDP2 GLT8D1 CBWD1 ACSS2 DMAP1 C20orf24 SLC25A40 DIABLO SERF1B PNO1 KIF15 ENTPD7 PCNP ZNF286A BIRC6 POLD4 ZNF410 NGB ALOXE3 TGIF2 SAV1 GPSM3 MCCC2 MAGEF1 SLC39A8 NCAPG LEPRE1 ELOVL1 MRPL40 TSEN34 EPC1 ULBP1 WDR23 PRR3 POLR1B WBSCR22
Alarmin/ Innate Immunity	*A1BG AAMP ABCA13 ABI1 ABI2 ABL1 ACAA1 ACLY ACP3 ACTB ACTG1 ACTR10 ACTR1B ACTR2 ACTR3 ADA2 ADAM10 ADAM8 ADGRE3 ADGRE5 ADGRG3 AGA AGER AGL AGPAT2 AHCYL1 AHSG AIM2 ALAD ALDH3B1 ALDOA ALDOC ALOX5 ALPK1 AMPD3 ANO6 ANPEP ANXA2 AOC1 AP1M1 AP2A2 APAF1 APEH APOB APP APRT ARG1 ARHGAP45 ARHGAP9 ARL8A ARMC8 ARPC1A ARPC1B ARPC2 ARPC3 ARPC4 ARPC5 ARSA ARSB ART1 ASAH1 ATAD3B ATF1 ATF2 ATG12 ATG5 ATG7 ATOX1 ATP11A ATP11B ATP6AP2 ATP6V0A1 ATP6V0A2 ATP6V0A4 ATP6V0B ATP6V0C ATP6V0D1 ATP6V0D2 ATP6V0E1 ATP6V0E2 ATP6V1A ATP6V1B1 ATP6V1B2 ATP6V1C1 ATP6V1C2 ATP6V1D ATP6V1E1 ATP6V1E2 ATP6V1F ATP6V1G1 ATP6V1G2 ATP6V1G3 ATP6V1H ATP7A ATP8A1 ATP8B4 AZU1 B2M B4GALT1 BAIAP2 BCL10 BCL2 BCL2L1 BIN2 BIRC2 BIRC3 BPI BPIFA1 BPIFA2 BPIFB1 BPIFB2 BPIFB4 BPIFB6 BRI3 BRK1 BST1 BST2 BTK BTRC C1orf35 C1QA C1QB C1QC C1R C1S C2 C3 C3AR1 C4A C4B C4B_2 C4BPA C4BPB C5 C5AR1 C5AR2 C6 C6orf120 C7 C8A C8B C8G C9 CAB39 CALM1 CALML5 CAMP CAND1 CANT1 CAP1 CAPN1 CAPZA1 CAPZA2 CARD11 CARD9 CASP1 CASP10 CASP2 CASP4 CASP8 CASP9 CAT CCL17 CCL22 CCR2 CCR6 CCT2 CCT8 CD14 CD177 CD180 CD19 CD209 CD247 CD300A CD300E CD300LB CD33 CD36 CD3G CD4 CD44 CD46 CD47 CD53 CD55 CD58 CD59 CD63 CD68 CD81 CD93 CDA CDC34 CDC42 CDK13 CEACAM1 CEACAM3 CEACAM6 CEACAM8 CEP290 CFB CFD CFH CFHR1 CFHR2 CFHR3 CFHR4 CFHR5 CFI CFL1 CFP CGAS CHGA CHI3L1 CHIT1 CHRNB4 CHUK CKAP4 CLEC10A CLEC12A CLEC4A CLEC4C CLEC4D CLEC4E CLEC5A CLEC6A CLEC7A CLU CMTM6 CNN2 CNPY3 COLEC10 COLEC11 COMMD3 COMMD9 COPB1 COTL1 CPB2 CPN1 CPN2 CPNE1 CPNE3 CPPED1 CR1 CR2 CRACR2A CRCP CREB1 CREBBP CREG1 CRISP3 CRISPLD2 CRK CRP CSNK2B CST3 CSTB CTNNB1 CTSA CTSB CTSC CTSD CTSG CTSH CTSK CTSL CTSS CTSV CTSZ CUL1 CXCL1 CXCR1 CXCR2 CYB5R3 CYBA CYBB CYFIP1 CYFIP2 CYLD CYSTM1 DBNL DCD DDOST DDX3X DDX41 DDX58 DEFA1 DEFA1B DEFA3 DEFA4 DEFA5 DEFA6 DEFB1 DEFB103A DEFB103B DEFB104A DEFB104B DEFB105A DEFB105B DEFB106A DEFB106B DEFB107A DEFB107B DEFB108B DEFB110 DEFB112 DEFB113 DEFB114 DEFB115 DEFB116 DEFB118 DEFB119 DEFB121 DEFB123 DEFB124 DEFB125 DEFB126 DEFB127 DEFB128 DEFB129 DEFB130A DEFB130B DEFB131A DEFB132 DEFB133 DEFB134 DEFB135 DEFB136 DEFB4A DEFB4B DEGS1 DERA DGAT1 DHX36 DHX58 DHX9 DIAPH1 DNAJC13 DNAJC3 DNAJC5 DNASE1L1 DNM1 DNM2 DNM3 DOCK1 DOCK2 DOK3 DPP7 DSC1 DSG1 DSN1 DSP DTX4 DUSP3 DUSP4 DUSP6 DUSP7 DYNC1H1 DYNC1LI1 DYNLL1 DYNLT1 ECSIT EEA1 EEF1A1 EEF2 ELANE ELK1 ELMO1 ELMO2 ENPP4 EP300 EPPIN EPPIN-WFDC6 EPX ERP44 F2 FABP5 FADD FAF2 FBXW11 FCAR FCER1A FCER1G FCGR1A FCGR2A FCGR3A FCGR3B FCN1 FCN2 FCN3 FGA FGB FGG FGL2 FGR FLG2 FOLR3 FOS FPR1 FPR2 FRK FRMPD3 FTH1 FTL FUCA1 FUCA2 FYN GAA GAB2 GALNS GCA GDI2 GGH GHDC GLA GLB1 GLIPR1 GM2A GMFG GNLY GNS GOLGA7 GPI GPR84 GRAP2 GRB2 GRN GSDMD GSDME GSN GSTP1 GUSB GYG1 GZMM HBB HCK HEBP2 HERC5 HEXB HGSNAT HK3 HLA-A HLA-B HLA-C HLA-E HMGB1 HMOX1 HMOX2 HP HPSE HRAS HRNR HSP90AA1 HSP90AB1 HSP90B1 HSPA1A HSPA1B HSPA6 HSPA8 HTN1 HTN3 HUWE1 HVCN1 ICAM2 ICAM3 IDH1 IFI16 IFIH1 IFNA1 IFNA10 IFNA13 IFNA14 IFNA16 IFNA17 IFNA2 IFNA21 IFNA4 IFNA5 IFNA6 IFNA7 IFNA8 IFNB1 IGF2R IGHE IGHG1 IGHG2 IGHG4 IGHV1-2 IGHV1-46 IGHV1-69 IGHV2-5 IGHV2-70 IGHV3-11 IGHV3-13 IGHV3-23 IGHV3-30 IGHV3-33 IGHV3-48 IGHV3-53 IGHV3-7 IGHV4-34 IGHV4-39 IGHV4-59 IGKV1-12 IGKV1-16 IGKV1-17 IGKV1-33 IGKV1-39 IGKV1-5 IGKV1D-12 IGKV1D-16 IGKV1D-33 IGKV1D-39 IGKV2-28 IGKV2-30 IGKV2D-28 IGKV2D-30 IGKV2D-40 IGKV3-11 IGKV3-15 IGKV3-20 IGKV3D-20 IGKV4-1 IGKV5-2 IGLC2 IGLC3 IGLV1-40 IGLV1-44 IGLV1-47 IGLV1-51 IGLV2-11 IGLV2-14 IGLV2-23 IGLV2-8 IGLV3-1 IGLV3-19 IGLV3-21 IGLV3-25 IGLV3-27 IGLV6-57 IGLV7-43 IKBKB IKBKE IKBKG IL1B ILF2 IMPDH1 IMPDH2 IQGAP1 IQGAP2 IRAG2 IRAK1 IRAK2 IRAK3 IRAK4 IRF3 IRF7 ISG15 IST1 ITCH ITGAL ITGAM ITGAV ITGAX ITGB2 ITK ITLN1 ITPR1 ITPR2 ITPR3 JUN JUP KCMF1 KCNAB2 KIR2DS1 KIR2DS2 KIR2DS3 KIR2DS4 KIR2DS5 KIR3DS1 KLRC2 KLRD1 KLRK1 KPNB1 KRAS KRT1 LAIR1 LAMP1 LAMP2 LAMTOR1 LAMTOR2 LAMTOR3 LAT LAT2 LBP LCK LCN2 LCP2 LEAP2 LGALS3 LGMN LILRA3 LILRB2 LILRB3 LIMK1 LPCAT1 LPO LRG1 LRRC7 LRRFIP1 LTA4H LTF LY86 LY96 LYN LYZ MAGT1 MALT1 MAN2B1 MANBA MAP2K1 MAP2K3 MAP2K4 MAP2K6 MAP2K7 MAP3K1 MAP3K14 MAP3K7 MAP3K8 MAPK1 MAPK10 MAPK11 MAPK12 MAPK13 MAPK14 MAPK3 MAPK7 MAPK8*

	MAPK9 MAPKAPK2 MAPKAPK3 MASP1 MASP2 MAVS MBL2 MCEMP1 MEF2A MEF2C MEFV METTL7A MGAM MGST1 MIF MLEC MME MMP25 MMP8 MMP9 MNDA MOSPD2 MPO MRE11 MS4A2 MS4A3 MUC1 MUC12 MUC13 MUC15 MUC16 MUC17 MUC20 MUC21 MUC3A MUC4 MUC5AC MUC5B MUC6 MUC7 MUCL1 MVP MYD88 MYH2 MYH9 MYO10 MYO1C MYO5A MYO9B NAPRT NBEAL2 NCF1 NCF2 NCF4 NCK1 NCKAP1 NCKAP1L NCKIPSD NCR2 NCSTN NDUFC2 NEU1 NF2 NFAM1 NFASC NFATC1 NFATC2 NFATC3 NFKB1 NFKB2 NFKBIA NFKBIB NHLRC3 NIT2 NKIRAS1 NKIRAS2 NLRC3 NLRC4 NLRC5 NLRP1 NLRP3 NLRP4 NLRX1 NME2 NOD1 NOD2 NOS1 NOS2 NOS3 NPC2 NRAS OLFM4 OLR1 ORM1 ORM2 ORMDL3 OSCAR OSTF1 OTUD5 P2RX1 P2RX7 PA2G4 PADI2 PAFAH1B2 PAK1 PAK2 PAK3 PANX1 PCBP2 PDAP1 PDPK1 PDXK PDZD11 PECAM1 PELI1 PELI2 PELI3 PFKL PGAM1 PGLYRP1 PGLYRP2 PGLYRP3 PGLYRP4 PGM1 PGM2 PGRMC1 PI3 PIGR PIK3C3 PIK3CA PIK3CB PIK3R1 PIK3R2 PIK3R4 PIN1 PKM PKP1 PLA2G2A PLA2G6 PLAC8 PLAU PLAUR PLCG1 PLCG2 PLD1 PLD2 PLD3 PLD4 PLEKHO2 PLPP4 PLPP5 PNP POLR1C POLR1D POLR2E POLR2F POLR2H POLR2K POLR2L POLR3A POLR3B POLR3C POLR3D POLR3E POLR3F POLR3G POLR3GL POLR3H POLR3K PPBP PPIA PPIE PPP2CA PPP2CB PPP2R1A PPP2R1B PPP2R5D PPP3CA PPP3CB PPP3R1 PRCP PRDX4 PRDX6 PRG2 PRG3 PRKACA PRKACB PRKACG PRKCD PRKCE PRKCQ PRKCSH PRKDC PROS1 PRSS2 PRSS3 PRTN3 PSAP PSEN1 PSMA1 PSMA2 PSMA3 PSMA4 PSMA5 PSMA6 PSMA7 PSMA8 PSMB1 PSMB10 PSMB11 PSMB2 PSMB3 PSMB4 PSMB5 PSMB6 PSMB7 PSMB8 PSMB9 PSMC1 PSMC2 PSMC3 PSMC4 PSMC5 PSMC6 PSMD1 PSMD10 PSMD11 PSMD12 PSMD13 PSMD14 PSMD2 PSMD3 PSMD4 PSMD5 PSMD6 PSMD7 PSMD8 PSMD9 PSME1 PSME2 PSME3 PSME4 PSMF1 PSTPIP1 PTAFR PTGES2 PTK2 PTPN11 PTPN4 PTPN6 PTPRB PTPRC PTPRJ PTPRN2 PTX3 PYCARD PYGB PYGL QPCT QSOX1 RAB10 RAB14 RAB18 RAB24 RAB27A RAB31 RAB37 RAB3A RAB3D RAB44 RAB4B RAB5B RAB5C RAB6A RAB7A RAB9B RAC1 RAC2 RAF1 RAP1A RAP1B RAP2B RAP2C RASGRP1 RASGRP2 RASGRP4 RBSN REG3A REG3G RELA RELB RETN RHOA RHOF RHOG RIPK1 RIPK2 RIPK3 RNASE2 RNASE3 RNASE6 RNASE7 RNASE8 RNASET2 RNF125 RNF135 RNF216 ROCK1 RPS27A RPS6KA1 RPS6KA2 RPS6KA3 RPS6KA5 S100A1 S100A11 S100A12 S100A7 S100A7A S100A8 S100A9 S100B S100P SAA1 SARM1 SCAMP1 SDCBP SELL SEM1 SEMG1 SERPINA1 SERPINA3 SERPINB1 SERPINB10 SERPINB12 SERPINB3 SERPINB6 SERPING1 SFTPA1 SFTPA2 SFTPD SHC1 SIGIRR SIGLEC14 SIGLEC15 SIGLEC5 SIGLEC9 SIKE1 SIRPA SIRPB1 SKP1 SLC11A1 SLC15A4 SLC27A2 SLC2A3 SLC2A5 SLC44A2 SLCO4C1 SLPI SNAP23 SNAP25 SNAP29 SOCS1 SOS1 SPTAN1 SRC SRP14 STAT6 STBD1 STING1 STK10 STK11IP STOM SUGT1 SURF4 SVIP SYK SYNGR1 TAB1 TAB2 TAB3 TANK TARM1 TAX1BP1 TBC1D10C TBK1 TCIRG1 TCN1 TEC TICAM1 TICAM2 TIFA TIMP2 TIRAP TKFC TLR1 TLR10 TLR2 TLR3 TLR4 TLR5 TLR6 TLR7 TLR8 TLR9 TMBIM1 TMC6 TMEM179B TMEM30A TMEM63A TNFAIP3 TNFAIP6 TNFRSF1B TNIP2 TOLLIP TOM1 TOMM70 TRAF2 TRAF3 TRAF6 TRAPPC1 TREM1 TREM2 TREX1 TRIM21 TRIM25 TRIM32 TRIM56 TRPM2 TSPAN14 TTR TUBB TUBB4B TXK TXN TXNDC5 TXNIP TYROBP UBA3 UBA52 UBA7 UBB UBC UBE2D1 UBE2D2 UBE2D3 UBE2K UBE2L6 UBE2M UBE2N UBE2V1 UBR4 UNC13D UNC93B1 VAMP8 VAPA VAT1 VAV1 VAV2 VAV3 VCL VCP VNN1 VPS35L VRK3 VTN WAS WASF1 WASF2 WASF3 WASL WIPF1 WIPF2 WIPF3 XRCC5 XRCC6 YES1 YPEL5 ZBP1 *MAPK9 MAPKAPK2 MAPKAPK3 MASP1 MASP2 MAVS MBL2 MCEMP1 MEF2A MEF2C MEFV METTL7A MGAM MGST1 MIF MLEC MME MMP25 MMP8 MMP9 MNDA MOSPD2 MPO MRE11 MS4A2 MS4A3 MUC1 MUC12 MUC13 MUC15 MUC16 MUC17 MUC20 MUC21 MUC3A MUC4 MUC5AC MUC5B MUC6 MUC7 MUCL1 MVP MYD88 MYH2 MYH9 MYO10 MYO1C MYO5A MYO9B NAPRT NBEAL2 NCF1 NCF2 NCF4 NCK1 NCKAP1 NCKAP1L NCKIPSD NCR2 NCSTN NDUFC2 NEU1 NF2 NFAM1 NFASC NFATC1 NFATC2 NFATC3 NFKB1 NFKB2 NFKBIA NFKBIB NHLRC3 NIT2 NKIRAS1 NKIRAS2 NLRC3 NLRC4 NLRC5 NLRP1 NLRP3 NLRP4 NLRX1 NME2 NOD1 NOD2 NOS1 NOS2 NOS3 NPC2 NRAS OLFM4 OLR1 ORM1 ORM2 ORMDL3 OSCAR OSTF1 OTUD5 P2RX1 P2RX7 PA2G4 PADI2 PAFAH1B2 PAK1 PAK2 PAK3 PANX1 PCBP2 PDAP1 PDPK1 PDXK PDZD11 PECAM1 PELI1 PELI2 PELI3 PFKL PGAM1 PGLYRP1 PGLYRP2 PGLYRP3 PGLYRP4 PGM1 PGM2 PGRMC1 PI3 PIGR PIK3C3 PIK3CA PIK3CB PIK3R1 PIK3R2 PIK3R4 PIN1 PKM PKP1 PLA2G2A PLA2G6 PLAC8 PLAU PLAUR PLCG1 PLCG2 PLD1 PLD2 PLD3 PLD4 PLEKHO2 PLPP4 PLPP5 PNP POLR1C POLR1D POLR2E POLR2F POLR2H POLR2K POLR2L POLR3A POLR3B POLR3C POLR3D POLR3E POLR3F POLR3G POLR3GL POLR3H POLR3K PPBP PPIA PPIE PPP2CA PPP2CB PPP2R1A PPP2R1B PPP2R5D PPP3CA PPP3CB PPP3R1 PRCP PRDX4 PRDX6 PRG2 PRG3 PRKACA PRKACB PRKACG PRKCD PRKCE PRKCQ PRKCSH PRKDC PROS1 PRSS2 PRSS3 PRTN3 PSAP PSEN1 PSMA1 PSMA2 PSMA3 PSMA4 PSMA5 PSMA6 PSMA7 PSMA8 PSMB1 PSMB10 PSMB11 PSMB2 PSMB3 PSMB4 PSMB5 PSMB6 PSMB7 PSMB8 PSMB9 PSMC1 PSMC2 PSMC3 PSMC4 PSMC5 PSMC6 PSMD1 PSMD10 PSMD11 PSMD12 PSMD13 PSMD14 PSMD2 PSMD3 PSMD4 PSMD5 PSMD6 PSMD7 PSMD8 PSMD9 PSME1 PSME2 PSME3 PSME4 PSMF1 PSTPIP1 PTAFR PTGES2 PTK2 PTPN11 PTPN4 PTPN6 PTPRB PTPRC PTPRJ PTPRN2 PTX3 PYCARD PYGB PYGL QPCT QSOX1 RAB10 RAB14 RAB18 RAB24 RAB27A RAB31 RAB37 RAB3A RAB3D RAB44 RAB4B RAB5B RAB5C RAB6A RAB7A RAB9B RAC1 RAC2 RAF1 RAP1A RAP1B RAP2B RAP2C RASGRP1 RASGRP2 RASGRP4 RBSN REG3A REG3G RELA RELB RETN RHOA RHOF RHOG RIPK1 RIPK2 RIPK3 RNASE2 RNASE3 RNASE6 RNASE7 RNASE8 RNASET2 RNF125 RNF135 RNF216 ROCK1 RPS27A RPS6KA1 RPS6KA2 RPS6KA3 RPS6KA5 S100A1 S100A11 S100A12 S100A7 S100A7A S100A8 S100A9 S100B S100P SAA1 SARM1 SCAMP1 SDCBP SELL SEM1 SEMG1 SERPINA1 SERPINA3 SERPINB1 SERPINB10 SERPINB12 SERPINB3 SERPINB6 SERPING1 SFTPA1 SFTPA2 SFTPD SHC1 SIGIRR SIGLEC14 SIGLEC15 SIGLEC5 SIGLEC9 SIKE1 SIRPA SIRPB1 SKP1 SLC11A1 SLC15A4 SLC27A2 SLC2A3 SLC2A5 SLC44A2 SLCO4C1 SLPI SNAP23 SNAP25 SNAP29 SOCS1 SOS1 SPTAN1 SRC SRP14 STAT6 STBD1 STING1 STK10 STK11IP STOM SUGT1 SURF4 SVIP SYK SYNGR1 TAB1 TAB2 TAB3 TANK TARM1 TAX1BP1 TBC1D10C TBK1 TCIRG1 TCN1 TEC TICAM1 TICAM2 TIFA TIMP2 TIRAP TKFC TLR1 TLR10 TLR2 TLR3 TLR4 TLR5 TLR6 TLR7 TLR8 TLR9 TMBIM1 TMC6 TMEM179B TMEM30A TMEM63A TNFAIP3 TNFAIP6 TNFRSF1B TNIP2 TOLLIP TOM1 TOMM70 TRAF2 TRAF3 TRAF6 TRAPPC1 TREM1 TREM2 TREX1 TRIM21 TRIM25 TRIM32 TRIM56 TRPM2 TSPAN14 TTR TUBB TUBB4B TXK TXN TXNDC5 TXNIP TYROBP UBA3 UBA52 UBA7 UBB UBC UBE2D1 UBE2D2 UBE2D3 UBE2K UBE2L6 UBE2M UBE2N UBE2V1 UBR4 UNC13D UNC93B1 VAMP8 VAPA VAT1 VAV1 VAV2 VAV3 VCL VCP VNN1 VPS35L VRK3 VTN WAS WASF1 WASF2 WASF3 WASL WIPF1 WIPF2 WIPF3 XRCC5 XRCC6 YES1 YPEL5 ZBP1*

Abbreviations: Pathway RespOnsive Genes for activity inference (PROGENy), bone marrow (BM).

Table S4. Demographics of TN-MF patients

Parameters	MYC negative patients (n = 11)	MYC positive patients (n = 12)	All patients (n = 23)
Median age at diagnosis, years (range)	62 (19-86)	65 (53-77)	63 (19-86)
Sex, n (%)			
Male	7 (64)	5 (42)	12 (52)
Female	4 (36)	7 (58)	11 (48)
Type of MF, n (%)			
PMF	9 (82)	10 (83)	19 (83)
Post-ET	2 (18)	2 (17)	4 (17)
Post-PV	0 (0)	0 (0)	0 (0)
Labs at Diagnosis (range)			
WBC, K/μL	8.5 (2.3-82.8)	6.0 (2.2-51.7)	6.6 (2.2-82.8)
Hemoglobin, g/dL	10.9 (7.7-15.6)	9.6 (3.4-12.8)	10.5 (3.4-15.6)
Platelet, K/μL	172 (48-967)	114 (8-378)	151 (8-967)
Monocyte, K/μL	0.3 (0.1-5.4)	0.4 (0.1-1.2)	0.3 (0.1-5.4)
BM assessment			
Blast, % (range)	0 (0-4)	0 (0-3)	0 (0-4)
Reticulin fibrosis, grade (mean)	2	2.4	2.2
Cytogenetics, n (%) *			
+8	1 (9)	5 (42)	6 (26)
+21	1 (9)	0 (0)	1 (4)
+1/dup(1q)	0 (0)	1 (8)	1 (4)
Tetraploidy	0 (0)	1 (8)	1 (4)
Complex karyotype **	1 (9)	0 (0)	1 (4)
DIPSS, n (%)			
Low	4 (36)	0 (0)	4 (17)
Intermediate-1	4 (36)	6 (50)	10 (43)
Intermediate-2	2 (18)	5 (42)	7 (30)
High	1 (9)	1 (8)	2 (9)

Abbreviations: Myelofibrosis (MF), triple negative MF (TN-MF), primary MF (PMF), essential thrombocythemia (ET), polycythemia vera (PV), white blood cells (WBC), absolute neutrophil counts (ANC), absolute lymphocyte counts (ALC), bone marrow (BM), Dynamic International Prognostic Scoring System (DIPSS).
*Cytogenetics were assessed by conventional karyotyping and/or Fluorescence In Situ Hybridization (FISH). **Complex karyotype was defined as 3 or more cytogenetic abnormalities.

Table S5. Clinical parameters of Mx1-Cre$^{+/-}$;Rosa26$^{LSL\text{-}MYC/LSL\text{-}MYC}$ studies

Parameters	Rosa26$^{+/+}$	Rosa26$^{LSL\text{-}MYC/+}$	Rosa26$^{LSL\text{-}MYC/LSL\text{-}MYC}$
Number of mice	38	44	54
Age at pIpC treatment, weeks	6-11	6-11	6-11
Female, n (%)	17 (45)	38 (86)	24 (44)
Median baseline body weight, mg (range)	19.0 (13.0-26.9)	18.7 (14.4-27.2)	19.1 (15.4-26.6)
CBC at baseline (range)*			
WBC, K/μL	8.72 (4.15-16.3)	11.13 (4.16-16.85)	9.67 (2.86-19.27)
RBC, M/μL	10.15 (8.92-10.91)	10.02 (8.68-11.67)	10.24 (8.40-11.57)
Platelet, K/μL	781.5 (15.4-1175)	790 (14.4-1207)	785 (15-1011)
Neutrophil, %	9.45 (4.1-35.9)	9.9 (2.5-49.4)	9.2 (3.5-45.2)
Monocyte, %	1.05 (0.6-2.4)	1.2 (0.4-3.6)	1.85 (0.2-3.9)
Lymphocyte, %	87.85 (61.3-93.8)	87 (47.5-95.3)	87.9 (51.6-94.2)
CBC at week 25-36 (range)			
WBC, K/μL	7.28 (2.12-18.9)	7.62 (0.13-18.7)	9.74 (1.82-20.32)
RBC, M/μL	10.97 (9.05-12.63)	10.29 (7.9-12.14)	9.27 (0.79-11.29)
Platelet, K/μL	1076.5 (17.1-1591)	1014 (14.8-1603)	994 (1-2013)
Neutrophil, %	12.1 (6.2-50.5)	11.7 (2.3-53.8)	11.45 (1.6-33.1)
Monocyte, %	2.4 (0.6-8.3)	2.9 (0-6.1)	5.05 (1.6-15.7)
Lymphocyte, %	78.5 (46.6-90.2)	78.6 (42.8-88.1)	76.9 (9.2-89.1)
Median spleen weight, mg (range)**			
At week 15-44	100 (80-130)	160 (90-940)	325 (130-720)
At week 45-62	110 (30-140)	205 (130-780)	1300 (1300-1300)
Median OS, days***	NR	385	258

Abbreviations: Polyinosinic-polycytidylic acid (pIpC), complete blood counts (CBC), white blood cells (WBC), red blood cells (RBC), overall survival (OS), and not reached (NR).

*Baseline CBC values were determined 1 week prior to pIpC injection.

**Spleen weight was measured at the time of death or at pre-defined endpoints. See Method.

***Overall survival was calculated from the first date of pIpC injection.

Table S6. Clinical parameters of Scl-CreERT$^{+/-}$;Rosa26$^{LSL\text{-}MYC/LSL\text{-}MYC}$ *in vivo* studies.

Parameters	Rosa26$^{+/+}$	Rosa26$^{LSL\text{-}MYC/+}$	Rosa26$^{LSL\text{-}MYC/LSL\text{-}MYC}$
Number of mice	20	25	15
Age at tamoxifen treatment, week	6-10	6-10	6-10
Female, n (%)	12 (60)	12 (48)	8 (53)
Baseline body weight, mg (range)	22.75 (17.2-24.6)	22.3 (19.7-31.2)	19.8 (19.1-24.4)
CBC at baseline (range)*			
WBC, K/µL	9.79 (5.16-14.04)	9.41 (5.9-12.39)	7.06 (5.25-9.63)
RBC, M/µL	10.46 (9.52-11.29)	10.72 (9.3-11.24)	10.98 (9.7-11.92)
Platelet, K/µL	881 (645-1200)	1063 (670-1315)	1022 (738-1197)
Neutrophil, %	9 (5.7-18.7)	8.45 (6.6-21.7)	9.3 (5.4-12.2)
Monocyte, %	1.8 (0.9-3.4)	1.4 (0.8-4.5)	1.6 (1-2.3)
Lymphocyte, %	87.6 (78.9-91.2)	88.45 (72.6-90.5)	86.4 (84.4-92.8)
CBC at week 25-36 (range)			
WBC, K/µL	9.11 (0.88-14.23)	7.3 (1.3-15.41)	8.78 (2.28-14.92)
RBC, M/µL	10.3 (8.46-11.64)	10.21 (7.74-11.37)	9.59 (8.94-10.68)
Platelet, K/µL	1282 (247-1634)	1172 (146-1785)	1364 (745-1774)
Neutrophil, %	13.3 (8.5-25)	12.6 (5.8-39)	15.25 (8.4-26.4)
Monocyte, %	1.8 (0.8-4.4)	2.4 (0.8-9.9)	4.9 (2-13)
Lymphocyte, %	83 (71.2-88)	82.1 (59.3-89.8)	79.9 (60.6-85.7)
Median spleen weight, mg (range)**	120 (80-140)	150 (110-230)	190 (120-440)
Median OS, days***	NR	427	339

Abbreviations: Complete blood counts (CBC), white blood cells (WBC), red blood cells (RBC), overall survival (OS), and not reached (NR).

*Baseline CBC values were determined 1 week prior to tamoxifen oral gavage.

**Spleen weight was measured at the time of death or at pre-defined endpoints. See Method.

***Overall survival was calculated from the date of first dose of tamoxifen oral gavage.

Table S7. Clinical parameters in competitive transplant studies

Parameters	Donor cells: Mx1-Cre$^{+/-}$;Rosa26$^{+/+}$	Donor cells: Mx1-Cre$^{+/-}$;Rosa26$^{LSL\text{-}MYC/LSL\text{-}MYC}$
Number of mice	4	5
Age at transplant, weeks	6	6
Female, n (%)	2 (50)	2 (40)
CBC at 20 weeks post-transplant (range)		
WBC, K/μL	5.485 (4.92-7.34)	5.36 (4.75-8.32)
RBC, M/μL	10.05 (9.15-10.56)	9.06 (8.8-9.37)
Platelet, K/μL	997.5 (558-1403)	635.5 (361-896)
Neutrophil, %	13.05 (9.8-15.5)	12.5 (9.2-15.5)
Monocyte, %	1.65 (1.6-2)	3.2 (2.6-3.2)
Lymphocyte, %	84.35 (80.8-88)	82.2 (80-86)
CBC at 36-40 weeks post-transplant (range)		
WBC, K/μL	6.76 (3.84-10.1)	6.875 (3.84-10.1)
RBC, M/μL	9.705 (9.23-10.01)	9.31 (1.01-9.54)
Platelet, K/μL	1252.2 (970-1634)	947 (5-1772)
Neutrophil, %	19.2 (10.6-26.4)	16.05 (11.9-32.9)
Monocyte, %	1.7 (0.7-2.9)	3.05 (1.5-9.7)
Lymphocyte, %	77.1 (68.6-86.9)	78.85 (51.4-84.8)
Median spleen weight, mg (range)*	90 (80-90)	170 (80-750)
Median OS, days**	NR	315

Abbreviations: Complete blood counts (CBC), white blood cells (WBC), red blood cells (RBC), overall survival (OS) and not reached (NR).

*Spleen weights of recipient mice transplanted with Mx1-Cre$^{+/-}$;Rosa26$^{LSL\text{-}MYC/LSL\text{-}MYC}$ BM cells were measured at the time of death or endpoints. Mice transplanted with Mx1-Cre$^{+/-}$;Rosa26$^{+/+}$ BM cells were sacrificed at the same time as control. See Method.

**Overall survival was calculated from the date of transplant.

Table S8. Comparison of gene expression profiles of Mx1-Cre$^{+/-}$;Rosa26$^{LSL\text{-}MYC/LSL\text{-}MYC}$ *vs.* Mx1-Cre$^{+/-}$;Rosa26$^{+/+}$ mouse

See “Table S8” file.

Table S9. List of genes used for PROGENy analysis of mouse BM cells

JAK/STAT	*Adipor1 Agap2 Ager Agt Agtr1a Akr1b3 Arl2bp Bcl3 Cav1 Ccl5 Cd40 Cd300a Cdk5 Cdk5r1 Cenpj Clcf1 Cnot7 Cntf Crlf1 Crlf3 Csf1r Csf2 Csf2ra Csf2rb Csf2rb2 Ctf1 Ctf2 Ctr9 Cxcl5 Cyp1b1 Dab1 Dot1l Egf Elp2 Ephb2 Epo Erbb4 Ercc6 Fer Fgfr3 Fyn Gadd45a Gbp3 Gbp7 Gfra2 Ggnbp2 Gh Ghr Gm13271 Gm13272 Gm13275 Gm13276 Gm13277 Gm13283 Hamp Hcls1 Hdac2 Hes1 Hes5 Hgs Hmga2 Hnf4a Hpx Hsf1 Ifna1 Ifna2 Ifna4 Ifna5 Ifna6 Ifna7 Ifna9 Ifna11 Ifna12 Ifna13 Ifna14 Ifna15 Ifna16 Ifnab Ifnb1 Ifne Ifng Ifnk Ifnl2 Ifnl3 Ifnz Igf1 Il2 Il3 Il4 Il5 Il6 Il6ra Il6st Il7r Il9 Il10 Il10ra Il10rb Il12a Il12b Il12rb1 Il12rb2 Il13 Il15 Il15ra Il18 Il20 Il21 Il22 Il22ra2 Il23a Il23r Il24 Inpp5f Irf1 Isl1 Jak1 Jak2 Jak3 Kit Lck Lep Leprot Lif Lyn Mir301 Mst1 Neurod1 Nf2 Nlk Notch1 Osbp Osm Parp9 Parp14 Pecam1 Pias1 Pias4 Pibf1 Pigu Pkd1 Pkd2 Prl Prl2a1 Prl2b1 Prl2c1 Prl2c2 Prl2c3 Prl2c5 Prl3a1 Prl3b1 Prl3c1 Prl3d1 Prl3d2 Prl3d3 Prl4a1 Prl5a1 Prl6a1 Prl7a1 Prl7a2 Prl7b1 Prl7c1 Prl7d1 Prl8a1 Prl8a2 Prl8a6 Prl8a8 Prl8a9 Prlr Prmt2 Ptger4 Ptk2b Ptk6 Ptpn2 Ptprc Ptprd Pwp1 Rac1 Ret Sac3d1 Sh2b3 Snhg20 Socs1 Socs2 Socs3 Socs5 Stat1 Stat2 Stat3 Stat4 Stat5a Stat5b Stat6 Stra6 Tnfrsf1a Tnfrsf18 Tnfsf18 Traf3ip1 Tslp Tyk2*
MAPK	*Abca7 Abl1 Abl2 Ace2 Ackr3 Acta2 Adam8 Adam9 Adam17 Adcyap1 Adipoq Adora1 Adra1a Adra1b Adra1d Adra2a Adra2b Adra2c Adrb2 Adrb3 Ager Agt Aida Ajuba Akap12 Akap13 Akt1 Alkal1 Alkal2 Alox12b Alox15 Angpt1 Ankrd6 Ankrd26 Apc Apip Apoe App Ar Araf Arhgap8 Arhgef5 Arl6ip5 Arrb1 Arrb2 Ash1l Atf2 Atf3 Atf7 Atp6ap2 Atp6v0c Avp Avpi1 Avpr1b Axin1 Bank1 Bcar3 Bcl10 Birc7 Bmp2 Bmp4 Bmp7 Bmp8b Bmper Bnip2 Braf Brap Btn2a2 C1ql4 C1qtnf1 C1qtnf2 C1qtnf3 C3 C5ar2 Calcr Camk2d Card9 Cartpt Casr Cav1 Cav2 Cav3 Cavin3 Cblc Cckbr Ccl1 Ccl2 Ccl3 Ccl4 Ccl5 Ccl6 Ccl7 Ccl8 Ccl9 Ccl11 Ccl12 Ccl17 Ccl19 Ccl20 Ccl21a Ccl21b Ccl21c Ccl22 Ccl24 Ccl25 Ccl26 Ccn1 Ccn2 Ccnq Ccr1 Ccr1l1 Ccr3 Ccr7 Cd4 Cd24a Cd27 Cd36 Cd40 Cd44 Cd74 Cd81 Cd84 Cd300a Cdc42 Cdc42ep5 Cdc42se1 Cdh2 Cdk5rap3 Cdk10 Cdon Ceacam1 Ceacam2 Cflar Chil1 Chrna7 Chrna9 Chrna10 Cib1 Clcf1 Cnksr3 Cntf Cntnap2 Cops5 Cracr2a Crhr2 Crkl Cryab Cryba1 Csf1r Csk Cspg4 Ctnnb1 Ctsh Cx3cl1 Cxcl12 Cxcl17 Cxcr4 Cyld Cysltr2 Dab2 Dab2ip Dact1 Dag1 Daxx Dcc Ddr2 Denn2b Dhx33 Dixdc1 Dkk1 Dlg1 Dmd Dnaja1 Dnajc27 Dok1 Dok2 Dok4 Dok5 Dok6 Drd2 Drd4 Dstyk Dusp1 Dusp2 Dusp3 Dusp4 Dusp5 Dusp6 Dusp7 Dusp8 Dusp9 Dusp10 Dusp13 Dusp15 Dusp16 Dusp19 Dusp22 Dusp26 Dusp27 Dusp29 Dvl2 Dvl3 Dynlt1b E130311K13Rik Ece1 Eda2r Edar Edn1 Edn3 Ednra Efna1 Egf Egfr Eif2ak2 Eif3a Emc10 Emilin1 Eno1b Epgn Epha2 Epha4 Epha7 Epha8 Ephb1 Ephb2 Epo Epor Erbb2 Erbb4 Ercc6 Ern1 Ern2 Erp29 Errfi1 Esr1 Esr2 Ezh2 Ezr F2r F2rl1 Fam83d Fas Fbln1 Fbxw7 Fcer1a Fcgr2b Fem1a Fermt2 Ffar4 Fga Fgb Fgd2 Fgd4 Fgf1 Fgf2 Fgf4 Fgf8 Fgf9 Fgf10 Fgf12 Fgf13 Fgf14 Fgf15 Fgf18 Fgf20 Fgf21 Fgf23 Fgfbp3 Fgfr1 Fgfr2 Fgfr3 Fgfr4 Fgg Fktn Flcn Flt1 Flt4 Fn1 Foxm1 Foxo1 Frs2 Fshr Fzd4 Fzd5 Fzd8 Fzd10 Gab1 Gadd45a Gadd45b Gadd45g Garem1 Gas6 Gata4 Gba Gcg Gcnt2 Gdf6 Gdf15 Gfral Ghr Ghrl Glipr2 Gnai2 Gpbar1 Gper1 Gpnmb Gpr37 Gpr37l1 Gpr39 Gpr55 Gpr183 Gps2 Grb2 Grb10 Grem1 Grik2 Grin2b Grm1 Grm4 Grm5 Gsdme Gsk3b Gstp1 Gstp2 Hacd3 Hand2 Havcr2 Hcrtr1 Hdac3 Hesx1 Hgf Hipk2 Hipk3 Hmgb1 Hmgcr Hras Hrh4 Hsf1 Hsph1 Htr2a Htr2b Htr2c Hyal2 Iapp Icam1 Id1 Igbp1 Igbp1b Igf1 Igf1r Igf2 Igfbp3 Igfbp4 Igfbp6 Igh-7 Ighm Il1a Il1b Il1rn Il3 Il6 Il6ra Il11 Il18 Il34 Ilk Inava Inpp5k Inppl1 Ins2 Insr Iqgap1 Iqgap3 Irak1 Irak3 Irak4 Itch Itga1 Itgav Itgb1bp1 Itgb3 Itpkb Jak2 Jcad Jun Kars Kdr Kiss1 Kiss1r Kit Kitl Kl Klb Klf4 Klhdc10 Klhl31 Kras Ksr1 Ksr2 L1cam Lamtor1 Lamtor2 Lamtor3 Laptm5 Lax1 Lbh Lemd2 Lep Lepr Lif Lilra5 Lilrb4a Lilrb4b Lmbrd1 Lmnb1 Lmo3 Lpar1 Lpar2 Lpar3 Lrp1 Lrrk2 Ltbr Lyn Madd Maged1 Magi3 Map2k1 Map2k2 Map2k3 Map2k4 Map2k5 Map2k6 Map2k7 Map3k1 Map3k3 Map3k4 Map3k5 Map3k6 Map3k7 Map3k10 Map3k11 Map3k12 Map3k13 Map3k15 Map3k20 Map3k21 Map4k1 Map4k2 Map4k3 Map4k4 Map4k5 Mapk1 Mapk3 Mapk6 Mapk7 Mapk8 Mapk8ip1 Mapk8ip2 Mapk8ip3 Mapk9 Mapk10 Mapk11 Mapk12 Mapk13 Mapk14 Mapkapk2 Mapkbp1 Marveld3 Mbip Mbp Mdfi Mdfic Mecom Mef2a Mef2c Men1 Met Mfhas1 Mid1 Mif Mink1 Mir504 Mlkl Mmp8 Mos Mst1r Mt3 Mturn Muc20 Myc Myd88 Mydgf Mylk2 Myoc Naip1 Naip2 Naip5 Naip6 Naip7 Nbr1 Ncor1 Ndrg2 Ndrg4 Ndst1 Necab2 Nek10 Nelfe Nenf Nf1 Nf2 Nfkb1 Ngf Ngfr Nlrp6 Nlrp12 Nmnat1 Nod1 Nod2 Nodal Notch1 Notch2 Nox1 Nox4 Npffr2 Nphs1 Npnt Nppa Npsr1 Nptn Npy Npy5r Nqo2 Nrbp1 Nrg1 Nrk Nrp1 Nrxn1 Ntf3 Ntrk1 Ntrk2 Ntrk3 Ntsr2 Nup62 Obox4 Olfr520 Olfr521 Oprk1 Oprm1 Osm Oxtr P2rx7 P2ry1 P2ry6 Pabpn1 Pafah1b1 Pak1 Pak2 Pak3 Pak4 Pak5 Pak6 Paqr3 Pbk Pbp2 Pdcd10 Pde5a Pde6g Pde6h Pde8a Pdgfa Pdgfb Pdgfc Pdgfd Pdgfra Pdgfrb Pea15a Pea15b-ps Pebp1 Peli2 Per1 Phb Phb2 Phlpp1 Pik3ap1 Pik3cb Pik3cg Pik3r2 Pik3r5 Pik3r6 Pin1 Pin1rt1 Pja2 Pkhd1 Pla2g5 Plcb1 Plce1 Plcg2 Plvap Pou4f2 Pparg Ppef2 Ppia Ppm1l Pramel7 Prdm11 Prdm15 Prdx1 Prdx2 Prkca Prkcd Prkce Prkcz Prkd2 Prmt1 Prmt5 Prok1 Prxl2c Psap Psca Psen1 Psmd10 Pten Ptger4 Ptk2 Ptk2b Ptpn1 Ptpn2 Ptpn5 Ptpn6 Ptpn11 Ptpn22 Ptprc Ptprj Ptprr Pycard Qars Raf1 Ramp3 Ranbp9 Rap1a Rap1b Rap2a Rapgef1 Rapgef2 Rara Rasgrp1 Rassf2 Rb1cc1 Rell1 Rell2 Ren1 Ren2 Ret Rgs2 Rgs14 Rhbdd3 Ripk1 Ripk2 Rit2 Rnf41 Rnf149 Robo1 Rock1 Rock2 Ror1 Ror2 Ros1 Rps3 Rps6ka6 Rras Ryk Sash1 Sbk2 Scg2 Scimp Sema4c Sema6a Sema7a Serpinf2 Setx Sfrp1 Sfrp2 Sfrp4 Sfrp5 Sh2b3 Sh3rf1 Sh3rf2 Sh3rf3 Shank3 Shc1 Sirpa Slamf1 Slc9a3r1 Slc11a1 Slc30a10 Smad1 Smad3 Smad4 Smpd1 Sod1 Sorbs3 Sorl1 Sox2 Sox9 Spag9 Sphk1 Spi1 Spred1 Spred2 Spred3 Spry1 Spry2 Spry3 Spry4 Src Sstr4 Stk3 Stk4 Stk25 Stk38 Stk39 Stk40 Stradb Styx Syk Syngap1 Synj2bp Tab1 Taok1 Taok2 Taok3 Tbc1d10c Tbx1 Tdgf1 Tek Tenm1 Tff2 Tgfa Tgfb1 Tgfb2 Tgfb3 Tgfbr1 Tgfbr3 Thbs1 Thpo Timp2 Timp3 Tirap Tlr2 Tlr3 Tlr4 Tlr6 Tlr7 Tlr9 Tlr13 Tmem106a Tnf Tnfaip8l3 Tnfrsf11a Tnfrsf19 Tnfrsf23 Tnfsf11 Tnik Tnip1 Tpbg Tpbpa Tpd52l1 Traf1 Traf2 Traf3 Traf4 Traf5 Traf6 Traf7 Trem2 Trf Trib1 Trim5 Trim12a Trim12c Trim30a Trim30d Trp73 Trpv4 Tsc2 Uchl1 Ulk4 Unc5cl Vangl2 Vegfa Vegfb Vrk2 Vrk3 Wdr54 Wnk2 Wnt5a Wnt7a Wnt7b Wnt16 Wwc1 Xbp1 Xcl1 Xdh Ywhae Ywhaz Zc3h12a Zdhhc17 Zeb2 Zfp36 Zfp36l1 Zfp36l2 Zfp110 Zfp622 Zmynd11*
EGFR	*Abl1 Abl2 Acp4 Adam17 Adgre4 Adora1 Adra2a Afap1l2 Agr2 Agt Akt1 Areg Arf4 Bcar1 Bcar3 Braf Btc Caml Cbl Cblb Cblc Ccdc88a Cdh13 Ceacam1 Ceacam2 Chmp6 Cnot9 Cpne3 Dab2ip Dgkd Dusp3 Efemp1 Egf Egfr Epgn Erbb3 Erbb4 Ereg Errfi1 Esr1 Esr2 Fam83a Fam83b Fasl Fbxw7 Fer Gab1 Garem1 Gper1 Gprc5a Grb2 Hap1 Hbegf Hip1 Hip1r Iqgap1 Itga1 Kif16b Lgmn Mapk1 Mmp9 Mvb12a Mvb12b Mvp Myoc Neu3 Neurl1a Nppa Nrg1 Nrg2 Nrg3 Nup62 Pde6g Pde6h Pigr Plaur Plce1 Plcg1 Psen1 Psen2 Ptk2 Ptk2b Ptpn2 Ptpn11 Ptpn12 Ptprf Ptprj Ptprr Rab7 Rassf2 Rbpj Rhbdf1 Rhbdf2 Rnf115 Rnf126 Rtn4 Sh3tc2 Shc1 Shkbp1 Slc30a10 Snx5 Socs4 Socs5 Sos1 Sox9 Src Tdgf1 Tfap2a Tgfa Tgfb1 Tsg101 Vil1 Vps25 Wdr54 Zfyve28 Zgpat*

PI3K	*Adora3 Agap2 Agt Akt1 Angpt1 Btn2a2 C1qbp Cat Cbl Ccl5 Cd28 Cd160 Ceacam1 Ceacam2 Cep55 Cntf Crnn Cryba1 Csf3 Dab2ip Dcn Dipk2a Edn1 Egf Egfr Entpd5 Erbb2 Erbb3 Erbb4 F2 F2r F2rl1 Fbxl2 Fgf2 Fgr Flt1 Fn1 Fshr Fyn Gata3 Gper1 Hax1 Hcls1 Hcst Hgf Htr2a Htr2b Igf1 Igf1r Il18 Inpp5e Insr Irs1 Jak2 Kbtbd2 Kdr Klf4 Lep Lime1 Ltk Maz Mydgf Myo16 Myoc Ncor1 Nedd4 Nf1 Nkx3-1 Nlrc3 Nop53 Nrg1 Ntrk1 Ntrk2 Ntrk3 Nyap1 Nyap2 Obscn Osm Pdgfa Pdgfb Pdgfc Pdgfd Pdgfrb Pear1 Pik3ap1 Pik3c2a Pik3c2b Pik3c2g Pik3ca Pik3cb Pik3cd Pik3cg Pik3ip1 Pik3r1 Pik3r2 Pld2 Plekha1 Plxnb1 Ppard Ppp1r16b Prex2 Prr5 Prr5l Pten Ptk2 Ptpn6 Ptpn13 Rara Rasgrp1 Reg1 Reln Rgl2 Ror1 Ror2 Selp Sema4d Serpina12 Serpine2 Sirt1 Sirt2 Slc9a3r1 Slc9a3r2 Sox9 Stambp Tek Tgfb2 Tpte Trem2 Tsc2 Twist1 Ube3a Unc5b Vegfa Wnt16 Xbp1 Zfp36l1*

MYC	*Dctn4 Rpl37 Mapre2 Zfy1 Zfy2 Slc12a2 Ptdss1 Eif2s3y Ndufb4 Zfp457 Zfp595 Srebf2 Sod1 Srp54a Srp54b Srp54c Zfp369 Abce1 Sap18 Ndufb5 Msh2 Daxx Abt1 Prkdc Anapc10 Ndufa1 Mccc2 Arhgef7 Ivns1abp Pcm1 Ttc33 Spag6l Calm2 Trib1 Vps52 Naga Ifnar1 Gm10320 Srd5a1 Exo1 Jarid2 Slc39a6 Tmed10 Pwp1 Nol7 Yif1a Zfp953 Gm49345 Zfp738 Rgl2 Pdcd10 Pigf M6pr Wdr46 Ndufa6 Asah1 Pigp Vps29 Rnps1 Appl1 Mgat2 Trip13 Pomt2 Slc39a7 Ch25h Ndufa2 Clcn6 Rpl19 Abcc4 Slc31a1 Ndufs6 Atxn10 Rrp9 Recql5 Ppp2r1b Etf1 Akap9 Sox12 Bckdha Nup153 Btbd1 Ddx10 Cish Tpp2 Lztr1 Ywhah Rcl1 Lamp1 Cacnb1 Eif3i Sdf2l1 Timm8b Rgs16 Arl1 Rps29 Alkbh1 Maea Gclc Ngb Kif20a Psmd7 Hsp90b1 Recql Rln1 Cdk6 Amd2 Ttc4 Sptlc2 Gm7075 Rbm15b Blk Rxrb Hspa9 Nfat5 Kpna3 Rfx5 Pex11b Slc25a40 Eea1 Kcnh4 Pycr2 Ctsc Pias3 Sav1 Spib Arfip2 Srp68 Pms1 Gins2 Syk Clcn2 Erlin1 Cox7c Psmc4 9130409I23Rik Magoh Glt8d1 Adam22 Rps6ka5 Eno2 Entpd7 Phb2 Snapc1l Snapc1 Vapa Man2a1 Hook2 Cks2 Gtf3c5 Cdc6 Rnf4 Rad51ap1 Cradd Etfa Dpysl3 Hmg20a Slc26a4 Mrpl40 Ly86 Arid4a Mpp6 Sertad1 Atm Sypl Sri Gmds Cops3 Vamp1 Ndufb1 Gpsm3 Snx3 Trap1 Smc1a Nudt6 Golga5 Gm28042 Pla2g4b Glra3 Zkscan5 Gm21992 Zfp174 Gabpa Sae1 Mettl1 Calr Diablo Cct8 Prep Khsrp Cdc16 Cyb561d2 Timm22 Ilk H6pd Mphosph6 Fads3 Gtf3c4 Clcn3 Ppt2 Azin1 Rasa1 Rassf1 Suclg1 Rpl5 Gns Prpsap1 Gm2000 Actr3 Sp4 Ddb1 Lage3 Aifm1 Tll2 Dnaja2 Ier5 Galc Aldh18a1 Ccdc6 Cox15 Tmf1 Hspa14 Cd164 Cxxc1 Ier2 Amd1 Cln3 Ranbp3 Nr1d1 Scd2 Scd4 Sap30 Mst1r Nubp2 Atg12 Eef1e1 Lta4h Pole3 Timm9 Psmd3 Cog5 Bckdhb Mtf2 Gdap1 Mapre1 Dgcr6 Tsc2 Gnb1l Cul5 Ociad1 Map4k5 Rps21 Fth1 Ptpn6 Ubqln1 Csf2rb2 Csf2rb Supt5 Htra2 Stx7 Scml2 Atf4 Cib1 Dpf1 Sco1 Xrcc6 Oaz1 Mbd4 Psmb5 Rps13 Tsen34 Rbm4 Polh Nufip1 Slc39a8 Pcyt1a Csde1 Uso1 Lipt1 Snx15 Naca Tpt1 Fxr2 Uxt Zfpl1 Ddx41 Spag5 Pde4c Lnpep Ftsj1 Ppp1r12a Dbp Tnfaip1 Pcf11 Polr3a Rps20 Polr1d Acad8 Pdk1 Hsf2bp Rab11a Mkrn1 Cndp2 Pex6 Cr2 Polr1c Rpl8 Coro1c Rpl13 Akap10 Epm2a Pou2f1 Pmvk Arfrp1 Aloxe3 Timm17a Rab8a Polr3k Uspl1 Acss2 Ptp4a1 Asb1 Dmtf1 Zfp593 Mtf1 Psmd8 Rras Mad2l1 Ppp2ca Gnl1 Nfs1 Ptov1 Rpl18 Stub1 Rad9a Trappc3 Ndufb2 Pdk3 Hebp1 Ube2d3 Ptges3 Rpl32 Flot2 Maff Trp53 Crebl2 Ahcyl1 Zmpste24 Maml1 Nubp1 Elovl1 Mbnl1 Prr3 Ubl3 Trim24 Rbm39 Chd1l Dap3 Ddx1 Map2k7 Gm49320 Gmip Scamp3 Rbbp8 Trim33 Med17 Atp6v1d Supt16 Rnf141 Zfp286 Tgif2 Cd2ap Smad3 Ifngr1 Pmpcb Rnf7 Nbr1 Slc7a1 Cdkn1b H2-T24 Gm11127 Gm7030 H2-M10.2 H2-M10.1 H2-M10.3 H2-M10.4 H2-M11 H2-M9 H2-M1 H2-M10.5 H2-M10.6 2410137M14Rik Hax1 Vasp Mkln1 Grk4 Mthfd1 Gnpat Atf6 Tnfrsf21 Rps27l Tubg1 Rpl27 Il17c U2af1 Cct7 Sugt1 Rac2 Rnaset2b Gm49721 Gm49673 Rnaset2a Blzf1 Eif2s1 Prmt5 Ppp3ca Epc1 Mat2b Ncbp2 Mmp15 Timm23 Hdac6 Fry Herc1 Snrpd3 Ercc6 Hsd17b7 Pmm2 Prkab1 Pla2g6 Cacybp Mapk7 Pycr1 Psmd10 Mcm3 Dmap1 Rps25 Lsm8 Arpc4 Fkbp11 Keap1 Tesk2 Fbxo5 Sgpl1 Dpagt1 Dync1li1 Rabgef1 Pde6d Cuta Rap2b Ndufs1 Rab3a Usp1 Ndufb3 Tuba1b Slc22a4 Ssb Ing1 Zfp410 Mfap1b Mfap1a Psma5 Ell Degs1 Zfp7 Ncl Xk Irf3 Arhgef16 Ddx17 Ppa1 Ash2l Gm5244 Rplp1 Yy1 Ammecr1 Eftud2 Psme3 Ddx3x Hspa2 Rheb Ndufv1 Snapc3 Rbl1 Prkcsh Rps6 Prkag1 Kif11 Psmb1 Tulp3 4933400A11Rik Parg Creb1 Cebpz Timm44 Wdr4 Rapgef6 Rad54l Eif2s3x Nagpa Pex3 Gm45928 Pold4 Igbp1 Mocs2 Pcmt1 Scand1 Rab3gap2 Spag6 Def6 Serp1 Vdac2 Sqstm1 Cntn2 Rpl15 Cox7a2l Nup62 Bard1 Thrap3 Pias1 Sdf2 Gsto1 Mcm5 Mt1 Ptprf Map2k5 Scly Ppme1 Prdx5 Abcb10 Ncapg Cnot4 Mknk1 Tle3 Mfng Pfkfb4 Cept1 Per1 Rraga Med20 Gm20517 Prps2 Slc22a3 Rps19 Sap18b Itgb3bp Mlx Fzd5 Agps Fabp5 Prkab2 Gak Ube2g2 Cpsf1 Cyba Ap4s1 Cnot2 Rps6ka2 Mycbp Birc6 Mrto4 Acox3 Topbp1 Ap4b1 Gm43064 Rad50 Tyk2 Ifi30 Madd Usp4 Lsm1 Usp11 Arl6ip5 Eif4e2 Cdkl3 Lats1 Hmmr Pkn2 Cad Uchl1 Vcp Gins1 Ap4e1 Plod3 Gm20716 Dpm1 Zfp105 Cstf3 Prkra Nr6a1 Psmb7 Slc2a4 Hadhb Stx16 Ncbp1 Tmod2 Tcf12 Tpr Fancf Ppp1cb Ndufb6 Mybbp1a Stom Vgf Idh3b Uqcrc2 Nup88 Dctn3 Jrkl Mdh1 Rab1a Lsp1 Slc5a6 Mocs3 St6galnac4 Dpm2 Dbi Ppp6c Eif4h Ripk2 Trim25 Ppia Zdhhc3 Gabarap Slc25a11 Snx5 Psmd14 Dnai1 Drg1 Ciao1 Khk Ggh Cacng3 Psmc5 Rps5 Mmp8 Slc43a1 Cd79b Psmd5 Pno1 Coil Abi3 Ldha Trim44 Zfp12 Nup54 Hs3st2 Nxt1 Zfp142 Pdk2 Cops2 Tagln2 Baz1b Rpl35 Trmt6 Gna12 Cdc25b Pex16 Lztfl1 Ptpn1 Lsr Zfp110 Polr1b Abcb6 Ddx5 Slc1a4 Pfn1 Mat2a Kif15 Styxl1 Nme1 Ddx58 Sh2d3c Pcna Apba3 Ap4m1 Arrb2 Hcfc2*
Alarmin	*Bgn Il33 Ager Rnase1 Itgb2l Tlr4 Hmgn1 Rnase2b Ear14 Rnase2a Hmgb1 Itgam Gm49368 Gm5849 Lgals9 Itgb2 S100a8 Ear6 Ear1 Ear10 Ear2 Cma1 Il1f9 S100a9*

Abbreviations: Pathway RespOnsive Genes for activity inference (PROGENy), bone marrow (BM).

Table S10. Cell-cell interaction analyses

See “Table S10” file.

Table S11. Clinical parameters of Mx1-Cre$^{+/-}$;Rosa26$^{LSL\text{-}MYC/LSL\text{-}MYC}$;*S100a9*$^{-/-}$ studies

Parameters	Rosa26$^{LSL\text{-}MYC/LSL\text{-}MYC}$	Rosa26$^{LSL\text{-}MYC/LSL\text{-}MYC}$;*S100a9*$^{-/-}$
Number of mice	13	6
Age at pIpC treatment, week	8-11	8-11
Female, n (%)	7 (54)	2 (33)
Baseline body weight, mg (range)*	21.4 (17.8-30.3)	20.8 (14.8-27.9)
CBC at baseline (range)*		
WBC, K/µL	9.38 (5.75-10.62)	9.55 (5.53-12.44)
RBC, M/µL	10.3 (8.99-11.12)	10.67 (9.73-11.22)
Platelet, K/µL	925 (721-1127)	1091 (725-1294)
Neutrophil, %	10.55 (8.9-32.9)	16.45 (11.9-21)
Monocyte, %	2.8 (0.9-6.4)	2.7 (1.8-3.3)
Lymphocyte, %	84.3 (75.4-88.5)	78.2 (75.6-83.7)
CBC at week 20-24 (range)		
WBC, K/µL	12.16 (8.12-16.46)	10.72 (5.53-12.44)
RBC, M/µL	8.55 (4.87-11.27)	9.58 (7.41-11.18)
Platelet, K/µL	1130 (157-1401)	1867 (1020-3032)
Neutrophil, %	12.9 (4.6-24.7)	13.3 (8.5-27.3)
Monocyte, %	4.55 (1.6-17.6)	2.85 (2.1-4.8)
Lymphocyte, %	81.6 (66.9-87.7)	82.7 (69.7-88.1)
Median spleen weight, mg (range)**	335 (187-1770)	230 (180-440)
Median OS, days***	225	NR

Abbreviations: Complete blood counts (CBC), white blood cells (WBC), red blood cells (RBC), overall survival (OS) and not reached (NR).

*Baseline body weight and baseline CBC were assessed 1 week prior to pIpC treatment.

**Spleen weights of Mx1-Cre$^{+/-}$;Rosa26$^{LSL\text{-}MYC/LSL\text{-}MYC}$ mice were measured at the time of death or endpoints. Mx1-Cre$^{+/-}$;Rosa26$^{LSL\text{-}MYC/LSL\text{-}MYC}$;S100a9$^{-/-}$ mice were sacrificed at ~32 weeks post-pIpC treatment.

***Overall survival was calculated from the date of first date of pIpC treatment.

Table S12. Clinical parameters of S100a9 transgenic mouse studies.

Parameters	Wild type control	S100a9Tg
Number of mice	20	56
Female, n (%)	10 (50)	26 (46)
CBC at month 3 (range)	N=5	N=6
WBC, K/µL	8.46 (6.82-11.46)	10.1 (6.42-14.57)
RBC, M/µL	11.25 (10.84-11.55)	10.63 (8.8-11.36)
Platelet, K/µL	963 (901-1149)	1074.5 (216-1546)
Neutrophil, %	9.4 (7.1-32.6)	11.2 (8.6-14.4)
Monocyte, %	1.3 (1.0-2.3)	1.85 (1.4-3.1)
Lymphocyte, %	87.2 (64.8-90.8)	85.5 (82.2-87.5)
CBC at month 12 (range)	N=4	N=34
WBC, K/µL	10.36 (6.41-11.04)	11.9 (4.47-164.59)
RBC, M/µL	9.89 (9.45-10.0)	10.00 (7.5-10.99)
Platelet, K/µL	1571.5 (1254-1625)	1357.5 (161-2383)
Neutrophil, %	12.45 (11.5-14.8)	15 (9.4-47.2)
Monocyte, %	3.1 (1.7-4.3)	4.25 (2.2-42.2)
Lymphocyte, %	83.05 (81.5-85.7)	80.8 (4.6-86.7)
Median spleen weight, mg (range)*	135 (90-230)	580 (80-3950)
Median OS, days***	NR	371

Abbreviations: S100a9 transgenic mouse (S100a9Tg), complete blood counts (CBC), white blood cells (WBC), red blood cells (RBC), and overall survival (OS).

*Spleen weights of S100a9Tg mice were measured at the time of death or at pre-defined endpoints. Age-matched control mice were sacrificed at the same time.

**Overall survival was calculated from the date of birth

Table S13. Clinical parameters of Tasquinimod efficacy studies in MYC-driven MF

Parameters	Regular water	Tasquinimod water
Number of mice	13	8
Age at pIpC treatment, week	8-11	8-11
Female, n (%)	7 (54)	5 (62.5)
Baseline body weight, mg (range)*	21.4 (17.8-30.3)	20.9 (16.3-24)
CBC at baseline (range)*		
WBC, K/µL	9.38 (5.75-10.62)	9.81 (6.46-13.45)
RBC, M/µL	10.3 (8.99-11.12)	10.41 (10.02-10.91)
Platelet, K/µL	925 (721-1127)	1030.5 (420-1260)
Neutrophil, %	10.55 (8.9-32.9)	7.4 (6.2-33.9)
Monocyte, %	2.8 (0.9-6.4)	2.1 (1.1-3)
Lymphocyte, %	84.3 (75.4-88.5)	88.05 (62.6-90.4)
CBC at week 20 (range)		
WBC, K/µL	12.16 (8.12-16.46)	11.07 (8.93-20.08)
RBC, M/µL	8.55 (4.87-11.27)	7.68 (4.69-9.02)
Platelet, K/µL	1130 (157-1401)	1615 (998-3084)
Neutrophil, %	12.9 (4.6-24.7)	27.7 (11.2-36.5)
Monocyte, %	4.55 (1.6-17.6)	5.4 (2.3-10.6)
Lymphocyte, %	81.6 (66.9-87.7)	64.85 (52.4-86.2)
Median spleen weight, mg (range)**	370 (212-1770)	240 (180-640)
Median OS, days***	208	251

Abbreviations: Complete blood counts (CBC), white blood cells (WBC), red blood cells (RBC), overall survival (OS) and not reached (NR).

*Baseline body weight and baseline CBC were assessed 1 week prior to pIpC treatment.

**Spleen weights of control mice (vehicle treatment) were measured at the time of death or endpoints. Mice treated with Tasquinimod were sacrificed at ~32 weeks post-pIpC treatment.

***Overall survival was calculated from the date of first date of Tasquinimod treatment.

Table S14. Clinical parameters of MYCi975 efficacy studies in MYC-driven MF

Parameters	Vehicle Treatment	MYCi975 Treatment
Number of mice	6	6
Age at transplant, week	12-15	12-15
Female, n (%)	6 (100)	6 (100)
Baseline body weight, mg (range)	21.2 (17.2-23.8)	20.35 (19.5-23.4)
CBC at baseline (range)*		
WBC, K/μL	6.952 (5.83-8.49)	8.35 (6.27-10.33)
RBC, M/μL	10.965 (10.5-11.34)	10.945 (10.6-11.2)
Platelet, K/μL	1041 (338-1210)	851 (479-1062)
Neutrophil, %	5.15 (3.7-8)	6.8 (4.3-7.7)
Monocyte, %	1.95 (0.9-2.6)	1.5 (1.3-2.9)
Lymphocyte, %	90.4 (86.9-94.4)	89.4 (88-92.9)
CBC at 32-36 weeks post-transplant (range)		
WBC, K/μL	7.345 (3.18-12.08)	9.6 (7.2-13.86)
RBC, M/μL	9.84 (8.66-10.12)	9.535 (8.77-10.08)
Platelet, K/μL	817 (440-884)	1153.5 (424-1801)
Neutrophil, %	9.85 (5-16.3)	10.2 (7.3-13.8)
Monocyte, %	6.25 (3.6-8.6)	2.45 (1.5-3)
Lymphocyte, %	81.1 (76.1-89)	84.25 (82.6-88.5)
Median spleen weight, mg (range)**	90 (80-90)	170 (80-750)
Median OS, days***	252	NR

Abbreviations: Complete blood counts (CBC), white blood cells (WBC), red blood cells (RBC), overall survival (OS) and not reached (NR).

*Baseline CBC values were determined 1 week prior to transplant.

**Spleen weights of vehicle treatment group were measured at the time of death or endpoints. MYCi975 treated mice were sacrificed at the same time for paired analysis.

***Overall survival was calculated from the date of transplant.

Table S15: Key Resources Table

REAGENTS	SOURCE	IDENTIFIER
Antibodies		
Anti-MYC	Santa Cruz	sc-4084
Anti-MYC	Abcam	Ab32072
Anti-p53	Santa Cruz	sc-126
Anti-S100a8	Sigma-Aldrich	HPA024372
Anti-S100a9	Sigma-Aldrich	HPA004193
Anti-phospho-STAT3	Cell Signaling	9131S
Anti-STAT3	Cell Signaling	9132S
Anti-phospho-ERK1/2 Tyr204	Santa Cruz	sc-7383
Anti-ERK1/2	Santa Cruz	sc-514302
Anti-phospho-AKT Thr308	Cell Signaling	4056S
Anti-AKT	Cell Signaling	4691S
Anti-Caspase 1	Cell Signaling	2225S
Anti-PARP	Cell Signaling	9542S
Anti-β-ACTIN	Cell Signaling	3700S
Anti-ASC	Santa Cruz	sc-514414
Mouse anti-Ter119-V450	BD biosciences	560504
Mouse anti-B220-PE	BD biosciences	553090
Mouse anti-Ly6G/Ly6C-APC	BioLegend	108412
Mouse anti-CD11b-BUV737	BD biosciences	612801
Mouse anti-CD3-BV786	BD biosciences	564379
Mouse anti-F4/80-BUV395	BD biosciences	565614
Mouse anti-CD34-PE	BD Biosciences	551387
Mouse anti-CD117 (c-Kit)-APC	BioLegend	105811
Mouse anti-Ly6A/Ly6E (Sca-1)-BB515	BD biosciences	565397
Mouse anti-CD150-PE-Dazzle 594	BioLegend	115935
Mouse anti-CD48-Brilliant Violet 711	BioLegend	103439
Mouse anti-CD16/CD32-BUV395	BD biosciences	740217
Mouse Lin cocktail-BV421	BioLegend	133311
Mouse anti-CD45.1-BUV737	BD Biosciences	564574
Mouse anti-CD45.2-APC-Cy7	BD Biosciences	560694
Mouse FC block (anti-CD16/CD32)	BD Biosciences	553142
Human anti-CD45-APC	BioLegend	368512
Human FC block	Miltenyi Biotec	130-059-901
Annexin V FITC	BD biosciences	556419
Ultracomp eBeads™ Compensation Beads	Life Technologies	01-2222-42
IRDye®R 800CW goat anti-mouse IgG	LI-COR	925-32210
IRDye®R 800CW goat anti-rabbit IgG	LI-COR	925-32211
IRDye®R 800CW donkey anti-mouse IgG	LI-COR	925-32212
IRDye®R 800CW donkey anti-rabbit IgG	LI-COR	925-32213
IRDye®R 680RD goat anti-mouse IgG	LI-COR	925-68070
IRDye®R 680RD goat anti-rabbit IgG	LI-COR	925-68071
Chemicals and recombinant proteins		
Zombie Near IR live/dead stain	BioLegend	423105
Propidium Iodide	Sigma-Aldrich	P4864
DAPI	Sigma-Aldrich	D9542
Ruxolitinib Phosphate	Selleckchem	S5243

Tasquinimod	Lawrence Lab	
MYCi975	Lee Lab	
Polyinosinic-polycytidylic acid (pIpC)	Sigma-Aldrich	P0913
Tamoxifen	MedChem Express	HY-13757A
Tamoxifen	Sigma-Aldrich	T5648
4OHT	Selleckchem	S8956
Sucrose	Fisher Scientific	AAA1558336
Ethanol	Fisher Scientific	BP2818500
PEG, BioUltra, 300	Sigma-Aldrich	90878
Dimethyl sulfoxide	Sigma-Aldrich	41640
Disuccinimidyl suberate	Thermo Scientific	21655
Ammonium persulfate	BIO-RAD	#161-0700
30% Acrylamide/Bis solution	BIO-RAD	#1610154
TEMED	BIO-RAD	#161-0801
Complete™, mini protease inhibitor cocktail	Sigma-Aldrich	11836153001
Sodium orthovanadate	Sigma-Aldrich	450243
Sodium fluoride	Sigma-Aldrich	S7920
PMSF	Sigma-Aldrich	P7626
Beta-glycerophosphate	Sigma-Aldrich	G9422
Corn oil	Sigma-Aldrich	C8267
Pierce™ 16% Formaldehyde (wt/vol)	Thermo Scientific	28908
37% Formaldehyde	Sigma-Aldrich	8.18708
Clarity™ Western ECL substrate	BIO-RAD	#1705061
Odyssey® Blocking Buffer (TBS)	LI-COR	927-50000
Odyssey® Blocking Buffer (PBS)	LI-COR	927-40000
Recombinant mouse IL-3	R&D system	403-ML
Recombinant mouse IL-6	R&D system	406-ML
Recombinant mouse SCF	R&D system	455-MC
Recombinant human TPO	PeproTech	300-18
Recombinant human FLT3L	PeproTech	300-19
Recombinant human SCF	PeproTech	300-07
Histopaque® 1077	Sigma-Aldrich	10771
Cell lines		
HEL	Kaufmann lab*	
SET2	Kaufmann lab*	
HL60	Kaufmann lab*	
Cell cultures		
RPMI media 1640	ThermoFisher	61870
DMEM media	ThermoFisher	10567014
Opti-MEM media	ThermoFisher	31985062
MethoCult™	STEMCELL Technology	M3434
MethoCult™	STEMCELL Technology	H4034
StemSpan™ SFEMII	STEMCELL Technology	09605
IMDM media	ThermoFisher	12440053
Bovine serum albumin	Sigma-Aldrich	A7906
Kits		
RNeasy Mini Kit	Qiagen	74104
DNeasy Blood & Tissue Kit	Qiagen	69504
NucleoBond® Xtra Maxi	Macherey-Nagel	740414
NucleoSpin® Plasmid EasyPure	Macherey-Nagel	740727

Chromium Single Cell 3' Reagent Kits (v2)	10x Genomics	PN-120237
Chromium Single Cell A Chip Kit (v2)	10x Genomics	PN-120236
Single Cell 3' Reagent Kits (v2) User Guide	10x Genomics	CG00052, Rev D
i7 Multiplex Kit, 96 rxn	10x Genomics	PN-120262
Mouse S100a8/S100a9 heterodimer DuoSet ELISA	R&D Systems	DY8596-05
CyQUANT LDH Cytotoxicity Assay Kit	Invitrogen	C20300
Masson's Trichrome Stain Kit	Agilent	AR173
Reticulin/Nuclear Fast Red Stain Kit	Agilent	AR179
Micro BCA™ protein assay kit	Thermo Scientific	23235
iScript™ cDNA synthesis kit	BIO-RAD	#170-8891
iTaq™ Universal SYBR® green supermix	BIO-RAD	#172-5124
SepMATE™	STEMCELL Technology	85450
Dead Cell Removal Kit	Miltenyi Biotec	130-090-101
LS columns	Miltenyi Biotec	130-042-401
Deposited Data		
scRNA-seq data_mouse bone marrow	This study	GSE240963
scRNA-seq data_human bone marrow	This study	GSE242730
Transgenic mice		
C57BL/6J Rosa26-CreERT2$^{+/-}$;Myc$^{+/+}$	Cleveland lab	
C57BL/6J Rosa26-CreERT2$^{+/-}$;Myc$^{fl/fl}$	Cleveland lab	
C57BL/6J Rosa26$^{DM\text{-}LSL\text{-}MYC/LSL\text{-}MYC}$	Murphy lab, Jackson Lab	033805
C57BL/6J Rosa26$^{DM\text{-}LSL\text{-}MYC/+}$	Murphy lab, Jackson Lab	033805
C57BL/6J Rosa26$^{+/+}$	Jackson Lab	000664
C57BL/6J Mx1-Cre$^{+/-}$	Jackson Lab	003556
C57BL/6J Scl-CreERT$^{+/-}$	Padron Lab	
C57BL/6J S100a9$^{-/-}$	Wright Lab	
C57BL/6J S100a9Tg	Wright Lab	
B6.SJL-Ptprc^{a} Pepc^{b}/BoyJ	Jackson Lab	002014
NSG-SGM3	Jackson Lab	013062
Software and Algorithms		
FlowJo version 9	FlowJo LLC	
Prism version 7	GraphPad	
Canvas version 11	Acdsee	
BiomaRt	R package	
ClusterProfiler v4.4.4		
CellChat	R package	
Liana	R package	
OmniPathR	R package	
ComplexHeatmap	R package	
fgsea	R package	

*All cell lines were verified by STR profiling in the Mayo Clinic Cytogenetics Shared Resources.

Table S16: Sequence Information

qRT-PCR primers	Forward (5' to 3')	Reverse (5' to 3')
Human *MYC*	TTCGGGTAGTGGAAAACCAG	AGTAGAAATACGGCTGCACC
Human *S100A8*	ATGCCGTCTACAGGGATGACCT	AGAATGAGGAACTCCTGGAAGTTA
Human *S100A9*	GCACCCAGACACCCTGAACCA	TGTGTCCAGGTCCTCCATGATG
Human *Ubiquitin*	ACCTGACCAGCAGCGTCTGATATT	TCGCAGTTGTATTTCTGGGCAAGC
Mouse *Myc*	TGATGTGGTGTCTGTGGAGAAGAG	AGTTGTGCTGGTGAGTGGAGA
Mouse *S100a8*	CAAGGAAATCACCATGCCCTCTA	ACCATCGCAAGGAACTCCTCGA
Mouse *S100a9*	TGGTGGAAGCACAGTTGGCAAC	CAGCATCATACACTCCTCAAAGC
Mouse *S100a9**	GACACCCTGACACCCTGAG	TGAGGGCTTCATTTCTCTTCTC
Mouse *Actin*	CATTGCTGACAGGATGCAGAAGG	TGCTGGAAGGTGGACAGTGAGG

*Used to detect *S100a9* mRNA expression levels in S100a9Tg mice